Smart Physics-Inspired Compositional Dimensionless Type Curves for Unconventional Enhanced Oil Recovery

By

Fahad Iqbal Syed

Submitted to the graduate degree program in the Department of Chemical & Petroleum Engineering and the Graduate Faculty of the University of Kansas in partial fulfillment of the requirements for the degree of Doctor of Philosophy.

Chair: Dr. Amirmasoud Kalantari Dahaghi

Dr. Shahin Negahban

Dr. Russell Ostermann

Dr. Chengwu Yuan

Dr. Prasad Kulkarni

Date Defended: December 1st, 2022

The thesis committee for Fahad Iqbal Syed certifies that this is the approved version of the following thesis:

Smart Physics-Inspired Compositional Dimensionless Type Curves for Unconventional Enhanced Oil Recovery

Dr. Amirmasoud Kalantari Dahaghi

Date Approved: December 1st, 2022

Abstract

Dimensionless Type curves have been developed and used in the Oil and Gas industry for primary production performance evaluation. To Date, there is no physics-based dimensionless performance type curve developed for Enhanced Oil Recovery (EOR) of even conventional hydrocarbon-producing reservoirs. Predicting the production performance of unconventional and tight hydrocarbon reservoirs is challenging. Each unconventional well drilling and completion normally cost a company $ 6-12 Million. Unconventional EOR (UEOR) is the next step in unlocking untapped unconventional and tight hydrocarbon reservoirs' full potential and helps in minimizing environmental footprints by targeting the remaining hydrocarbon left behind and consequently avoiding unnecessary drilling and minimizing carbon emission.

To conduct a successful UEOR project, oil and gas companies perform comprehensive simulation studies to screen and select candidate wells (pilot) for UEOR, predict their response to the UEOR methods and agents, and forecast the performance of wells' ongoing UEOR. This requires running thousands of simulation cases that might take several months to complete comprehensive techno-economic assessment and evaluation. AI-empowered Dimensionless Type Curves that honor physical laws can offer fast-track screening and accurate solutions.

In this dissertation, Smart Physics-Inspired Compositional Dimensionless Type Curves (SPiC TC_D) for UEOR are presented that aim to address the above-mentioned problem and save millions of dollars by optimizing the UEOR practice and consequently reducing the carbon emission and environmental footprints and using subsurface resources in an environmentally beneficial way, which is the current portfolio of the oil and gas industry.

SPiC TC_D respond to operators' W_3H questions (**W**here to inject, **W**hen to inject, **W**hat to inject, and **H**ow to inject an EOR solvent) while performing comprehensive field screening and designing unconventional EOR pilot(s). W_3H methodology provides fast-track AI-aided physics-inspired solutions based on historical wells' performance with existing subsurface reservoir and fluid descriptions and

hydraulic fracture geometries and flow properties. This technique enables operators to make quick decisions on unconventional EOR pilot candidates' selection and design to optimize design criteria such as the choice of injection solvent type and volume estimation, the optimum start of injection and soaking time as well as the frequency of this cyclic process and estimation and the soaking duration for the optimum oil recovery.

To generate Smart Physics-Inspired Compositional Dimensionless Type Curves, a manageable number of numerical simulation cases are defined through the Physics-Guided Design of Experiment workflow. The workflow covers a wide range of operational design parameters pertaining to W_3H criteria, reservoir rock and fluid properties, hydraulic fracture design, and their corresponding flow-related parameters such as fracture conductivity, fracture half-length, fracture height, fracture spacing, and the number of hydraulic fracture clusters per stage.

Conventional design of experiment workflows fails in case of dealing with a system that operates based on known governing physical laws. This affects the accuracy of the proxy models and probabilistic modeling. Therefore, a detailed workflow is developed which is a physics quality control module to evaluate the response of the generated cases using the design of experiment techniques. It ensures the generated multidimensional distribution of the input parameters creates physically meaningful responses when solving the fluid flow equations. The next step is to train a family of machine-learning algorithms. Deep neural network algorithms are employed to build the proxy models for Smart UEOR dimensionless type curve generation. Upon completion of the training, the physics-based blind hindcasting and model response evaluation according to the physical laws are conducted. The generated physics-based AI proxy models are capable of generating thousands of cases based on the different reservoir and fluid descriptions as well as hydraulic fracture properties and W_3H operational design criteria within an hour instead of months. It enables fast and accurate decision-making for optimal UEOR practice in unconventional and tight oil reservoirs.

Acknowledgment

First and foremost, I want to express my gratitude to the Almighty Allah Ta'ala for enabling me to accomplish this challenging journey. Secondly, let me thank my graduate advisor, Dr. Amirmasoud Kalantari Dahaghi, for his technical expertise, insight, exceptional help, patience, visionary thinking, and real personal devotion to this comprehensive research. He was always available to me for both emotional and technical help. I could not have finished my dissertation without his consistent guidance and sound recommendations. Additionally, I want to thank Dr. Shahin Negahban for enabling me to attend the University of Kansas (KU). His kind demeanor, considerate actions, extensive professional experience, and technical expertise played an important role for completion of this study.

I also appreciate the enthusiasm and commitment of my research committee to enhancing the caliber of my dissertation. In addition, I would like to express my sincere gratitude to my fellow peers at the Center of Net Carbon Zero GeoEnergy Intelligence and Sustainability, who have been indispensable in helping me finish this work. Also, I would like to acknowledge the Chemical and Petroleum Engineering Department at KU for the financial support by offering Graduate Teaching Assistant appointments and, I'm also thankful to the United States' Department of Energy (DOE) and the Tertiary Oil Recovery Program (TORP) at KU for funding my Graduate Research Assistant appointments at KU for a couple of semesters.

Finally, I must express my sincere gratitude to my respected parents, wife, and siblings for their unwavering love, care, and moral support during this challenging and prolonged journey.

Dedication

To my beloved parents Prof. Mussarat Jabeen and Engr. Mehmood Iqbal

Table of Contents

List of Figures

List of Tables

Abbreviations

ANN	Artificial Neural Network
BERG	SPE Bleeding Edge of RTA Group
BHFP	Bottom Hole Flowing Pressure
CMG	Computer Modeling Group – Numerical Simulation Tool
CMOST	CMG AI Assisted Module
CNN	Convolutional Neural Network
CSI	Cyclic Solvent Injection
C_t	Rock Compressibility
DCA	Decline Curve Analysis
DNN	Deep Neural Network
DoE	Design of Experiment
EIA	Energy Information Administration
EOR	Enhanced Oil Recovery
EoS	Equation of State
ERD	Extended Reached Drilling
FC	Fracture Conductivity
FC	Fracture Conductivity / Fracture Flow Capacity
F_cD	Dimensionless Fracture Conductivity
FT	Fluid Type
GNN	Graphical Neural Network
GOR	Gas Oil Ratio
GUI	Graphical User Interface
h	Formation Thickness
HC	Hydrocarbon Gas
h_f	Fracture Height
HI	Hydrogen Index
HnP	Huff-n-Puff
IFT	Oil–water interfacial tension
K_f	Fracture Permeability
K_m	Matrix Permeability
K_{NFZ}	Permeability of None Fractured Zone
LGR	Local Grid Refinement
LHS	Latin Hypercube Sampling
MAE	Mean Absolute Error
MBE	Material Balance Equation
mD	Milli Darcy
MMP	Minimum Miscibility Pressure
MMP	Minimum Miscibility Pressure
MRC	Maximum Reservoir Contact
nD	Nano Darcy

Øf	Fracture Porosity
Øm	Matrix Porosity
OOIP	Original Oil in Place
OWC	Oil Water Contact
P_c	Critical Pressure
PDE	Partial Differential Equation
P_e	Peclet Number
PG-DoE	Physics-Guided Design of Experiment
P_i	Initial Reservoir Pressure
PINN	Physics Inspired Neural Network
PM	Proxy Model
P_{res}	Reservoir Pressure
P_{sat}	Saturation Pressure
PTA	Pressure Transient Analysis
qD_g	Dimensionless Oil Gas Rate
qD_o	Dimensionless Oil Flow Rate
R&D	Research & Development
ReLU	Rectified Linear Unit
R_o	Thermal maturity
RTA	Rate Transient Analysis
S_f	Spacing between two adjacent fractures
SHAP	SHapley Additive exPlanations ML library
SPE	Society of Petroleum Engineers
$SP_iC\ TC_D$	Smart Physics Inspired Compositional Dimensionless Type Curves
SRV	Stimulated Reservoir Volume
Swi	Initial Water Saturation
T_c	Critical Temperature
TC	Type Curve
TC_D	Dimensionless Type Curve
TDS	Brine Total Dissolved Solids
tD_xf	Dimensionless Time
Tmax	Thermal Maturity
TOC	Total Organic Carbon
TOR	Tight Oil Reservoirs
T_{res}	Reservoir Temperature
uD	Micro Darcy
UEOR	Unconventional Enhanced Oil Recovery
W_3H	Software Package; Where to inject, When to inject, What to inject, and How to inject an EOR solvent
W_f	Fracture Width
W_f	Fracture Width
X_f	Fracture Half Length

1

INTRODUCTION

Tight reservoirs are hydrocarbon-bearing formations with ultra-low permeability, often found in shale and tight sandstone. Economically, these formations are tough to develop due to tight matrix permeability and poor inter-pore connectivity. Such reservoirs are commonly developed with a large number of independent horizontal producers aided by a complex hydraulic fracture network to provide maximum reservoir contact. In addition to long horizontal wells and hydraulic fractures, early EOR application may improve and sustain the oil recovery from tight oil reservoirs. Unlike conventional reservoirs, the key performance indicators for the EOR pilot selection criteria in unconventional tight reservoirs are not well established yet. In this thesis, a detailed workflow is presented for quick screening based on the prior production history, reservoir characteristics, and the hydraulic fracture design parameters through Smart Physics Inspired Compositional Dimensionless Type Curves (SPiC TC_D). In this chapter, a detailed stepwise workflow is presented to generate SPiC TC_D and their application to answer operators' W_3H questions i.e. Where to inject, When to inject, What to inject, and How to inject an EOR solvent for the enhanced oil recovery from tight oil reservoirs.

1.1. Background

Tight oil reservoirs are contributing a major role to fulfill the overall crude oil needs, especially in the US. However, the dilemma is their ultra-tight permeability and an uneconomically short-lived primary recovery factor. Therefore, the application of EOR in the early reservoir development phase is considered effective for fast-paced and economical tight oil recovery. To achieve these objectives, it is imperative to determine the optimum EOR potential and the best-suited EOR application for every individual tight oil reservoir to maximize its ultimate recovery factor. Since most of the tight oil reservoirs are found in wide spatial source rock with complex and compacted pores and poor geophysical properties, they hold high saturation of good quality oil, and therefore, every single percent increase in oil recovery from such huge reservoirs potentially provides an additional million barrels of oil.

Due to poor rock quality, the common practice to develop tight reservoirs is to drill long horizontal wells to provide maximum reservoir contact and the wellbores are further subjected to massive multi-stage hydraulic fracturing to provide extensive support to the reservoir fluid to flow through artificial flow channels. However, with all such artificial support, the natural energy consumption, i.e., in-situ reservoir pressure, declines too rapidly during natural depletion which results in rapid oil production decline. Generally, more than half of the original well productivity diminishes within the first year of the well production life which results in poor reservoir fluid recovery.

To overcome the highlighted issue, an easy solution to uplift the recovery factor is to provide effective energy support. Water and different gases are the most studied injectants at both laboratory and numerical simulation scales. In addition, a few actual field pilots are also performed in the United States with CO_2, associated & lean hydrocarbon gas injection through huff and puff, and water flooding. Water did not show any appreciated response to improve the oil recovery; however, CO_2 and hydrocarbon injection presented mixed results that are subjected to further investigation. The detailed observations on numerical simulation, laboratory, and field pilot tests are presented in the following chapter.

From the above context, it can be concluded that the EOR application in tight oil reservoirs is quite essential to boost the oil recovery at an early stage, and it would help individual well productivity to sustain for a longer period to improve the recovery factor. However, the process of selecting the best-suited injection solvent and designing an EOR operation in such complex reservoirs is not straightforward. Unlike conventional reservoirs, due to only a few actual field pilot studies, there is limited field data available that is inconclusive to generalize field development planning for a tight oil reservoir. The physical understanding of EOR applications in different circumstances from laboratory to field scale is the key to success and similarly, the fundamental physical concepts of fluid flow dynamics under non-unique confinement conditions play an important role.

The precise selection of a particular EOR application type based on the reservoir rock, fluid, and petrophysical characteristics as well as the heterogeneity distribution are the pillar points to conducting a successful EOR application for optimum incremental hydrocarbon recovery. In addition, the prior production history, and the pre-existing hydraulic fracture design (if exist) are equally important for the EOR operational design and field implementation planning. After having the entire list of contributing factors in hand, the next and most critical step is to perform techno-economical evaluations to determine the most optimal EOR solution.

It is always risky and expensive to implement a full field EOR application at once especially when the available data has some uncertainty and/or does not have sufficient data to build numerical models with enough confidence. The best solution to cope with this issue is to conduct multiple actual field pilots in different regions to understand the reservoir response with various EOR planning strategies for optimum oil recovery.

There are multiple steps to conduct an actual field pilot as listed below.

- Representative region selection based on the common reservoir properties, fluid saturation distribution, and the production history that could represent the entire or at least a major portion of the field.
- Candidate wells selection mainly based on their location and the production/ injection history
- Mechanistic or fine-scale numerical model development and history matching
- EOR process identification
- Running hundreds of simulation cases to determine the most effective EOR plan to answer W_3H questions i.e. Where, When, What, and How to implement an EOR pilot.
- Collect all possible surface and sub-surface data from multiple pilots and update the numerical model, such that to prepare a full field EOR development plan.

As mentioned earlier, it is time-consuming and computationally expensive work to do even in conventional reservoirs. For unconventional reservoirs, the process is more complicated because of multiple additional limitations. Therefore, in this thesis, a physics-based, automated, and quick workflow and an automated tool are introduced that can easily perform the entire job in no time. The only requirement for this tool is to have the primary flow performance data that would be used as a reference to provide multiple physics-based techno-economical EOR options to provide W_3H answers. The automated data-driven tool "**W_3H**" is developed using a huge data set, generated using a commercial compositional numerical simulator 'CMG-GEM'.

1.2. Problem Statement and Dissertation Contribution

Since the classical ages of the oil and gas industry, the reservoir characterization, development planning, and flow performance monitoring of the conventional reservoirs are being done through a well-testing approach normally using pressure transient analysis (PTA). The working procedure is to match the bottom hole flowing pressure response with multiple type curves to determine the reservoir and the near-wellbore approximated formation properties. The only problem with this approach is the subjectivity of the well test and due to multiple possibilities of type curve matches, the accuracy is always been an issue even

for the conventional reservoirs. For the unconventional reservoirs, this approach is technically not possible due to poor rock type and isolated in-situ pressure support system that would take years to show any pressure build-up response on shutting in a producer and that is not economical at all. Therefore, pressure transient analysis is not an option for tight reservoirs, and it is practically not easy to completely alter the engineering operational practice therefore, the petroleum engineers came up with a similar approach to evaluate tight reservoirs through rate transient analysis (RTA) using the similar correlations and the equations. The only difference in this approach is to use the production rate along with the pressure data.

The RTA application on tight wells is not straightforward like PTA on conventional reservoirs that are usually completed with vertical, slanted, or horizontal wells with shorter horizontal sections as compared to the tight reservoirs. Tight reservoirs are normally completed with long horizontal sections and massive multiple-staged hydraulic fractures and hence have a huge well surface area that makes the analysis complicated. In such hydraulically fractured long horizontal wells, the transient response is the combination of multiple factors including, reservoir matrix properties, reservoir fluid composition, and their PVT properties as well as the hydraulic fracture properties such as fracture half-length, fracture height, fracture conductivity, etc.

However, most of the operators are using the RTA approach, though it's not accurate but economical, easy, and not much time-consuming. On contrary, the latest advancement in numerous reservoir simulations, laboratory, and actual field data made it possible to understand the physics and the possible response of in-situ hydrocarbons in different circumstances. Using those limited but reliable data, numerical simulation model development would be a more accurate solution but not economical at all. It would require a lot of computational and human effort and operational time. Since most of the tight reservoirs especially in the U.S. developed so quickly in the last couple of decades with thousands of hydraulically fractured long horizontal wells that later or sooner must be subjected to EOR to boost up the production as the economical primary recovery from such wells hardly last from few months to a couple of years.

As far as the EOR application is concerned in tight oil reservoirs, it requires detailed physics-based investigation based on individual wells' historical performance. Though multiple operators invested a lot of their R&D time and finances to build numerical simulation models subjected to their reservoirs to determine the most suitable candidate for EOR pilot out of thousands of their pre-existing producers. But still, no generalized and robust tool is available that would provide quick and physics-based reliable solutions for not only EOR pilot candidate selection but also provide a complete EOR operational design for the given reservoir rock and fluid properties as well as the pre-existing hydraulic fracture design. Detailed reservoir simulation is an ideal technique to investigate physics-based analysis with numerical accuracy and come up with a plan but it's not computationally economical to run thousands of simulation cases that would take years to explore all possible techno-economic options.

Therefore, a quick and robust solution is required for designing an EOR application. EOR candidate selection and its operational planning is a critical procedure that is based on several aspects. Typically, the following are the key **W_3H** factors that are required to be addressed.

a. **WHERE** to inject – best-suited EOR pilot/development well selection based on the primary recovery performance and the oil saturation in place.
b. **WHEN** to inject – to decide the suitable EOR timeline after primary production.
c. **WHAT** to inject – the selection of an EOR solvent based on the reservoir rock and fluid properties.
d. **HOW** to inject – EOR application design including the injection solvent volume and the soaking time.

The motivation of this work is to address all the above-listed factors and in this dissertation, I introduce an automated and smart tool that provides quick Physics-Inspired Compositional Dimensionless Type Curves (SPiC TC_D) to address W_3H factors. Based on the said motivations, the smart tool is named '**W_3H – Smart Unconventional EOR Solutions**'. The working phenomenon of this tool is inspired by Rate Transient Analysis (RTA) type curve matching technique. It provides a quick, physics-based solution for selecting the most suitable EOR pilot candidate among thousands of wells having different operational

histories as well as, drilled in different regions of a reservoir with different rock and fluid properties. It also provides multiple techno-economic options to an engineer to come up with an estimated additional oil recovery subjected to the EOR operational design. Table 1.1 presents a quick timeline comparison using the conventional ways that most of the operators use versus **W_3H** and the workflow presented in this dissertation.

Table 1.1 A quick comparison of a tight oil reservoir development conventional vs. smart W_3H timeline

Field Development Workflow	**Conventional Timeline**	**Smart W_3H Timeline**
Data Gathering & Analysis	Days to weeks	Less than an hour
Numerical Model Generation	Weeks to months	–
History Matching for Model validation	Weeks to months	Less than an hour
EOR forecasting using different solvent slug sizes & soaking time	Weeks to months	Less than an hour
The entire project – An estimated timeline to explore all possible techno-economic options	Months to year	Few hours to a couple of days

The entire study is performed in several steps; however, the major phases of this work are presented in a detailed workflow shown in Figure 1.1.

Initially, a detailed literature review is performed to collect the most representative data to develop meaningful ranges of reservoir rock, fluid, and hydraulic fracture design parameters. Secondly, using typical tight oil reservoir rock and fluid properties and the commonly adopted hydraulic fracture design parameters, a numerical simulation model is generated using a compositional commercial reservoir simulator 'CMG-GEM'. Categorically, the generated reservoir model is tuned and validated using the time-based typical tight oil well flow responses observed in multiple wells performance data publicly available at the Society of Petroleum Engineers (SPE) data repository.

For different circumstances, a thorough physical understanding is developed from the generated reservoir model followed by thousands of physics-based numerical simulation cases generation using different reservoir rock and fluid properties as well as the hydraulic fracture design parameters. The EOR operational design parameters are also utilized as one of the key sets of parameters to generate simulation cases. The entire reservoir matrix, fluid, and hydraulic fracture-related parameters were randomly

distributed to cover the entire possible range found in the literature using the Latin Hypercube Sampling (LHS) technique as a Physics-Guided Design of Experiment (PG-DOE).

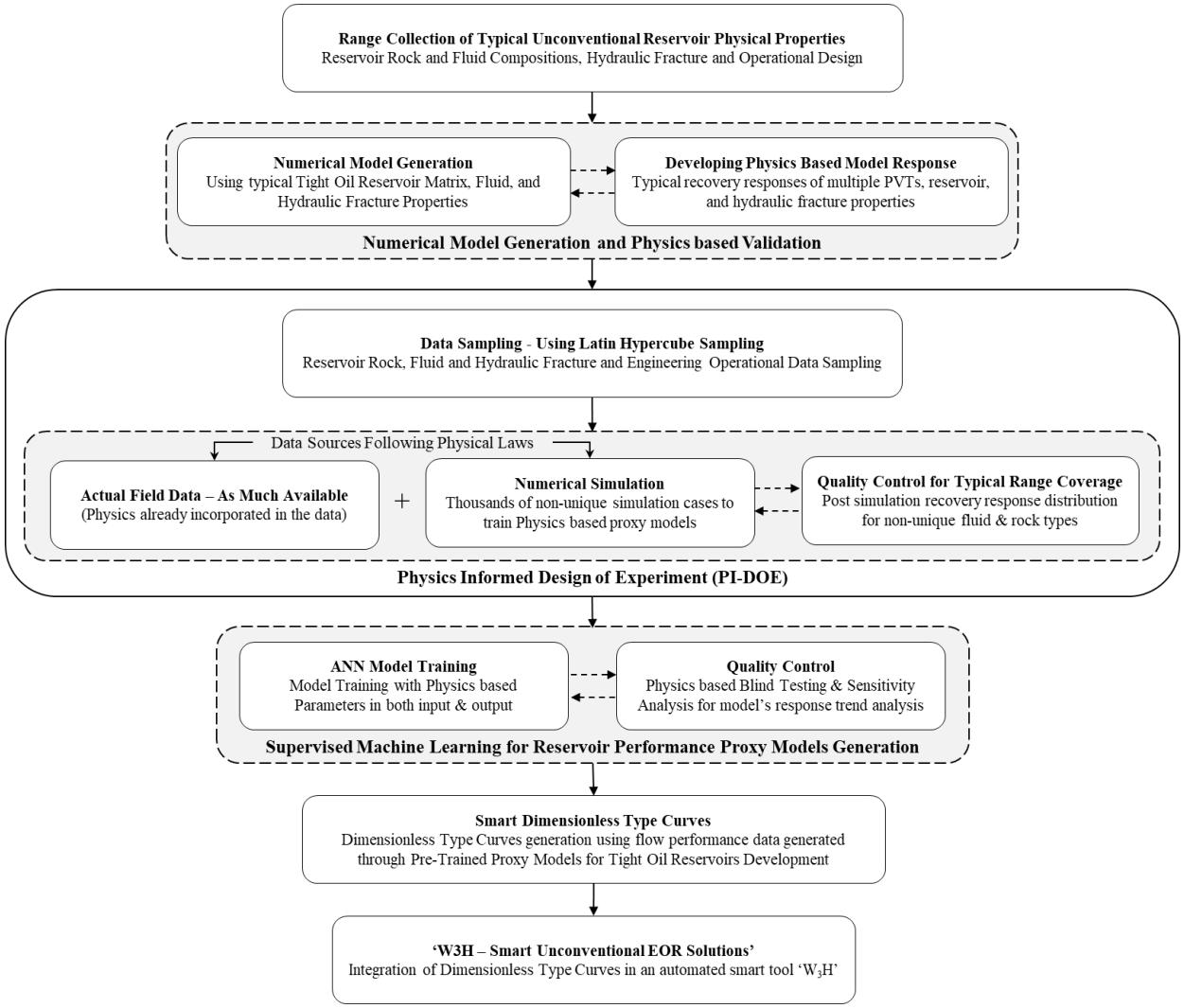

Figure 1.1 Complete study workflow

In the next step, a data-driven machine-learning approach is applied to train an automated model for the generation of uncounted proxy models for the numerous combinations of reservoir rock and fluid as well as hydraulic fracture design parameters. Lastly, an automated graphical user-interface-based application '**W_3H**' is generated that is a plug-n-play type of application for quick EOR solutions to develop tight oil reservoirs.

1.3. Dissertation Organization

This dissertation is comprised of a total of seven chapters that are organized as below:

Chapter 1: Introduction

In this chapter, a brief overview of tight oil reservoirs, their strategic development planning, and their unique characteristics are presented that support EOR application to accelerate and boost the overall oil recovery process. In addition, a detailed project workflow is presented in this chapter.

Chapter 2: Literature Review

This chapter presents a comprehensive literature review on tight oil reservoirs and their multi-dimensional characteristics. In addition, the observations and reservoir simulation, laboratory, and EOR field pilots-based performance evaluation are presented such that to collect all necessary reservoir rock and fluid information, hydraulic fracture design parameters ranges, and the possible EOR operational design limits to develop a comprehensive numerical simulation-based database to train proxy models.

Chapter 3: Reservoir Numerical Model Development

In this chapter, a numerical mechanistic compositional reservoir simulation model is created for the physics-based database utilizing the usual tight oil reservoir rock and fluid properties. Through consideration of various reservoir rock and fluid characteristics, hydraulic fracture design parameters, and various EOR operating designs, sensitivity analysis is used to generate a full physical knowledge of several aspects.

Chapter 4: Spatio-Temporal Database Development

Using the history-matched compositional mechanistic paradigm, this chapter discusses the creation of spatiotemporal databases. The reservoir rock and fluid characteristics, hydraulic fracture design parameters, and the operational design for EOR are all considered while creating a database. To account for a wide range of individual parameters, random sampling is carried out using an experimental design that enables the creation of a database for the full magnitude range of each parameter using a small number of simulation cases with randomly chosen combinations of various parameters.

Chapter 5: Smart Physics-Inspired Compositional Dimensionless Type Curves

In this chapter, novel Physics-Inspired Smart Compositional Dimensionless Type Curves are introduced. Additionally, a generalized end-user poster is assembled in this chapter to cover all potential scenarios with various reservoir rock properties, in-situ fluid types, hydraulic fracture designs, and EOR operational designs for a quick and efficient primary and UEOR performance match as well as incremental hydrocarbon recovery predictions.

Chapter 6: Smart Physics-Inspired Proxy Models Development

In this chapter, a methodical approach and steps are discussed for creating random samples for a numerical simulation-based comprehensive data library, using a Physics Guided Design of Experiment, followed by the Deep Neural Network structure considered for the smart physics-inspired proxy models development.

Chapter 7: Physics-Inspired Proxy Models Quality Check & Case Studies

This chapter presents the prediction performance of the proxy models using both training and non-training datasets. Several actual case studies are then presented and analyzed to show how the proxy models respond to the techno-economic unconventional EOR pilot screening.

Chapter 8: W_3H – User Manual

This chapter introduces W_3H, a physics-based alternative to computationally expensive numerical simulation tools that provides results in a matter of hours, helping to reduce the number of prospective UEOR pilot wells that need to be thoroughly studied. W_3H is a straightforward and user-friendly tool that imports historical well performance data, information on the rock and fluid quality of the reservoir, and hydraulic fracture design parameters. After matching the primary recovery performance with the W_3H dimensionless type curves, the smart tool offers multiple EOR options with the optimum incremental oil recovery.

2

LITERATURE REVIEW

This chapter presents a comprehensive literature review on tight oil reservoirs and their multi-dimensional characteristics. In addition, the observations and reservoir simulation, laboratory, and EOR field pilot-based performance evaluation are presented. Also, the significance of micro to the macro-scale assessment of tight oil reservoirs is presented in comparison to a conventional reservoir for the full field development planning and the EOR applicability. The fluid flow mechanisms and the physical laws are also included in the chapter that controls the in-situ fluid flow through nano-confined pore spaces. The typical ranges of tight oil reservoir rock and fluid properties are also listed in the chapter which is the most important part of this dissertation that is used to develop the entire dataset.

2.1. Introduction

Crude oil from tight oil reservoirs (TOR) is the fastest-growing hydrocarbon resource worldwide and these reservoirs are being developed usually through horizontal drilling and multistage hydraulic fracturing. According to Energy Information Administration (EIA), the technically recoverable shale hydrocarbon resources are summed up to more than 350 billion barrels, globally. These reserves are present in shale formations laying under different international territories which is almost 10% of the total known fossil oil in the world. The estimated amount of technically recoverable top 10 shale oil reserves are listed in Table 2.1. Among the top 10 countries with maximum shale oil reserves, the United States falls in 2nd place after Russia with approximately 17% of the total global shale oil. China, Argentina, and Libya are the next biggest shale oil holders (EIA, 2013). The regional estimate of the technically recoverable shale oil share to the world is shown in Figure 1.1. This distribution is based on 46 countries across the world with North America having the highest technically recoverable share due to competitive technical advancement (EIA, 2017).

Table 2.1 Top 10 countries with technically recoverable shale oil resources; data collected and summarized from multiple sources (EIA, 2013, 2021a, 2021b)

Rank	Country	Shale Oil (Billion bbl.)	Global Shale Oil Reserves (%)
1	Russia	75	21.7
2	USA	58	16.8
3	China	32	9.8
4	Argentina	27	7.8
5	Libya	26	7.5
6	Australia	18	5.2
7	Venezuela	13	3.7
8	Mexico	13	3.7
9	Pakistan	9	2.6
10	Canada	9	2.6
	Total	345	

Figure 2.2 presents the significance of the U.S. shale oil production that is contributing to more than half of the whole U.S. oil production as of 2022. Among seven different regions of the U.S., the Permian basin located in the Southwest region alone contributed the most to the total U.S. shale crude oil production. It can be noticed in Figure 2.2 that the overall shale U.S. crude oil production jumped from 5 to 8 MMbbl per day just in a couple of years i.e., from 2018 to 2020 and the progressive trend of the U.S. shale reservoirs' rapid development can be noticed in the

same figure. In early 2020, due to the global pandemic situation, oil production was significantly cut down, globally, which is getting back on the same trend as pre-pandemic in 2022. Table 2.2 summarizes the reserves distribution based on individual basins and/or reservoirs (EIA, 2017; Long, 2022).

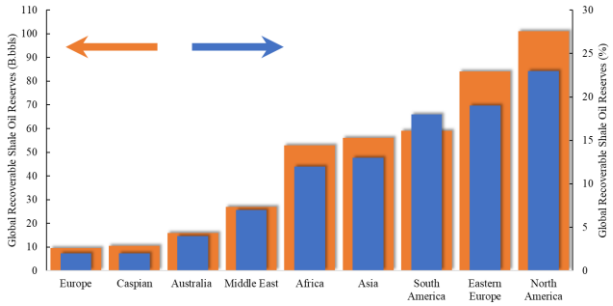

Figure 1.1 Regionally technically recoverable shale oil reserves (Data collected and summarized from EIA, 2013, 2021a, 2021b; Syed et al., 2022)

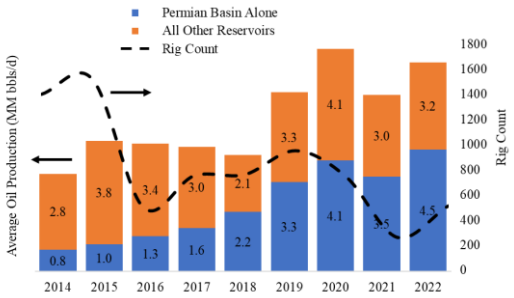

Figure 2.2 U.S. tight oil recovery performance and the tight oil reservoirs development through rig counts

Based on the experiences shared in this chapter from laboratory to field scale, a fact is established that the process of finding the most effective way to develop a shale reservoir is critical and time-consuming because of multiple factors including extremely small pore size, low and dual porosity distribution, and most importantly the ultra-tight permeability distribution (Du et al., 2019). In the last decade, considerable advancement is done to finally acknowledge a couple of techniques including horizontal well drilling and multistage massive hydraulic fracturing in tight formations as the most successful ones to develop TORs more effectively. A rapid increase in total oil production using these techniques is evidence of their success that could be noticed that resulted in a boost in total oil production to almost double since 2010 (EIA, 2021b). Figure 2.3 is presenting the production history and the projection of the U.S. shale oil production that is expected to hit the peak of 12 million barrels per day by the end of this decade using the current technology. However, these anticipated numbers would increase with further advancements in technology over time. In Figure. 2.3, it is notable that tight oil is even today contributing around 70% to the total oil production (Syed et al., 2021a; 2021b; 2022; Usman Ahmed, 2016). EIA also reported that only 15% of the total crude oil in the U.S. used to be produced through horizontal wells which jumped to 96% of the entire oil production by the end of 2018 through optimized horizontal drilling mainly in TORs. However, in parallel about 88,000 pre-existing vertical wells are also producing but to a very minor contribution towards the total volume and are considered to keep

producing until they become uneconomic. Figure 2.4 shows the status of the total vertical and horizontal well count in the major unconventional plays of the U.S. as of 2019 (EIA 2019; Kurtoglu, et al., 2013a; Perrin, 2019).

Table 2.2 Technically recoverable shale oil resources in the U.S. per basin/ reservoir as of January 2020 (EIA, 2017)

Region	Basin/ Reservoir	Technically Recoverable Shale Oil per Region (Billion bbl.)
East	Appalachian	4.4
	Illinois	
	Michigan	
Gulf Coast	Black Warrior	31
	TX-LA-MS Salt	
	Western Gulf (Eagle Ford)	
Midcontinent	Anadarko	2.6
	Arkoma	
	Black Warrior	
Southwest	Fort Worth	112.6
	Permian	
Rocky Mountain/ Dakotas	Denver	25.1
	Grater Green River	
	Paradox	
	Powder River	
	San Juan	
	Southwestern Wyoming	
	Uinta Piceance	
	Wind River	
Northern Great Plains	Montana Thrust Belt	18.9
	North Central Montana	
	Powder River	
	Williston (Bakken)	
West Coast	Columbia	0.4
	San Joaquin/Los Angeles	

Apart from tight hydrocarbon (oil and gas) reservoirs, deep natural gas, geo-pressurized zones, coalbed methane, and methane hydrate reservoirs are also commonly referred to as unconventional reservoirs. For such complex reservoirs, a horizontal well provides comparatively greater contact to the reservoir and enhances the wellbore exposure to produce plenty of additional hydrocarbons that is why horizontal wells are also known as Maximum Reservoir Contact (MRC) wells, and their drilling process is called Extended Reached Drilling (ERD) (Syed, et al., 2016). However, MRC wells and hydraulic fractures make a great combination to generate greater

exposure of the hydrocarbon to flow from the matrix to the fractures through primary depletion with a higher differential pressure across the wellbore that results in an incredible increase in production (Butler, et al., 2021; Muther, et al., 2020a; Sprunger, et al., 2021; Syed, et al., 2021). Nevertheless, it has been a common observation in almost all the TORs that the resulting increased oil production does not sustain for long and comes to a rapid decline after some time that ranges between a few months to a couple of years (Syed et al., 2021c; Khan, et al., 2016; Todd and Evans, 2016). A schematic of a horizontal well with induced hydraulic fractures deep into the matrix is shown in Figure 2.5 concerning a vertical well.

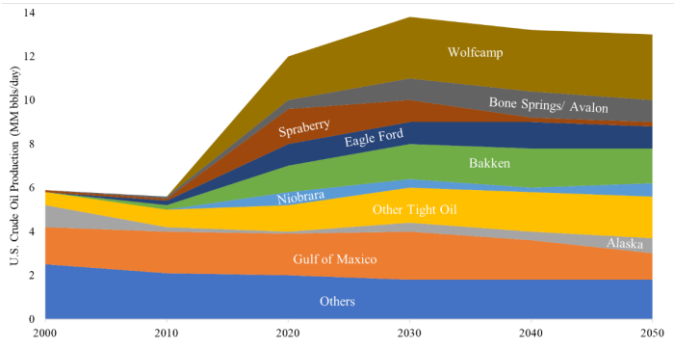

Figure 2.3 Projected U.S. tight oil production profiles of all major plays (Data collected and summarized from multiple sources as mentioned in the context)

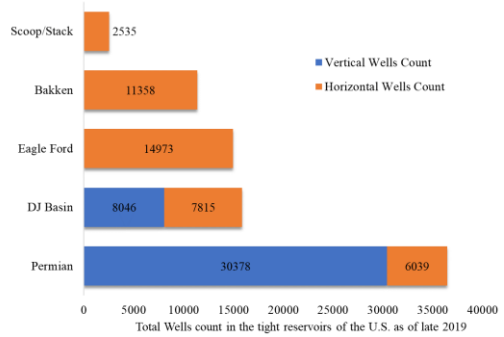

Figure 2.4 Existing vertical and horizontal well count in the U.S. reservoirs as of 2019 (Data collected and summarized from Kurtoglu, et al., 2013a; Perrin, 2019)

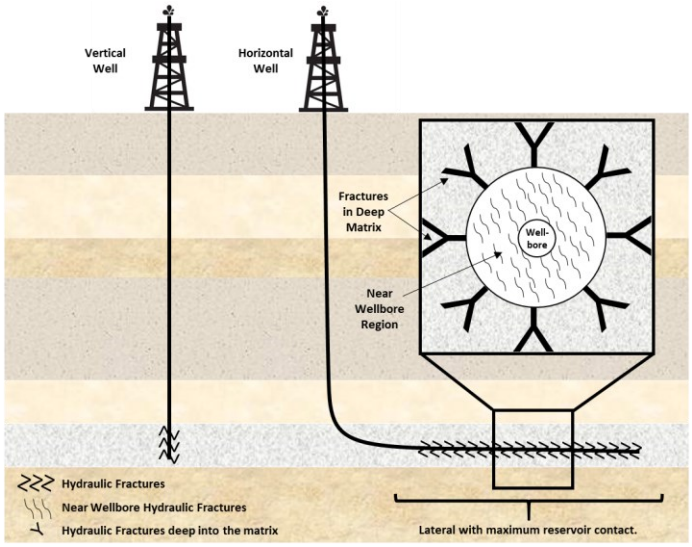

Figure 2.5 Horizontal well schematic with stimulated hydraulic fractures and the vertical well for reference.

2.2. Major Shale Oil Plays

Bakken play is one of the most producing U.S. shale oil plays that is aerially lying over Montana and North Dakota in north-central America and a part of it lying in south-central Canada. This play is relatively thin layering in

the central part and quite deep at the Williston Basin and it includes both conventional as well as unconventional reservoirs. The entire Bakken formation is consisting of three major parts, lower, middle, and upper Bakken, out of which, middle Bakken is the primary production zone. The original oil in place is estimated at approximately 300 to 900 billion barrels while the technically recoverable reserves based on today's technology are approximately 5 to 25 billion barrels (Li, et al., 2018; Wang, et al., 2020)

Eagle Ford is the second highest producing play that is lying in south Texas with approximately 5 to 30 billion barrels of original oil in place. It mainly consists of higher carbonate shale percentage i.e., around 70% mainly in south Texas with Kerogen Type II while possessing higher shale content in the northwest region. The higher carbonate content makes it more brittle and hence it becomes more conducive for hydraulic fracture operations. Currently, Eagle Ford is contributing under 1 million barrels of oil production per day (DiStefano, et al., 2019; Liang and Zhao, 2019; Zhao, et al., 2020)

Another major shale oil play in the U.S. is Wolfcamp which is lying in the midland basin, which is a major oil resource of the Permian Basin. It is having approximately 30 billion barrels of original oil in place. The Kerogen type for this play is found to be varying in the overall region between Type II and Type III. It is one of the most developed shale oil resources with more than 6500 producers and over 200 active rig counts (Casey, et al., 2018; Gherabati, et al., 2020; Smye, et al., 2020).

The next is the Niobrara shale formation that is lying northeast of Denver, Colorado, with the presence of both conventional and unconventional oil resources. The Niobrara is consisting of three isolated zones i.e., Niobrara A, B, and C which are sitting on the top of Codell and Greenhorn formations. It is one of the deepest shale formations in the U.S. with approximately 7000 ft vertical depth with the formation thickness ranging between 150 to 300 ft (Heart Energy 2020; McCormack, et al., 2021; Yue, et al., 2021).

The Utica shale is another important shale oil play in the U.S. that is a stacked play, that includes both the Utica formation and the underlying Point Pleasant formation of the Late Ordovician age. The formation extends in the subsurface from New York State in the north to northeastern Kentucky and Tennessee in the south. The typical depth of the formation varies from 2000 to 14000 ft and a wide range of thicknesses covers 70 to 750 ft (Heart Energy 2020; Gittings and Roach, 2020; Goodman, et al., 2019). Figure 2.6 is presenting the boundaries, structure (elevation of the opt contours), and isopachs (thickness contours) of all five plays discussed above. While Table 2.3 summarizes the

overall characteristics of all five plays. Multiple oil & gas companies are operating simultaneously on every individual play.

Table 2.3 Summary of U.S. tight oil plays characteristics

U.S. Plays	Bakken	Utica Shale	Eagle Ford	Wolfcamp	Niobrara
Geological Age	Late Devonian & Early Mississippian	Middle Ordovician	Early Cretaceous	Permian	Late Cretaceous
Basin	Williston Basin	Appalachian	Maverick Basin	Permian	Denver-Julesburg
Geographic location	North Dakota & Montana	Eastern United States	South Texas	West Texas & SE New Mexico	NE Kansas, NE Colorado, SW Nebraska & SE Wyoming
Average depth, ft	6000	5000 – 11000	7000	10000 – 12000	3000 – 14000
Average thickness, ft	22	100 – 400	200	1200 – 2000	450
Average porosity, %	8	2 – 8	9	5 – 9	6 – 9
TOC, %		5 – 8	4.25	2 – 5	3

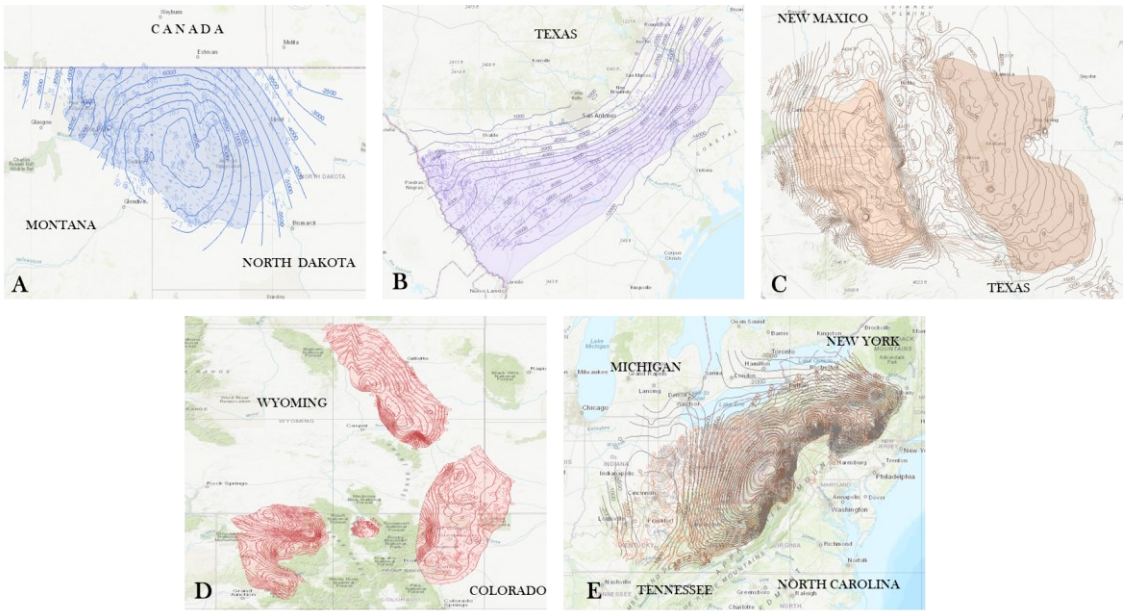

Figure 2.6 Boundary, structure (elevation of the top contours), and isopachs (thickness contours) of (A) Bakken (B) Eagle Ford (C) Wolfcamp (D) Niobrara (E) Utica Shale (Maps gathered from EIA 2022)

Apart from the U.S., Russia, and China are having the largest shale oil resources with approximately 75 and 32 billion barrels of technically recoverable oil. Globally, shale oil resources are facing the same issue of short production life and very low ultimate oil recovery that typically ranges between 3% to 10%. Figure 2.7 presents an image of a typical well's average annual production rate decline percentile for the first year of production from different major shale oil plays in the U.S. It can be observed that oil production decreases rapidly as high as 50% of

the initial flow rate. Therefore, to increase the oil recovery factor and the reservoir's overall potential, secondary/tertiary oil recovery must be considered from day one of the field development. Due to ultra-tight permeability, gas injection is the only best-suited option that has been tested in a few pilots and found considerable results, especially with CO_2 injection.

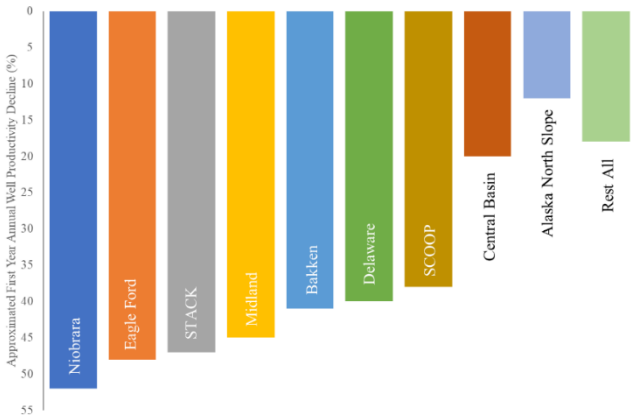

Figure 2.7 First-year annual oil production rate decline percentile (Data collected and summarized from Barree, et al., 2009)

2.3. Field Development Planning

Conventional reservoirs with good permeability distribution are more likely to be developed with natural depletion drive. Whereas water flooding is the most economical secondary drive mechanism that aids oil recovery improvement, usually followed by Enhanced Oil Recovery (EOR)/tertiary recovery applications. The most common EOR applications include HC and non-HC gas injection for miscible and immiscible gas flooding, etc. The EOR processes are those that improve recovery from the injection of non-native fluid or energy deep into the reservoir. Chemical and thermal EOR methods are also very commonly adopted to develop and/or to re-develop conventional oil reservoirs (Syed, et al., 2011; 2016; 2019). But unlikely, the unconventional oil reservoirs do not give any response to natural depletion or water injection due to very low water injectivity because of ultra-tight permeability and the poor rock pores and pore throat size distribution that keep the oil isolated and trapped droplets (Sheng and Chen, 2014; Sheng, 2015). The contribution of rock structures and their mineralogy cannot be neglected either which is responsible for creating such ubiquitous matrix nature. For example, Figure 2.8 presents a schematic of pore throat size, structure, and types for unconventional reservoirs concerning conventional reservoirs. The hydrocarbon accumulation in conventional reservoir rock usually possesses a pore throat diameter of 1 micrometer that causes reservoir fluid accumulation and migration based on buoyancy factors. On contrary, unconventional reservoirs usually own pore

throats with lesser than 1-micrometer diameter, and fluid migration and accumulation happen by different mechanisms including overpressure, buoyancy, stable temperature, and pressure.

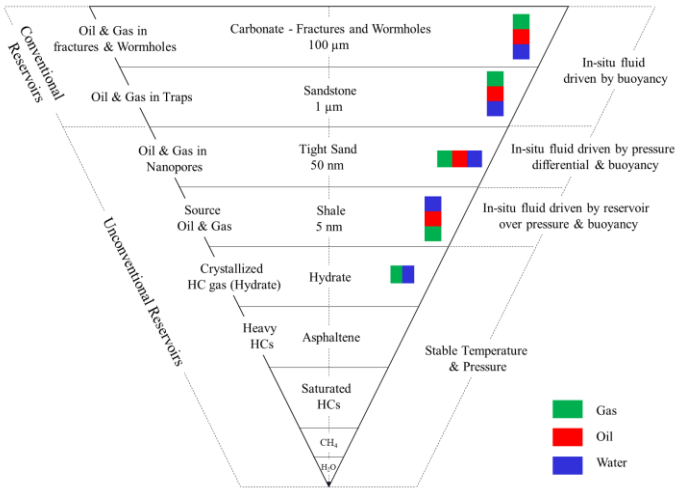

Figure 2.8 Type, size, and structures of pore throats in conventional and unconventional reservoirs (modified from Hoteit and Firouzabadi, 2006)

Considering the facts discussed above, EOR projects are capitally intensive, time-consuming, and highly uncertain processes that commercially require careful and systematic evaluation for successful unconventional field development planning. A well-defined staged evaluation process for field development mainly relies on consistent comparison of processes and the involvement of updated available and applicable technology. The maximum chances of success depend on the process of minimizing efforts spent on inappropriate scenarios and the communication with multi-disciplinary teams as well as commercial stakeholders. To present the complex nature of unconventional reservoirs, multiple formation rock & fluid characteristics, and rock mineralogy are summarized in Table 2.4.

The unconventional resources tend to be laterally extensive but only developed through diffusion-based processes since the unconventional hydrocarbons are not found within the discrete closures. That is why the presence of huge but inherent heterogeneities requires hundreds of wells to target sweet spots for commercial-scale field development. Table 2.5 enlists all the major reservoir specifications and the field development considerations usually considered while developing two different types of reservoirs.

Table 2.4 Typical rock/ formation and fluid properties of shale oil reservoirs

Reservoir Formation, Rock and Fluid Properties	Typical Range (Collected from Literature)	References
Permeability	1E-5–0.1 mD	Alvarez and Schechter, 2016; Alfarge, et al., 2017a, 2017b; Alvarez, et al., 2017; Alharthy, et al., 2018a, 2018b; Adel, et al, 2018; Aziz, et al, 2021; Biresselioglu, 2016; Caineng, et al., 2013; Cho, et al., 2016; Dawson, et al., 2015; Fragoso, et al., 2018; Jin, et al., 2016; Kurtoglu, et al., 2013b; Kurtoglu, et al., 2014; Karimi, et al., 2019; Kerr, et al., 2020; Li, L., et al., 2019; Morsy, et al., 2013; Morsy and Sheng, 2014; Pu and Li, 2016; Rassenfoss, 2017, 2014; Sanaei, et al., 2018; Valluri, et al., 2016; Wang, D., et al., 2016, 2014, 2012, 2011; Wang, D., et al., 2016; Yu and Sheng, 2016; Yu, et al., 2014; Yin, et al., 2017; Zhang, et al., 2013b; Zhang, 2016
Porosity	2%–18%	
Reservoir temperature	200–240 °F	
Formation pressure	3000–8000 Psi	
Saturation pressure	2500–3500 Psi	
Ney pay thickness	8 –2600 ft.	
Formation depth	2000–14000 ft.	
Drive mechanism	Poor sweep and low-pressure connectivity	
Initial water saturation	25%–50%	
Pressure gradient	0.42–0.7 psi/ft	
Rock type	Mixed-silt, limestone, sand & shale	
Thermal maturity (Ro)	0.6%–1.8%	
Wettability	Mixed to oil-wet	
Contact angle	80°–145°	
Oil–water interfacial tension (IFT)	17–34 mN/m	
Natural fracture intensity	0–32 per ft	
Clay content	7%–30%	
Total organic content	0.1%–12%	
Bulk density	2.3–2.5 g/cm^3	
Grain density	2.5–2.7 g/cm^3	
Rock grain size	Below 62.5 µm	
Average pore radius	0.01–0.03 µm	
Oil viscosity	Below 4.2 cP	
Oil API gravity	25 to 50°	
Gas oil ratio (GOR)	500–1800 scf/stb	
Oil polarity	More towards paraffinic	
Fluid PH	Acidic	
Total acid number	0.02–0.36 mg KOH/g	
Total base number	0.12–1.16 mg KOH/g	
Brine specific gravity	Heavy	
Brine salinity	High	
Brine total dissolved solids (TDS)	228500–285000	

Table 2.5 Reservoir specifications and field development differences between conventional & unconventional

	Conventional Reservoirs	Unconventional Reservoirs
Reservoir Specifications	Found in localized structural traps	Found in aerially continuous thin formation deposits
	Relatively smaller original oil in place	Relatively larger original oil in place
	Higher to moderate porosity	Moderate to lower porosity
	Possesses inter-granular porosity	Other/ Complex Porosity Types
	Permeability ranges > 0.1mD	Permeability ranges << 0.1mD
	A strong relationship between porosity & permeability	Generally, permeability increases with porosity but no strong relationship
	Follow traditional phase behavior	Mostly works on complex PVT behavior
	API may vary from 7º to 50º	API varies greatly within the range of 25º -50º
	Primary recovery ranges between 15% - 35%	Primary recovery ranges between 2% - 8%
Field Development Planning	Shows sustainable Production & Injection operations	Rapidly declines production and shows poor injectivity
	Few wells are reliable enough for commerciality	Several wells are required for commercial field development
	Field development assessments before development drilling	Field development assessments during development drilling and the development plan keep on updating based on the regional flow performance
	Field development uncertainty/ risk factor ranges from Low to medium	Always high uncertainty and the field development risk factor
	Both vertical and horizontal wells work with hydraulic fractures	Horizontal wells are necessarily required with hydraulic fractures to maximize reservoir contact
	Follow the natural depletion process	Artificial / manufacturing process
	Hard to find – Easy to produce	Easy to find – Hard to produce

Whereas Table 2.6 lists the summary of typical well properties drilled in different U.S. TORs to give an idea about the estimated cost for individual well drilling operations and the expected estimated ultimate oil recovery for the net profit approximation.

Table 2.6 Typical wells information from major U.S. shale oil plays. (Heart Energy, 2020)

	First Production	Well Cost ($MM)	EUR (Million bbl.)	Well Spacing (ft.)	Avg. Well Lateral (ft.)
Bakken	2008	Approx. 8.5 -9	700	160	8500 – 10000
Eagle Ford	2006	Approx. 6 - 9	600	40 – 80	6000 – 7000
Wolfcamp	2011	Approx. 7 – 8	650 – 750	80	4500 – 6700
Niobrara	2006	Approx. 3 – 5.5	250 – 450	160	4000 – 5100
Utica	2011	Approx.6 – 8	3.6 – 5.4	160	500 – 900

2.3.1. Field Development Stages and Planning Strategy

It is a common practice to develop TORs in multiple stages and each stage could take several years to complete, therefore, the development of such reservoirs is comparatively expansive and becomes a mega-multibillion-

dollar project. In the initial stage, the exploration has performed confirmation of the existence of the technically recoverable hydrocarbons. The geological investigation of the existing wells in the neighboring areas could be an easy start to have clear signs of hydrocarbons in the targeted area. On positive signs, detailed preliminary geological and geophysical surveys have performed the confirmation of the hydrocarbon's existence. During the same stage, the land acquisition and the drilling permits are obtained from the local and federal authorities (if needed), which could take a year. The second stage involves the seismic survey, its evaluation, and its characterization. The major objectives of this survey include the overall formation extent determination to define formation boundaries, a rough reserves estimation, and the most favorable exploratory well drilling spot determination.

For exploration purposes, initially, a vertical well is drilled to obtain multiple well logs and core samples for the actual reservoir formation and in-situ fluid characterization. While developing unconventional reservoirs, comprehensive Rock-Eval pyrolysis is performed to determine basic properties including total organic carbon (TOC), thermal maturity (T_{max}), hydrogen index (HI), etc. In addition, the geochemical properties such as rock traceability and the brittleness index are also measured in this step which is compulsorily needed for the optimum sweet spot determination while hydraulic fracturing the well. This entire exploration process approximately takes more than a year which is usually followed by drilling a few horizontal wells aided with multi-stage hydraulic fracturing networks for the early stage, usually single well based, hydrocarbon productivity estimation. Usually, micro-seismic surveys are also conducted to evaluate the hydraulic fracturing treatments and completion techniques optimization. In the development of tight hydrocarbon reservoirs, the application of massive and multi-staged hydraulic fractures is a common practice to provide optimum reservoir contact and flow channels for the in-situ fluid that does not flow easily from tight matrix pores.

The next stage is comprised of hydrocarbon production potential analysis, analytically and numerically. After having enough confidence in the collected data and their analysis, a commercial field development plan is prepared. As a part of a commercial development plan, full-field drilling permits, pipelining, and facility construction permits are acquired from the concerned authorities. Finally, after having all the legal permits, the entire field is developed on a commercial scale that might include drilling smaller spaced a few hundred to more than a thousand horizontal wells. Not only primary production but also EOR application could be part of the full field development planning.

Due to ultra-tight permeably, usually, TORs are developed regionally through the individual well-based huff-n-puff mechanism that is also known as a cyclic solvent injection (CSI). Apart from the well completion design, the hydraulic fracture design plays an important role to improve the EUR, however, a detailed sensitivity analysis on every individual well is necessarily required to determine the optimum well design and the hydraulic fracture design as well as the EOR operational design (Muther, et al., 2020a; 2020b; Syed, et al., 2022b). A detailed numerical simulation study is performed to evaluate the effects of multiple cluster count as presented in Figure 2.9, as well as the effects of fracture half-length, fracture spacing, and fracture effective permeability (Muther, et al., 2021b; 2022b; Syed, et al., 2021b; 2022b; 2020c). A few results of the numerical simulation-based study are presented in Figure 2.10 which clearly illustrates that the increasing number of clusters per fracture helps to improve the oil recovery, but the stimulated reservoir volume (SRV) is the limiting factor that determines the optimum number of clusters required in each scenario. In addition, the effect of incremental fracture half-length, spacing, and the effective permeability or fracture conductivity positively improves the recovery factor significantly.

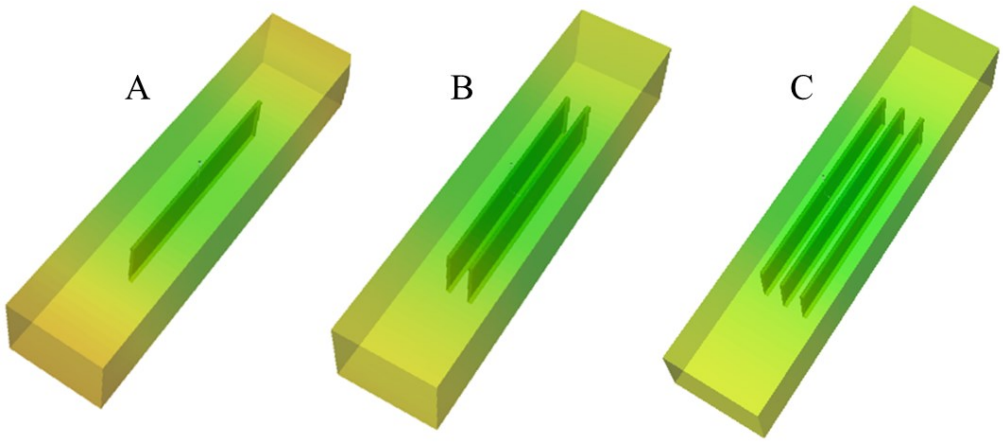

Figure 2.9 3D Numerical model representation of (a) a single, (b) dual, and (c) triple clusters per fracture

In addition to the hydraulic fracture design, the huff-n-puff operational scheme is also an important factor to consider with any injection solvent for the development of an unconventional oil reservoir. Considering CO_2 as an example, the incremental number of huff-n-puff injection and soaking cycles play an effective role to improve the oil recovery significantly as presented in Figure 2.11. It can be noticed from the first figure that the ultimate oil recovery significantly improved with an incremental number of huff-n-puff cycles. However, the recovery/fluid-flow response deteriorates because of every individual cycle in a row due to reducing residual oil saturation near the wellbore and near the fractured zone (Syed, et al., 2022b).

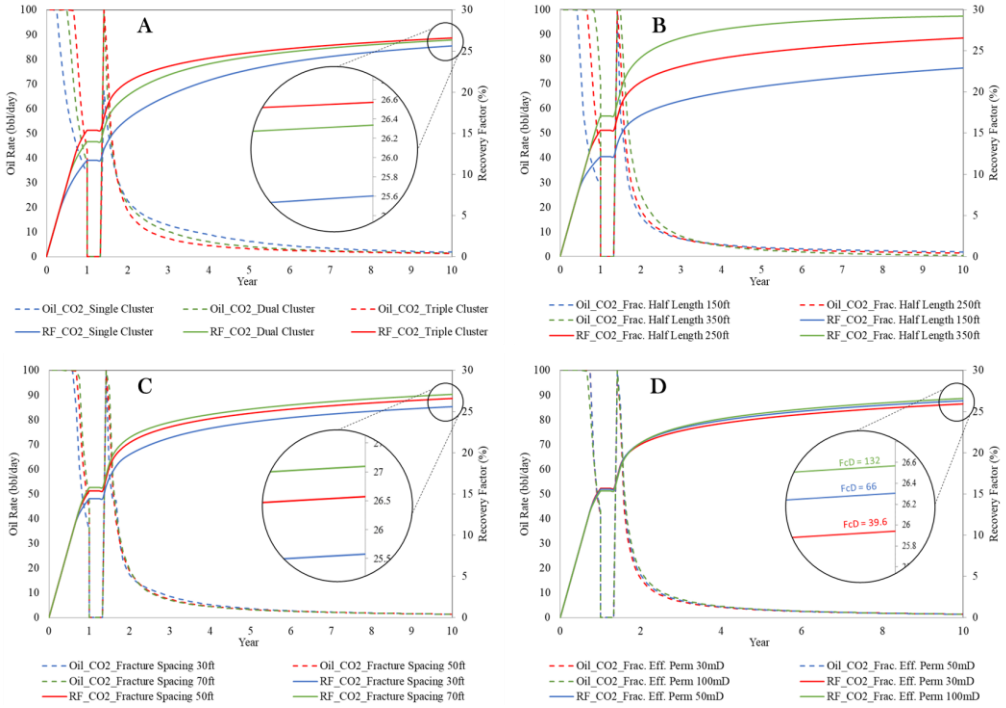

Figure 2.10 Recovery response for (a) cluster count per fracture, (b) fracture half-length, (c) fracture spacing, and (d) effective fracture permeability as presented by Syed, et al. (2022b)

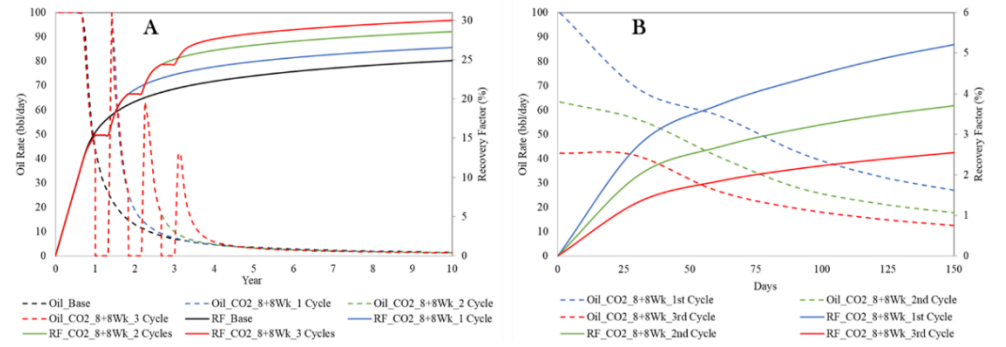

Figure 2.11 Effect of multiple huff-n-puff cycles on (a) ultimate oil recovery, and (b) individual fluid-flow and recovery response after each huff-n-puff cycle as presented by Syed, et al. (2022b)

2.3.2. Conventional Vs. Unconventional EOR

In the bigger picture, the exploration and development of tight reservoirs require early integration of geoscience and engineering skills. In addition, the early development decisions for the TORs must be made without the benefit of local well production data because over large areas, the unconventional/tight hydrocarbon accumulations can contain extremely large in-place volumes (Balasubramanian, et al., 2018). Horizontal wells and infill drilling is one of the commonly applied short-term practices to increase rapid production, the maximum reservoir contact and the spacing between the wells vary based on the rock and the stimulated reservoir volume as well as the fluid quality

(Al-Farsi, et al., 2012). Lower the quality of oil and the rock permeability; closer will be the infill wells with extended lateral lengths (Syed, et al., 2021; 2022b). Before getting into more details about the EOR applications applicable in the TORs, let us look at the major differences between the conventional and the unconventional EOR schemes as briefly listed in Table 2.7.

Table 2.7 Conventional vs. unconventional EOR mechanisms and development strategies

Conventional EOR	**Unconventional EOR**
Long-term increase in EUR	Only short-term production restoration
Considerable recovery enhancement	Quick hydrocarbon production acceleration
Sustained injection of external fluids	Unable to sustain injection/limited external fluid injectivity
The fluid flow mechanism observed through the matrix	Complex fluid flow through natural fractures and nano-pores
Fluid flow physics is relatively well understood	Fluid flow physics & chemical processes are still not completely explainable
IFT, wettability, and miscibility improvements are the key parameters to improving oil recovery	The effects of these parameters are still not completely understood
Targets in-place reservoir volume	Only near-wellbore/ locally fractured areas (SRV) are the goal
Development plans based on multiple productions & injection wells	Usually, individual well (huff-n-puff) development plans work more efficiently
It's a mid to late life-cycle application	Early life-cycle application
Shows low to medium uncertainty and risk factor	Mostly uncertain applications with a high-risk factor

2.3.4. From Laboratory to Field Scale – Lessons Learned

Because of the complicated nature of TORs, the EOR applications in conjunction with horizontal drilling are getting significant attention and motivation as discussed earlier. However, due to a poor understanding of geological constraints and the fluid flow performance in a TOR, the proper selection of an optimal EOR application, hydraulic fracture design, and the planned operational strategy is still a big challenge (Syed, et al., 2021; 2022b). There has been a lot of development research conducted over the years regarding the implementation of EOR in different U.S. TORs. A summarized evaluation of different EOR techniques based on laboratory analysis, numerical simulation, and field implementation is provided in Table 2.8. Whereas several experimental research projects are conducted on a laboratory scale is summarized in Table 2.9.

Based on the collective learnings from the experimental core scale and the numerical field-scale simulation studies, several pilots were historically planned and conducted in the U.S. Some of them presented impressive

recoveries because of CO_2 EOR, while a few of them ended up with no success but left lots of learning for better assessment and implementation in the future. A typical description of different US field development pilot projects for unconventional reservoirs is summarized in Table 2.10.

2.4. Potential Unconventional EOR Techniques & Recovery Mechanisms

As discussed in Table 2.6, the EOR applications in TORs are quite different in comparison to conventional reservoirs due to complex reservoir rock mineralogy and flow behavior. Due to the rapid production decline of unconventional tight hydrocarbon wells and low EUR, IOR/EOR techniques are essentially required to improve and sustain the production profile, economically. The only viable unconventional EOR technique so far is gas (CO_2, enriched/associated hydrocarbon) injection. In recent years, numerous studies have been conducted on various types of EOR applications in TORs and a large volume of material has been presented in technical literature by academia and industry researchers (Alfarge, et al., 2017a; 2017b; Syed, et al., 2021; 2022b).

Gas injection and most importantly the combination of the huff-n-puff process is the more frequently adopted technique to develop shale reservoirs in the U.S. since 2010, and most of the recent wells are drilled as MRC wells. The multi-stage fracturing is another factor that adds value to the process with either continuous gas injection in closed-spacing infill wells or huff-n-puff on widely spaced individual wells (Hoffman, 2018b; Thomas, et al., 2016; Todd and Evans, 2016). It was found from the literature that most of the recent research on U.S. TORs is conducted on Eagle Ford, Bakken, and Barnett formations to understand the applicability of different EOR techniques (Alfarge, et al., 2017a). From the IOR and EOR standpoint, several applications have been successfully tested in conventional fields but unfortunately, due to different reservoir rock architecture, mineralogy and the fluid flow performance in ultra-tight pores and the pore throats make it almost impossible to adopt any of the conventional applications at least without any modifications. There are hundreds of studies found to be very impressive in literature with improved recovery but at the same time, many other studies strongly contradict their findings (Alvarez, et al., 2014; Dawson, et al., 2015; Sanchez-Rivera, et al., 2015; Shuler, et al., 2011; Wang, et al., 2011; 2012;).

The recovery mechanisms are not the same for the unconventional tight reservoirs as the conventional reservoirs due to different rock properties and heterogeneity distribution, fluid phase behavior as well as fluid flow mechanism, and mass transfer mechanism (Dawson, et al., 2015; Syed, et al., 2022a). The most expected mechanisms during gas (CO_2 or HC) injection through the huff-n-puff processes include molecular diffusion in nano-pores, single-way mass

transfer, or gaseous phase evolution/expansion (Luo, et al., 2018). In addition, the cyclic pressurization and the resultant phenomenon of near wellbore/fracture oil swelling, viscosity reduction, and vaporizing gas drive are the expected mechanisms. With the above discussion, the EOR potential in major U.S. plays is listed in Figure 2.12 and consequently, a huge number of studies are conducted from laboratory scale to field pilot scale. The distribution in percentage is shown in Figure 2.13 for both, studies conducted on various scales and the major U.S. plays for which these studies are conducted.

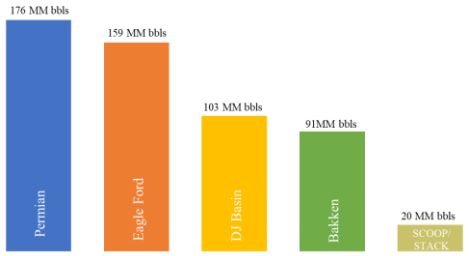

Figure 2.12 EOR potential in the U.S. reservoirs as of 2020

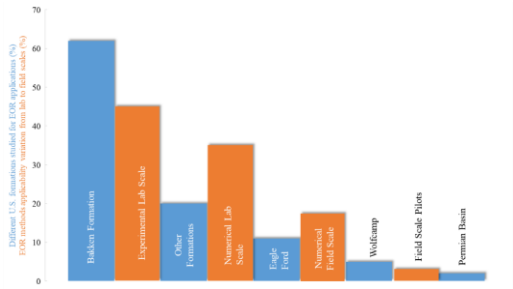

Figure 2.13 Formations & the tools (lab to field scale) used for the EOR applications on tight oil reservoirs of the United States

Table 2.8 Working phenomenon and lab/ simulation/ field tests of different EOR techniques in tight oil reservoirs

EOR	Base Phenomenon	Observations & Learnings	References
Miscible & immiscible gas injection (CO_2, HC, lean natural gas, and N_2)	• Molecular diffusion • Capillary pressure, wettability, fluid density, and viscosity reduction • High compressibility to push the oil toward the producer • Pressure maintenance • Oil swelling • Combination of all or some of the working mechanisms listed above	• Tested in almost all the U.S. reported TORs including Eagle Ford and Upper, Middle, and Lower Bakken formations. • Most importantly, reservoir pressure maintenance and oil swelling were the dominant factors to provide a considerable recovery factor. • Huff-n-puff proved to be an important player with cyclic miscible (CO_2, HC gas) as well as immiscible (N_2) gas injection in field pilots. • CO_2 is being tested more often in both the field and the lab tests. • Apart from field tests, there are several simulation and lab tests reported in the literature. • In lab and numerical studies, the gas molecular diffusion phenomenon is found to be more important to make a remarkable recovery in comparison. • Also, huff-n-puff gas injection is found to be considered successful in most of the simulation studies.	Chen, et al., 2016 Hawthorne, et al., 2019; Hoffman, 2012, 2018a; Kurtoglu and Salman, 2015; Li, et al., 2015; Sheng, 2015; Sheng and Chen, 2014; Song and Yang, 2017; Syed, et al., 2020a, 2020b; Todd, et al., 2017; Tovar, et al., 2018;

Chemical flooding (Alkaline, surfactant & polymers)	• Oil-water interfacial tension reduction • Wettability alteration	• A couple of field pilots were tested but no conclusive recovery performance review is presented in the literature. • In the lab, surfactants showed considerable results. • Also, anionic, and non-ionic surfactants are tested in the lab. • Most of the lab experiments are performed on the core samples taken from the Bakken formations. • Additionally, on a field scale, simulation studies are conducted that present promising results.	Akbar, et al., 2021; Dawson, et al., 2015; Karadkar, et al., 2019; Nguyen, et al., 2014; Sanchez-Rivera, et al., 2015; Shuler, et al., 2011; Wang, et al., 2012; 2011; Zhang, et al., 2018
Low salinity water flooding	• Clay swelling • Shale mineral cracking • Wettability alteration • Water imbibition • Osmotic Effect	• No field trials are found in the literature • However, several experimental studies are conducted • Most of the studies in the lab are conducted on a core scale • Remarkable recovery performance is observed, noticeably due to shale cracking by clay swelling • But not conclusively understood to apply in the field. Most probably due to clay swelling that might play a negative role to make the permeability worse. • Also, poor sweep and conformance control is expected.	Morsy and Sheng, 2014; Morsy, et al., 2013; Valluri, et al., 2016; Wang, et al., 2011, 2014; Zhang, J., et al., 2013b (?)
Carbonated water flooding	• Oil viscosity reduction • Oil swelling – increase in oil saturation and the relative permeability • Reduction in oil-water interfacial tension	• Lab experiments are performed, and remarkable results are found to reduce residual oil saturation to as low as 15% under reservoir operating conditions. • Also, water alternate gas with CO_2 is tested in the lab and found good results • Requires limited modifications on surface water flooding facilities to implement in fields. • Comparatively more suitable in certain environments such as places with a limited supply of CO_2 & difficult to build a recycling plant to capture or recycle CO_2.	Dong and Hoffman, 2013; Li, S., et al., 2019; Zou, et al., 2018
Carbonated silk water	• Used for hydraulic fracturing and post-fracturing EOR • Near wellbore & fracture. • Oil viscosity reduction • Oil swelling – increase in oil saturation and the relative permeability • Reduction in oil-water IFT	• During lab experiments, fractures induced by pure CO_2 are much more complex with larger surface areas compared to fractures induced by water. • A significant reduction in viscosity as a function of shear rate is observed with silk water in comparison to water or foamed water under reservoir operating conditions.	Ribeiro, et al., 2017; Wan, et al., 2015; Yin, et al., 2017; Zhang, et al., 2017

Table 2.9 Experimental research conducted on the U.S. shale reservoir rock and fluid samples.

Core Samples	Permeability, mD	Porosity, %	Injection Gas	Recovery Mechanism	Oil Recovery Factor, %	Reference
Eagle Ford	<0.001	4.4	N_2	Flooding	17.94	Sheng and Chen, 2014
	0.004	13.1			19.88	
	<0.001	4.4		Huff-n-puff	22.52	
	<0.001	13.1			24.13	
	0.0024	7.28	CO_2	Huff-n-puff 7-hour soaking	56.8	Li L., et al., 2019
	-	-	CO_2 Miscible	Huff-n-puff 5 cycles	31	Alvarez, et al., 2017; Hawthorne, et al., 2019
			CO_2 Above miscible	Huff-n-puff 3 cycles	41	
			CO_2 Way above miscible	Huff-n-puff 6 cycles	49	
			CO_2 Immiscible	Huff-n-puff 2 cycles	0.9	
	0.005	5	N_2	Cyclic gas injection	14.23–39.66	Zhu, et al., 2021
	-	7.7	CO_2		20–71	Todd and Evans, 2016
Mancos	-	5			10–63	
	-	-	N_2	Cyclic gas injection 1-day soaking	13.5	Jin, et al., 2019
				Cyclic gas injection 2-day soaking	16.96	
				Cyclic gas injection 3-day soaking	19.59	
Bakken	0.27 – 0.83	18.6 – 23.1	CO_2	Near miscible Huff-n-puff 40-hour soaking	63	Syed, et al., 2020a; Wang, et al., 2010
				Miscible Huff-n-puff 60-hour soaking	61	
				Immiscible Huff-n-puff 60-hour Soaking	42.8	
	0.29 – 0.44	18.9 – 23.6	Water + CO_2	CO_2 WAG	80.1–88.1	Dong and Hoffman, 2013; Yang, et al., 2015
Upper Bakken	-	-	CO_2	Oil extraction	10–43	Sheng, 2015
Middle Bakken	0.081 – 1.03	4.4 – 5.4	C_1		>90	Sheng & Chen, 2014
			C_2		~100	
			$C_{1\text{-}85\%}$ - $C_{2\text{-}15\%}$		>90	
			CO_2		>90	
			N_2		26	
Lower Bakken	0.081 – 1.03	4.4 – 5.4	C_1		~18	
			C_2		~27	
			$C_{1\text{-}85\%}$ - $C_{2\text{-}15\%}$		~32	
			CO_2		<10	
	-	-			8–48	Sheng & Chen, 2014
Barnett	-	-	N_2	Cyclic gas injection 1-day soaking	6.5–17.79	Sheng & Chen, 2014

Table 2.10 Observations and learnings collected from the field pilots conducted on unconventional shale reservoirs of the U.S.

Res.	Year	Injectant	EOR	Observations & Learnings	References
Bakken	2008	CO_2	Huff-n-Puff	Reported a successful injectivity test with no incremental oil recovery because of injection. The injectivity was successful due to 1-2 miles of horizontal well and a massive hydraulic fracturing network.	Sheng and Chen, 2014
	2009			Found a successful injectivity test with a minor increase in oil rate and recovery. The minor increase is likely caused by frac-hits.	
	2012	Water		Successful injectivity test with water but almost no incremental recovery. After multiple huff-n-puff cycles, observed an incremental oil response possibly due to the late reach of CO_2 deeper into the formation.	Adel, et al., 2018; Kurtoglu, et al., 2013b; Song and Yang, 2017; Sheng & Chen, 2014
	2012		Flooding	Limited success in waterflood conductivity test with no incremental oil recovery and early water breakthrough (within a month). The oil rates were reduced because of the large amount of water restricting oil flow.	
	2014	CO_2	Gas injection	Reported unsuccessful experience because of CO_2 breakthrough at an offset well on the same day with a huge CO_2 content possibly due to a connected thief zone among the two wells.	
	2014	Water	Flooding	Successful water flooding injectivity test with no incremental oil recovery due to early water breakthrough and its rapid increase (within a week) in one of the offset wells.	Sheng and Chen, 2014
	2014	Produced HC gas		After an unsuccessful experience with water flooding in 2012, produced HC gas with around 90% of C_1 and C_2 mixture injected for a couple of months that partially resulted in improved oil recovery from the offset wells. But, due to some major stimulation events and high GOR in offset neighboring wells made this experience quite complicated to call a success story.	

Eagle Ford	2012	Produced lean HC gas	Huff-n-Puff	However, the provided operational data including GOR trends seems unrealistic (GOR was found to be low during the HC gas injection) but still, the overall recovery performance was found good with a cyclic trend of improved oil rates after every injection and soaking cycle of 4 to 6 weeks.	Hoffman, 2018b Thomas, et al., 2016
	2015	Produced HC gas	Gas injection	Based on the decline curve analysis, both pilots showed a considerable incremental recovery with natural gas injection.	Hoffman, 2018b
	2015	Produced HC gas			
	2015	Produced HC gas	Huff-n-Puff	Like previous experience, also this pilot showed promising results with an incremental oil recovery because of hydrocarbon gas injection.	
	2015	Produced rich HC gas		It is quite difficult to conclude results for these pilots due to the unavailability of enough performance data.	
	2015				
	2016	Produced HC gas		It is a huge huff-n-puff, multiple wells-based field-scale pilots started in mid-2016 that showed impressive results with notable incremental oil recovery.	

2.5. UEOR Physics & Fluid Flow Mechanism at Nano-Pore Scale

As discussed in earlier sections hydraulic fractures are compulsorily generated to develop unconventional reservoirs but proper dealing with the interaction between the matrix and the hydraulically induced fractures is very important. Hydraulic fractures are usually in macro size as compared to the natural fractures that are found in micro size; therefore, hydraulic fractures help to enhance the economical fluid flow through improved flow channels for the hydrocarbons from matrix nano-pores. As a part of post-fracture operations, the micro seismic data is gathered to understand the effectiveness of hydraulic fractures and the subsequent development of the fracture network (Barree, et al., 2015; Shuler, et al., 2011; Xie, et al., 2015). Due to tight permeability and poor injectivity as well as productivity, the huff-n-puff is the most preferred gas injection/EOR mechanism that is applied in TORs. The huff-n-puff operation is performed in three steps as explained on a micro/ pore-scale level in Figure 2.14. During huff-n-puff, CO_2 is injected into the reservoir through the fractures while the concentration gradient pushes CO_2 to invade the matrix in the first step. During the second step, the well is shut in which allows CO_2 to interact with the formation of oil resulting in oil swelling and oil viscosity reduction. Finally, in step 3, the miscible or immiscible oil and CO_2 migrate out of the pores

towards the fracture by diffusion, injected CO_2 equalizes pressure inside the rock pores, and the excess CO_2 plus the heavy hydrocarbons stay back into the rock pores.

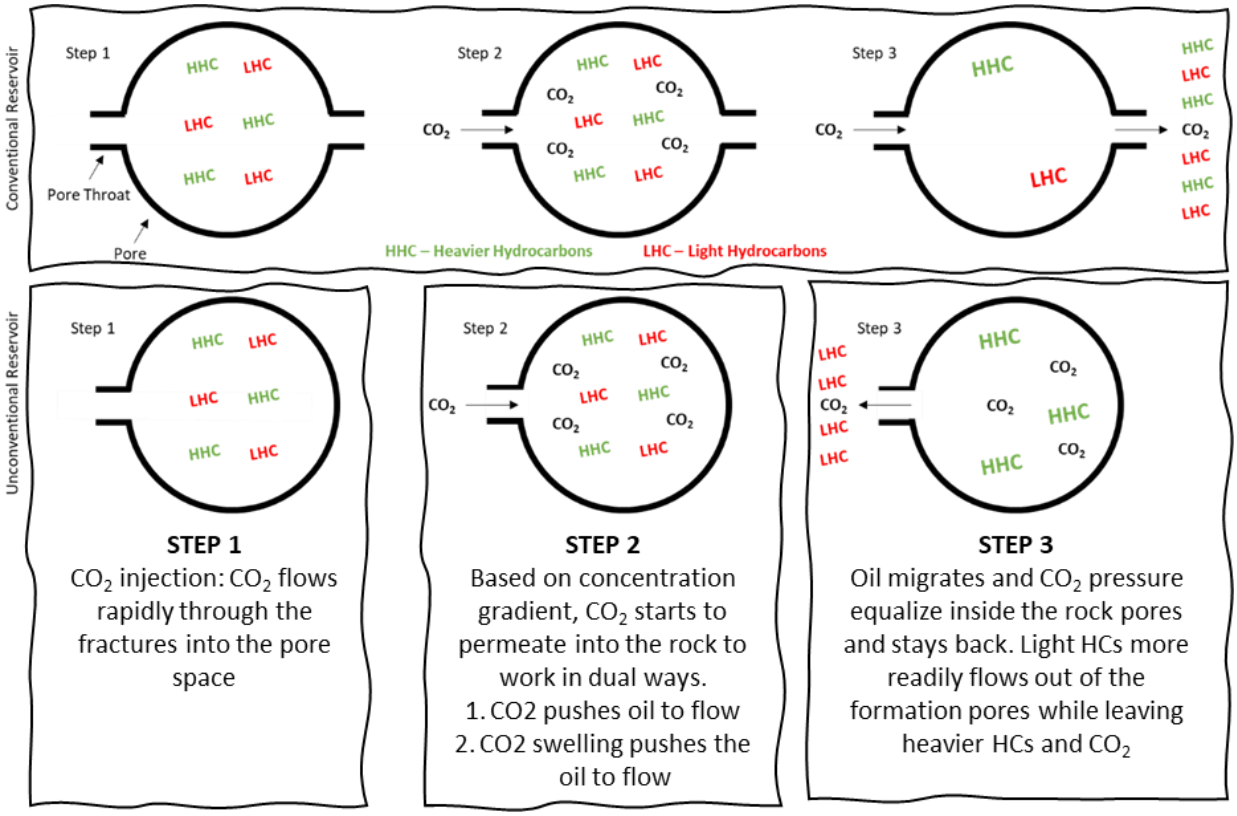

Figure 2.14 Stages of CO_2 huff-n-puff in fractured oil reservoir on a micro/ pore level in comparison to continuous gas injection in conventional oil reservoirs (Syed, et al., 2022b)

It is foremost important to study the dynamic fluid flow properties under nano-confinement. However, it is not easy, time-consuming, and expensive to capture physics through experimental studies at a nano-pore scale therefore dynamic molecular simulation has become a powerful tool to analyze the molecular structure and their dynamic behavior. There are two commonly used simulation methods in molecular modeling including Monte Carlo (Alder and Wainwright, 1959) and molecular dynamics (Alder and Wainwright, 1957; EIA 2021a). There are several studies recently conducted on different EOR/fluid-fluid and fluid-nano-pore interaction mechanisms. Most importantly, each EOR mechanism behaves differently to target different fluid-fluid and fluid-nanopore interaction properties. Table 2.11 presents a summary of a few UEOR physics-based dynamic molecular simulation studies for different injection solvents.

Table 2.11 UEOR physics-dynamic molecular simulation studies

EOR Mechanism	Fluid-Fluid & Fluid-Nano-Pore Interaction Mechanisms	References
CO_2 injection	Oil Swelling	Li, C., et al., 2019a; Liu, et al. 2016; Muther, et al., 2021a
	Viscosity reduction	Muther, et al., 2021a; Zhao, et al., 2015
	Oil/water interfacial tension (IFT)	de Lara, et al., 2012; Makimura, et al., 2013; Zhang, et al., 2013a
N_2, CH_4 & C_2H_6 injection	Oil/water interfacial tension (IFT)	Li, et al., 2020; Muther, et al., 2021a; Syed, et al., 2012; 2021a Syed, 2012
	Minimum miscibility pressure (MMP)	Chun, et al., 2015; Peng, et al., 2018
Surfactant–chemical EOR	Self-assembly structure	Cai, et al., 2018; Jalili and Akhavan, 2009; Ruiz-Morales & Romero-Martínez, 2018; Tang, et al., 2014
	Surface adsorption	Memon, et al., 2020; 2021; Muther, et al., 2021a; 2022a; 2022c; Qu, et al., 2016
	Temperature sensitivity	Chen and Xu, 2013; Sammalkorpi, et al., 2007
	Salt resistance	Li, C., et al., 2019b; Sammalkorpi, et al., 2007; Yan, et al., 2010
	Effect of surfactant or surfactant/nanoparticles on oil/water IFT	Metropolis and Ulam, 1949; Vu and Papavassiliou, 2019

CO_2 or any other solvent injection process into the reservoir matrix through fractures, at first helps to maintain the reservoir pressure, and secondly, the miscibility between the oil and the gas is expected to be achieved after multiple contacts. Molecular diffusion mainly determines the rate and the maturity of the miscibility between oil and the injected gas. Figure 2.15 presents a three-step miscibility development from the lower to higher pressure in a visual PVT cell for an oil sample taken from one of the U.S. unconventional reservoirs. In the first step i.e., the swelling pressure range, the CO_2 dissolves into the oil phase that causing the oil volume to increase (oil swelling). While it can be observed in the transition from the 2nd to 3rd step, with further increase in pressure, the oil volume decreased and

the gas color on the top changed that indicating that oil got extracted into the gas phase where the pressure point exists before the pressure reaches MMP. The discussed example leads to the conclusion that unidirectional diffusion can be considered for the low-pressure gas injection and production process but mostly, the reservoir pressure is well above the MMP, especially for the TORs. Therefore, careful binary interaction and multicomponent diffusion coefficient selection is the key to performing realistic physics-based numerical simulation, and the upscaling process from lab to field scale will be more meaningful with the correct diffusion parameters selection.

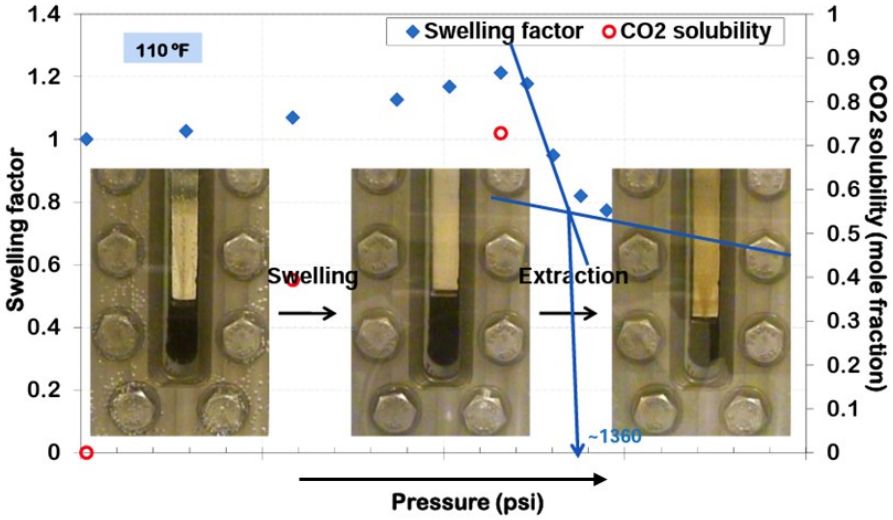

Figure 2.15 Interactions (swelling and solubility) between CO_2 and crude oil under different pressure conditions (Tsau, 2011).

It is a well-understood fact that gravity drainage, physical diffusion, viscous flow, and capillary forces are the driving forces for fluid flow in porous media. However, one force is usually found more dominating over others depending on the reservoir rock and fluid properties as well as on the operating conditions. In unconventional reservoirs with ultra-low matrix permeability, gravity drainage is considered inefficient; molecular diffusion plays an important role in fluid flow. Molecular diffusion is defined as the molecular movement caused by Brownian motion or fluid composition gradient in a mixture of fluids (Yu, et al. 2014). As discussed previously, most of the TORs are developed through EOR application, either continuous injection or the huff-n-puff technique, which is mainly led by the molecular–diffusion mechanisms. The correct identification of molecular diffusion is necessarily important in the numerical simulation process that defines the miscibility process between the injected gas and the formation. In literature, a dimensionless number called Peclet number (Pe) is widely used to measure the relative importance of molecular diffusion flow to the convention flow. The Pe is expressed as shown below;

$$P_e = \frac{\text{Diffusion time}}{\text{Convection time}} = \frac{L^2/D}{L/v} = Lv/D \quad \text{Eq. 2.1}$$

where; v is the bulk velocity, L is a characteristic length, and D is the molecular diffusion coefficient. Mathematically, Pe below unity defines the molecular diffusion-based fluid flow and the dispersion flow is considered when the Pe ranged between unity to 50 and above 50, convection is considered the dominant flow in the porous media (Mohebbinia and Wong, 2017).

2.5.1. Molecular Diffusion

Hawthorne et al. (2013) extensively investigated the CO_2 diffusion-mechanism on a laboratory scale using core samples gathered from the Bakken formation and conceptually concluded that the injected solvent (CO_2) flows into and through the fractures and it floods the rock driven by the pressure differential across the injection and the outlet points. It is also concluded that the oil migrates from nano-pores to bulk fractures via swelling and reduced viscosity on mixing with the injected solvent, and as the pressure gradient reduces, the oil production process gradually shifts from pressure gradient to concentration-gradient diffusion from pores into the fractures (Alfarge, et al., 2017c; Hawthorne, et al., 2013; Sigmund, 1976).

Generally, a couple of empirical correlations driven by Sigmund (Holm and Josendal, 1980; Sigmund, 1976), and Wilke & Chang (1955) are used in commercial simulators, such as CMG GEM, for the diffusion coefficient estimation in the bulk phase. In Sigmund correlation, the binary interaction coefficient (D_{ij}) between two components is given by;

$$D_{ij} = \frac{\rho_k^0 D_{ij}^0}{\rho_k}(0.99589 + 0.096016\rho_{kr} - 0.22035\,\rho_{kr}^2 + 0.032874\,\rho_{kr}^3) \quad \text{Eq. 2.2}$$

where $\rho_k^0 D_{ij}^0$ is the zero-pressure limit of the density-diffusion coefficient product in phase k; ρ_k and ρ_{kr} are the molar density and reduced molar density of the diffusion mixture, respectively. Also, $\rho_k^0 D_{ij}^0$ and ρ_{kr} are mathematically defined as;

$$\rho_k^0 D_{ij}^0 = \frac{0.0018583\,T^{1/2}}{\sigma_{ij}^2 \varepsilon_{ij} R}\left(\frac{1}{M_i} + \frac{1}{M_j}\right)^{1/2} \quad \text{Eq. 2.3}$$

$$\rho_{kr} = \rho_k \frac{\sum_{i=1}^{n_c} y_{ik} v_{ci}^{5/3}}{\sum_{i=1}^{n_c} y_{ik} v_{ci}^{2/3}} \quad \text{Eq. 2.4}$$

where M_i is the molecular weight of component i; σ_{ij} is the collision diameter; ε_{ij} is the collision integral of the Lennard-Jones potential; y_{ik} is the mole fraction of component i in phase k; v_{ci} is the critical volume of component i. Whereas, the components σ_{ij} and ε_{ij} are calculated using the following expressions;

$$\sigma_{ij} = \frac{\sigma_i + \sigma_j}{2} \quad \text{Eq. 2.5}$$

$$\sigma_i = (2.3551 - 0.087\omega_i)\left(\frac{T_{ci}}{P_{ci}}\right)^{1/3} \quad \text{Eq. 2.6}$$

$$\varepsilon_{ij} = \frac{1.06036}{T_{ij}^{0.1561}} + \frac{0.193}{\exp(0.47635T_{ij})} + \frac{1.03587}{\exp(1.52996T_{ij})} + \frac{1.7674}{\exp(3.89411T_{ij})} \quad \text{Eq. 2.7}$$

where ω is the acentric factor; T_{ci} and P_{ci} are the critical temperature and pressure, respectively. Finally, the diffusion coefficient of component i in a multicomponent mixture of phase k is calculated by;

$$D_{ik} = \frac{1-y_{ik}}{\sum_{i\neq j}\left(y_{jk}/D_{ij}\right)} \quad \text{Eq. 2.8}$$

Similarly, Wilke-Chang proposed a diffusion coefficient based on a series of laboratory measurements for various hydrocarbon solvents and other systems in the literature (Christiansen and Haines, 1987). The mathematical expression is given below;

$$D_{ik} = \frac{7.4 \times 10^{-8}(M'_{ik})^{1/2}T}{\mu_k v_{bi}^{0.6}} \quad \text{Eq. 2.9}$$

$$M'_{ik} = \frac{\sum_{j\neq i} y_{jk}M_j}{1 - y_{ik}} \quad \text{Eq. 2.10}$$

where M'_{ik} is the molecular weight of the solvent; μ_k is the viscosity of phase k; and v_{bi} is the partial molar volume of component i at the boiling point.

2.5.2. Minimum Miscibility Pressure

Minimum miscibility pressure (MMP) is the lowest pressure at which the interfacial tension (IFT) between the two fluids (oil and injected solvent) vanishes completely after multiple contacts and both fluids become miscible. MMP is usually measured in the lab through multiple techniques including the sand-packed slim tube method (Rao, 1997), the rising bubble method (Stalkup, 1987), and the vanishing IFT method (Zick, 1986). The presence of porous media is not a compulsory factor for the measurement of MMP and that is fine for the conventional reservoirs where the large pores phase behavior is not affected by confinement. However, measuring MMP with real confinement for the unconventional tight formation is a significant challenge and practically it is not yet well defined. Therefore, MMP

measurement with good accuracy can be determined numerically through fluid-flow and thermodynamic phase-equilibrium principles.

Numerically, there are multiple approaches to calculating MMP including 1D compositional gas-oil fluid-flow slim tube simulation (Wang and Orr Jr, 1997), no-flow predetermined mixing technique using single or multiple connecting cells (Teklu, et al., 2014), and the method of characteristics (Muther, et al., 2022c). Teklu, et al., (2014) investigated MMP for Bakken oil samples with CO_2 as the effects of capillary pressure, the change in critical-property on phase behavior, and the IFT in the thermodynamics in nano-pores. Table 2.12 presents the unconventional Bakken reservoir oil composition, gas composition, and other reservoir and fluid properties that were invested in the study. Figure 2.16 presents the MMP results of 100% CO_2 gas injection in the Bakken oil sample for the pore radii of 4 and 20 nm with the reference of no confinement case.

Compared with the unconfined case, the MMP for the Bakken oil was reduced approximately by 130 psi for the 4 nm case in comparison to the unconfined case. As far as the 20 nm case is concerned, a similar MMP is noticed in the unconfined case (Muther, et al., 2022a). Another study suggests that Ethane is a strong EOR solvent (MMP – 1343 psi) as compared to CO_2 (2523 psi) at 100 ^oC for the Bakken oil. Whereas methane and nitrogen are having considerably high MMPs of 4510 and 14706 psi, respectively (O'Bryan and Bourgoyne, 1990).

Table 2.12 Bakken oil composition and EOS parameters – T_{res} = 241 ^oF (Teklu, et al., 2014)

Components	**Oil**	**T_c, ^oF**	**P_c, psi**	**ω**	**Binary Interaction Coefficients**		
					CO_2	C_1	C_2
CO_2	–	87.60	1071	0.225	–	–	–
C_1	0.367	-124.66	655.02	0.010	0.100	–	–
C_2	0.148	89.97	721.99	0.102	0.130	0.0050	–
C_3	0.093	205.97	615.76	0.152	0.135	0.0035	0.0031
C_4	0.057	299.208	546.46	0.189	0.130	0.0035	0.0031
C_{5-6}	0.064	415.479	461.29	0.268	0.125	0.0037	0.0031
C_{7-12}	0.158	593.25	363.34	0.429	0.120	0.0033	0.0026
C_{13-21}	0.073	872.10	249.61	0.720	0.120	0.0033	0.0026
C_{22-80}	0.037	1384.5	190.12	1.015	0.120	0.0033	0.0026

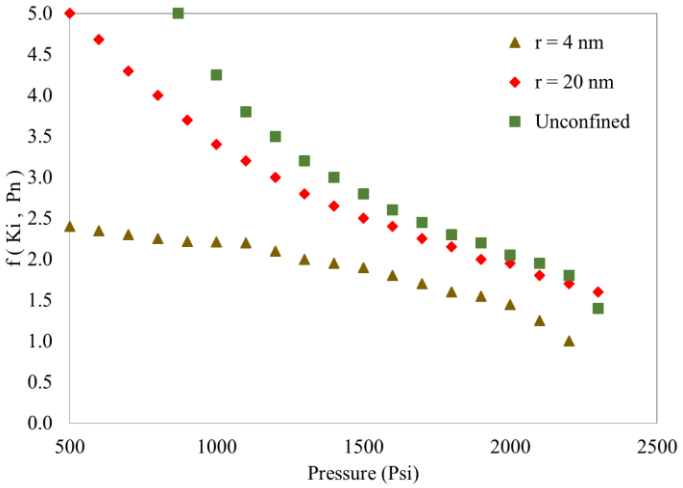

Figure 2.16 The $f(K_i, p^n)$ vs. pressure for Bakken oil & 100% CO_2 inj. at different pore radii (modified from Teklu, et al., 2014)

$$f(K_i, P^n) = \min\left[\sqrt{\sum_{i=1}^{N_c}(1 - K_i)^2}\right] \quad \text{Eq. 2.11}$$

where K is the equilibrium constant; P represents pressure, and N_c is the number of components in the above expression.

2.5.3. Solubility

Solubility is defined as the ability of a solvent to dissolve in oil that directly influences oil recovery. Higher solubility factor causes oil swelling and oil viscosity reduction, and both help the oil to migrate from nano-pores to wellbores via fractures. The pressure-composition experiments are evident that CO_2 is the most likely soluble solvent in oil (Williams, et al., 2004). However, methane and CO_2 both show high solubility, but CO_2 achieves a certain number solubility level at a much lesser pressure than methane needs to achieve (Li and Luo, 2017). This effect can also be defined through the gas-oil ratio (GOR) for the oil saturated with CO_2 as a function of pressure. Figure 2.17 is a good example of measured GOR of live oil with different high-pressure solvents (Habibi, et al., 2017b). It is noticeable that natural gas and enriched natural gas showed reasonable solubility and adding CO_2 into the system improved the solubility significantly at lower saturation pressure.

2.5.4. Oil Swelling

Oil swelling due to dissolved high-pressure injection solvents is another important factor to highlight that generates a localized pressure gradient, which causes oil to migrate from pores to fractures. Therefore, solvents that cause more swelling of the reservoir oil are good candidates for the EOR. An excellent visual example of crude oil

swelling due to the dissolution of high-pressure CO_2 and Nitrogen injection is presented in Figure 2.18 (Habibi, et al., 2017a, Pereira, et al., 2016). The oil volume increased significantly with CO_2 in comparison to nitrogen at the same elevated pressure observed after the same period.

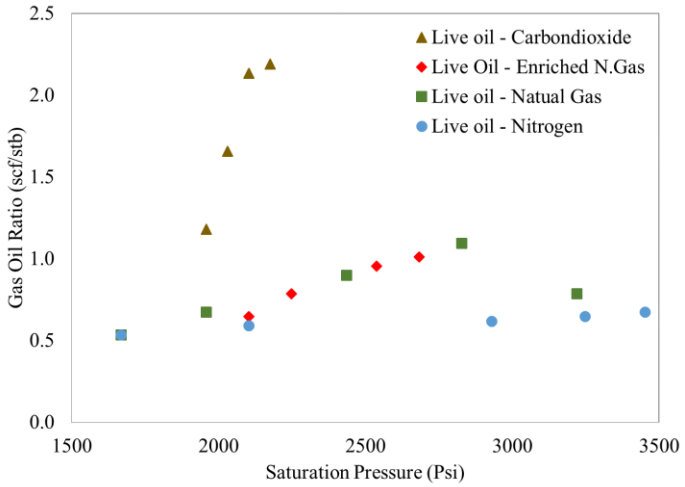

Figure 2.17 Measured gas/oil ratios of live oil with different high-pressure gases (modified from Habibi, et al., 2017b)

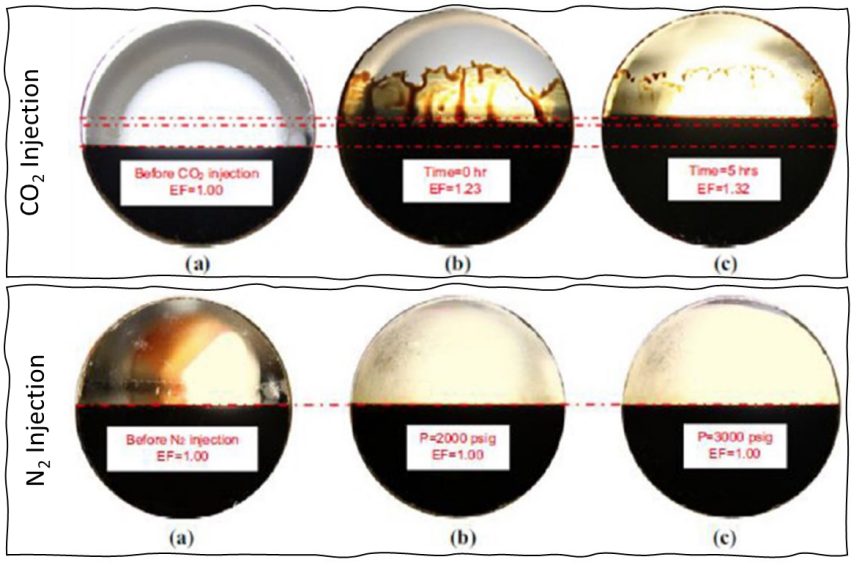

Figure 2.28 Oil interface with CO_2 and N_2 injection at elevated pressure. (**a**) Only crude oil, (b) oil with injection solvents at elevated pressure, (**c**) oil with injection solvents at elevated pressure after 5 hr (Habibi, et al., 2017a)

2.5.5. Oil Viscosity

Another important interaction parameter is the reduced oil viscosity as the result of high-pressure solvent dissolution into the crude oil. The reduced oil viscosity aids the oil in its displacement from the pores to fractures. This effect of viscosity reduction is more prevalent with CO_2 as compared to any other solvents. Figure 2.19 is an

excellent example of the effect of dissolved CO_2 and other solvents on the viscosity of a live oil sample taken from the Bakken formation (Zhao, et al., 2015). It is clear from the figure that, as the saturation pressure increases, the viscosity of the crude oil and CO_2 mixture rapidly declines in comparison to other solvents.

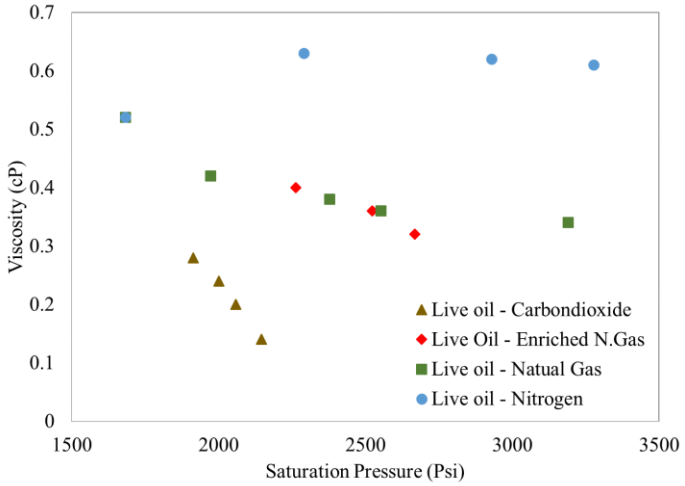

Figure 2.19 Measured viscosities of live oil with different elevated pressure solvents (modified from Habibi, et al., 2017b).

2.5.6. Interfacial Tension (IFT)

Interfacial tension (IFT) reduction due to the dissolution of elevated pressure solvents into crude oil is a critical parameter that helps to improve oil recovery. The IFT reduction with increasing pressure is the most dramatic in the gas phase. Focusing on CO_2 injection, as the pressure increases, CO_2 invades into a less compressible liquid phase causing a decrease in IFT with an increase in pressure. However, the IFT plays a major role in conventional reservoirs but not in the TORs where the CO_2 is pushed into the pores primarily by diffusion processes (EIA 2022).

2.5.7. Adsorption & Desorption – Solvent Trapping Mechanism

The adsorption and desorption of the injected solvents on the nanopores surfaces are important especially while dealing with the tight formation for the solvent injection process efficiency. The overall system's efficiency mainly depends on the total organic content (TOC). The adsorption of CO_2 can significantly reduce the gas saturation in the rock pores. It is considered the second-order mechanism or the by-product of CO_2 miscibility into the formation liquid and the effect of adsorption would be more substantial in the formations with higher TOC. Table 2.13 shows a comparative study conducted on major U.S. tight formations for the maximum absolute adsorption capacity.

Table 2.13 Maximum absolute adsorption capacities for different U.S. tight reservoirs (Heller, R. and Zoback, M., 2014)

Major U.S Tight Formations	Total Organic Content (%)	Maximum Absolute Adsorption Capacity at 2000 Psi and 104 oF (Scf/ton)
Barnett and Montney	5.3	151
Marcellus	1.2	64
Eagle Ford	1.8	33

The phenomenon of CO_2 adsorption into the nano-pores and on the pore surfaces aids CO_2 molecular diffusivity into the tight reservoirs and the effect is more prominent with the higher TOC and the combination of these phenomena theoretically justifies the essential CO_2 trapping mechanism. The trapped CO_2 can be a large fraction of the total injected solvent volume into liquid-rich shale plays that mainly depends on the TOC content and the CO_2 diffusion coefficient. In this study, the Langmuir multicomponent isotherm model is utilized that was initially established for the coal formations (Arri, L.E., et al., 1992, Hall, F.E., et al., 1994), the mathematical expression is given below:

$$\gamma_i = \gamma_{max,i} \frac{y_i \delta_i p}{1 + p \sum_{k=1}^{N_c} y_k \delta_k} \qquad \text{Eq. 2.12}$$

where $\gamma_i$and γ_{max} are the moles of adsorbed component and the Langmuir maximum morels of adsorbed component *i* per unit mass of rock (gmol/lb.), respectively. δ_i represents the Langmuir constant (Psi^{-1}), p and y_i denotes the gas phase pressure and the mole fraction of the adsorbed component *i* in the gas phase, respectively. Whereas Nc characterizes the total number of components that contribute to adsorption.

It is important to note that the adsorption and desorption interlink with the pressure paths. Therefore, in the huff-n-puff process, in which a single well contributes to injection and production, both phenomena actively participate i.e., adsorption of solvent occurs during injection and desorption during production. It is also worth noticing that the adsorption and desorption paths for CO_2 are not similar and they showed a hysteresis effect under moderate pressure conditions (Culp, J.T., et al., 2008). Figure 2.20 is showing a schematic of injected solvent desorption as the function of the initial pressure point that appears to be pressure path dependent. During gas injection, the formation pressure increases that causing adsorption followed by pressure depletion due to production from different pressure points showing dissimilar desorption paths. This phenomenon is similar to the capillary pressure and relative permeability hysteresis effect that works based on the wetting phase saturation as the common scale for multiple phases, whereas the adsorption and the desorption are the single-phase phenomenon.

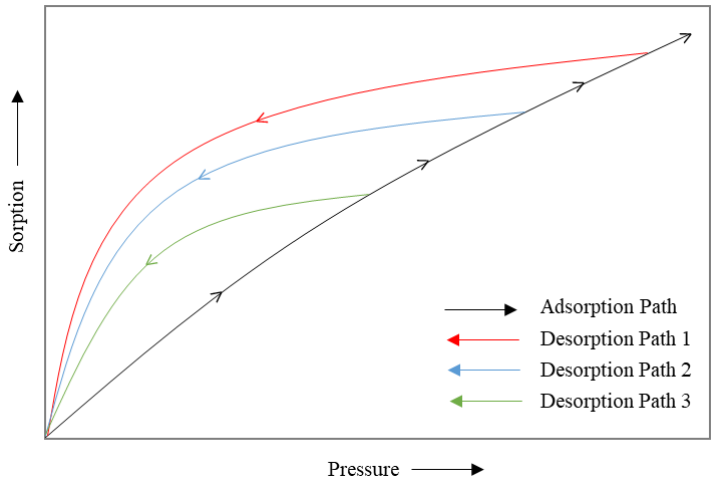

Figure 2.20 Schematic of Injected solvent (CO_2) adsorption and desorption paths during the huff-n-puff process at different pressures. The phenomenon is explained by Jesson et al. (2008) for a fixed temperature and TOC.

2.6. Smart Physics Inspired Compositional Dimensionless Type Curves – SPiC TC_D

Generally, reservoir rock & fluid characterization and hydrocarbon production forecasting is performed based on historical production performance and there are not many techniques being used classically. For example, pressure transient analysis is a 'high frequency/ high resolution' data analysis technique that depends on historical production performance data and for which, he data quality is the key. The most adopted technique for production forecasting was introduced almost a century back based on the empirical analysis of the historical production performance, the technique is called 'Decline Curve' analysis (DCA). It is important to note that the objective of introducing DCA was economic analysis, not technical (Cutler, W.W., 1924). Later with time, multiple techniques were introduced that were presented in different representations such as Cartesian, log-log, and semi-log scale plots. In 1944, Arps introduced exponential and hyperbolic families of decline curves (Arps, J.J., 1944) that were transformed into log-log type curves by Fetkovich (Fetkovich, M.J., 1973), however, this technique provides an empirical solution but seems to work as a general tool, is that more of a coincidence or theory…found no answer in the literature.

Moving further down the road, a promising analytical solution was introduced by van Everdingen and Hust in 1949, which was re-plotted by Fetkovich (Fetkovich, M.J., 1973). Fetkovich further extended the work and introduced composite decline-type curves that were generated on multiple assumptions including; a single well based on constant bottom hole flowing pressure and the radial flow in a finite radial reservoir system. The analysis based on this technique is theoretically simple and practical to be performed using dimensionless type curves that can use the field

data, but it has a drawback i.e., limited by the solution model as well as the data quality (Whitson, C.H. and Sognesand, S., 1990).

In this dissertation, initially, the numerical physics-based huge dataset is developed using multiple realizations with the combinations of different reservoir rock and fluid properties, including multiple reservoir fluid compositions representing different fluid types, as well as the hydraulic fracture design parameters. Secondly, the dimensionless type curves are generated for the entire dataset to be matched with the reservoir flow performance data in log-log format. The well flow performance library and the dimensionless numerical type curves are then used to train and develop an AI-assisted neural network model for the generation of numerous proxy models and smart dimensionless semi-empirical compositional type curves.

For hydraulically fractured horizontal wells, the dimensionless types are usually plotted on a log-log plot, having a dimensionless flow rate 'q_D' on the y-axis against the dimensionless time 't_{Dxf}' on the x-axis. The equations of both parameters are reported in the literature by multiple authors (Gringarten, A.C., et al., 1974; 1975; Chukwu, I.F., 1989; Cox, D.O., et al., 1996; Chen, C.C. and Raghvan, R., 1997) as given below;

$$Dimensionless\ flow\ rate = \ q_D = \frac{141.2\ q\ B\ \mu}{k\ h\ (P_i - P_{wf})} \quad \text{Eq. 2.13}$$

$$Dimensionless\ time = \ t_{Dxf} = \frac{0.0063\ k\ t}{\emptyset\ \mu\ c_t x_f^2} \quad \text{Eq. 2.14}$$

where; q is the liquid flow rate, and B and μ are the liquid formation volume factor and viscosity, respectively. k, Ø, and h are the permeability and the matrix porosity, and the formation thickness, respectively. Similarly, Pi and Pwf are the initial reservoir pressure and the bottom hole flowing pressures, respectively. c_t is the total compressibility, X_f represents the hydraulic fracture half-length, and t is time.

2.7. Artificial Neural Network – Proxy Reservoir Performance Modeling

The concept of the neural network was introduced long back in the mid-20th century (McCulloch, W.S. and Pitts, W., 1943) and was studied by several scientists and researchers based on their needs on the applicability in different industries. The artificial neural network (ANN) is introduced as an information-processing technique that has worked with a particular set of performance characteristics like the biological neural networks found in human brains (Mohaghegh, S., 2000). In other words, as in a biological system, all organisms are composed of cells and neurons that form a complex nervous system that mainly comprises a cell body, an axon, and dendrites as shown in Figure 2.21. Multiple types of ANNs have been implemented by several users based on the nature of the data. Deep Neural Networks (DNN), Convolutional Neural Networks (CNN), Graphical Neural Networks (GNN), and Physics Inspired Neural Networks (PINN) are a few commonly applied and reported ANNs in the literature (Zou, J., et al., 2008).

The working phenomenon of ANN is inspired by the biological neuron system, as shown in Figure 2.21, that works directionally by passing a piece of information into a cell body that enters through the input terminals called dendrites that generate an output response which travels through myelin sheat towards the axon terminal that works as an output terminal as well as an input receiving end for another neuron. In the case of the connected neuron, the generated response from the first neuron acts as input information for the second neuron and this process similarly goes on. Typically, a human brain contains around 10 to 500 billion neurons (McClelland, J.L. and Rumelhart, D.E., 1989) that are characteristically divided into different sections and each section consists of about a further 500 neurons (Stubbs, D.F., 1988). Biologists estimated that each neuron network consists of more than 100,000 neurons that connect (Mohaghegh, S., 2000). The actual neuron system is very complex that cannot be mimicked 100% therefore, for the mathematical calculations; ANNs are developed based on a few assumptions including; the information that passes through elements called neurons, and each connection that links up the neurons have its weightage.

In this work, DNNs are utilized to generate reservoir performance and proxy models. DNN consists of several hidden layers and each layer consists of several neurons. These networks are capable of processing complex data and algorithms. A typical DNN works on the phenomenon explained in the schematics shown in Figure 2.22.

The provided input information multiplies by the connection links weightage and the resultant product, enters a neuron where all the inputs are summed up and the defined activation function of the neuron is applied that leads to an output. Thus, a neuron typically has multiple inputs and only a single output. The typical DNN consists of a single

input layer and one or multiple hidden layers that result in a single output layer. The input and output layers determine the input and the outputs of the given problem while the hidden layers are responsible for the extraction features from the provided dataset. The training of any type of ANNs requires huge datasets, however, a huge amount of data requires exceptional computing power. Data preprocessing is an essential step that mainly controls the quality of the dataset as well as the training quality of the ANN model. It is a fact that any neural network is only as good as the quality of the input data that is used to train the model (Parmar, 2018).

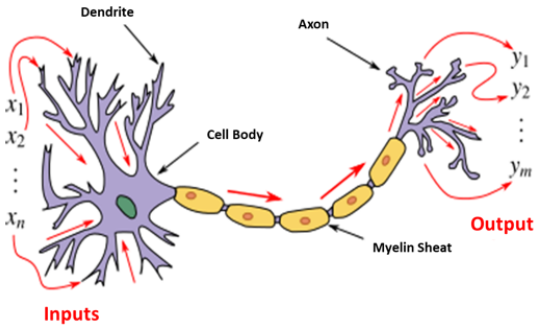

Figure 2.21 Typical biological neuron system - Two Bipolar Neurons (Conte, E., et al., 2006)

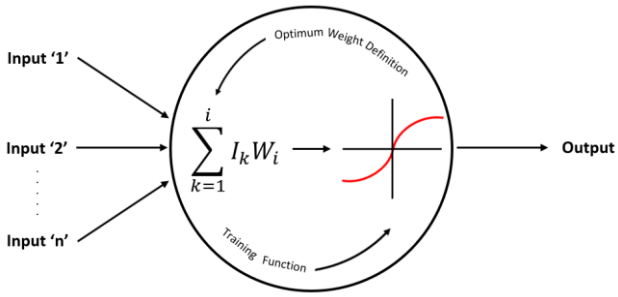

Figure 2.22 Schematic of Artificial Neuron Network (ANN) working phenomenon (Syed, et al., 2022a)

2.7.1. Working Phenomenon of Deep Neural Network (DNN) Application

Like any other engineering application, usually, the supervised DNNs are applied for reservoir engineering as well as the EOR problems. The basic steps include representative input data collection and their characterization to be used for the training, testing, and verification process. Data normalization is an important step to perform for the balanced weightage distribution that is being done while providing the input data. Lastly, the optimized number of hidden layers and the training function is defined. Once the model is set, data testing and training are performed, followed by data de-normalization for the confidence-building before using the prediction model for any future operation (Abdullah, M., et al., 2019, Khamidy, N.I., et al., 2019, Moosavi, S.R., et al., 2019, Sun, Q. and Ertekin, T., 2020).

The input data for each DNN model is considered different depending on the application. The selected data could be a collection of experimental testing, numerical simulation, or actual field operational data, etc. Practically, most of the reservoir engineering operations are supervised, therefore; both input and outputs are required to be provided while defining the sample data in the first step. Typically, the provided data set is divided into three sections including training, testing, and verification. The training data I used to develop the DNN model while the provided output data set helps to determine the weights of each input. The weight calibration is performed through the

feedforward backpropagation algorithm that is being done through error backpropagation in the network. While the testing dataset is used to measure the network generalization and it is a continuous process that keeps running until the generalization stops improving. Finally, the remaining dataset i.e., the verification dataset is utilized for the evaluation of the overall network performance. Keeping in mind that the verification dataset is not used in any step of network building or testing (Demuth, H., et al., 2007).

One of the most important factors to highlight in this section is the data normalization that is necessarily done on the dataset especially when the magnitude of input or the output data are too different, therefore, scaling of the data is required to be performed (Saeedi, A., et l., 2007, Zabihi, R., et al., 2011). One of the most common methods of data normalization is to scale all the data between 1 and -1 using Equation 1 (Demuth, H., et al., 2007).

$$X_i' = 2\left(\frac{X_i - X_{min}}{X_{max} - X_{min}}\right) - 1 \qquad \text{Eq. 2.15}$$

where X_i is the original value of the given parameter, X_i' is the normalized value of X_i while X_{min} and X_{max} are the minimum and the maximum values of X_i, respectively.

Another important step is the calculation of the optimum number of hidden layers and the cumulative neurons in each hidden layer. The first part is achieved through an iteration process while the second part is usually done either through total average absolute deviation or through the mean square of the error process. That means, starting with a single neuron and keeping that number increasing until reached the lowest stabilized error. Finally, the training function is chosen to minimize the error. A few examples of commonly used training functions include variable learning rate backpropagation, resilient backpropagation, scaled conjugate gradient, etc. (Demuth, H., et al., 2007). In general, Equation 2 (Huang, Y.F., et al., 2003) explains the entire DNN working process i.e., the calculation of an output based on a neural '*j'* defined in layer '*k'*.

$$u_{jk} = F_k\left(\sum_{i=1}^{N_{k-1}} w_{ijk}\, u_{i(k-1)} + b_{jk}\right) \qquad \text{Eq. 2.16}$$

where 'w_{ijk}' and 'b_{jk}' are the defined connection weight and anti-weight of the network that works as the fitting parameters of the respective model.

The generalized objective is to obtain a relationship from the given multidirectional input parameters to an output. The goal is to obtain the difference between the predicted and the actual sample values in the output vector with the least possible error. Here comes the role of fitting parameters that keep on modifying automatically over each iteration until an error criterion between the input and the output is satisfied based on the geometric characteristics of

a DNN and its defined learning strategy. Whereas the linked weights are defined as the learning process based on the DNN input/output training and the testing process.

2.7.2. Application of DNN in Reservoir Engineering

In recent years, the DNNs have been used to solve several complicated problems in the oil industry, not only in the reservoir but also in exploration, and drilling engineering domains. Several success stories of DNN applications have been published in the literature. In reservoir engineering, lots of work has been done in recent years, especially for reservoir characterization (Zabihi, R., et al., 2011), reservoir fluid and rock properties (Yang, H.S. and Kim, N.S., 1996, Alcocer, Y. and Rodrigues, P., 2001), reservoir monitoring (Denney, D., 2001), well testing (Denney, D., 2003), formation damage determination (Saeedi, A., et l., 2007), and hydrocarbon resources estimation (Armstrong, R.T., et al., 2015). Also, a few studies are conducted on EOR applications including SCAL, relative permeability interpolation, low salinity chemical flooding (Dang, C., et al., 2018), steam-assisted gravity drainage (Najeh, A., et al., 2010), and CO2 injection for naturally fractured reservoirs (Hamam, H. and Ertekin, T., 2018, Syed, F.I., et al., 2021d, Sprunger, C., et al., 2021).

2.8. Discussion

Tight reservoirs are well-known hydrocarbon-bearing formations that have recently been under focus for unconventional oil and gas exploration in several countries. Specifically, tight oil is a liquid hydrocarbon resource found in ultra-low porosity and permeability rocks such as shale, siltstone, sandstone, and carbonate, which are mostly considered the source rock. TORs are usually found in the depressions and slopes of basins, close to extensive, mature, and organic-rich source rocks. These are considerably large-scale reservoirs with nanoscale pore networks and the local sweet spots with easier oil production regions. The sweet spots in tight reservoirs are mainly recognized with the key features including the source type, lithology, reservoir quality, rock brittleness i.e., related to Young's modulus and Poisson's ratio, oil-bearing property, and the stress anisotropy. The United States is having the world’s second-largest technically recoverable shale oil resources. Among seven different regions of the U.S., the Southwest region is having most of the tight oil resources. The main reservoirs in this region include the Permian and Fort Worth Basins. Eagle Ford, Bakken, Wolf-Camp, and Niobrara are also major and well-known shale oil plays that are situated in South Texas, Montana and North Dakota, Midland Basin, and Denver, Colorado.

The tricky part while developing TORs is sustainable hydrocarbon production that barely lasts from a few months to a couple of years without any external support because of their complex geology. Oil wells in almost all major tight oil plays including Eagle Ford, Bakken, Niobrara, etc. face the same problem of rapid production decline within the first year of their production life. On average, the daily production rate declines to half within a year, therefore EOR application along with the massive stimulation (hydraulic fracturing) on individual well bores is nowadays considered a compulsory factor for its development. In addition, because of limited inter-pore connectivity, TORs are mostly developed through an independent huff-n-puff process. In most of the numerical simulation and laboratory cases, it is observed in the literature that even though the ultimate oil recovery does not improve but the recovery significantly accelerates. It is important to note that even a single percent increase in EUR could result in extra million barrels of oil; therefore, even a single percent increase is significant while developing TORs.

For the huff-n-puff process, there are various factors to keep under consideration including the well and the hydraulic fracture design, selection of the injection solvent type, slug size, the soaking time, etc. Hydraulic fracture design parameters mainly include fracture half-length, height, and the number of stages as well as the number of clusters per stage. The fracture stress shadow is another important factor to keep in mind, especially while designing a hydraulic fracture numerically because it is unlikely to have all fractures operational in the actual field. Hydraulic fracture design optimization depends on the rock quality, its brittleness and rock stresses, etc. Usually, in TORs, the individual wells are designed with multiple stages and clusters depending on the targeted area of interest, the lateral length of the drilled horizontal well, and the neighboring wells. As far as the injection solvent type is concerned, CO_2 and the produced hydrocarbon gas are the most common choices because of the poor injectivity response from most of the tight reservoirs. Due to the ultra-low permeability of the formation rock, only highly volatile fluids i.e., gases can easily be injected, CO_2 is a greenhouse, and the critical gas with lower minimum miscibility pressure is an ideal candidate that mainly depends on its economical availability. Figure 2.23 presents the maximum availability of CO_2 and the multiple sources currently available in different regions of the United States. While the cost of CO_2 from natural sources is tied to the crude oil price while for the industrial sources of CO_2, the overall expenses cover the capturing, compressing, and transportation costs. Table 2.14 summarizes the average overall cost of CO_2 per million cubic feet taken from different industrial sources.

Table 2.14 Overall average cost of CO_2 capture, compression, and transportation from various industrial sources (EIA 2017)

CO_2 Industrial Source	**Average Overall $/Million Cubic Feet of CO_2**
Hydrogen plants	7.8 – 22.2
Ammonia Plants	2.9 – 3.0
Ethanol Plants	2.3 – 5.4
Cement Plants	6.5 – 15.7
Natural Gas Processing	2.1 – 4.0

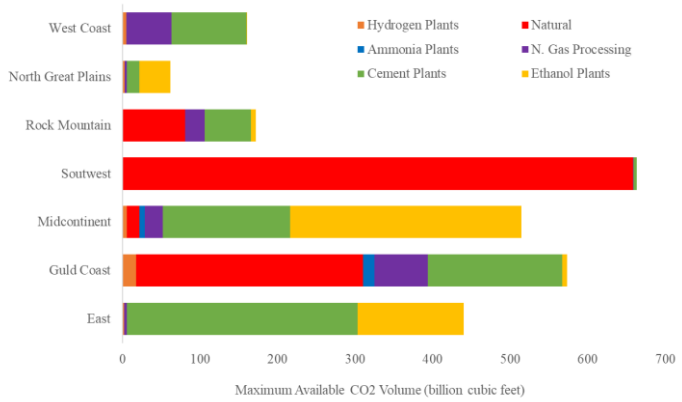

Figure 2.23 Maximum availability and the sources of CO_2 from different regions of the United State as of March 2022

There are several laboratory and field-scale EOR applications reported in the literature that were conducted with different injection solvents including miscible and immiscible gases, chemicals, low-salinity water, carbonated and silk water, etc. Gas injection mainly helps to improve oil recovery through molecular diffusion, capillary pressure, wettability, in-situ fluid density, and viscosity reduction while chemical flooding targets the interfacial tension reduction and the wettability alteration. The low salinity water flooding improves oil recovery through clay swelling, shale mineral cracking, and wettability alteration. Similarly, the carbonated and silk water flooding aids oil recovery through in-situ oil swelling and the reduction in reservoir oil viscosity and interfacial tension.

Most of the laboratory-scale research was conducted on core samples collected from the U.S. reservoirs including Eagle Ford, Mancos, Bakken, and Barnett through CO_2 injection under miscible and immiscible conditions. While the actual field EOR pilots were conducted with CO_2 and produced hydrocarbon gas in Bakken and Eagle Ford formations. The initial EOR pilots conducted in the Bakken formation with CO_2 huff-n-puff showed limited oil recovery improvement while the later pilot in the same formation with water flooding followed by produced hydrocarbon gas injection wasn't found successful due to poor injectivity and early gas breakthrough in the neighboring well. Whereas

the pilots conducted in Eagle Ford with produced hydrocarbon gas injection showed limited recovery improvement with both gas flooding and cyclic gas injection.

2.9. Summary

In closing, the lessons learned from all the experiences discussed from lab to field-scale unconventional EOR studies are summarized below;

- Apart from hydraulically induced artificial hydraulic fracture networks, the EOR application is a must thing to develop an unconventional reservoir for fast-paced economical oil recovery.
- Depending on the original oil in place, a single percent increment in oil recovery through a single or multiple EOR applications on a tight oil reservoir could add up to several extra billion barrels of oil.
- CO_2 and produced hydrocarbon injection are proven successful EOR applications for decades in TORs however, its success in unconventional reservoirs is so far inconclusive due to limited information availability of the actual field pilots.
- However, from the available field pilots, laboratory experiments, and numerical studies, CO_2 and produced HC gas with huff-n-puff operation managed to provide an extra couple of percent of incremental oil recovery.
- Along with EOR applications in TORs, hydraulic fracturing and re-fracking operation in multiple stages could further improve oil recovery.
- Based on individual well operation, the huff-n-puff cycling EOR technique has also provided limited yet promising results in the field to improve oil recovery.
- There is a high risk in UEOR due to a lack of long-term production. In addition, the UEOR mostly does not increase the overall recovery but accelerates the production significantly.

Exploring all the possible options to develop a tight reservoir requires huge computational run time and manpower that leads to an uneconomical situation for any operating company. This work would help operators to save a lot of their time and finances. I understand that this work would have some marginal error in results accuracy depending on the actual reservoir heterogeneity, fluid types, and the hydraulic fracture design, but still, this workflow and the tool introduced in this dissertation would narrow down the screening process for the reservoir development to save millions of dollars and the project timeline.

3

RESERVOIR NUMERICAL MODEL DEVELOPMENT

In this chapter, a numerical mechanistic compositional reservoir simulation model is developed using the typical tight oil reservoir rock and fluid characteristics for the physics-based database development. The model is purposely made simple enough to save computational run time and is computationally detailed enough to capture all possible technical aspects. A thorough physical understanding of multiple factors is developed through sensitivity analysis for different reservoir rock and fluid properties, hydraulic fracture design parameters, and multiple EOR operational designs.

3.1. Introduction

In this chapter, multiple aspects are discussed including typical tight oil reservoir rock, fluid and geophysical data collection, a mechanistic compositional reservoir simulation model generation, and its tuning and validation through its fluid flow response comparison with a few publicly available tight oil wells performance data. The reference tight oil wells data are taken from the Society of Petroleum Engineers (SPE) data repository that is referred to as SPE wells in the dissertation. For the physical understanding, multiple scenarios are studied, and their responses are discussed in detail for different reservoir initial pressure, rock properties, and hydraulic fracture design parameters for multiple reservoir fluid compositions. Finally, a systematic procedure of generating a huge database using a physics-guided design of experiments (PG-DOE) is presented that is mainly used to train an AI-based data-driven model to generate proxy models. Following Figure 3.1 presents an integrated workflow for the based model development, its quality check, and the database development using the physic-guided design of the experiment.

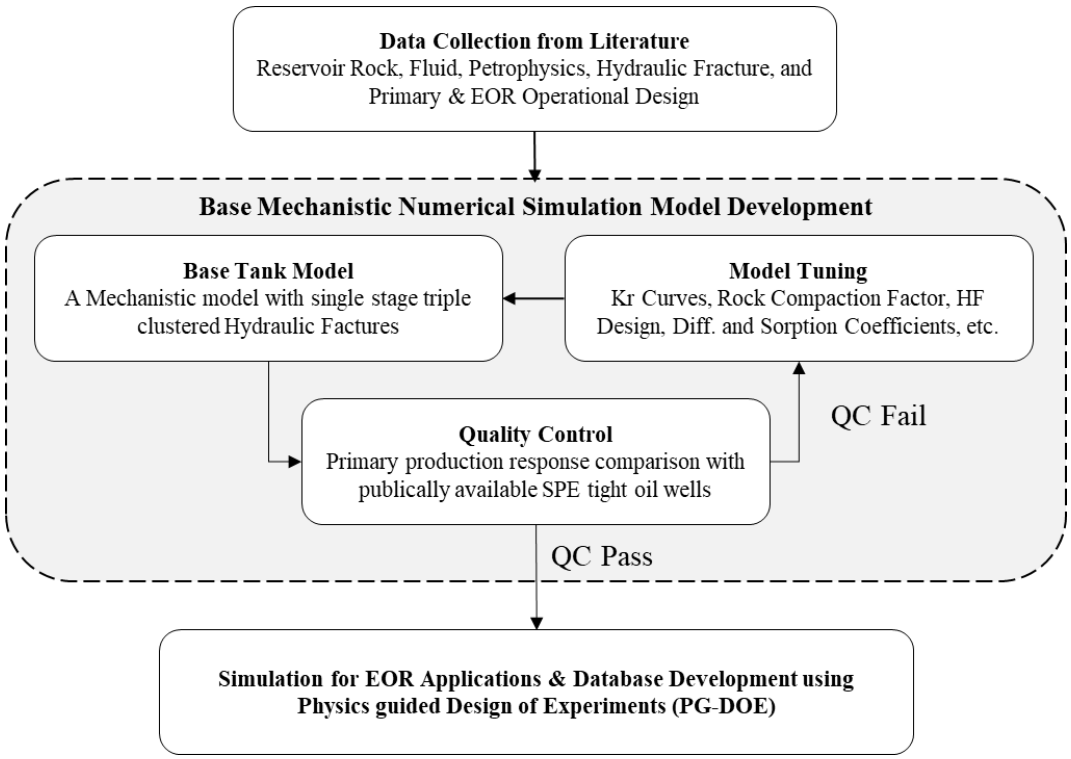

Figure 3.1 An integrated workflow of a base numerical reservoir simulation model and the database development

3.2. Reservoir Simulation Model Development

The significance of the entire study depends on the database used to train a data-driven model that is used as an engine to generate thousands of proxy models representing multiple scenarios based on the combination of different

reservoir rock and fluid properties as well as the hydraulic fracture design parameters. Therefore, no compromise was made on the accuracy of the base simulation model. Due to no availability of history matched or a verified model authenticated by an oil operator to use as a reference model for this work, therefore, typical unconventional tight oil reservoir rock and fluid properties are gathered and a 3D mechanistic reservoir simulation model was built from scratch using a commercial reservoir simulator, CMG–GEM. Following are the flow governing equations used to model the total mass balance in oil and gas phases;

$$\frac{\partial}{\partial t}\left(\emptyset \sum_{x=1}^{N_p} \rho_x S_x w_{ix}\right) + \vec{\nabla}.\left(\sum_{x=1}^{n_p} \rho_x w_{ix} u_x - \emptyset \rho_x S_x \bar{\bar{K}}_{ix} \nabla w_{ix}\right) - r_i = 0 \qquad \forall: \quad i = 1, \dots, N_c \qquad Eq.\,3.1$$

where; $\emptyset$ is the formation porosity, ρ_x & S_x represent density and saturation of phase x , respectively. Whereas r_i are the injection or the production mass rate and the negative sign shows the sink as a fluid flow source. Also, N_c and N_p in the above flow, the equation represents the number of components and the phases, respectively. w_{ix} and $\bar{\bar{K}}_{ix}$ represents the mass fraction and the dispersivity coefficient of the i^{th} the component in x phase per unit volume, respectively. Lastly, u_x represents Darcy's flow velocity, which is expressed as;

$$u_x = -\frac{\bar{\bar{k}}}{\mu_x}(\bar{\nabla} p_x - \rho_x \bar{g}) \qquad Eq.\,3.2$$

where; $\bar{\bar{k}}$ represents the formation of rock permeability in a tensor format, μ_x is the fluid viscosity for the x phase. The dispersivity coefficient $\bar{\bar{K}}_{ix}$is mathematically expressed as;

$$\bar{\bar{K}}_{ix} = \frac{\bar{\bar{D}}_{ix}}{\tau} + \frac{\overline{\alpha_x}\,|\overline{u_x}|}{\emptyset S_x} \qquad Eq.\,3.3$$

where; $\overline{\alpha_x}$ are the dispersivity coefficient of phase x in the longitudinal direction and two transverse directions, τ is the tortuosity, $\bar{\bar{D}}_{ix}$ is the diffusion coefficient of the i^{th} the component in phase x. The Sigmund correlation is used to measure the diffusion coefficients of CO_2 in the oil and gas phases in this study.

Conventional fractured reservoirs can typically be modeled using dual porosity/dual permeability standards, however, tight reservoirs have extremely low permeability and slow pressure transients, making it impossible to adequately simulate fluid flow using these methods. To address this issue, hydraulic fractures are specially treated in tight reservoir numerical models by explicitly modeling the flow behavior. Using CMG-Builder, hydraulic fractures are designed in the model using the planer fracture template that defines hydraulic fractures with logarithmically spaced, locally refined, dual-permeability distribution. A fine-gridded layer(s) of the matrix is essentially defined to

correctly capture the fluid flow and the pressure transient effect around the fractures to avoid sudden shock to the reservoir fluid while flowing from ultra-tight matrix to high permeability fractures, directly. The logarithmic refinement solves the issue of having more refinement closer to the centerline of the fracture where it is needed and less refinement far away from the fracture.

3.2.1. Data Collection – Typical Tight Oil Reservoir Properties

To initiate this study, it was the most critical step to gather as much data as possible with accuracy in the data quality. Most of the data, listed in Table 3.1, are collected from published literature and EIA reports.

Table 3.1 Model Initialization data used for the base case and the typical range found in tight oil reservoirs

Property	Typical Range in TORs	Data Used in Base Model
Initial Res. Pressure (P_i)	5000 – 10000 Psi	7000 Psi
Matrix Porosity ($Ø_m$)	2 – 12%	5 %
Matrix Permeability (K_m)	1E-5–0.1 mD	0.001 mD
Fracture Porosity ($Ø_f$)	-	2 %
Fracture Permeability (K_f)	5-50 mD	30 mD
Permeability of None Fractured Zone (K_{nfz})	-	0.1 mD
Reservoir Formation Top	2000-14000 ft	8200 ft.
Formation Thickness (h)	100-1000 ft	180 ft
Oil Water Contact (OWC)	-	12000 ft.
Free Gas	-	None
Initial Water Saturation (S_{wi})	20-50%	35 %
Rock Compressibility (C_t)	-	1E-5 Psi^{-1}
Total Clusters per Fracture	5-15	3
Fracture Half Length (X_f)	100-300 ft	250 ft
Fracture Width (W_f)	-	0.33 ft
Fracture Height (h_f)	50-200	130 ft
Fracture Conductivity (FC)	5-50 ft. mD	30
Fracture Orientation	-	J Direction
Spacing between two adjacent fractures (S_f)	25-100 ft	50 ft
Perforations per cluster in each fracture	-	5
Reservoir Fluid Compositions	Light to Medium Oil	Fluid Type 4 (Ref. Figure 3.10)
Reservoir Fluid API Gravity	25 – 50°	40
Reservoir Fluid Initial GOR	500 – 1800 scf/stb	575 scf/stb
Matrix Grid Blocks	-	23 × 50 × 18
Model Dimensions	-	230ft × 1000ft × 180ft
Fracture Grid Blocks	-	5 × 3 × 1
Fracture Gridding Style	-	Logarithmic LGR

The typical ranges of reservoir matrix & fluid properties and the hydraulic fracture design parameters are listed in the following table, also model initialization data is included in the same table. The most important realization of this study is the reservoir fluid composition which is the most dynamic property that varies significantly within a

reservoir aerially and vertically, and the fluid properties that vary significantly over time with the alteration in reservoir pressure. As discussed in the prior chapter, the poor connectivity of reservoir pores in tight oil reservoirs, the reservoir pressure support is quite minimal that causing a rapid decline in near-wellbore reservoir pressure. For any strategy-based reservoir development planning it is important to address all the possible static and dynamic reservoir matrix and fluid properties, therefore, multiple reservoir fluid compositions are taken under consideration to generate the entire database. The details on all the considered ranges of individual parameters are discussed in the following section.

3.2.2. Base Reservoir Model Description

For this study, a 3D Cartesian grid small-scaled mechanistic model is built, consisting of 23 grids in X, 50 in Y, and 18 in the Z-direction. In total, the model is consisting of 20,700 grid blocks and the reservoir dimensions of the model are 230ft.×1000ft.×180ft. which represents the width, length, and thickness, respectively. For our objectives, only a single horizontal well is placed in the x-direction with a lateral length of 110ft. Using logarithmic local grid refinement (LGR), a single staged planer fracture with triple clusters is introduced into the model as shown in Figure 3.2. The specifics of the reservoir and hydraulic fracture design parameters used for the model initialization are listed in Table 3.1.

Tight oil reservoirs are usually found with huge variations in their rock and fluid properties aerially and vertically. The typical matrix permeability and porosity ranges reported in the literature are found as 0.00001 to 0.1 mD and 2 to 12 %, respectively. Similarly, a huge variety of fluid types are found in different U.S. tight oil reservoirs including condensate, volatile, and high to medium-quality in-situ oil. For this study total of seven fluid templates are generated representing the entire range of U.S. tight oil reservoirs' fluid types based on their critical properties and the phase envelopes, to generate the database library that was later used to train data-driven proxy models. Figures 3.3 and 3.4 are showing the reservoir fluid composition and its corresponding phase envelope for one of the reservoir fluid types that are used to develop the base model. The same model is used for the model validation by comparing its flow performance with the typical flow performances of the SPE wells. Similarly, Figures 3.5 and 3.6 are presenting the relative permeability curves for the reservoir matrix and the hydraulic fractures. While the critical reservoir fluid properties and the binary interaction coefficients used for the equation of state (EoS) development are listed in Table 3.2 and 3.3, respectively that are used to generate the compositional base reservoir model.

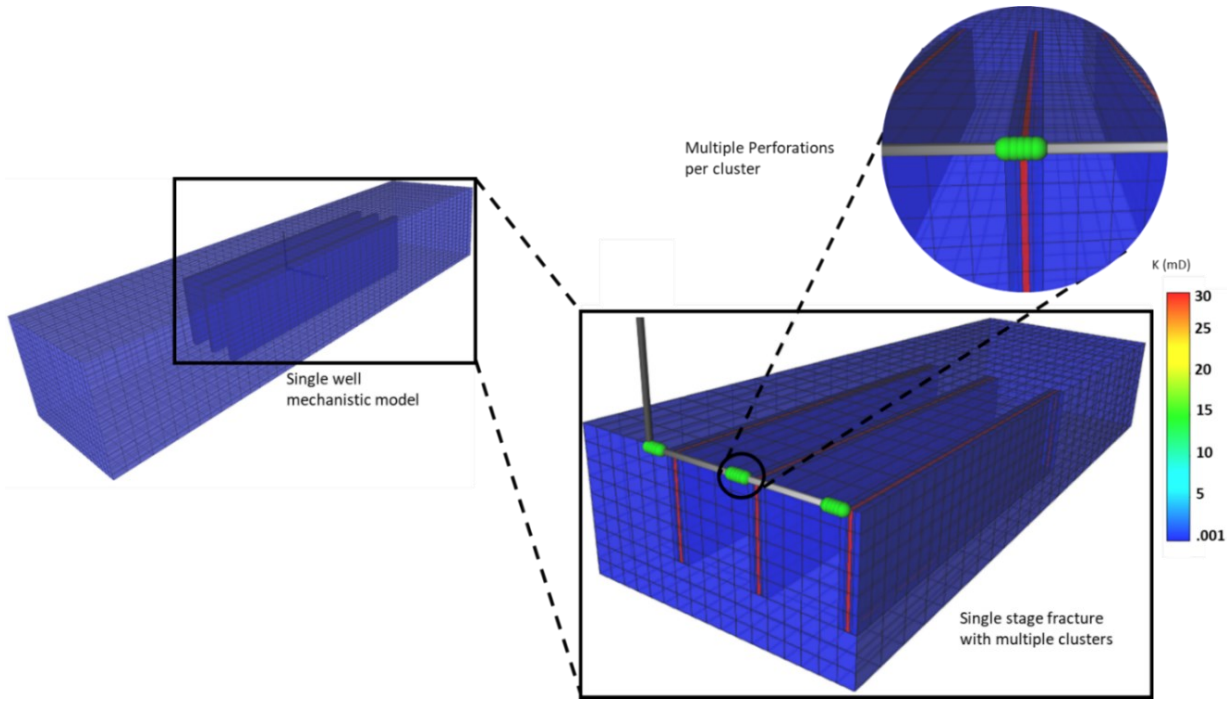

Figure 3.2 Cross-sectional views of the model highlighting the fractures and the perforations connected with individual clusters

Table 3.2 Reservoir fluid pseudo components and the critical properties used to generate a compositional model

Component	Mol. Wt. (g/gmol)	Tc (K)	Pc (Psi)	Acentric Factor
N_2-H_2S	37.37	222.09	815.56	0.148
CO_2	44.01	304.20	1069.86	0.225
C_1	16.04	193.19	667.19	0.008
C_2-C_3	35.31	331.15	673.27	0.118
iC_4-C_6	68.58	455.25	513.09	0.224
C_7-C_{17}	139.81	610.40	292.58	0.615
C_{18}-C_{21}	267.58	798.87	253.20	0.799
C_{22}-C_{27}	326.94	879.47	197.94	0.944
C_{28+}	515.41	935.33	141.24	1.301

Table 3.3 Binary interaction coefficients used to generate a compositional model

Component	N_2-H_2S	CO_2	C_1	C_2-C_3	iC_4-C_6	C_7-C_{17}	C_{18}-C_{21}	C_{22}-C_{27}	C_{28+}
N_2-H_2S	-	-	-	-	-	-	-	-	-
CO_2	0.0000	-	-	-	-	-	-	-	-
C_1	0.0718	0.1300	-	-	-	-	-	-	-
C_2-C_3	0.0915	0.1300	0.0019	-	-	-	-	-	-
iC_4-C_6	0.1098	0.1300	0.0076	0.0020	-	-	-	-	-
C_7-C_{17}	0.1129	0.1300	0.0185	0.0089	0.0025	-	-	-	-
C_{18}-C_{21}	0.1129	0.1300	0.0339	0.0205	0.0099	0.0025	-	-	-
C_{22}-C_{27}	0.1129	0.1300	0.0391	0.0247	0.0130	0.0042	0.0002	-	-
C_{28+}	0.0214	0.1300	0.0547	0.0378	0.0231	0.0107	0.0029	0.0015	-

For the model performance characterization, firstly, the reservoir fluid type is selected based on the typical light hydrocarbon content i.e., C_1-C_3, to represent one of the SPE well that is reported in the SPE data repository to be

taken from the Eagle ford reservoir. The typical initial GOR and the API gravity are the key parameters used to select fluid type for the base model's performance validation. The second most critical parameter for the model initialization is to select the representative relative permeability (K_r) curves. The Kr. curves shown in Figures 3.4 and 3.5 are built for the matrix and the hydraulic fractures separately through repeated trial and error procedures using CMOST, which is an automated tool of CMG. It is important to notice the shapes and the endpoints of the K_r curves to characterize the in-situ fluid flow performance. The matrix K_r curves are representing a mixed to an oil-wet system that is most likely the scenario in tight oil/ shale oil reservoirs. While the endpoints of the matrix Kr curves show highly restricted flow from the reservoir matrix in comparison to the hydraulic fracture's K_r curves that provide highly conductive fluid flow channels between the reservoir matrix and the wellbore.

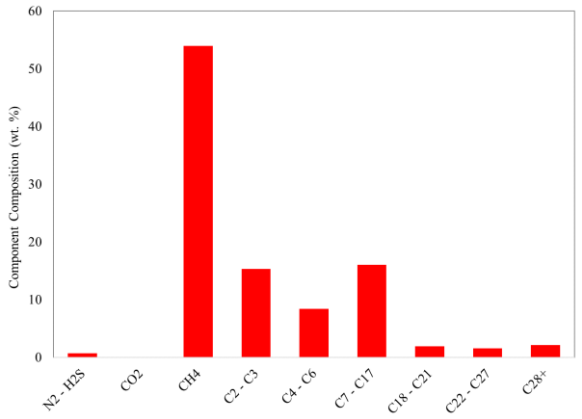

Figure 3.3 Reservoir fluid composition for the based model

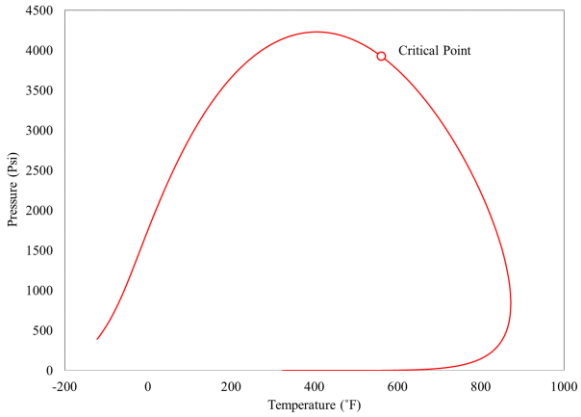

Figure 3.4 Reservoir fluid phase envelop for the base case

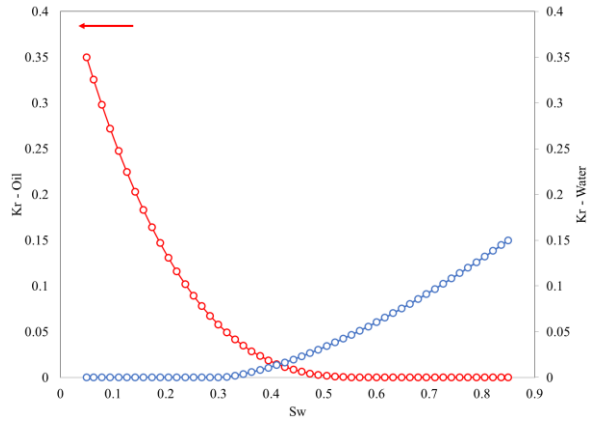

Figure 3.5 Reservoir matrix – Relative permeability cures

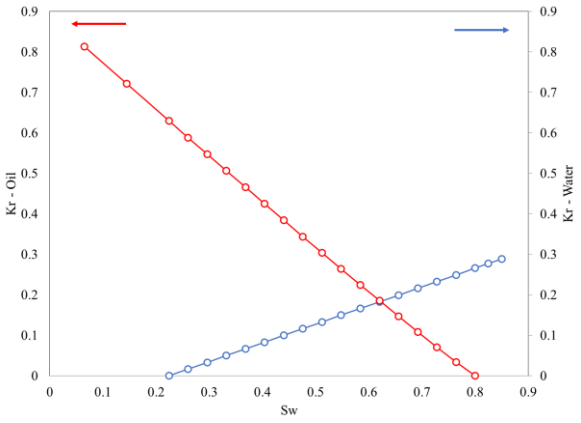

Figure 3.6 Hydraulic fractures – Relative permeability cures

3.3. Base Simulation Model Performance and Validation

As discussed in the prior section that the validation performance of the base simulation model is the most critical step that defines the creditability of the entire study. Unfortunately, due to having no history-matched model or verified from the O&G operator using the actual field case, a trial and error-based work was performed to match the model's flow performance in comparison to the publicly available tight oil SPE wells. Figure 3.6 is presenting the comparison of the base model's bottom-hole flowing pressure (BHFP) profile with the typical tight oil SPE wells' performance having similar reservoir rock and fluid properties as well as the hydraulic fracture design including fracture half-length and fracture conductivity, etc. Keep in mind that the SPE wells performance shown below is normalized for a single-stage hydraulic fracture design same as the base case (refer to Figure 3.2) for an apple-to-apple comparison and the SPE wells datasets presented below are also cleaned from all the operational effects and extrapolated using the logarithmic slope trends. Notably, the subject SPE well is having the closest BHFP match. Therefore, the base model's flow profiles are compared with the same well (i.e., SPE Well 6) for the further model's performance validation as shown in Figure 3.8. While Figures 3.9 and 3.10 are presenting reservoir pressure and saturation distribution profiles over time through 3D model cross-sections.

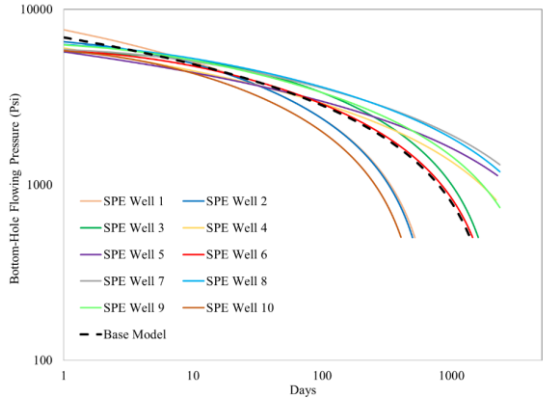

Figure 3.7 BHFP performance of base model vs. typical tight oil wells (using SPE well7 as a ref. well)

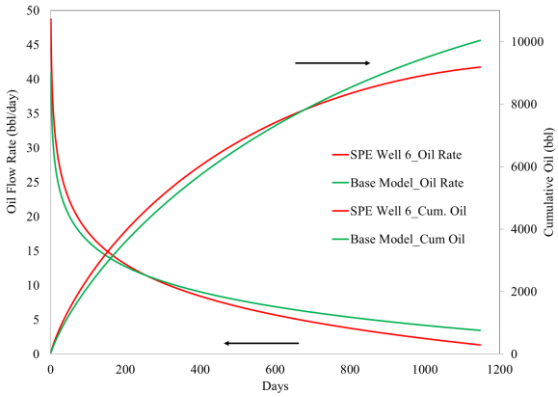

Figure 3.8 Oil flow performance of base model vs. typical tight oil well (using SPE well7 as a ref. well)

It can be noticed from the following figures that the in-situ reservoir fluid saturation alters quickly in the hydraulic fractures and the reservoir matrix region associated with the fractures due to rapid pressure drawdown in the subject regions. This effect of rapid pressure drop is because of a couple of reasons including the existence of highly conductive fractured fluid flow channels with super-increased permeability and the limited to no pressure support from the matrix due to ultra-tight permeability contrast of the reservoir matrix formation in comparison. It is

important to keep in mind that the flow performance in the following figures is shown for a primary recovery mechanism-based scenario i.e., reservoir fluid flow with no external pressure support.

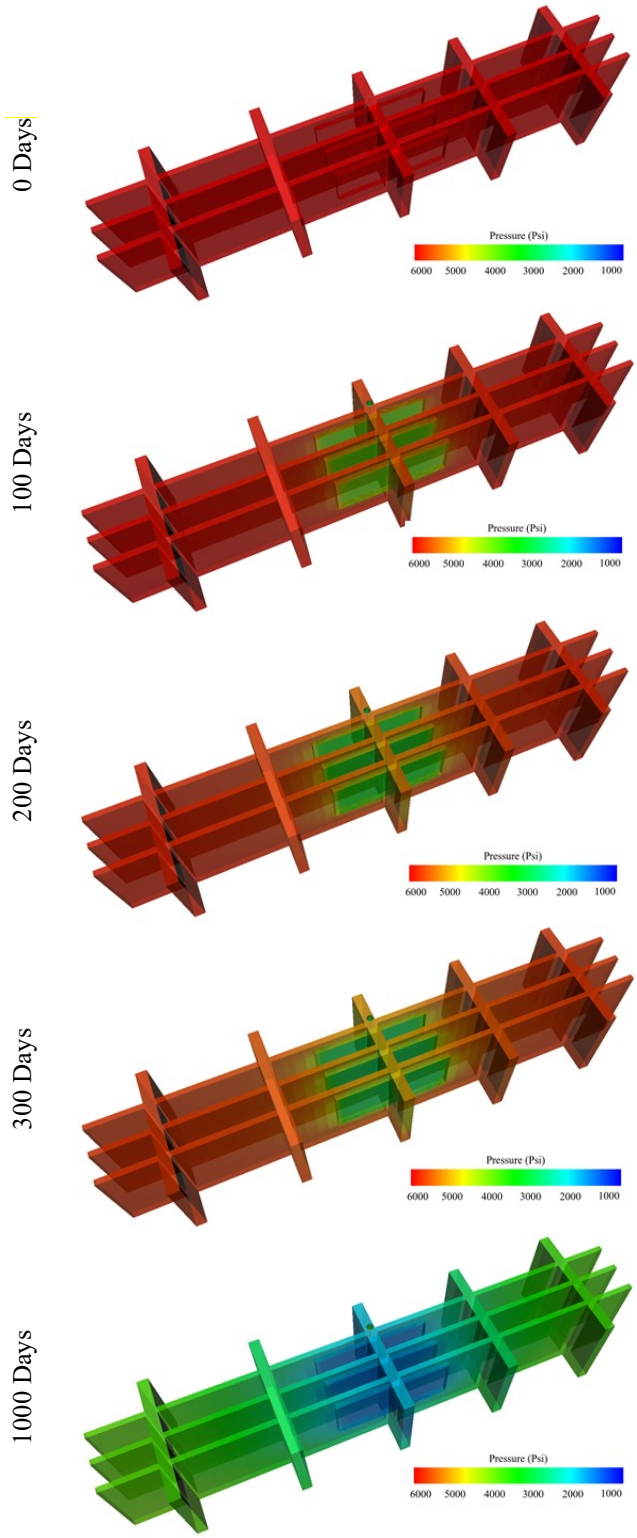

Figure 3.9 Base model's reservoir pressure distribution contrast in reservoir matrix & hydraulic fractures

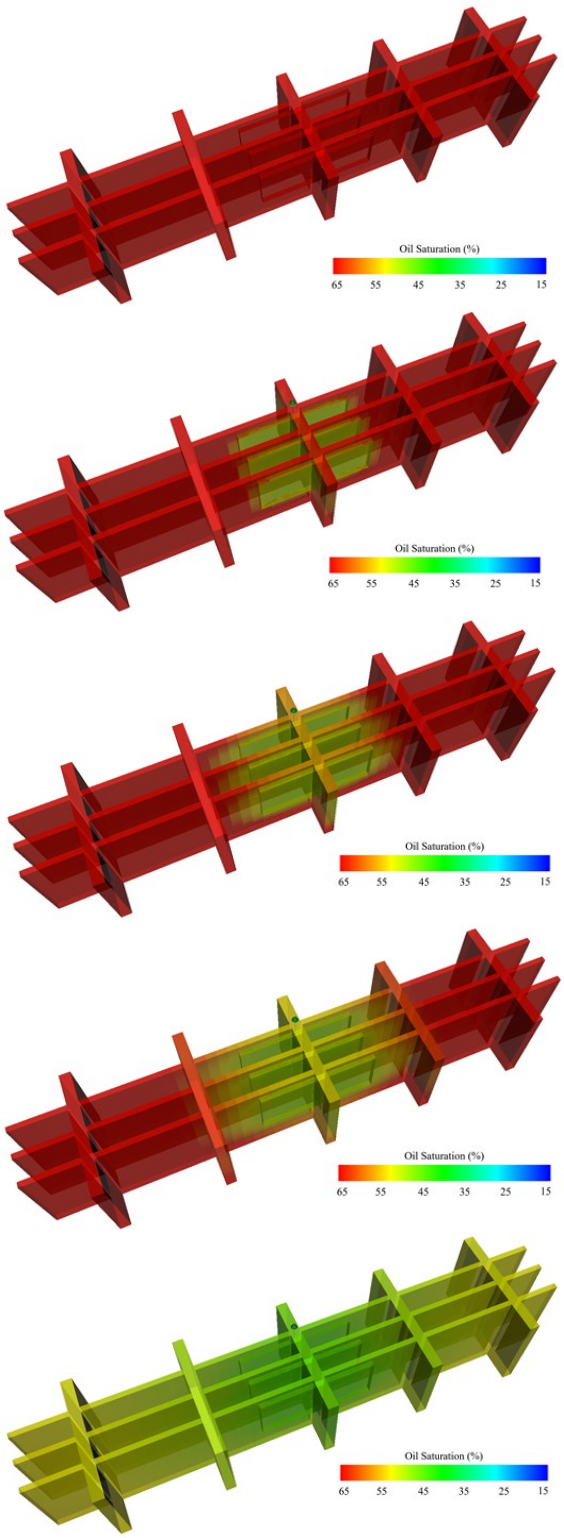

Figure 3.10 Base model's oil saturation distribution contrast in reservoir matrix & hydraulic fractures

As the objective of this piece of study is to develop a physical understanding concerning the fluid flow response as the function of the different reservoir and hydraulic fracture design properties, therefore, the model is purposely designed as simply as possible. However, no reservoirs are found with homogenous reservoir properties distribution, and no O&G operator drills a horizontal well with single-stage hydraulic fractures. Typically, to develop a tight reservoir, the horizontal wells are drilled with multiple thousand feet of horizontal section aided with multiple staged hydraulic fractures with a variable number of clusters in each stage.

Due to limited pressure support and rapid in-situ fluid flow decline, it would be effective to consider external pressure support through early EOR application by injecting low viscous fluids, due to poor injectivity, to boost up the overall recovery factor and it would help in recovery acceleration. Among different injection solvents, produced hydrocarbon gas and CO_2 are the most effective options due to lower minimum miscibility pressure (MMP).

3.4. Reservoir Simulation Model Flow Response – Developing Physical Understanding

After having a reasonable base model flow performance match with one of the typical tight oil wells (SPE well 6), numerous simulation cases using the base model are generated to develop a physical understanding of the model with different parameters for a given model initialization dataset. This is an integrated step for the data-driven model validation and more importantly, the learnings are used to develop the physics-guided design of experiments (PG-DoE) to make sure that the dataset is not just developed based on random sampling but has a physical meaning. For the PG-DoE, the Latin Hypercube sampling method is utilized which is discussed in detail in the following section.

As we know that the quality of a data-driven/ artificial neural network (ANN) model depends on the dataset quality, and it is unlikely to have any physics involved in the ANN model training or prediction. Therefore, it is important to evaluate the proxy ANN model through blind-physics-based sensitivity analysis. Thus, in this step, around 200 simulation/physics-based sensitivities are developed that are used in the later step for the data-driven ANN model testing and its validation for physics compliance and explainability.

As stated in the prior section that the reservoir fluid composition is a sensitive parameter that significantly varies aerially and vertically in reservoir formations, also its properties dramatically alter over time as a function of pressure. Therefore, reservoir fluid compositions are considered the compulsory parameter for the said analysis. In addition, reservoir porosity, fracture half-length, and fracture conductivity are also used for the blind-physics-based sensitivity analysis. The range of all the considered sensitivity parameters is listed in Table 3.4.

Table 3.4 Parameters range for blind physics-based sensitivity analysis

Sensitivity Parameter	Range
Reservoir Fluid Types	7 Fluid Compositions
Reservoir Matrix Porosity (%)	4, 6, & 8
Fracture Half Length (ft)	100, 200, & 300
Fracture Conductivity (mD. Ft)	10, 20, & 30

3.4.1. Reservoir Fluid Types

From the literature, multiple fluid types are found from different U.S. tight oil reservoirs that show significant variation in their fluid composition and the phase envelops as shown in Figure 3.11. It is notable from the figure that all the phase envelopes are non-unique because of having a huge variation in their compositions representing condensate, volatile, and high to medium-quality in-situ oils. The API gravities of the subject oil compositions range between 25 to 50^{o} while the saturation pressure contrasts between 2500 to 3500 Psi and the oil viscosity is found below 4.2 cP. The typical initial gas-oil ratio (GOR) for all fluid types ranges between 500 to 1800 scf/stb.

To capture the entire range of different reservoir fluid types found in most of the U.S. tight oil reservoirs (as found from the literature), a total of seven standard fluid compositions are designed synthetically as shown in Figure 3.9 overlapping most of the phase envelops representing the typical US tight oil reservoirs fluid types. The corresponding standard fluid compositions are shown in Figure 3.12. The reason for generating these standard fluid types is to use them as one of the parameters to develop a numerical database. As discussed earlier, the numerical database is generated as the function of multiple parameters including reservoir rock, fluid (fluid types), and hydraulic fracture properties such that to capture the reservoir recovery response under all possible scenarios representing the U.S. reservoirs. The saturation pressure and the CO_2 MMP values are shown in Figure 3.13; these thermodynamic calculations are performed using CMG-WinProp. The utilization of the saturation and the miscibility pressure values are discussed in the later section while discussing the enhanced oil recovery (EOR) performance with CO_2 and hydrocarbon gas injection.

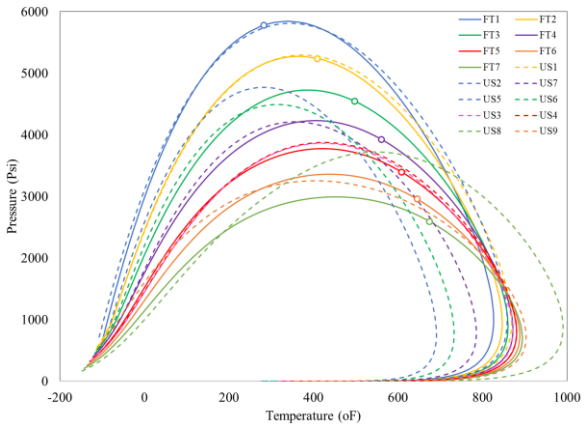

Figure 3.11 Phase envelops (PT Diagram) of U.S. reservoir fluids and the fluid templates

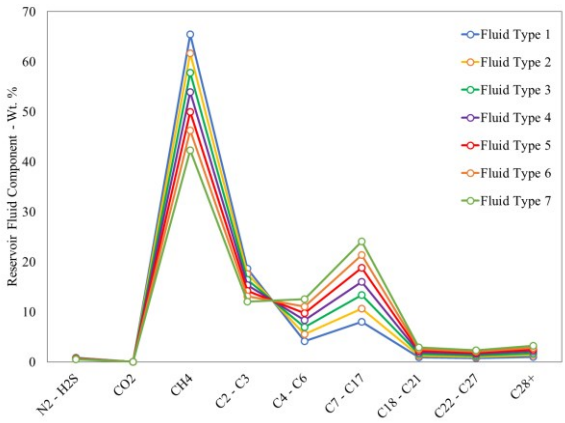

Figure 3.12 Fluid composition of all seven templates used to generate the database

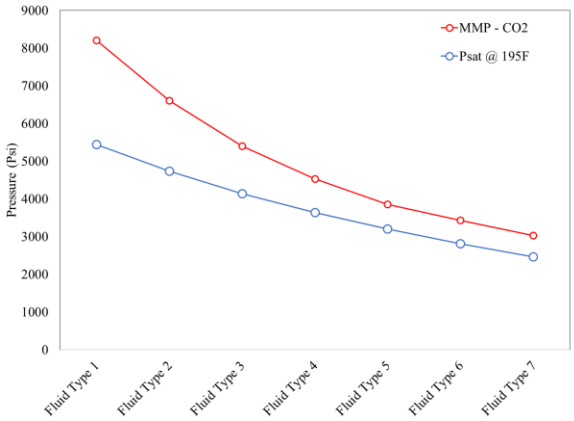

Figure 3.13 Saturation & minimum miscibility pressures of all seven reservoir fluid templates

3.5. Physics-Based Model Flow Response using Blind Sensitivities

The objective covered in this step is to generate benchmark responses of a physics-based numerical reservoir simulation model as the function of different reservoir flow performance controlling parameters including reservoir fluid type, reservoir matrix, as well as the hydraulic fracture design properties. This piece of work provided a detailed physical understanding as a reference that was used for the validation of the ANN proxy models for their physics compliance and explainability.

3.5.1. Effect of Reservoir Matrix Porosity

The model's physics compliance, oil flow rate, gas-oil ratio (GOR), and cumulative flow performance profiles are used in this section as the dynamic key performance indicators for all the considered scenarios. Initially, the effect of reservoir matrix porosity is presented in Figure 3.14. Keeping in mind that all the other parameters except matrix porosity are kept constant such that to observe the effect of porosity on the flow profiles, alone. It is clear from

the flow profiles that incremental formation porosity provides additional reservoir fluid volume that helps to sustain the formation fluid to flow for a longer period.

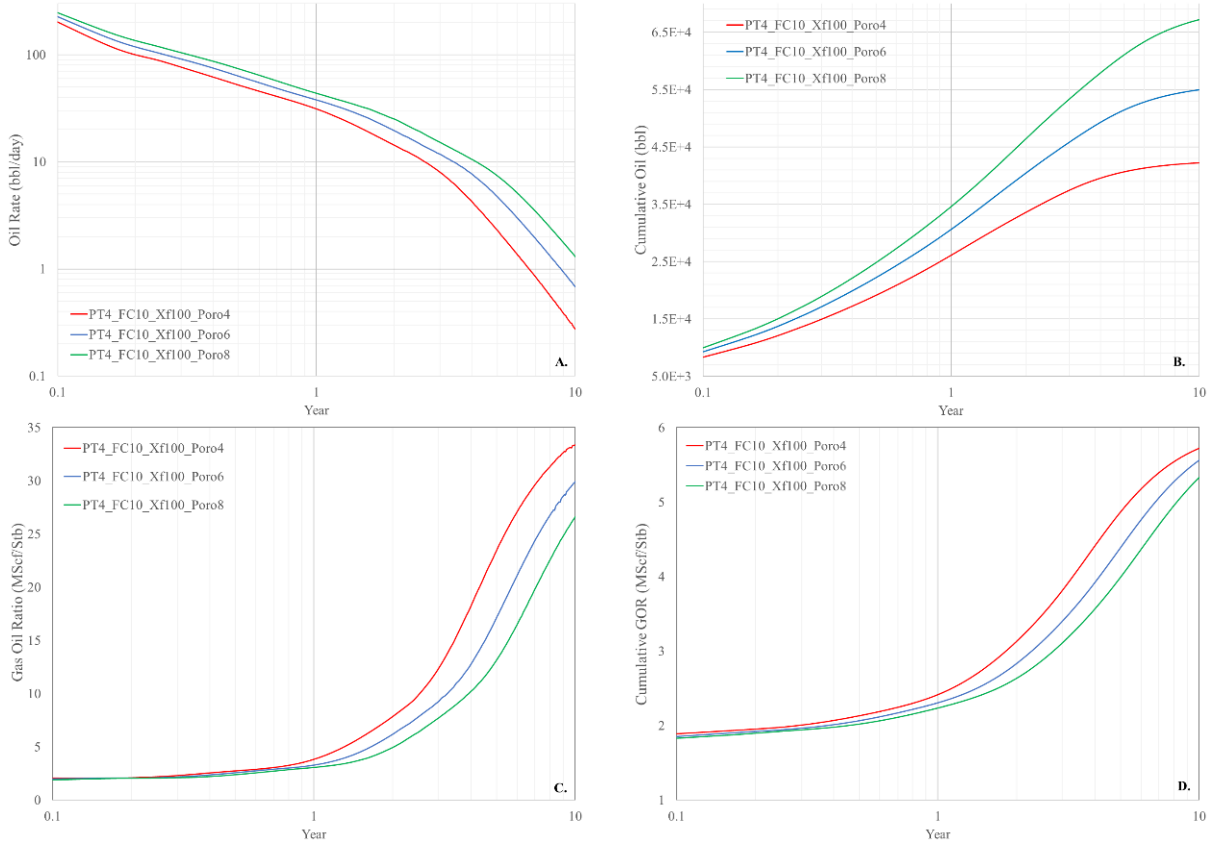

Figure 3.14 Base model flow responses as the function of matrix porosity (A) Oil flow rate, (B) Cumulative oil, (C) GOR, & (D) Cumulative GOR

Therefore, it can be observed from the instantaneous and cumulative oil flow profiles that the higher the porosity, the higher will be the produced fluid volume due to a couple of reasons i.e., comparatively, additional fluid volume to flow and the additional pressure support. On the other hand, for the same draw-down/bottom-hole flowing pressure profiles over time, lower GOR and cumulative GOR profiles are observed for the incremental formation porosity numbers. These GOR responses are logical i.e., the higher the porosity, the higher will be the pressure support due to additional formation fluid volume that would cause a delay in attaining the saturation pressure that directly causes to increase in the GOR. Therefore, the conclusions from this exercise are, at a certain time-step, the oil flow rate and the cumulative oil volume are directly proportional to the reservoir matrix porosity while inversely proportional to the GOR and the cumulative GOR.

3.5.2. Effect of Hydraulic Fracture Conductivity

Hydraulic fracturing is a process of initiation of and propagation of a heavy load of an external fluid composition that generates artificial flow into the tight hydrocarbon formations to create highly conductive flow channels for the in-situ reservoir fluid to flow from the reservoir matrix to the wellbore. The process of fracturing mainly consists of a couple of steps. In the first step, the hydraulic fracturing fluid is injected into the formation at an elevated injection rate and pressure than exceeds the formation's least principal stress to create fractures in the formation next to the wellbore. With the continuation of injection at the higher injection rates, these fractures propagate and grow deeper into the formation. While in the second step, the slurry i.e., the combination of fracturing fluid and proppant injected into the fractures keep the fractures open and avoid them from collapsing.

The hydraulic fractures are generated perpendicular to the least principal stress. Usually, the hydraulic fractures are induced vertically in most of the tighter and the deeper formations depending on the formation rock mechanics i.e., their geomechanical properties, which are also the key players that define the hydraulic fracture design geometry. In addition, the fracturing operation including the fracturing fluid and the proppant injection design plays an important role to define the fracture design parameters.

The key design parameters of a hydraulic fracture include fracture half-length (X_f), fracture height (H_f), and fracture width (W_f). Typically, X_f and H_f are found great in magnitude i.e., hundreds of feet, while W_f typically ranges between less than an inch to a couple of inches. The combination of these parameters describes the fracture conductivity or fracture flow capacity (FC) i.e., the efficiency of a fracture to transmit fluid efficiently from the reservoir formation to the wellbore. Mathematically, FC is the product of fracture permeability and the propped W_f as shown in the following equation;

$$FC = K_f \times W_f \qquad Eq.3.4$$

where FC is the fracture conductivity, K_f is the effective fracture permeability, and W_f is the effective/ propped fracture width.

Fracture conductivity is usually reported in 'mD.ft' and the correlation is defined as, the higher the fracture conductivity, the greater will be the fluid flow through the fracture, therefore, FC can be used as the measure of success for the hydraulic fracturing treatment. From the fluid flow type perspective, higher FC represents an infinite fracture flow response on the derivatives and leads to linear fracture flow while lower FC represents a finite fracture flow

response and typically shows a bilinear flow. The bilinear flow consists of the initial linear flow from the matrix to the fractures and the second linear flow represents the fluid flow from the fracture to the wellbore. A typical hydraulic fracture schematic is shown in Figure 3.15.

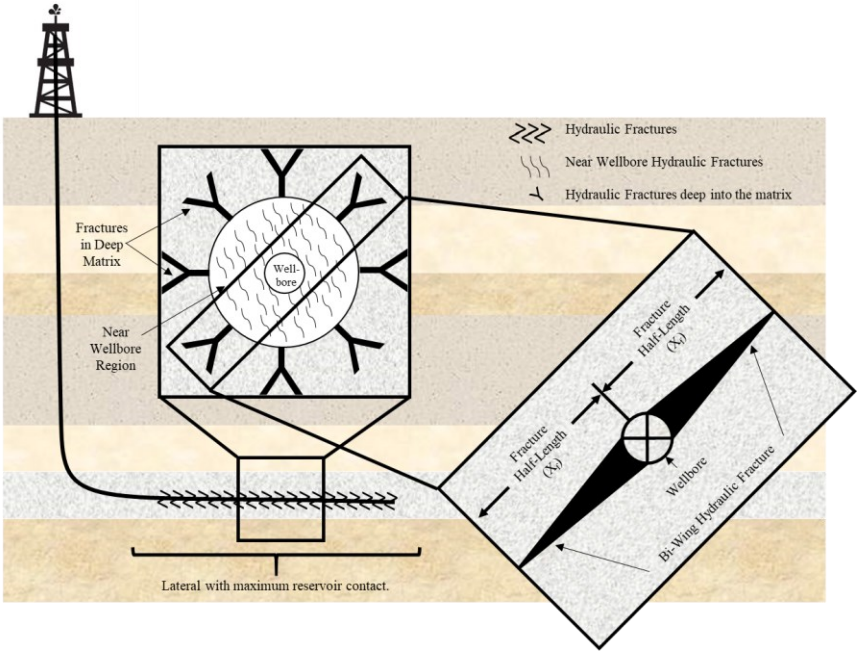

Figure 3.15 Typical hydraulic fracture schematic

There is another important correlation called dimensionless fracture conductivity (F_cD) that mathematically describes the combined effect of fluid flow response from the formation to the fracture and from fracture to the wellbore. The mathematical expression of FcD is shown below;

$$F_CD = \frac{K_f \times W_f}{K_m \times X_f} \qquad Eq.3.5$$

where; F_cD is the dimensionless fracture conductivity, K_f is the effective fracture permeability, W_f is the effective/ propped fracture width, K_m is the formation matrix permeability, and X_f is the fracture half-length.

Based on different numerical and experimental studies, it is concluded that the FcD greater than 10 is sufficient for the optimum in-situ fluid productivity from both matrix and the hydraulic fractures, and it is assumed that the FcD greater than 50 shows no incremental effect on productivity. Figure 3.16 evident this theory of having a significant incremental effect on productivity with the increase in fracture conductivity, however, no considerable increment in cumulative oil production is found in the simulation cases with F_cD greater than 50. Figure 3.13 shows the formation fluid flow response i.e., oil rate, gas oil ratio, and their cumulative for multiple cases with fracture conductivity ranges between 0.1 to 50 mD.ft and their corresponding F_cD ranges between 0.2 to 100.

The overall productivity of the model with the lowest fracture conductivity could be noticed from the following figures is comparatively lower due to the insufficient flow ability of the fluid from the matrix to the fractures due to ultra-tight matrix permeability and the same restricted flow from fractures to the wellbore due to comparatively lower fracture conductivity. While the opposite flow behavior can be noticed in the reservoir model with the higher FC.

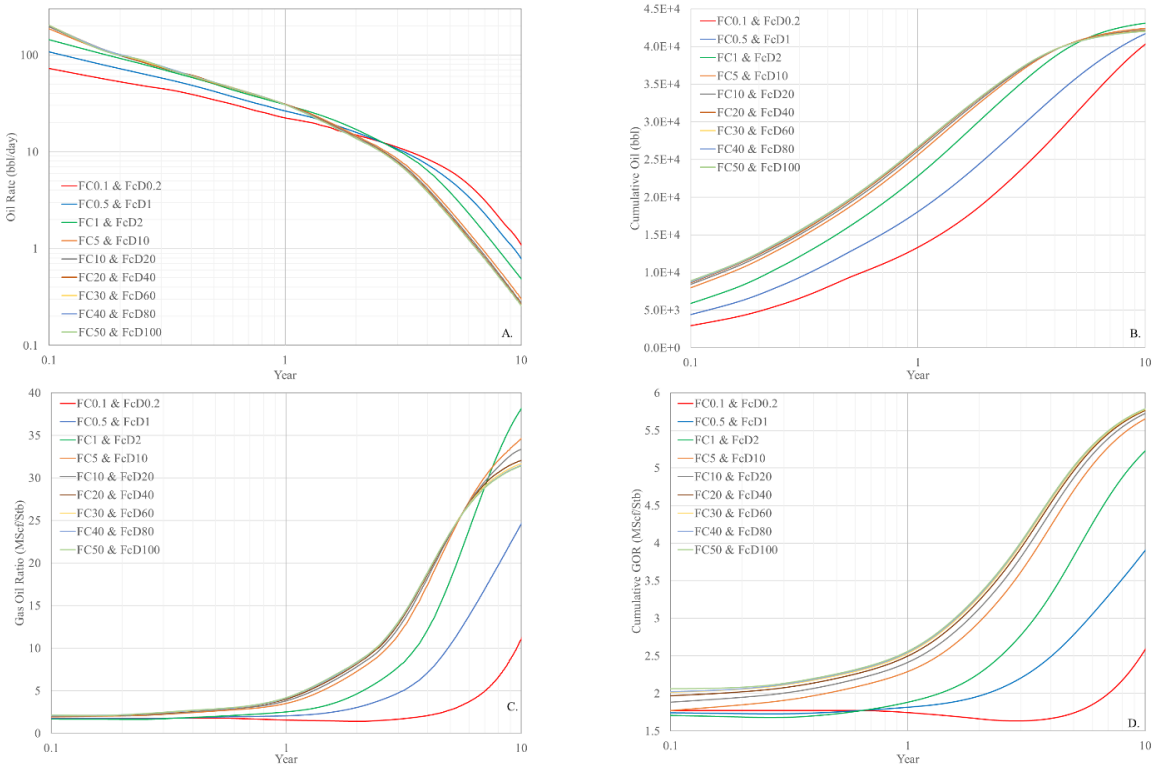

Figure 3.16 Base model flow responses as the function of hydraulic fracture conductivity (A) Oil flow rate, (B) Cumulative oil, (C) GOR, & (D) Cumulative GOR

3.5.3. Effect of Hydraulic Fracture Half-Length and Reservoir Fluid Types

Hydraulic fracture design parameters including fracture half-length, fracture height, and fracture width are practically the most uncertain parameters that are difficult to characterize with accuracy after having an actual field stimulation treatment. However, while designing a hydraulic fracture based on the formation properties, fracture half-length is usually on the top of the priority list as it plays the most critical role to boost the oil recovery from the tight oil reservoirs through the greater surface contact area. The typical range of fracture half-lengths found in the literature ranges between 100 to 300ft.

Most of the studies found in the literature concluded that the incremental fracture half-length is more favorable for enhanced oil recovery through the single well-based huff-n-puff process in comparison to the primary

recovery. The impact of longer half-length is more prominent for the EOR application because of more contact area with the reservoir that results in surplus CO_2 diffusion in a larger portion of the reservoir that results in a higher recovery factor. Almost all the studies reported in the literature focused on the impact of different hydraulic fracture design parameters for a single fluid type. However, it is important to consider the effect of reservoir fluid types because it significantly affects the overall instantaneous in-situ fluid flow behavior and its flow profile over time. This work comprehensively focuses on the impact of different reservoir fluid types as well as the hydraulic fracture design parameters. Figure 3.17 is presenting the primary recovery performances of various scenarios highlighting the effect of hydraulic fracture half-lengths (i.e., 50ft, 100ft, 150ft, & 200ft) individually for seven different fluid types (Figure 3.17 A to G) and the combined flow performance comparison with different fluid types in Figure 3.17.H.

Fluid types 1 to 7 are representing lighter to a heavier oil with $C_{1\text{-}3}$ ranging from 85% to 55%. For an apple-to-apple comparison, all the reservoir and hydraulic fracture design parameters, except the fracture half-length, were kept the same in all the cases. In addition, all the cases were simulated using the same bottom-hole flowing pressure (BHFP) profile. As we know, the reservoir fluid flow profiles including oil rate and gas-oil ratio (GOR), are the function of pressure. The GOR abruptly changes as soon as the saturation pressure is achieved, that's why it was important to use the same BHFP profile for all the cases for a fair comparison. It can be noticed in Figure 3.17, for all fluid types, the instantaneous initial oil flow rate is higher for the larger fracture half-length in comparison. A simultaneous effect of pressure drawdown and the fracture half-length size can be noticed i.e., larger fracture half-length results in faster in-situ fluid withdrawal due to rapid pressure drawdown and the simultaneous effect is of the attainment of the saturation pressure. As the same BHFP profiles are used in all the cases, the saturation pressure of each fluid type is achieved at different periods such that the saturation pressure of the lighter fluid type is achieved earlier than the heavier fluid type. Thus, it can be noticed that the flip over of the performance profiles from fluid type 1 to 7 was delayed which also impacted the cumulative oil recoveries in comparison as shown in Figure 3.18. Ideally, fluid type 7 shows the most reported flow behavior in the literature as the function of fracture half-length that shows more oil production over time with a larger fracture half-length and less production with a smaller half-length. Similarly, the cumulative GOR profiles are shown for the same cases with different fracture half-lengths and reservoir fluid types in Figure 3.19. The effect of fracture half-lengths is prominent on the cumulative GOR profiles such that, the larger the half-length, the more will be the cumulative GOR due to comparatively faster pressure drawdown and the rapid in-situ fluid withdrawal.

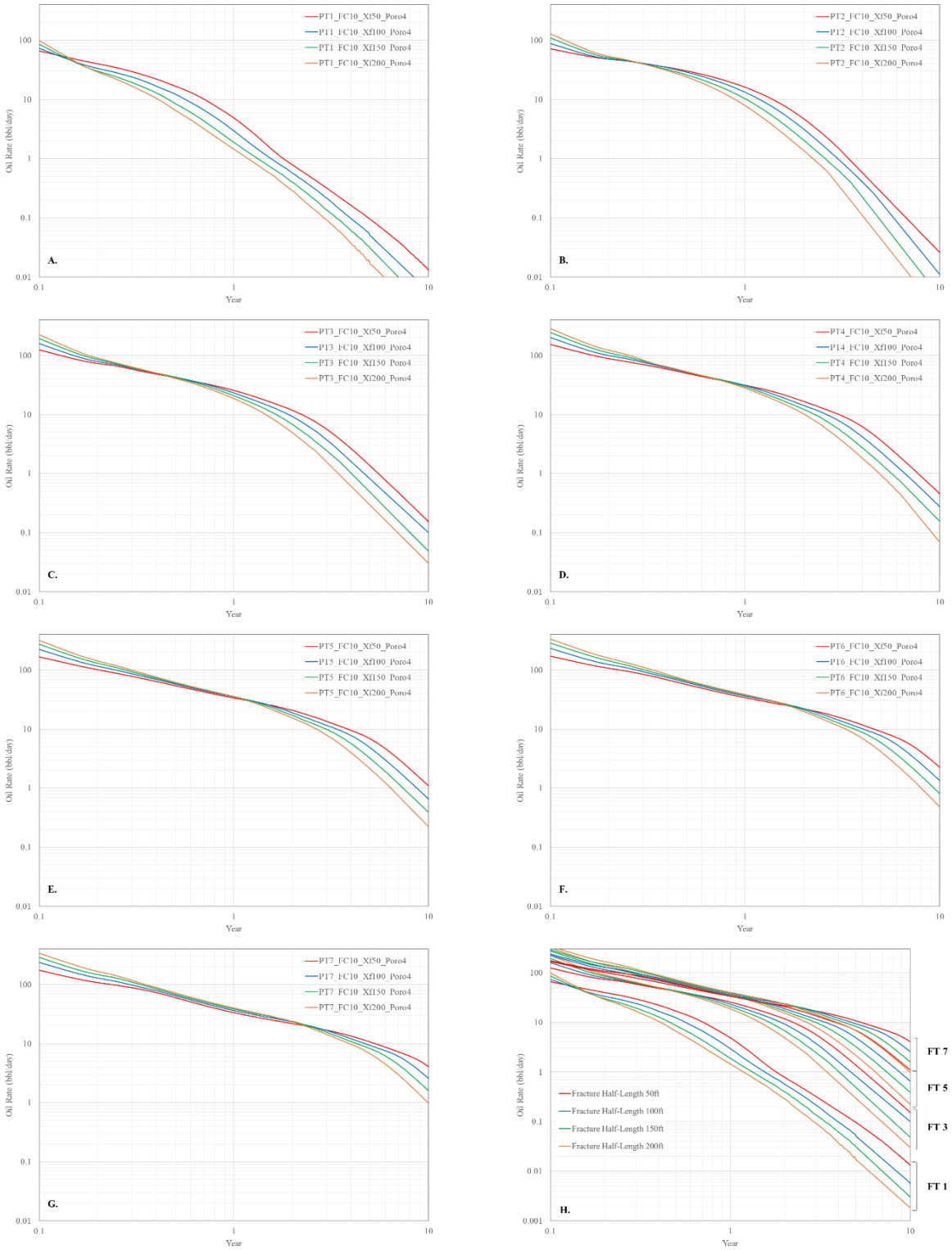

Figure 3.17 Blind physics-based sensitivities on the oil flow behavior as the function of hydraulic fracture half-length and the reservoir fluid types. Individual plots are showing the effect of fracture half-lengths for multiple fluid types i.e. (A) Fluid Type 1, (B) Fluid Type 2, (C) Fluid Type 3, (D) Fluid Type 4, (E) Fluid Type 5, (F) Fluid Type 6, and (G) Fluid Type 7. (H) The combined effect of all fluid types for overall comparison

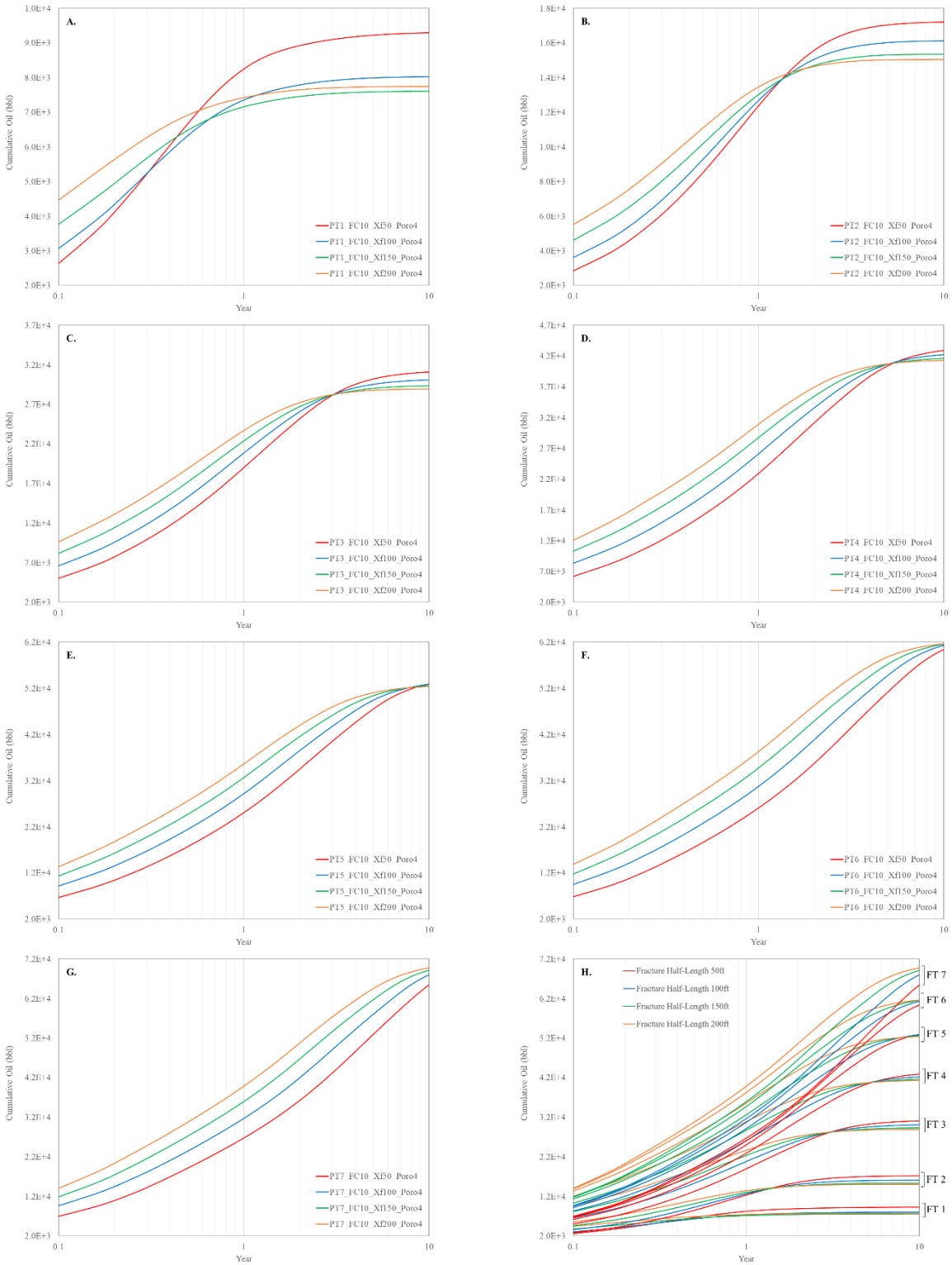

Figure 3.18 Blind physics-based sensitivities on cumulative oil production as the function of hydraulic fracture half-length and the reservoir fluid types. Individual plots are showing the effect of fracture half-lengths for multiple fluid types i.e. (A) Fluid Type 1, (B) Fluid Type 2, (C) Fluid Type 3, (D) Fluid Type 4, (E) Fluid Type 5, (F) Fluid Type 6, and (G) Fluid Type 7. (H) The combined effect of all fluid types for overall comparison

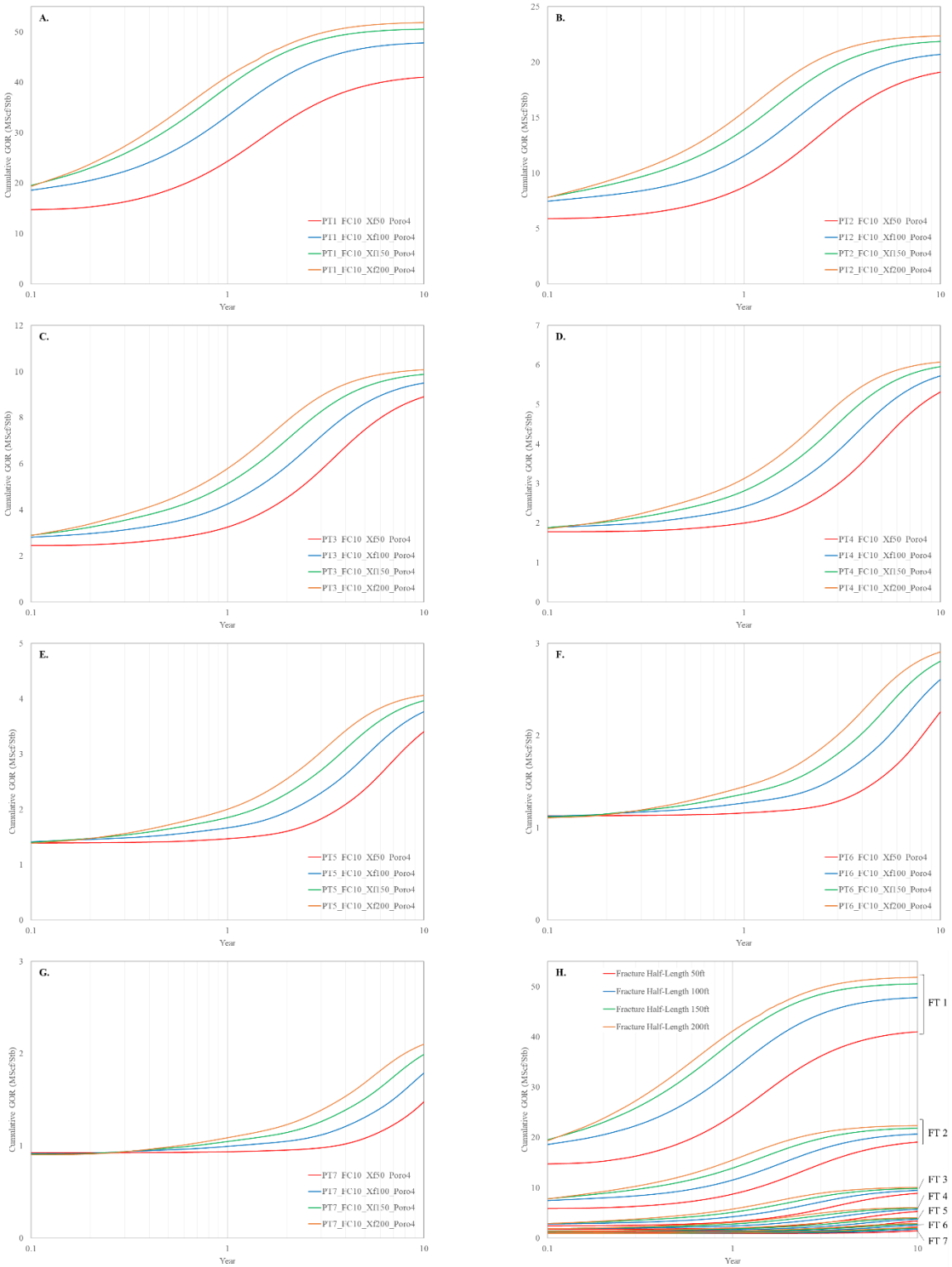

Figure 3.19 Blind physics-based sensitivities on cumulative GOR as the function of hydraulic fracture half-length and the reservoir fluid types. Individual plots are showing the effect of fracture half-lengths for multiple fluid types i.e. (A) Fluid Type 1, (B) Fluid Type 2, (C) Fluid Type 3, (D) Fluid Type 4, (E) Fluid Type 5, (F) Fluid Type 6, and (G) Fluid Type 7. (H) The combined effect of all fluid types for overall comparison

It is concluded from the above discussion that it is critical to perform a detailed hydraulic fracture design optimization based on the reservoir fluid type, reservoir pressure, and the operational design that defines the BHFP profile or the drawdown pressure over time. This extensive exercise is performed to develop a physical understanding of the reservoir model used in this study such that to expect a similar response from the data-driven proxy models. While generating proxy models, it is important to have physics compliance and explainability. Data-driven proxy models' generation and their physics compliance tests are discussed in detail in the next chapter.

3.6. Unconventional Enhanced Oil Recovery Response

Performing an EOR operation in tight oil reservoirs is not as simple as in conventional reservoirs. First, not all EOR techniques are applicable in tight reservoirs due to ultra-low matrix permeability and hence the poor injectivity. Therefore, CO_2 and hydrocarbon gas injection-based EOR techniques are more favorable to the tight system. Secondly, due to poor inter-pore connectivity, individual well-based EOR techniques are considered more effective to perform EOR through the huff-n-puff process. Lastly, as explained in the prior sections, hydraulic fractures are considered a mandatory application to develop tight reservoirs therefore, the hydraulic fracture design is extremely critical for an optimum unconventional EOR application. In this section, the numerically simulated results are discussed in a couple of steps including, the effect of EOR operational design and the optimum hydraulic fracture design on EOR recovery. Secondly, the potential CO_2 storage is also discussed as the byproduct of CO_2 injection for EOR through a single staged huff-n-puff technique.

The objective of this section is to develop a physics-based understanding of the reference EOR response under different situations. In addition, it is important to highlight that for all the EOR cases, we considered an additional case without any solvent injection, while the well/producer kept close for the same duration as the solvent injection and soaking period is considered in the EOR cases. It is strongly recommended to perform this step for all the EOR field development practices to understand the usefulness of the EOR process in a way to differentiate the effect of EOR simply from pressure buildup if there will be any. However, it is almost impossible but just in case, if the recovery performance of the two cases i.e., EOR and the shut-in case are comparable with a minimal difference then there is no significant need for such a huge investment in an EOR application.

3.6.1. EOR Operational Design

The general perception these days for the EOR application in a conventional reservoir system is not a difficult task anymore because of several EOR field applications in similar systems. The EOR selection mainly depends on the architecture, geophysics, and geochemistry of a reservoir formation, as well as the reservoir fluid characteristics. However, the situation is not that simple for unconventional reservoirs because of limited field applications and lack of field data availability. The unconventional reservoir properties are not well defined and most of the literature is based on the best-guessed data.

It is a great deal to make the unconventional tight oil flow from tiny matrix pores to the wellbore through the conductive hydraulic fractures. Among the limited EOR solvent selection, CO_2 and produced hydrocarbon (HC) gas are the commonly adopted EOR solvents for UEOR applications and thus in this section, the physical understanding is developed through numerical trend analyses for different scenarios through a couple of EOR options in comparison to being used as a reference for the EOR.

First, for an EOR application, it is strongly recommended to compare EOR performance with the base cases i.e., primary production with continuous fluid flow and a similar case with a shut-in period. The shut-in period must be equivalent to cover the entire EOR application timing including the injection and the soaking periods. This comparison is techno-economically important to eliminate the effect of wellbore storage and to encounter the pressure buildup and the wellbore storage effects. Therefore, before analyzing multiple EOR scenarios, no-injection base cases with different time duration of shut-in are compared as presented in Figure 3.20. The results with different shut-in time duration i.e., 8:8 (16 weeks), 4:4 (8 weeks), and 8:4/4:8 (12 weeks) are compared, and no significant differences are found. Infect, on a closer look, it is observed that the shut-in negatively affected the recovery performance and because of ultra-tight permeability, no pressure support is gained from the deeper reservoir. It can be concluded that the unconventional reservoirs locally behave as an independent part of the reservoir that reflects no pressure and fluid transient communication into the formation. As observed, no near-wellbore pressure build-up is observed at least for a shorter period of a well shut-in that would be more economical for the operators. There might be a different effect of longer shut-in but of course, that will not be an economical approach for any operator to shut in their producers for a longer period.

In addition, to the EOR technique and the hydraulic fracture design, the reservoir formation fluid type is also an important factor that plays a critical role in a successful EOR application. After developing our physics-based understanding of the multiple reservoirs and hydraulic fracture characteristics using a single type of reservoir fluid, the EOR response to different reservoir fluid types is discussed in the last section of this chapter.

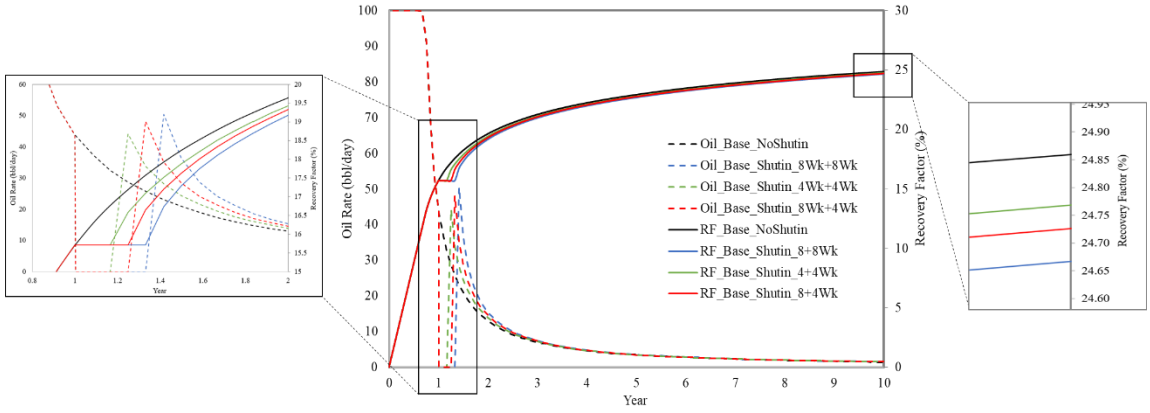

Figure 3.20 Reference cases with shut-in for the same period as EOR solvent injection and soaking duration

3.6.1.1. Effects of Solvent Injection Volume & Soaking Period

Figure 3.21 shows the EOR recovery performance comparison with CO_2 and the produced HC gas injection. Both solvents are injected at the same injection rate and the injection pore volume is controlled through the injection time duration. It can be noticed that CO_2 significantly improved the oil recovery in comparison to HC gas. The observed EOR responses from both solvents make perfect sense as the CO_2 being a supercritical fluid is more effective than the other injectants because of its lower minimum miscibility pressure and higher solubility that helps the trapped reservoir fluid to flow from tiny matrix pores into the main flow stream.

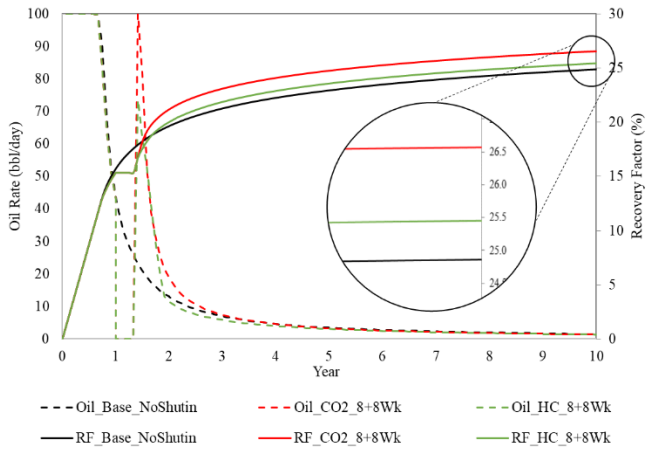

Figure 3.21 Recovery performance comparison with different EOR injection solvents

A detailed sensitivity analysis is performed with different injection and soaking time durations, with a fixed injection rate, using CO_2 as the most efficient EOR solvent for a significant EOR response. Figure 3.22A is presenting four different scenarios with 8:8, 4:4.8:4, and 4:8 weeks of injection and soaking. An interesting response was noticed that the two cases with higher CO_2 injection volume (i.e., 8:8 and 8:4 weeks) showed comparatively higher recovery. However, larger soaking time shows a considerable increment in the other couple of cases with approximately four weeks of CO_2 injection at a constant injection rate, however, the effect is not as significant as the CO_2 injection volume showed in comparison. It is also important to keep in mind that the longer soaking period might improve the overall recovery because of oil swelling, viscosity reduction, diffusion, and pressure buildup but the longer shut-in would affect the project economics, negatively. A similar observation was made with the lean HC gas injection as shown in Figure 3.22B.

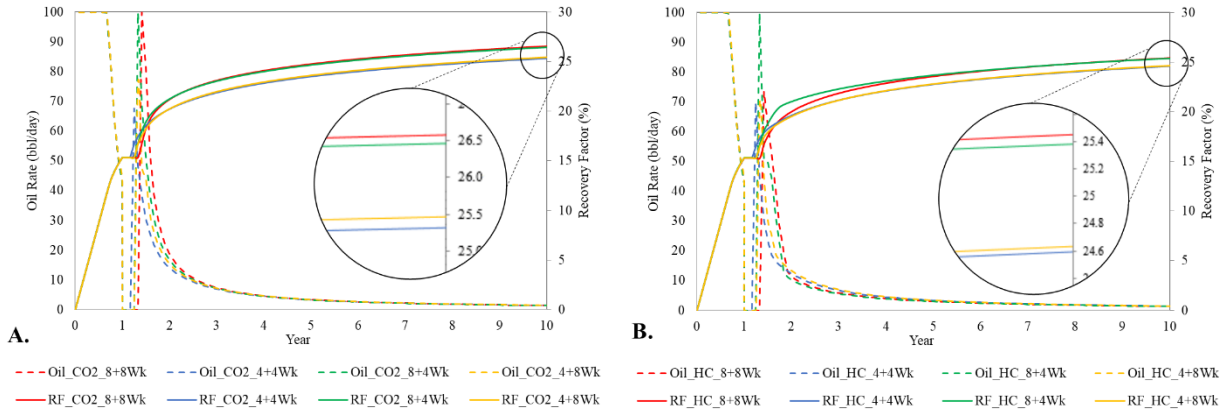

Figure 3.22 EOR Recovery performance comparison for different injection and soaking periods with (A) CO_2 and (B) HC

3.6.1.2. Effects of Huff-n-Puff Cycles Initiation

Along with the EOR solvent type, its injection volume, and the soaking period, the EOR initiation timings and the duration of every individual huff-n-puff cycle are equally important that significantly affect the ultimate oil recovery from tight oil reservoirs. Figure 3.23 is presenting the recovery performance comparison of four different scenarios with three huff-n-puff cycles in each case with different huff-n-puff duration. The first case shows significantly higher recovery in comparison, which initially applies EOR after 6 months of primary production and is followed by the 2nd and 3rd cycle after every 6 months of production. In the second, third, and fourth cases, the EOR initiated after 12, 18, and 24 months of primary production, respectively, followed by the next cycles after the same duration each time. A couple of conclusions can be drawn from the recovery performance, the oil recovery from a

tight reservoir is sensitive to EOR start timing after primary production and secondly, the timings for individual huff-n-puff application on the same well is also critically important to recovery response. Therefore, it is strongly recommended to design a cyclic huff-n-puff EOR application with smaller periods to achieve optimal oil recovery.

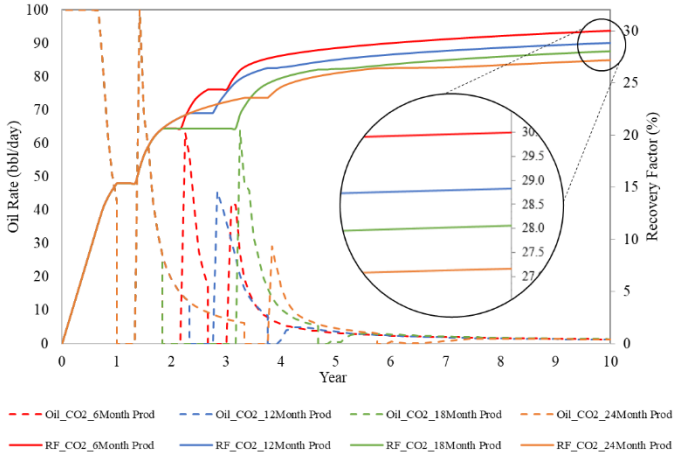

Figure 3.23 Recovery performance comparison for multiple Huff-n-Puff cycles injection after 6, 12, 18, and 24 months

3.6.1.3. Effects of Huff-n-Puff Cycles

As noticed from the prior discussions, solvent injection aids to boost the oil recovery significantly from tight oil reservoirs as an instant effect through the huff-n-puff technique. However, the oil flow rate declines rapidly because of the limited injectivity due to ultra-tight permeability and nano-pore throat size distribution. The injected solvent usually does not invade too much into the matrix but most likely into the near-fractured zones, only. The invaded solvent requires some time to be soaked into the matrix, therefore the well is kept close for a defined pace of time that allows the injected solvent and the reservoir fluid to potentially achieve multi-contact miscibility through back-n-forth condensation and evaporation that causes oil swelling and viscosity reduction. But this phenomenon requires longer well shut-in, which is not economically feasible for the operators. Therefore, the repeated cyclic huff-n-puff approach is more reasonable. Using this approach, an excellent sensitivity analysis is performed as shown in Figure 3.24, three different scenarios with single, dual, and triple huff-n-puff cycles are applied numerically.

Approximately 16% pore volume of the total original oil in place (OOIP), CO_2 is flooded into the reservoir in each huff-n-puff cycle that resulted in 1.2 to 3% incremental oil recovery in each cycle and cumulatively, a 5% increment is noticed after three continuous cycles (see Table 3.5). In addition, the incremental oil recovery after the 2nd and 3rd cycles reduced in a linear trend. This observation of decreased incremental oil recovery is logical i.e., with

every additional huff-n-puff cycle; a lesser amount of oil would remain in place to be contacted with the injected solvent beyond the hydraulic fractures.

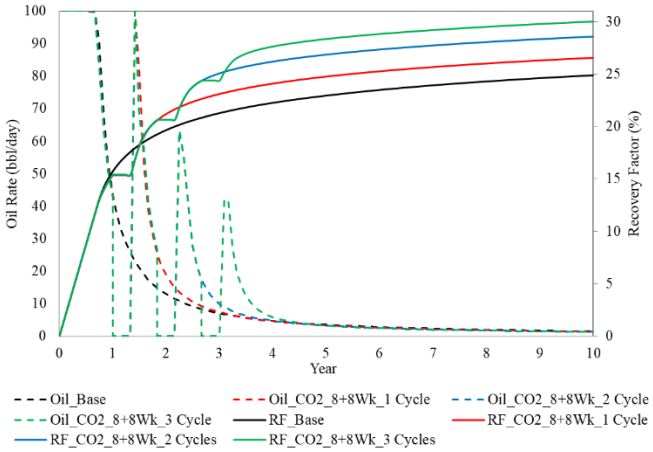

Figure 3.24 CO_2 EOR recovery performance comparison for one, two, and three huff-n-puff cycles

Table 3.5 CO_2 injection, production, and trapping summary

Cycles	CO_2 Injection (ft^3)	CO_2 Produced (ft^3)	CO_2 Trapped in Reservoir (%)	Cum. CO_2 Trapped in Reservoir (%)	Cum. Inc. Oil Recovery (%)	Consecutive Increment (%)
1st	6.90E+07	6.60E+07	4.35	4.35	2.0	2.0 (Inc. over the base case)
2nd	7.30E+07	6.90E+07	5.48	4.93	3.8	1.8 (Inc. over the previous cycle)
3rd	7.20E+07	6.70E+07	6.94	5.61	5.0	1.2 (Inc. over the previous cycle)
Total	2.14E+08	2.02E+08	5.61	-	-	5.0

Nanopore confinement is another important factor that directly affects the hydrocarbon recovery factor from nano-pores (tight reservoir with nano-Darcy permeability), but that effect can be modeled numerically for a reservoir with non-uniform permeability distribution i.e., a reservoir with different pores sizes. However, its effect is minimal when the average reservoir pressure is considerably higher than the bubble point pressure. The bubble point suppression and changes in fluid properties in nanopores can be modeled through varying critical properties i.e., critical temperature and pressure of the fluid components. In brief, the effect of nano-pore confinement can be achieved numerically by varying the critical properties of the confined fluids as a function of the pore size, and for that, multiple correlations can be applied to shift the phase envelop at critical pore sizes based on the shale mineralogy. Numerically, a dual permeability model can be set up to achieve this objective with explicit modeling of the stimulated reservoir volume (including both hydraulic fracture and the connected natural fractures if present in the model) and the unstimulated reservoir volume (with unconnected natural fractures). As part of the methodology, multiple PVT regions

are required to be defined and associated with different pores sizes i.e., for example; nanopores with maximum shifted phase envelop, mesopores with partially shifted phase envelop, and macropores to be considered with the original PVT. These PVTs to be assigned in the model associated with the non-uniform matrix as the function of the pore size distribution which may perhaps be correlated with the permeability for a set maximum percentage of matrix blocks (based on the formation properties and the rock pore size distribution) assigned the mesopores and nanopores. Through this approach, the alteration in fluid properties as the function of bubble point suppression under confined nanoscale pores and the resultant effect on the oil recovery can be captured for different types of reservoir fluids.

In addition, Figure 3.25 is presenting the oil recovery and the flow rate plots for each huff-n-puff cycle. Similarly, an increment in CO_2 trapped volume is witnessed with every individual huff-n-puff cycle as shown in Figure 3.26 in terms of total CO_2 volume injected and produced back.

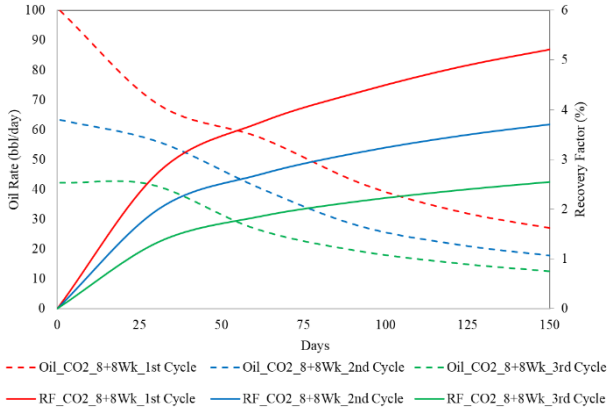

Figure 3.25 Individual flow rates and recovery performance of every individual huff-n-puff cycles

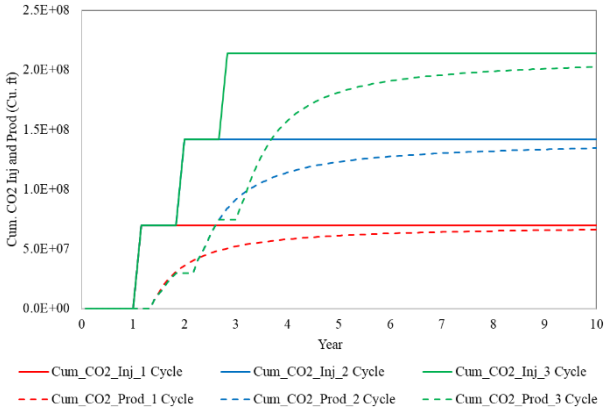

Figure 3.26 Comparison of cumulative CO_2 injection and its backflow response for one, two, and three huff-n-puff cycles

3.6.1.4. Effects of Reservoir Fluid Types

One of the biggest constraints and the reservoir development controlling factors is the reservoir fluid composition. Without accurate information, no EOR and the injected solvent selection can be done properly. For the numerical simulation, binary interaction coefficients are necessarily required to be defined for each fluid component in the simulator for the condensation and vaporization mechanism that defines the diffusion and the solubility phenomenon. Figures 3.27 and 3.28 are presenting the CO_2-EOR performance comparison through a single huff-n-puff cycle with their reference base cases and the incremental oil recovery, respectively, for seven different fluid types as discussed in the prior section.

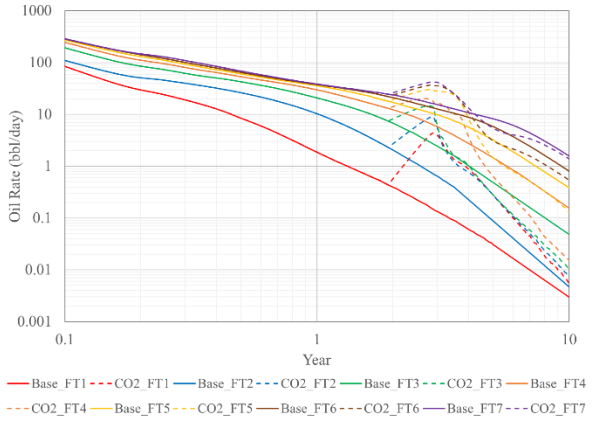

Figure 3.27 Reservoir flow performance comparison for different reservoir fluid types

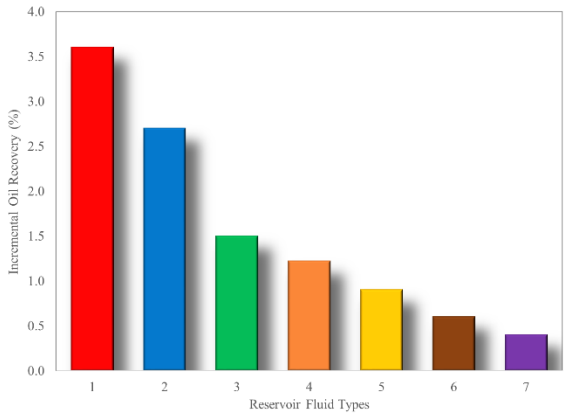

Figure 3.28 Incremental oil recovery comparison for different reservoir fluid types

3.6.2. Hydraulic Fracture Design

Hydraulic fractures provide considerable channels for the reservoir fluid flow and the maximum reservoir contact for the injected EOR solvent that helps to improve oil recovery. Multiple hydraulic fracture design parameters, directly and indirectly, affect the reservoir recovery performance. The most critical parameters include fracture half-length, effective permeability (i.e., after having proppant in place), and height. Fracture width is also an important design parameter but since it is comparatively a much smaller number the fracture is half-length and height, therefore, its effect is minimal. The total clusters count per fracture, the spacing between each fracture, and the number of fracture stages is also imperative parameters. Since there is no rule of thumb to generate a fracture design, therefore, a similar approach is applied in this study as observed in a few field practices, shared in the literature.

3.6.2.1. Clusters Count

The total clusters in each fracture provide significant operational quality of a fracture through reservoir contact area improvement with the wellbore. This effect is even more prominent for the long horizontal wells that are completed through multiple staged hydraulic fractures. However, there are a few limitations to consider while designing hydraulic fractures including local oil in place (i.e., stimulated reservoir volume, SRV), reservoir rock quality (mainly the matrix permeability), formation fluid characteristics, and the reservoir pressure to feed the fractures. In this study, three distinct scenarios with single, double, and triple clusters, as shown in Figure 3.29, are considered to review the recovery performance with a single staged horizontal well.

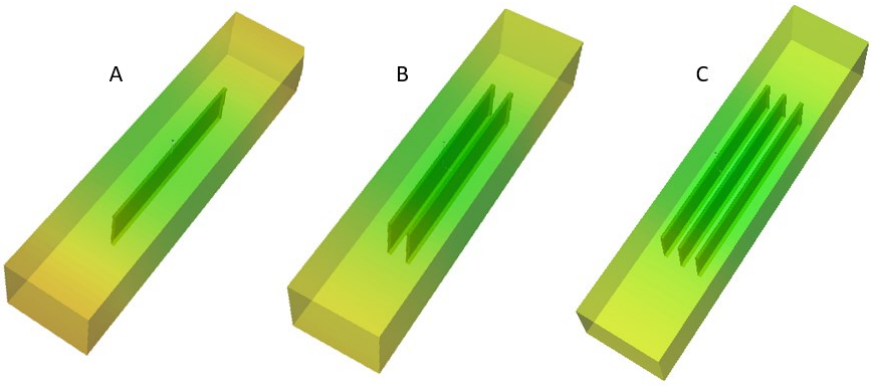

Figure 3.29 Cross-sections of reservoir models with A. Single, B. Double, and C. Triple clusters per fracture

The recovery comparison plots are shown in Figure 3.30 and the results make perfect sense i.e., significantly more oil is recovered with the triple cluster scenario as compared to the single cluster case. However, the recovery difference between double and triple clusters is minimal because of the limited oil in place. Hence, it can be concluded that it is important to determine the optimum number of clusters per fracture based on the local SRV for individual fractures.

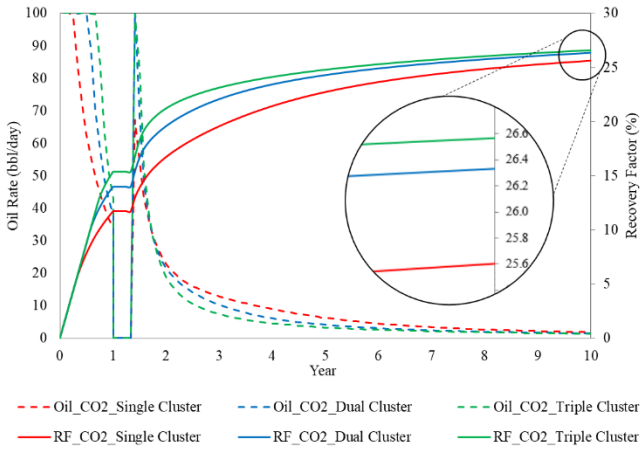

Figure 3.30 Comparing recovery performance with single, double, and triple clusters per fracture

3.6.2.2. Fracture Half Length

Another important fracture design parameter is the fracture half-length which significantly affects the oil recovery performance because it determines the stimulated area linked to the wellbore and provides an easy path for the reservoir fluid to flow. The bigger the fracture half-length on both ends of the fracture, the more will be its contact with the reservoir and hence more drawdown. However, it is not that easy to achieve a higher fracture half-length due to operational constraints, but it is important to consider the offset wells spacing while designing the half-length to avoid any frac-hits. Figure 3.31 is showing the oil recovery performance comparison for a single stage with triple

clustered fracture, and it can be concluded that fracture half-length is having a significant impact on the oil recovery. It is observed from the results that the half-length is directly proportional to the oil recovery; however, the incremental recovery trend is found to reduce with an increment in the half-length. Therefore, similar to the fracture counts, also the fracture half-length selection requires optimization depending on the reservoir rock quality, formation fluid characteristics, and most importantly the local oil in place counter in SRV.

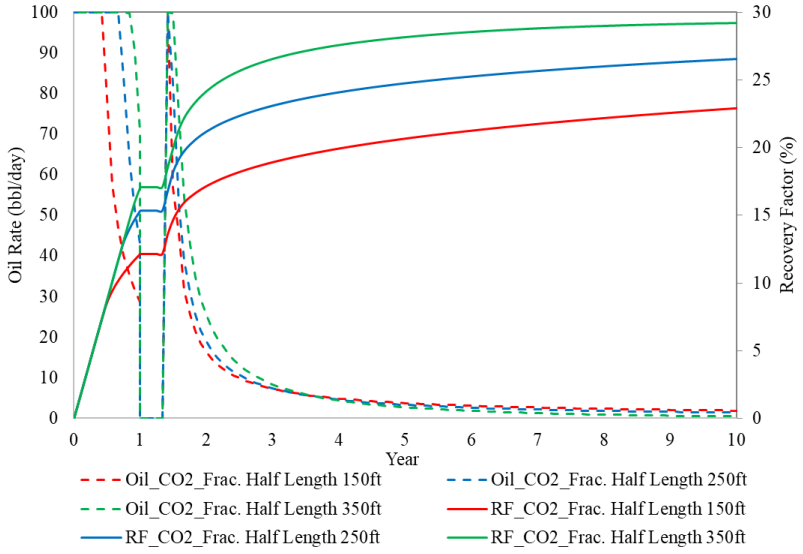

Figure 3.31 Comparing recovery performance for different fracture half-lengths

3.6.2.3. Fracture Spacing

The fracture spacing is also a critical parameter while designing an overall well completion plan that depends on the reservoir rock characterization and the sweet spot distribution in a tight reservoir. Generally, hydraulic fractures and individual cluster placement are defined in a model based on the matrix permeability distribution between the two consequent fractures, locally oil in place, and the pressure distribution. Theoretically, the same phenomenon of infill drilling is applied here in this scenario, which defines the wells' placements depending on the remaining oil saturation in place, locally and it is a fact that closer the fracture, provides more oil recovery until there is some transient interference with the other fractures. Therefore, a denser fracture network with closer fracture placement would be more considerable for optimum oil recovery. In addition, it is important to keep in mind while designing a fracture network, there will be an optimized fracture spacing and half-length for each scenario for a given set of reservoir characteristics. Figure 3.32 is showing the recovery performance comparison for three cases with 30, 50, and 70 feet

of fracture spacing, while keeping all the other reservoir and fracture specifications, fixed. A similar performance trend as fracture half-length is observed in this case i.e., more fracture spacing results in comparatively higher oil recovery. While the incremental oil recovery reduced with higher spacing because of limited oil in place. Therefore, it is worth concluding that the two parameters, fracture half-length, and spacing show a simultaneous impact on oil recovery performance as shown in a contour plot shown in Figure 3.33.

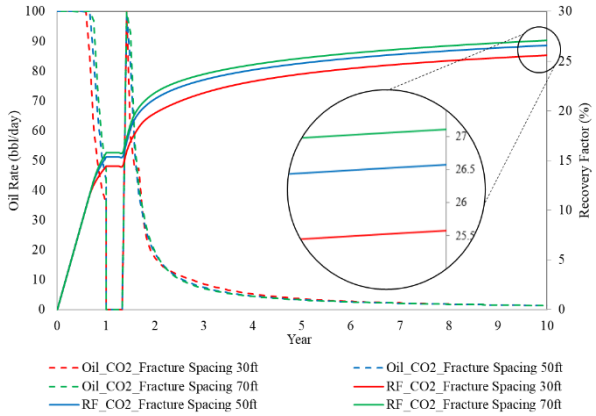

Figure 3.32 Comparing recovery performance for different fracture spacing

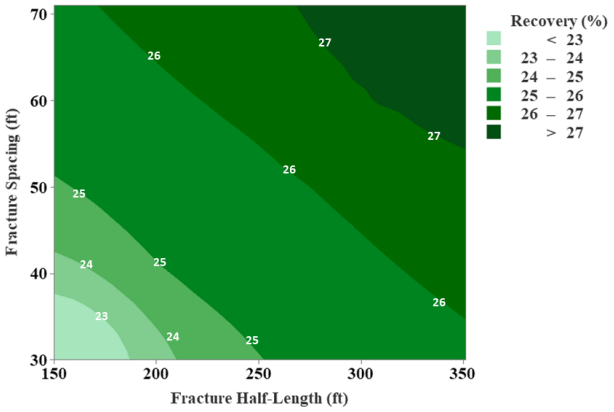

Figure 3.33 Simulation-based contour plot for the simultaneous effects of Fracture half-length and fracture spacing

3.6.2.4. Fracture Permeability

Fracture effective permeability is included in this study as the last sensitivity and one of the most important hydraulic fracture parameters that significantly determine the fluid flow from the tight reservoir. In general, the higher the fracture permeability, the higher will be the fracture conductivity and that will ultimately result in higher fluid flow and so the oil recovery. The dimensionless Fracture conductivity (F_cD) is given by the following correlation between fracture and reservoir matrix properties.

$$FcD = \frac{Fracture\ Permeability\ \times Fracture\ Width}{Matrix\ Permeabiltiy\ \times Fracture\ Half\ Length} \qquad Eq.\ 3.6$$

Figure 3.34 is showing the recovery performance comparison for three different fracture permeability values i.e., 30, 50, and 100 mD. Though the differences are not much but still there is an increasing trend that can be noticed such that to have higher recovery with the higher fracture effective permeability.

In addition, the simultaneous effect of fracture permeability and half-length is shown in Figure 3.35, as expected the increase in both parameters results in considerable improvement in the oil recovery. The figure is presenting

directional results for the given set of parameters; however, a similar trend should be expected from any other set of reservoir and fluid properties while developing a tight oil reservoir.

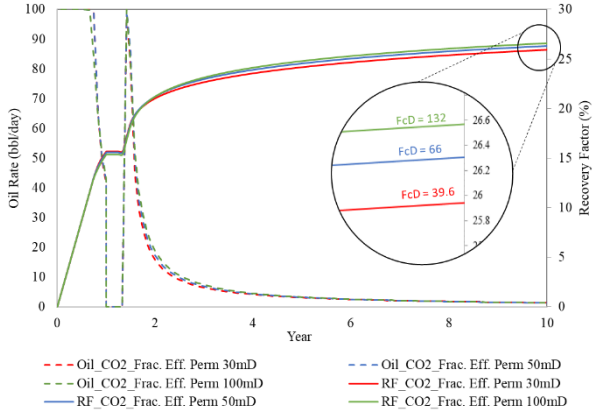

Figure 3.34 Comparing recovery performance for different fracture permeability and fracture conductivity

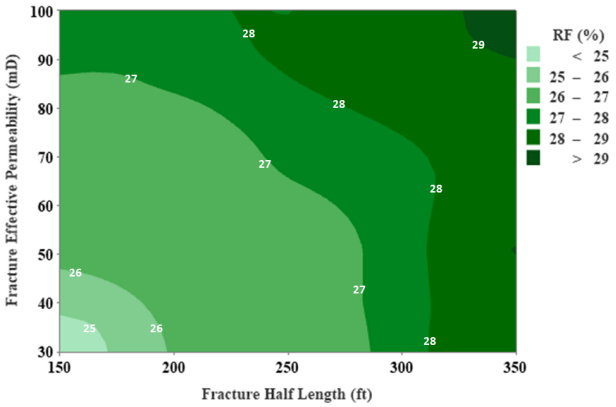

Figure 3.35 Simulation-based contour plot for the simultaneous effects of Fracture half-length and fracture permeability

3.6.3. Sub-Surface Injected Solvent Storage

CO_2 injection into the tight oil reservoirs not only plays an important role to improve oil recovery from the tight oil reservoirs but also helps to achieve the net carbon zero objectives through CO_2 footprint reduction from the planet earth. During the huff-n-puff process, a significant amount of injected CO_2 is usually produced back to the surface that is recycled into the reservoir to further improve the oil recovery. However, a significant amount of CO_2 stays back into the formation replaces oil, and gets trapped in the nanopore spaces. The CO_2 trapping mechanism is explained in the prior section i.e., through adsorption, desorption, and capillary force hysteresis. The combined effect of CO_2 adsorption, desorption, capillary force hysteresis, as well as the solubility of CO2 into the formation oil, became the reason for its trapping/ storage in the reservoir. The solubility of the injectant solvent causes swelling and the oil viscosity reduction that eventually helps to improve the oil recovery and along with the residual oil saturation, the additional amount of the solvent becomes trapped into the nanopores. It is observed in different studies that the phenomenon of CO_2 trapping is more pronounced when the solvent is injected at a pressure below its minimum miscibility pressure under reservoir conditions. A simple method to measure the total amount of CO_2 trapped in the formation is through retention factor that is defined as;

$$Retention = \frac{CO_2\ Remaining\ into\ the\ subsurface\ formation}{Total\ CO_2 Injected\ Volume} \times 100 \qquad Eq.\ 3.7$$

Reservoir temperature and pressure are critical parameters for the CO_2 trapping mechanism. Usually, the concept of retention is considered for the tertiary recovery (EOR) and higher retention is considerably obtained when the CO_2

is injected into a reservoir at or above MMP. Under such conditions, the injected CO_2 drives out the oil from the nanopores through dissolution into the oil which causes oil swelling and reduction in viscosity and interfacial tension. In this study, refer to Figure 3.22, there are the following facts to notice;

i. In each huff-n-puff cycle, not the complete amount of the injected CO_2 is produced back because of its trapping into the formation.

ii. The amount of trapped CO_2 increases for each ascending huff-n-puff cycle.

Using the limited statistics obtained from this study, a contour plot is prepared as shown in Figure 3.36 for an approximation of CO_2 trapping percentage as the function of injected CO_2 pore volume and the number of huff-n-puff cycles. It is obvious from the plot that both the parameters directionally improve the CO_2 trapping phenomenon. Multiple other parameters are also usually considered critical for the trapping mechanism such as reservoir geology, average reservoir pressure, injection pressure, soaking time, and the presence of aquifer or the formation brine, etc.

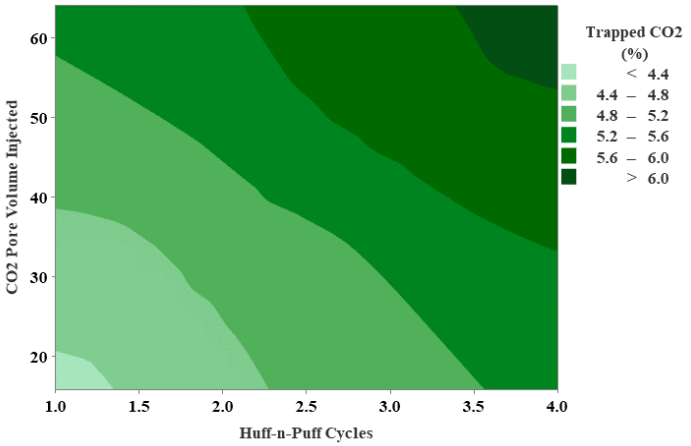

Figure 3.36 Simulation-based contour plot for the simultaneous effects of Fracture half-length and fracture permeability

3.7. Summary

A numerical simulation study is conducted to compare the recovery response from a tight oil reservoir for different injection solvents, operating conditions, and hydraulic fracture designs using the huff-n-puff technique. Purposely, this study is performed on a uniform reservoir model to eliminate the effects of heterogeneity such that to understand the physics at both micro and macro scales. The results are found marginally optimistic due to reservoir homogeneity and the size of the mechanistic model in comparison to the stimulated reservoir volume, however, the directional trends with the actual reservoir properties would remain the same. Following are a few conclusions that can be drawn;

1. Early application of EOR significantly improves oil recovery and based on the sensitivity analysis, CO_2 and the carbonated water injection significantly improve oil recovery from tight oil reservoirs.
2. Both, the injection solvent volume, and the additional number of huff-n-puff cycles significantly improve the oil recovery. The performance further improves from the reservoirs with lighter components.
3. The soaking time is critical for EOR, though, it helps to provide more time for diffusion and solubility, but the longer shut-in directly affects the economics.
4. Cluster count, fracture spacing, half-length, and fracture effective permeability are critically important parameters that are directly proportional to the recovery performance from a tight oil reservoir.

Huff-n-puff is an excellent technique that not only improves oil recovery significantly but also helps to achieve net carbon zero objectives through CO_2 trapping into unconventional reservoirs.

4

SPATIO-TEMPORAL DATABASE DEVELOPMENT

In this chapter, spatio-temporal database development is discussed using the history-matched compositional mechanistic model. For database development, multi-dimensional aspects are considered including reservoir rock and fluid properties, hydraulic fracture design parameters, and the EOR operational design. To accommodate a wide range of individual parameters, random sampling is performed using a design of experiment such that to develop a database for an entire range of magnitudes of each parameter using a limited number of simulation cases having random combinations of different parameters.

4.1. Introduction

The spatio-temporal database generation is the first and foremost important step towards the data-driven proxy model development. However, deciding the extent of the database representation for the reservoir matrix and fluid properties, hydraulic fracture design parameters, and the reservoir operational design limits for both primary as well as EOR is challenging. Therefore, it is recommended not to avoid any of these parameters to generate a meaningful and representative database that covers the entire possible range of multi-dimensional properties.

Usually, a database for a dynamic flow system includes the pairs of input and output datasets for the proxy model training process. For a dynamic system such as a reservoir simulation scenario, typically the static data is considered as the inputs such as reservoir and hydraulic fracture characteristics, initialization parameters, operational constraints, etc. while the outputs generally consist of the production data. However, in this study, not only the primary but also the EOR production is trained and that requires multiple additional parameters such as EOR agent/ injection fluid type, injection duration, soaking period, etc. which are also considered as the supplementary dynamic input parameters.

In addition, there are multiple assumptions and model limitations are kept under consideration for the simulation cases development as listed below;

1. A mechanistic homogeneous, isotropic, and isothermal reservoir model with a single distribution is designed.
2. The model is having a uniform reservoir thickness and consists of a single layer with 18 grid blocks in the z-direction.
3. The overall reservoir model dimensions are kept the same in all simulations i.e., L:230ft×W:1000ft×H:180ft.
4. A single horizontal well is placed at the center of the model with a single staged triple planner fracture perpendicular to the horizontal section of the well.
5. All three fractures are equally spaced along the horizontal section of the well.
6. All individual fractures are having the same design and characteristics for every individual simulation case; however, the fracture design varies for each simulation. The fracture properties include fracture conductivity, fracture half-length, fracture height, and fracture effective permeability.
7. Both, finite and infinite fracture conductivity values are assumed in different simulations to develop a variety of hydraulic fracture-driven flow behaviors. From the database development experience, the fracture

conductivity greater than 20 ft. mD produce optimum in-situ fluid recovery and the fractures are found to have infinite conductivity. A similar response for the dimensionless fracture conductivity (F_{cD}) is observed when its value is 50.

8. Wellbore storage and skin effects are not considered in the model.
9. For each simulation, the formation fluid is single-phase and slightly compressible with fixed PVT and rheological properties. However, for the database development, seven different reservoir fluid types are used representing most of the reservoir fluid compositions present in US unconventional tight oil reservoirs ranging between light and volatile to slightly heavier oils.
10. Depending on the reservoir and the hydraulic fracture design, linear and bilinear flow are observed during the early time region, while radial and compound linear flow are observed in the middle time region. Similarly, the late radial and boundary dominant flow regions are observed in the late time region. From the flow type perspective, in both formation and fractures, the laminar flow type is considered.

It is also important to understand that a petroleum reservoir is a pressure-driven system i.e., the production response (for both primary and EOR) is directly linked with the reservoir/ bottom hole flowing pressure and that is a dynamic property. Thus, in this study, input training parameters have not only included static but also dynamic properties are included. It is also important to make sure that the generated proxy models honor the physical laws and for that, its validation through blind sensitivities is essential.

The concept of Design of Experiment (DoE) is usually adopted to cover the entire possible range of multiple static and dynamic parameters such that to generate a meaningful database. However, for a dynamic system that works on physical law, is not necessary that the considered DoE would cover the entire range of the output response. Therefore, it is also significantly important to perform a quality check for the input parameters distribution as well as the output response of the system. For that purpose, a concept of a Physics guided Design of Experiment (PG-DoE) is introduced in this study that is focused on the output responses for the dynamic systems that follow the physical laws.

Figure 4.1 presents a schematic of a conventional DoE that shows the random distribution of the samples across the given range but for a physics-defined system, not necessarily; the simulated dynamic outputs cover the entire range. As shown in the following figure, the first output is a typical example of cumulative production while the

second output represents the instantaneous production rates over time with multiple missed spaces. Therefore, a DoE should be smart enough to generate data samples such that to cover the output response range more importantly than the input samples. In addition, the samples should be distributed in a way to avoid duplication of the output responses. Figure 4.2 presents an ideal output response that covers the entire range that also shows no overlapping of the output responses.

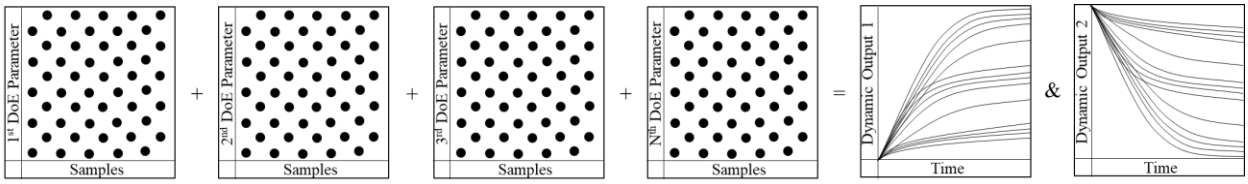

Figure 4.1 Schematic of a typical conventional Design of Experiment (DoE)

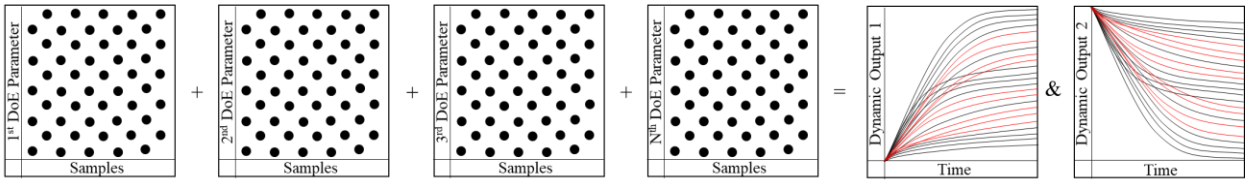

Figure 4.2 Schematic of an ideal Physics Guided Design of Experiment (PG-DoE)

4.2. Design of Experiment

The concept of DoE was introduced in the early 20th century to investigate the probabilistic behavior of static systems. DoE gained a lot of attention and become a normal practice in engineering that help engineers to reduce the computational cost, significantly. The samples of a given DoE are generated using a couple of approaches including domain-based (or non-adaptive or model-free) and the response-based (or adaptive or model-based or sequential) approaches. Multiple types of DoEs are mainly distributed in three types classical sampling (i.e., deterministic and space-filling), random sampling, and Quasi-random sampling. Figure 3 is showing a detailed distribution of different types of DoEs.

4.3. Samples Distribution & Quality Control

In this study, the sampling distribution is performed using Latin Hypercube (LHS) DoE. It is one of the most widely used random sampling techniques for the proxy modeling approach that evenly distributes samples over a given sampling space. The samples generated using the LHS technique are known as controlled random samples that are often applied in Monte Carlo uncertainty quantification analysis because it can dramatically reduce the number of

simulations that need to achieve accurate results. Similarly, for a huge database development using a deterministic simulation approach, LHS help to reduce the sampling points significantly. In this study, initially through a factorial approach, thousands of organized samples were generated because of a wide range of every individual parameter that was reduced to around eight hundred samples through the LHS sampling technique that was used to generate the numerical simulation database.

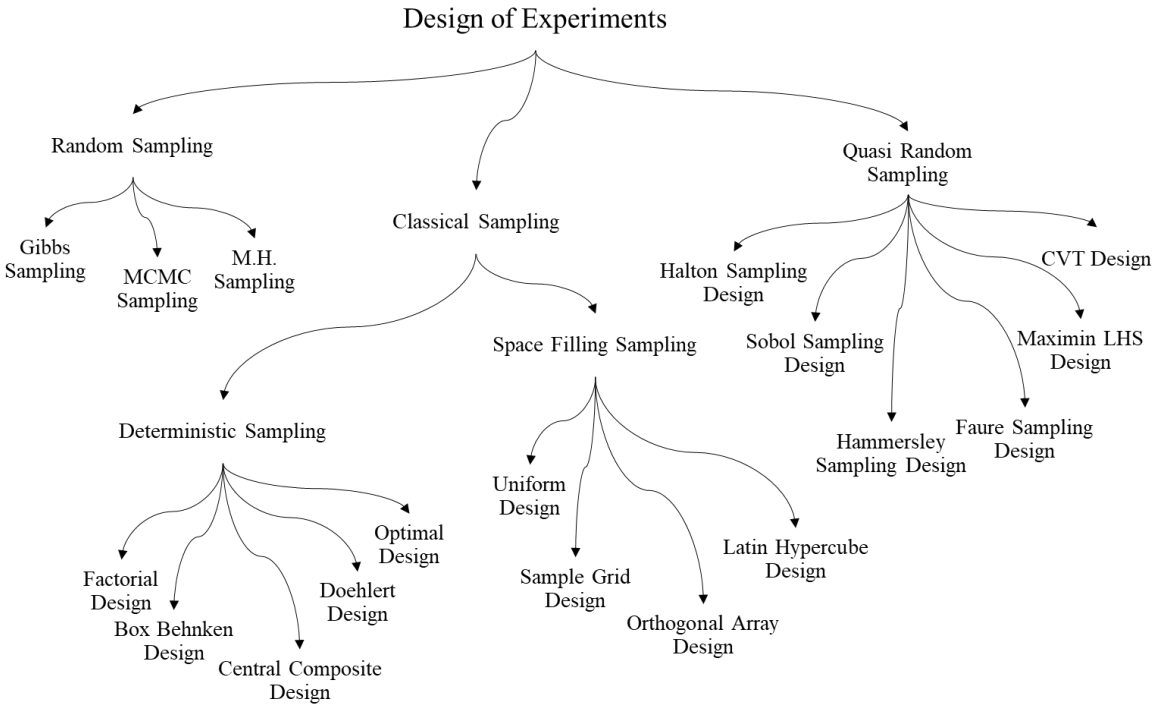

Figure 4.3 Different types of design of experiments for data sampling

As explained in the prior sections, multiple parameters control the fluid flow response from a tight oil reservoir. Therefore, the database for this work is developed using a random distribution of the major reservoir parameters including reservoir pressure, matrix porosity & matrix permeability and hydraulic fracture design, fracture half-length, fracture height, and fracture conductivity, etc. which mainly play the most critical role in flow dynamics. The following figures are presenting the cumulative probability and the probability mass distribution of the subject parameters in both Y-axes and their sampling range on the X-axis. The actual samples found from the literature are also included in all the figures that are overlaying the cumulative probability distribution plot for a quick sampling distribution comparison.

For both primary and enhanced oil recoveries from tight formations, apart from the reservoir and the hydraulic fracture characteristics, the reservoir fluid type and the reservoir pressure play a critical role in the reservoir fluid recovery. Therefore, a wide range of reservoir pressure is considered in this study ranging between 4000 to 12000 Psi. Figure 4.4 is presenting the normal/ Gaussian distribution of reservoir pressure values for the given range. It is important to note that the actual reservoir pressure values are found more towards the lower end which lies between the P50 to P90 range of the distribution of the sample. But still, there are a few reservoir pressure points found at the upper bound which is why an extended pressure range is taken under consideration for the database generation.

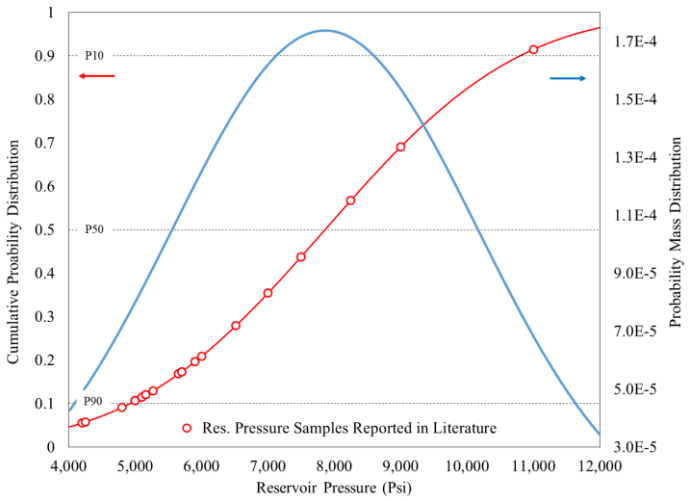

Figure 4.4 Random sampling distribution – Reservoir Pressure

Similarly, Figures 4.5 and 4.6 are presenting the sampling distribution for the reservoir matrix porosity and permeability. Most of the tight oil reservoirs in the United States are found with a variety of matrix porosity that was typically found between 4 to 12% and it is noticeable in the following figure that the porosity values are uniformly distributed across the entire considered range. While the reservoir matrix permeability is found to be very tight i.e., mostly ranging between 0.0001 to 0.05mD.

Similar considerations are applied to generate random sampling data-point distribution for the hydraulic fracture design parameters. Figure 4.7 through Figure 4.10 are presenting the random data sampling distribution and their cumulative mass distribution for fracture permeability, fracture conductivity, fracture half-length, and fracture height, respectively.

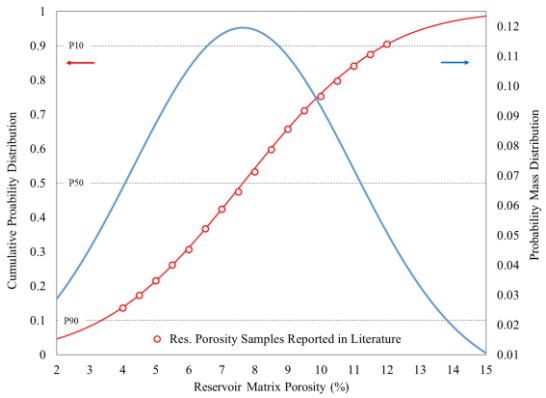

Figure 4.5 Random sampling distribution – Matrix Porosity

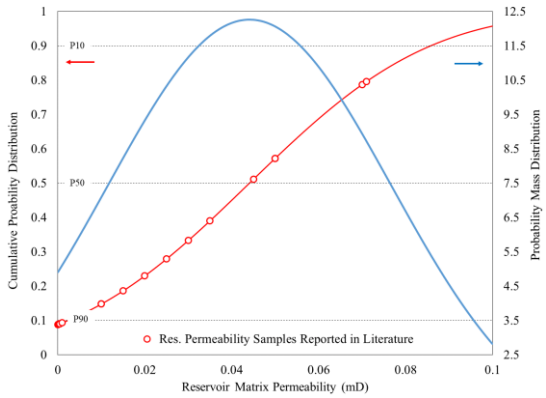

Figure 4.6 Random sampling distribution – Matrix Permeability

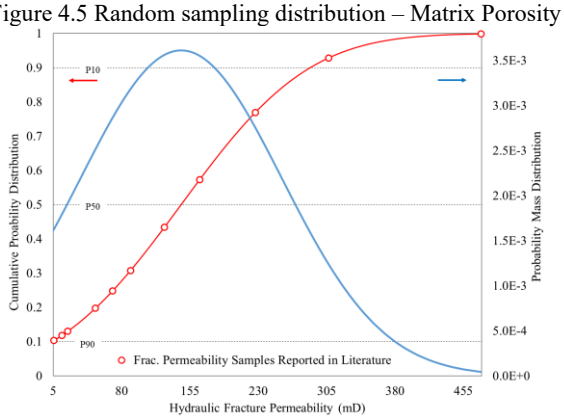

Figure 4.7 Random sampling distribution – HF Permeability

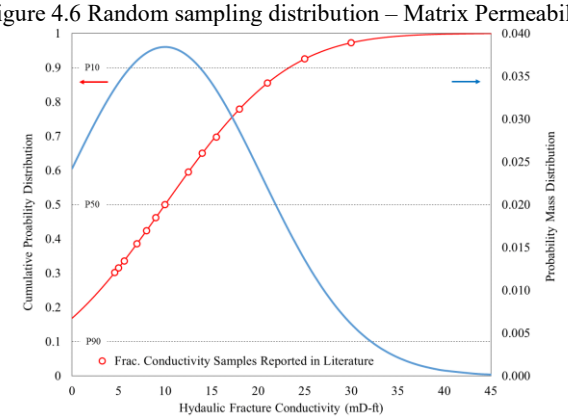

Figure 4.8 Random sampling distribution – HF Conductivity

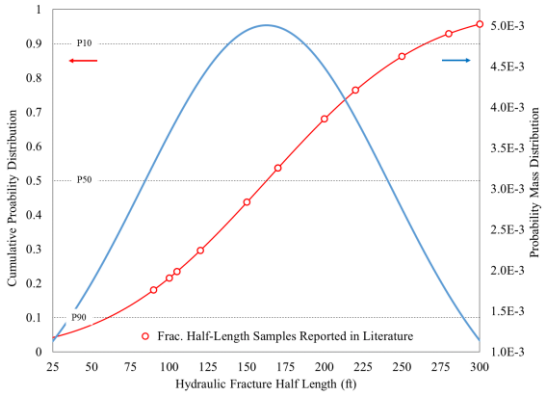

Figure 4.9 Random sampling distribution – HF Half-Length

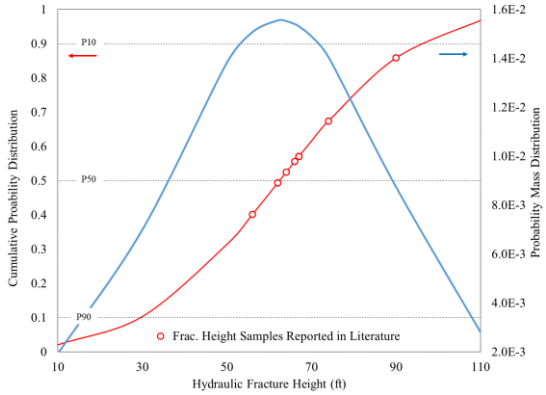

Figure 4.10 Random sampling distribution – HF Height

4.3.1. Sampling Quality Control

The data sampling quality control is performed in two major steps i.e., Pre and Post simulations sampling quality control.

Step 1: As the reservoir fluid types are the basic and the most important factor of the generated database, therefore the pre – simulation quality control is performed initially on the distribution of the random sample through visual inspection for every individual parameter corresponding to each fluid type to make sure that the samples are

randomly distributed all over the sampling space. In addition, it is to make sure that cumulatively all the samples are randomly distributed majority of the sampling space with no major blank area in the sampling space.

Step 2: The post-simulation quality control step explains the physics-based design of the experiment such that to have simulation response of the entire database is evenly distributed as discussed in the prior section.

Figures 4.11 and 4.12 are schematically presenting the pre- and post-random data sample distribution quality checks. In the first figure, different parameters are represented through dissimilar colors that are distributed with the correspondence of multiple fluid types such that to have random distribution to cover the entire sampling space without any major overlapping of the samples. Similarly, the second figure shows the simulation response of multiple output responses. The number of output responses may vary in different cases; however, the simulation response mainly signifies the sample distribution qualitatively and quantitatively.

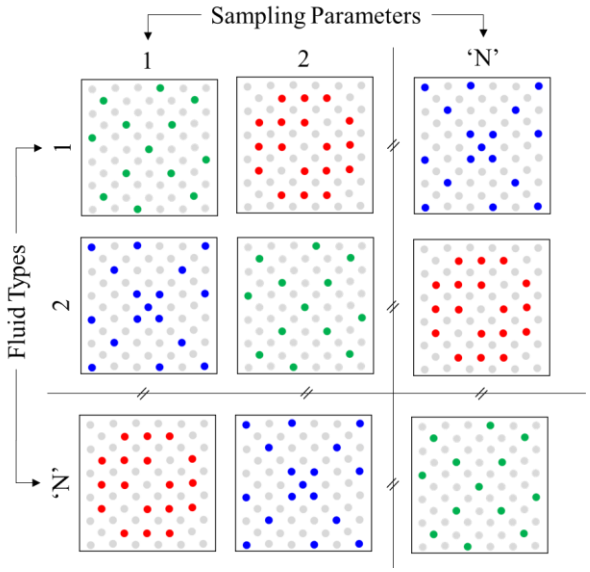

Figure 4.11 Pre-simulation random data sampling quality check through visual samples distribution

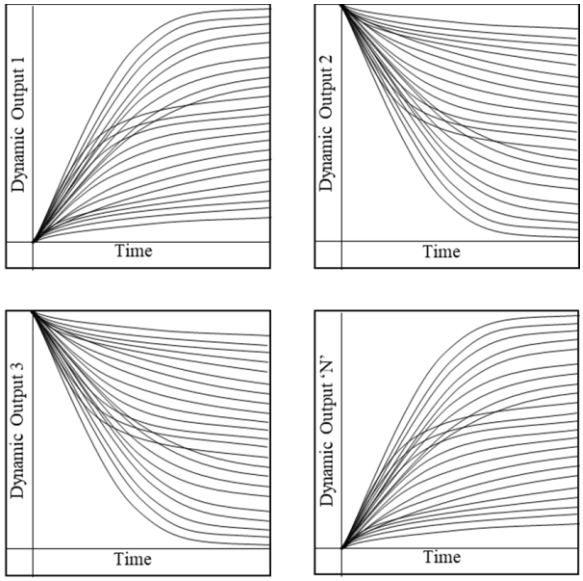

Figure 4.12 Post-simulation random data sampling quality check through dynamic simulation response

4.3.2. Pre and Post Simulation Sampling Quality Check

Using the discussed approach, initially, all the data samples were randomly distributed using the LHS sampling technique without distinguishing or dominating any reservoir/ hydraulic fracture parameter or the fluid types followed by a manual sampling distribution check for all parameters with different reservoir fluid types. A few of the considered parameters are shown below in Figure 4.13.

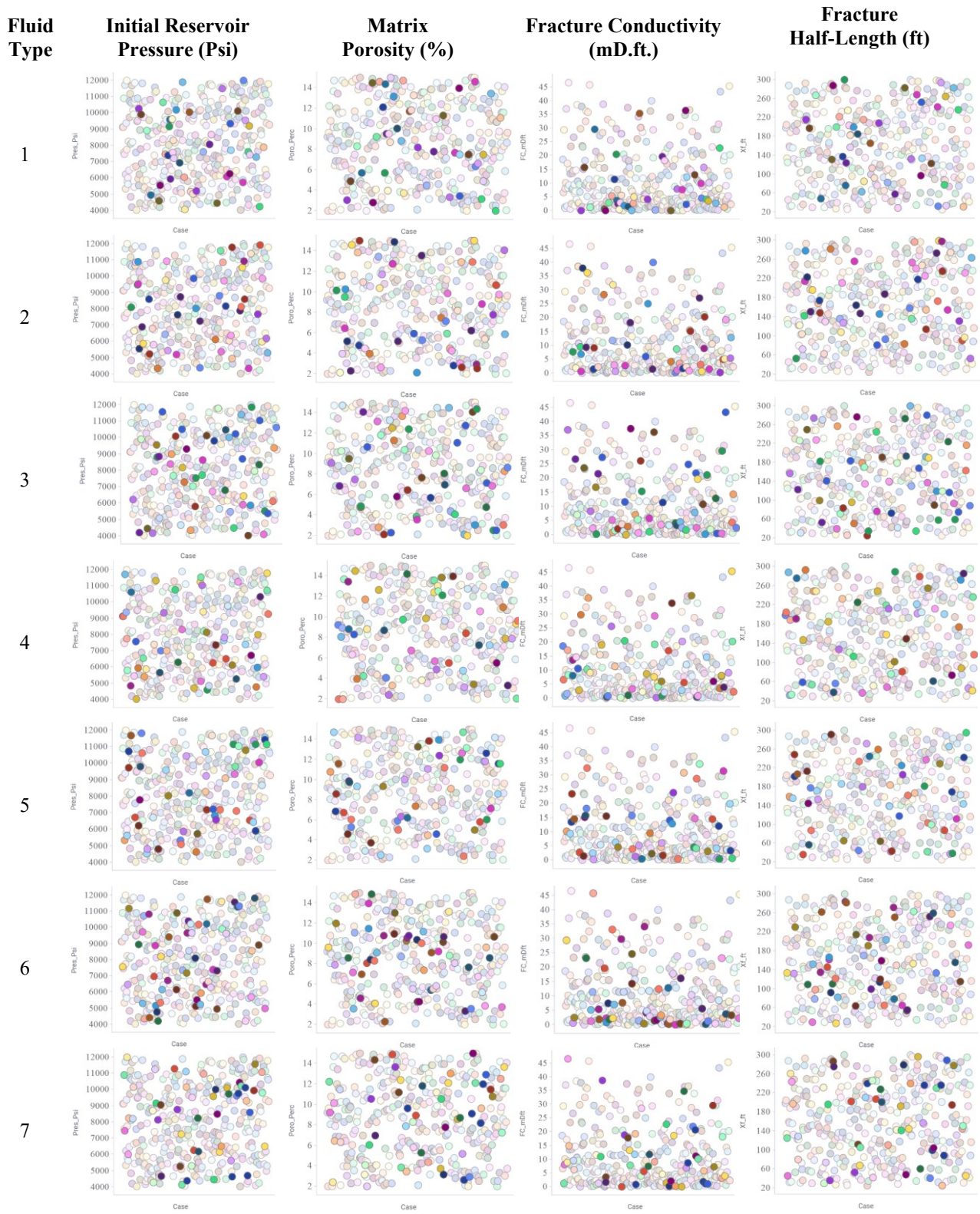

Figure 4.13 Pre-simulation random data samples distribution corresponding to different reservoir fluid types

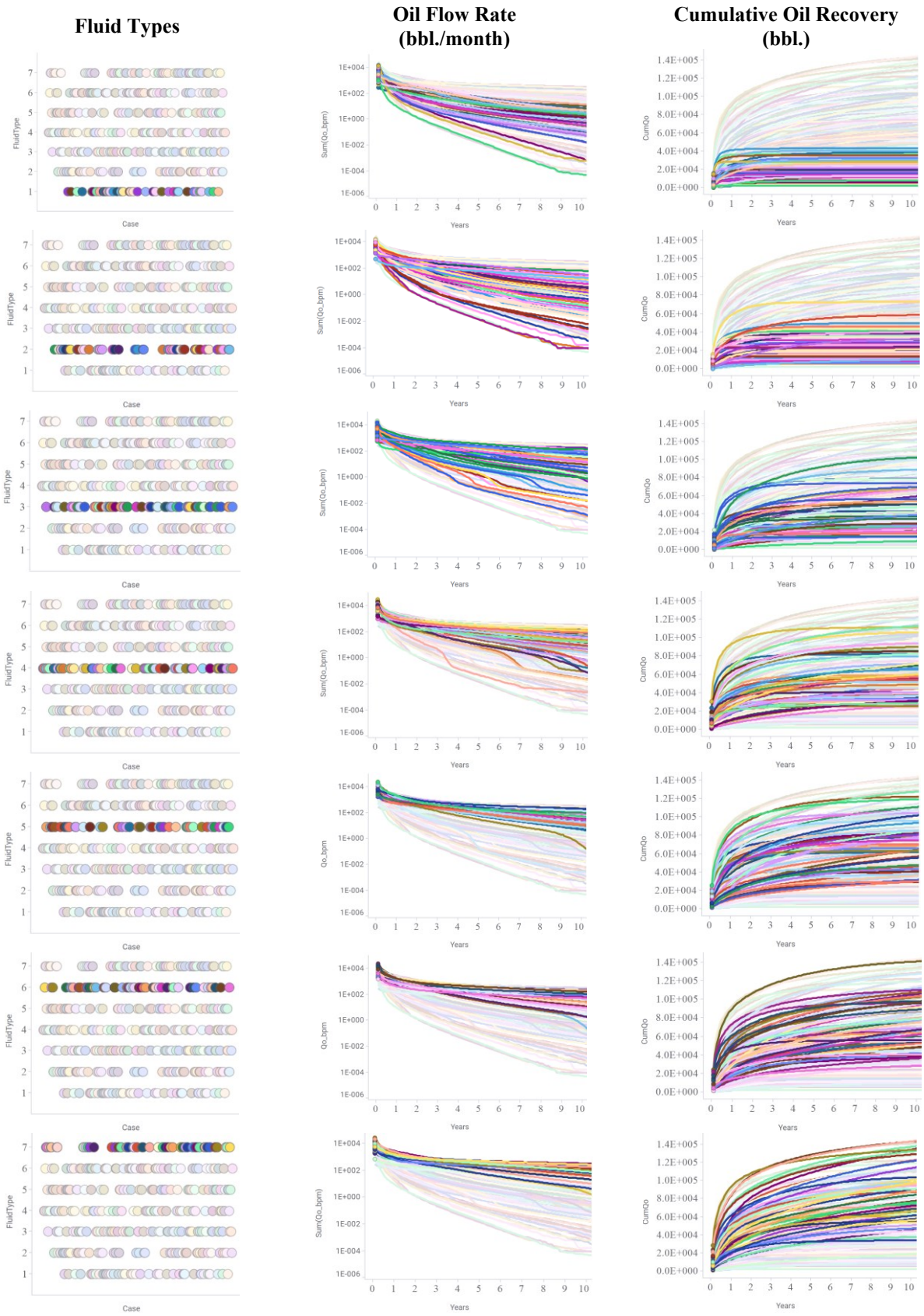

Figure 4.14 Post-simulation responses (oil flow rate & cum. Oil production) corresponding to different reservoir fluid types

4.4. Discussion

In the prior sections of this chapter, the steps and the quality of spatial-temporal database development are discussed. In addition, it is highlighted that not only the random distribution of the input parameters is important, but the simulation response/ outputs are more important to developing a physics-inspired database generation for the proxy models development.

In this section, another approach is adopted for the database quality check through reservoir recovery responses that are established as the resultant factor for the combination of the different reservoir and hydraulic fracture parameters. The objective is to develop a physical understanding of the subject parameters with the reservoir recovery response and to make sure that the recovery responses are unbiased towards any specific reservoir or hydraulic fracture property.

Following is the list of parameters and their distribution ranges used for the recovery responses. It is important to note that, the recoveries shown in Figure 4.15 are the result of the combination of the reservoir and hydraulic fracture parameters. While the incremental oil recovery is the response of not only the reservoir and hydraulic fracture parameters but also the EOR operational design including the EOR solvent injection volume and the injected solvent soaking period.

Table 4.1 Reservoir and hydraulic fracture parameters range distribution for model's recovery response representation

Parameter	Low Range	Medium Range	High Range
Reservoir Fluid Types (Ref. Figure 3.11)	1 – 2	3 – 4	5 – 7
Initial Reservoir Pressure (Psi)	4000 – 6000	6000 – 9000	9000 – 12000
Hydraulic Fracture Half-Length (ft.)	25 – 100	100 – 200	200 – 300
Hydraulic Fracture Conductivity (ft. mD)	0.02 – 1	1 – 10	10 – 50
Hydraulic Fracture Height (ft.)	10 – 30	30 – 60	60 – 110
Matrix to Fracture Permeability Ratio	$<1\times10^{-6}$	1×10^{-6} - 1×10^{-5}	$> 1\times10^{-5}$

It can be noticed from the following figures that reservoir fluid type is influencing both primary and incremental oil recoveries i.e., comparatively higher oil recovery from heavier reservoir fluid

type. Partially the same effect of fracture conductivity is observed such that, higher fracture conductivity produces more oil from the reservoir. Rest all other parameters show no major influence on oil recovery.

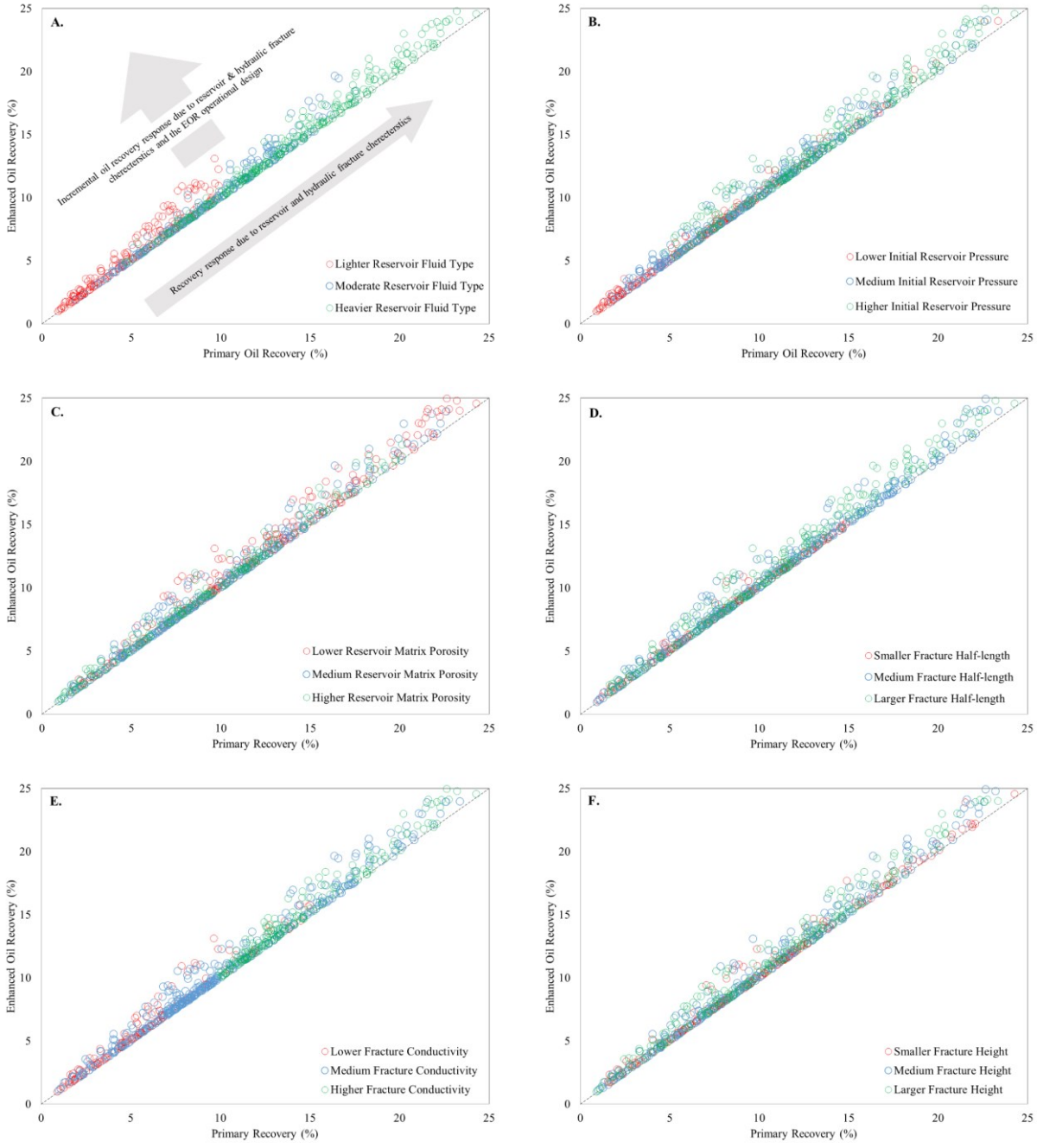

Figure 4.15 Primary and enhanced oil recovery cross-plots as the function of (A) Reservoir Fluid Type (B) Initial Reservoir Pressure (C) Matrix to Fracture Permeability Ratio (D) Hydraulic Fracture Half Length (E) Hydraulic Fracture Conductivity (F) Hydraulic Fracture Height

5

SMART PHYSICS-INFORMED COMPOSITIONAL DIMENSIONLESS TYPE CURVES

Smart Physics Inspired Compositional Dimensionless Type Curves (SPiC TC_D) is a novel technique for the Unconventional Enhanced Oil Recovery (UEOR) pilot designing and its performance analysis that are developed using a huge compositional numerical simulation-based database. The dimensionless type curves for the UEOR are developed as an extension to the primary recovery using modified Fetkovich RTA for a multi-fractured horizontal well in tight permeability formations. In this chapter, the development and interpretation of the SPiC TC_D are discussed. Also, a generalized end-user poster is compiled in this chapter discussing all possible scenarios with different reservoir rock properties, in-situ fluid types, hydraulic fracture design, and the EOR operational designs for a quick and effective primary and UEOR performance match and incremental hydrocarbon recovery predictions.

5.1. Introduction

Unconventional tight oil reservoirs are found with a fine pore network structure, poor interpore-connectivity, and limited pressure support. Therefore, the development of such reservoirs is only considered economical through long horizontal wells aided with massive mechanical stimulation i.e., an artificially induced hydraulic fracture network that provides easy fluid flow channels deep into the reservoir matrix for the sub-surface reservoir hydrocarbons to produce from the tight matrix and nano-pores (Syed, F.I., *et al.*, 2022).

An unsaid rule of thumb for a healthy and economical reservoir development is to perform reservoir diagnostics locally on every individual producer to understand the reservoir fluid flow signatures (Lin, M., *et al.*, 2015). These signatures are found in the form of fluid flow responses that not only distinguish different reservoir and wellbore characteristics but also characterize hydraulic fracture design parameters. The common approach for such diagnostics is through pressure-time relationships (commonly called Pressure Transient Analysis or PTA) that provide comparatively better and focused reservoir characterization due to high-resolution pressure data. While another approach is based on a rate-time relationship (commonly called Rate Transient Analysis or RTA). RTA is performed using low-resolution pressure data that lumps up the entire production life of a well into the analysis (Jiang, R., *et al.*, 2014).

The biggest drawback of PTA is the loss of hydrocarbon production because the high-resolution pressure data is normally collected in response to a producer shut in. On the other hand, RTA is performed with the production rate data (hence no need to shut in a producer) while the reservoir and the wellbore flowing pressures are embedded in the dimensionless flow rate and time equations. The working phenomenon of RTA is based on the combination of Darcy's law for fluid flow in porous media with the equation of state (EoS), and the Material Balance Equation (MBE). The same analysis could be performed analytically through Partial Differential Equations (PDEs). However, RTA is performed through a rate-time relationship but still, it incorporates pressure into the flow performance diagnostics. Therefore, for tight reservoirs, RTA is the only suitable option because the wells drilled in such reservoirs with limited

pressure support show rapid pressure decline locally due to poor interpore connectivity and do not provide enough high-resolution pressure data.

It is important to highlight that there are several well-performance behaviors can be observed for horizontal wells drilled in a reservoir depending on reservoir characteristics, including both reservoir fluid and rock properties, and the stimulated hydraulic fracture designs. The main hydraulic fracture design parameters include but are not limited to fracture half-length, fracture height, fracture effective permeability, fracture conductivity, etc. (Syed, F.I., *et al.*, 2022). In this chapter, initially, the conceptual numerical compositional simulation model is presented for a combination of reservoir characteristics and a single staged – triple clustered hydraulic fracture. In the following step, a detailed understanding is developed through several simulation cases for all possible flow responses resulting from a reservoir model with the combination of different reservoir fluid & rock types and hydraulic fracture designs. The exact range of the model's parameters is the same as discussed in the prior chapter to generate a numerical simulation database using a random sampling technique called Latin Hypercube Sampling.

The impacts of multiple combinations are studied through multiple sequences of flow regimes that could be obtained from a tight oil reservoir. Lastly, novel and advanced flow responses for an additional factor of EOR application in tight oil reservoirs are presented. The EOR application showed interesting flow responses that are significant for an unconventional tight oil reservoir development and due to the rapid production decline, it is wisely suggested to develop tight oil reservoirs with early-life EOR applications. However, due to the complex and locally isolated nature of tight reservoirs, huff-n-puff is the most suitable option and due to poor injectivity because of the tight nature of the matrix, not many EOR options are recommended except CO_2 and hydrocarbon gas injection.

These physics-informed flow responses are presented in the form of dimensionless type curves in log-log plots that generalizes the effects of reservoir fluid types, reservoir rock properties, hydraulic fracture design, EOR type, and the EOR operational design for any tight oil reservoir. For the first time in the oil industry, a detailed set of smart physics-informed compositional dimensionless type curves for

unconventional EOR applications are presented, and lastly, a generalized set of dimensionless type curves diagnostics are presented for easy and quick understanding of the reservoir fluid flow response based on any possible combination of the reservoir, hydraulic fracture, and EOR operational characteristics.

5.2. Typical Flow Regimes

As discussed earlier, the proper identification and interpretation of the sequence of flow regimes are very important to determine the most possible flow event. The flow regimes sequence is always found critical for multi-fractured horizontal wells because the interpreted flow response could be because of single or multiple factors including reservoir characteristics or the hydraulic fracture design. In addition, the effect of EOR operation could also be another factor resulting in a flow response. Therefore, proper interpretation of each flow response is necessary. Figure 5.1 is presenting the typical flow regimes encounter from the hydraulically multi-fractured horizontal wells plotted on a log-log scale.

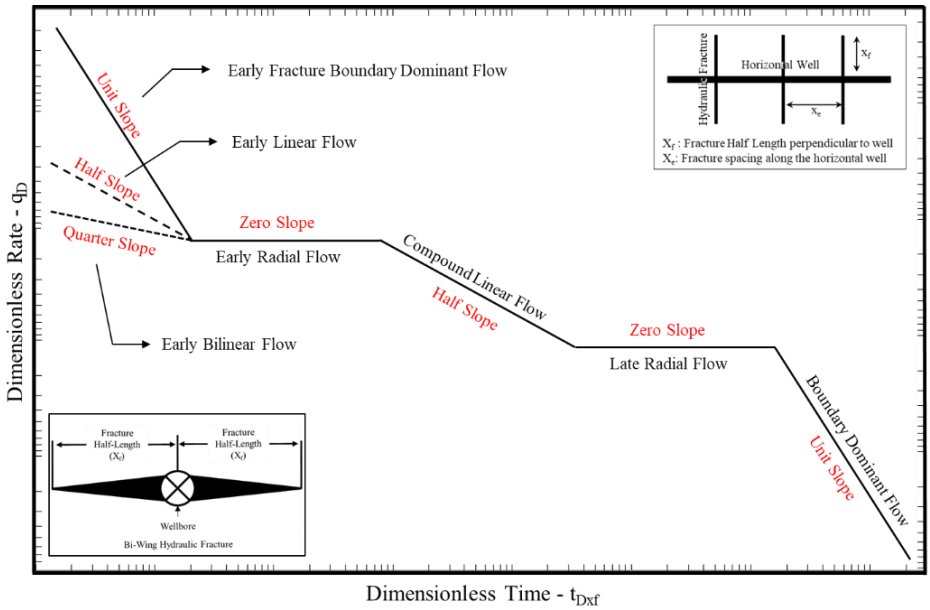

Figure 5.1 Schematic of typical flow regimes sequence encounter for a hydraulically multi-fractured horizontal well in a homogeneous reservoir

The early fracture boundary dominant flow (unit slope on a log-log plot) may occur for the light and volatile reservoir fluid types with high compressibility to represent the early pseudo-steady state flow. This effect is noticed when the flow transient reaches the hydraulic fracture boundaries that act as a no-flow boundary. Similarly, early bilinear fracture flow is a common observation with the quarter slope on a

log-log scale for hydraulic fractures with greater fracture half-length than the fracture height. The flow is called bilinear because two linear flow behaviors occur simultaneously i.e., a linear flow from matrix to fracture and the linear flow from fracture to a wellbore.

Similarly, an early linear flow with a half slope may occur for the infinite fractures with higher effective fracture permeability and fracture conductivity such that the pressure distribution in the entire fracture is theoretically found equal. During the early time flow region, after early linear flow, early radial flow is another flow regime that could be observed with zero slopes on the same scale only when the hydraulic fractures are far apart. Early radial flow occurs right after the early linear flow, and it ends as soon as the flow interference between two consequent fractures starts.

During the middle time region, the compound linear flow with a half slope may be observed representing the interference of fluid flow from multiple fractures. This flow type is only possible with larger well spacing in the same flow region and it lasts as soon as the flow transients from different wells interfere with each other.

Lastly, zero and unit slopes are possibly observed representing the late radial and boundary dominant flow regimes, respectively. The late radial flow can only be observed in an undeveloped field or a field with wells drilled very far apart because this flow regime requires an extremely long time to develop without any pressure transient interference. While the boundary dominant flow occurs due to pseudo-steady state flow in the late time region when the pressure transient hits any type of no-flow boundary including sealing fault, or the no-flow caused due to nearby producing wells. Further details on the discussed observations are listed in Table 5.1.

Table 5.1 Flow regimes for multi-fractured horizontal wells

Flow Regime	Slopes	Event
Early Fracture Boundary Dominant Flow	Unit Slope	Early pseudo-steady state flow occurs, with lighter/ volatile reservoir fluid type having high compressibility when the flow transient reaches the fracture boundaries that act as no-flow boundaries. This effect is only dominant in early time with higher hydraulic fracture conductivity and fractures size causing hydraulic fractures to behave as a tank and that causes pressure in the SRV region to decrease at the same.
Early Bilinear Fracture Flow	Quarter Slope	Bilinear fracture flow occurs in hydraulically fractured horizontal wells with finite fracture conductivity and when $X_f > H_f$. In this flow regime, two types of linear flow occur one from the matrix to the fracture and one from the fracture to the wellbore.
Early Linear Flow	Half Slope	Linear fracture flow occurs in hydraulically fractured wells when the conductivity of the fracture is infinite. In this situation, the permeability of the fracture is so high that the pressure throughout the fracture is constant.
Early Radial Flow	Zero Slope	It would be observed after the end of the Early Linear Flow i.e., linear flow from matrix to fractures, but before the fractures start interfering with each other. It is only seen if the fractures are far apart and are not likely to be observed with the close fracture spacing.
Compound Linear Flow	Half Slope	Once the fractures have interfered with each other, compound linear flow may be observed. It is defined by the flow from an outer zone towards the region stimulated by the fractures. This can be observed in fields where well spacing is sparse. However, with close well spacing, it will not be observed before interference from adjacent producing wells occurs.
Late Radial Flow	Zero Slope	This flow regime will only be observed if the well exists all alone, in an undeveloped field, and would require an extremely long time and area to develop in tight unconventional formations. As such, it is unlikely to be observed in practice.
Boundary Dominant Flow	Unit Slope	Pseudo-steady state (PSS) flow occurs during the late time region when the outer boundaries of the reservoir are all no-flow boundaries. This includes not only the case when the reservoir boundaries are sealing faults, but also when nearby producing wells cause no-flow boundaries to arise. During the PSS flow regime, the reservoir behaves as a tank. The pressure throughout the reservoir decreases at the same, constant rate

5.3. Smart Physics Informed Dimensionless Type Curves for Primary Recovery

Starting with J.J. Arps's empirical Decline Curve theory explained in the 1940s, a comprehensive set of equations was introduced defining the exponential, hyperbolic, and harmonic declines (Arps, J.J., 1945). The concept was further investigated by multiple researchers for their specific needs and defined circumstances. Brons and Miller in the early 1960s (Brons, F. and Miller, W.C., 1961) Fetkovich in the late 1980s (Fetkovich, M.J., *et al.*, 1987) applied constant pressure solution to the diffusivity equation and after several realizations, claimed that the exponential decline curve successfully represents the single phase, incompressible fluid flow from a closed/ finite system. It was a breakthrough moment for the industry to find out that decline curve analysis (DCA) is more than an empirical curve fitting method. Fetkovich further extended his work and introduced dimensionless type curves to enhance the application of DCA that is conventionally being used for the near-well bore reservoir permeability and the wellbore skin measurements analytically. Fetkovich's methodology provides a combined solution for the early-time region and the late-time region that represent the transient flow and the boundary-dominated flow, respectively, that were originally introduced by Arps in his decline curve theory.

The Fetkovich type curve presenting the early-time region characterizes an infinite-acting reservoir that provides a constant-pressure analytical solution of transient flow equations, while the late-time data is determined through Arps's decline curves using boundary-dominated flow equations based on empirical exponential, hyperbolic, and harmonic decline curve solutions (Fetkovich, M.J. 1973). During the mid-1990s, Doublet and Blasingame introduced a theoretical basis for combining transient and boundary-dominated fluid flow for the pressure transient solution to the diffusivity equation (Doublet, L.E. and Blasingame, T.A. 1995). After several advancements, the dimensionless type curves become a routine practice for reservoir characterization through reservoir fluid flow behavior analysis.

For a horizontal well with multiple fractures, the dimensionless type curves are represented on a log-log scale as dimensionless flow rate (q_D) versus dimensionless time (t_{Dxf}) (Gringarten et al., 1974; Chen and Raghavan, 1997). The equations for dimensionless liquid rate and time are shown below;

$$q_{Do} = \frac{141.2\ q\ B\ \mu}{k_{SRV}\ h\ (P_i - P_{wf})} \qquad Eq.5.1$$

$$t_{Dxf} = \frac{0.00633\ k_{SRV}\ t}{\emptyset\ \mu\ C_t\ x_f^2} \qquad Eq.5.2$$

Similarly, the dimensionless gas rate and time equations are given below;

$$q_{Dg} = \frac{1.417 \times 10^6\ q\ T}{k_{SRV}\ h\ (P_{pi}^* - P_{pwf}^*)} \qquad Eq.5.3$$

$$t_{Dxf} = \frac{0.00633\ k_{SRV}\ t_a^*}{\emptyset\ \mu\ C_t\ x_f^2} \qquad Eq.5.4$$

where; q is the reservoir fluid flow rate, B is the formation volume factor, μ is the produced fluid viscosity, k_{SRV} is the permeability of the stimulated reservoir volume, h is the net pay thickness, T is the reservoir temperature, Pi and Pwf are the initial and bottom hole flowing pressure, respectively, t represents time, t_a is the modified pseudo-time to account for slippage effect for the gas production, similarly P^*_{pi} and P^*_{wf} represent the modified pseudo-pressure considering the slippage effect while gas production at initial conditions and the wellbore flowing pressure, respectively. Lastly, Ø is the formation porosity while C_t and x_f represent total compressibility and the fracture half-length, respectively.

A huge database is generated using numerical simulation (as discussed in chapter 04) for the physics-informed dimensionless type curves database development. The subject database is developed using an isothermal and homogeneous mechanistic reservoir model equipped with a single horizontal well aided with a single staged, triple clustered planer hydraulic fracture. The database is developed using multiple simulation scenarios considering a defined range of reservoir fluid types, reservoir matrix characteristics, hydraulic fracture design parameters, and multiple operational designs.

Figure 5.2 to 5.4 are presenting the combination of dimensionless type curves for different reservoir fluid types, namely FT1 to FT7 representing lighter to heavier fluid types, respectively (further details on fluid types are provided in chapter 3). It is noticeable that the type curves become leaner as the fluid type

becomes heavier and from the positioning perspective, the curves vertically shift upward as the reservoir fluid becomes heavier. Apart from the reservoir fluid types, the effect of different reservoir matrix porosity is also prominent in Figure 5.2 such that the type curves shift horizontally towards the left for increasing reservoir matrix porosity. The similar effects of hydraulic fracture half-length are shown in Figure 5.4. The overall effect of porosity and fracture half-length is similar on type curves shape and their placement as both provide near wellbore and near hydraulic fracture reserves to produce.

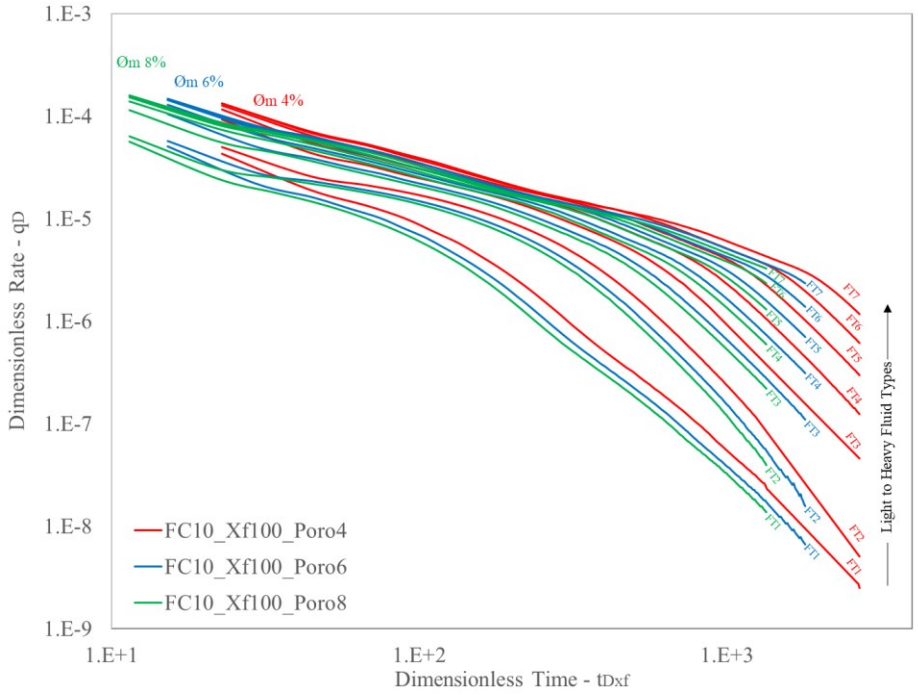

Figure 5.2 Typical dimensionless type curves for a multi-fractured horizontal well showcasing the effect of different reservoir fluid types and reservoir matrix porosity.

For all scenarios, early-time linear flow is a common observation represented by ½ slope that depicts the in-situ fluid flow from the reservoir matrix to the hydraulic fractures. Also, the bilinear flow, representing fluid flow from matrix to fracture and the flow from fractures to the wellbore, is a common observation for long horizontal wells with large hydraulic fractures. The impact of fluid flow from fractures would not be significant for the smaller fractures. Similarly, late-time boundary dominant flow represented through unit slope is another common observation regardless of the reservoir characteristics and the hydraulic fracture design as well as the fluid type. In addition to the prior observations, Figure 5.3 and Figure 5.4 represent the effects of hydraulic fracture half-length and conductivity on the dimensionless type

curves shape and their shifts both vertically and horizontally. A detailed discussion on the slopes of every individual flow region according to the reservoir formation and hydraulic fracture characteristics is presented in the later section.

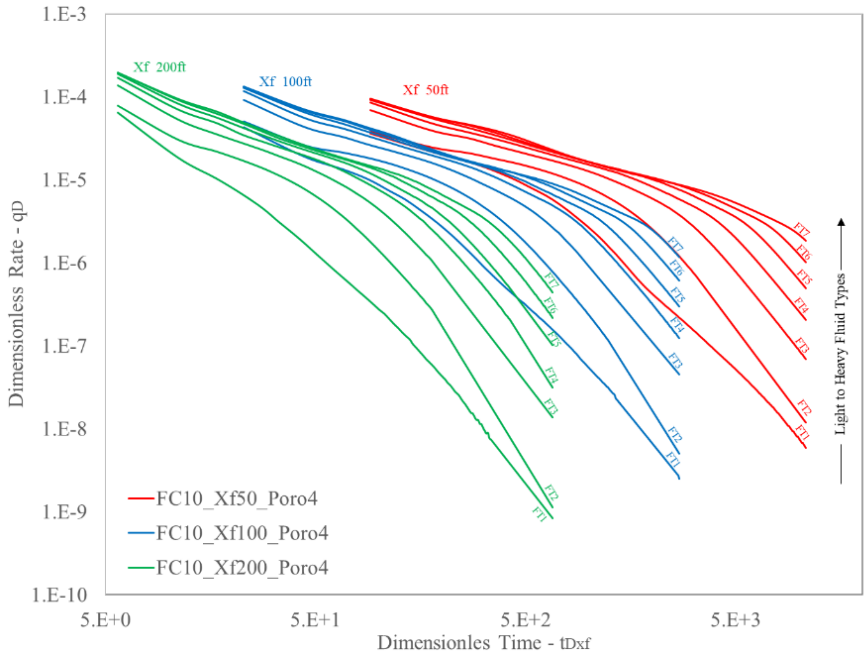

Figure 5.3 Typical dimensionless type curves for a multi-fractured horizontal well showcasing the effect of different reservoir fluid types and hydraulic fracture half-length.

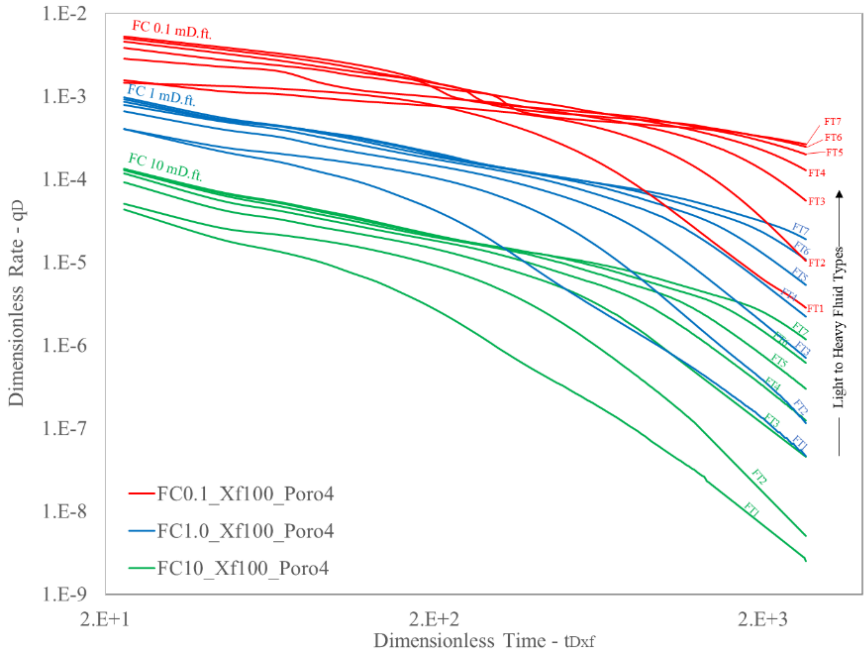

Figure 5.4 Typical dimensionless type curves for a multi-fractured horizontal well showcasing the effect of different reservoir fluid types and hydraulic fracture conductivity.

5.4. Unconventional Enhanced Oil Recovery – Fluid Flow Response

Starting from the primary recovery fluid flow behavior and their possible responses for the closed boundary reservoir system with a horizontal well aided with multiple fractures, the next step is to apply EOR application such that to improve the oil recovery. Figure 5.5 represents the operational design schematic that initiates with primary recovery followed by injection and soaking. Finally, the producer is kept in production for the enhanced oil recovery until the set economic limits. Every operator follows a different operational design such that after a certain level of primary recovery based on the well flow performance or the economic limits, the EOR application is initiated that starting with the EOR solvent injection. The injection period is a critical step that depends on the injection fluid volume, injection rate, and maximum injection pressure. The injection pressure typically ranges between 75 to 85% of the initial or the current average reservoir pressure such that to avoid hitting the formation fracture pressure.

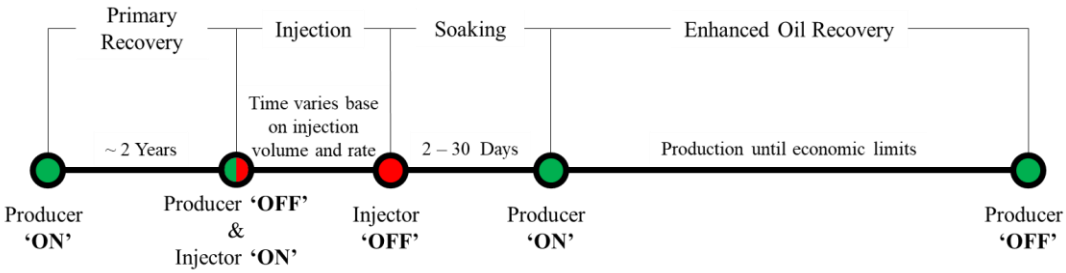

Figure 5.5 Typical Enhanced Oil Recovery operational design

It is obvious from the prior discussion and the observations made in Figures 5.2 to 5.4 that the reservoir fluid types play an important role in reservoir fluid flow performance. Therefore, it is important to review the effects of EOR applications under different circumstances, most importantly with different reservoir fluid types. Apart from the fluid type, the hydraulic fracture design including hydraulic fracture half-length, height, and fracture conductivity play important roles. Figure 5.6 to 5.7 are presenting the well flow performance (flow rate over time) under the primary recovery mechanism and overlaid by enhanced oil recovery through CO2 injection after 2 years of primary recovery. There are multiple numerical simulation cases are presented in the figure for different reservoir fluid types. Keeping in mind that the presented examples are only included for the workflow demonstration with a single Huff-n-Puff cycle that shows limited incremental oil recovery while the multiple cycles provide a considerable trapped volume of

in-situ oil that moves out of their tiny pore spaces because of back-and-forth CO_2 vaporization and condensation until multi-contact miscibility is achieved. The following results conclude that every individual reservoir fluid type shows a non-unique response as the phenomenon of achieving multi-contact miscibility is not the same with different reservoir oil compositions. In a nutshell, medium-quality oil comparatively shows the highest oil recovery because of the optimum effect of achieving miscibility, oil swelling, and viscosity reduction. However, a typical heavy oil shows minimal response because of the least chances of CO_2 miscibility.

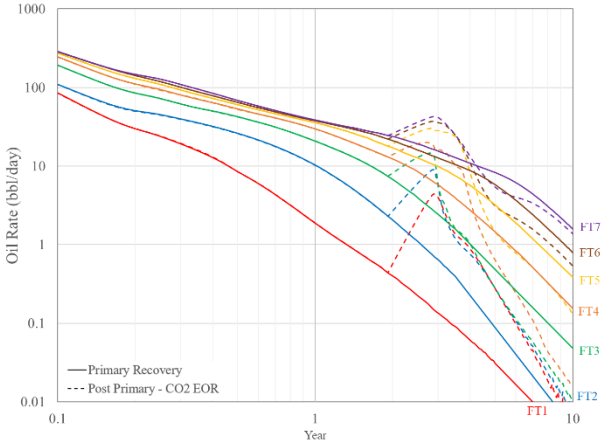

Figure 5.6 Comparative primary and EOR oil flow performance for different reservoir fluid types

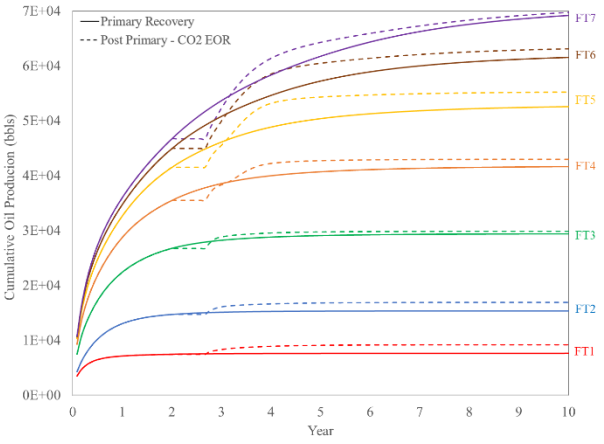

Figure 5.7 Comparative primary and EOR cumulative oil recovery for different reservoir fluid types

5.5. Compositional Dimensionless Type Curves for Unconventional EOR

Using the same approach as discussed in the prior section for the dimensionless type curve generation for the primary recovery through the modified Fetkovich approach, the type curves are further extended for the unconventional EOR. For the EOR section, the type curves response (shape, position, and slopes) is found non-unique as the function of reservoir fluid type and reservoir petrophysical characteristics as well as the hydraulic fracture design. The EOR type curve response also includes an additional controlling factor i.e., EOR operational design, mainly consisting of EOR solvent type, injection volume, and the soaking time. In addition, EOR application initiation timing would also impact the shape and the slopes of the type curves. Figure 5.8 is presenting a few examples of physics based UEOR dimensionless type curves as the function of reservoir fluid type and the hydraulic fracture half-length. The responses for each parameter are found noticeably different that are generalized and discussed in the following section.

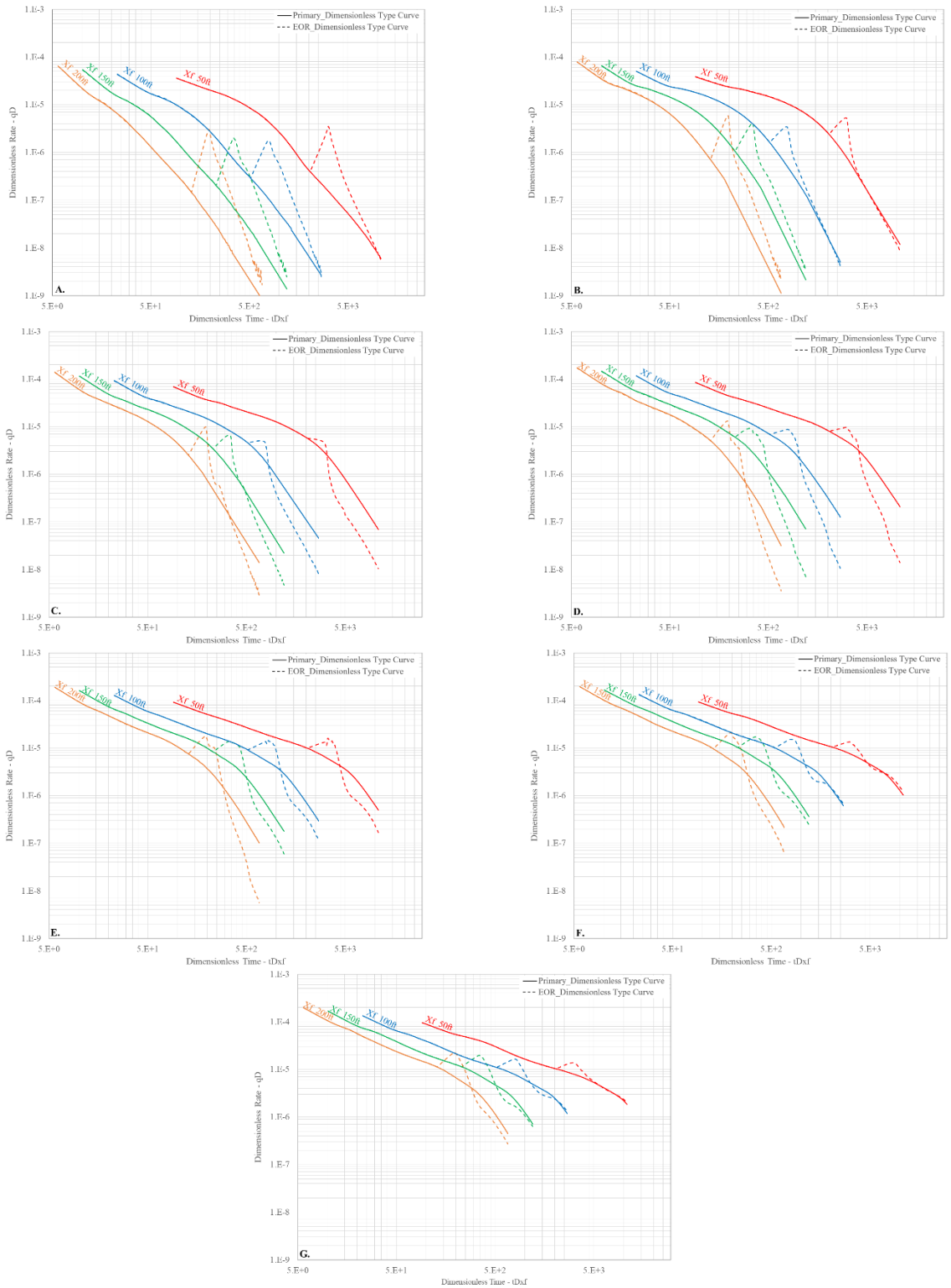

Figure 5.8 Compositional dimensionless type curves representing oil flow behavior as the function of hydraulic fracture half-length, and the reservoir fluid types for both primary and EOR recovery. Individual plots are showing the effect of fracture half-lengths for multiple fluid types i.e. (A) Fluid Type 1, (B) Fluid Type 2, (C) Fluid Type 3, (D) Fluid Type 4, (E) Fluid Type 5, (F) Fluid Type 6, and (G) Fluid Type 7. Fluid types 1 to 7 is characterized as lighter to heavier hydrocarbon oil.

5.6. Smart Physics-Informed Compositional Dimensionless Type Curves - SPiC TC_D

Using the workflow as presented in Figure 1.1, a collection of numerical simulation-based EOR responses for all possible circumstances are generated that are mandatory for developing an unconventional tight oil reservoir through a multiple-fractured horizontal well. The EOR responses are designed to be evaluated through Rate Transient Analysis (RTA). In this section, all-possible RTA-based Smart Physics-Inspired Compositional Dimensionless Type Curve (SPiC TC_D) are presented for the Oil production and the associated solution gas production in a generalized format to be used by an end-user for a quick and effective primary and UEOR performance match and incremental recovery predictions.

Description of an individual set of SPiC dimensionless type curves for both enhanced oil and associated gas recoveries are given below. It is important to note that the ensuing examples are illustrative of SPiC Dimensionless Type Curves for CO_2 and hydrocarbon gas EOR, however, the defined approach is not only limited to these types of unconventional enhanced oil recovery applications.

Figure 5.9A: SPiC TC_D for oil recovery with vertically downward shift for heavier to lighter reservoir fluid type. The slopes range from ½ to unit slope for the primary recovery while the EOR slopes vary between half slope to as high as 2 slope for different types of reservoir fluid types.

Figure 5.9B: SPiC TC_D for oil recovery with a horizontal shift towards left for increasing reservoir porosity. The slope remains unchanged for the primary recovery, i.e., unit slope, while the EOR slopes vary between unit slope, i.e., for higher matrix porosity, to as high as greater than 2 slope for the smaller porosity values.

Figure 5.9C: SPiC TC_D for oil recovery with vertically downward and horizontally towards left shift for increasing hydraulic fracture half-length. Slopes remain unchanged for the primary recovery, i.e., ½ slope, while the EOR slopes vary between unit slope, i.e., for smaller half-length, to as high as greater than 2 slopes for the larger half-length values. Also, the TCs shape becomes leaner for increasing fracture half-length.

Figure 5.9D: SPiC TC_D for oil recovery with vertically downward shift for increasing hydraulic fracture height. The slopes range from ½ to unit slope for the primary recovery while the EOR slopes vary between unit slope to as high as over 2 slope for increasing hydraulic fracture height.

Figure 5.9E: SPiC TC_D for oil recovery with vertically downward shift for increasing hydraulic fracture conductivity. The slopes range from ½ to unit slope for the primary recovery while the EOR slopes vary from unit slope to as high as over 2 slope for increasing hydraulic fracture conductivity.

Figure 6.10A: SPiC TC_D for associated gas recovery with counterclockwise shift for lighter to heavier reservoir fluid type. The slopes range from unit to ½ slope for the primary recovery while the EOR slopes vary between half slope to as high as 2 slope for different types of reservoir fluid types.

Figure 5.10B: SPiC TC_D for associated gas recovery with a horizontal shift towards left for increasing reservoir porosity. The slope remains unchanged for the primary recovery, i.e., unit slope, while the EOR slopes vary between unit slope, i.e., for higher matrix porosity, to as high as greater than 2 slope for the smaller porosity values.

Figure 5.10C: SPiC TC_D for associated gas recovery with vertically upward and horizontally towards left shift for increasing hydraulic fracture half-length. The slopes range from unit to ½ slope for the primary recovery while the EOR slope for the associated gas recovery is found greater than 2 slope for a variety of hydraulic fracture half-lengths.

Figure 5.10D: SPiC TC_D for associated gas recovery with vertically downward shift for increasing hydraulic fracture height. The slopes range from ½ to unit slope for the primary recovery while the EOR slopes vary from unit slope to as high as over 2 slope for increasing hydraulic fracture height.

Figure 5.10E: SPiC TC_D for associated gas recovery with vertically downward shift for increasing hydraulic fracture conductivity. The slopes range from Half to Unit slope for the primary recovery while the EOR slopes vary from unit slope to as high as over 2 slope for increasing hydraulic fracture conductivity.

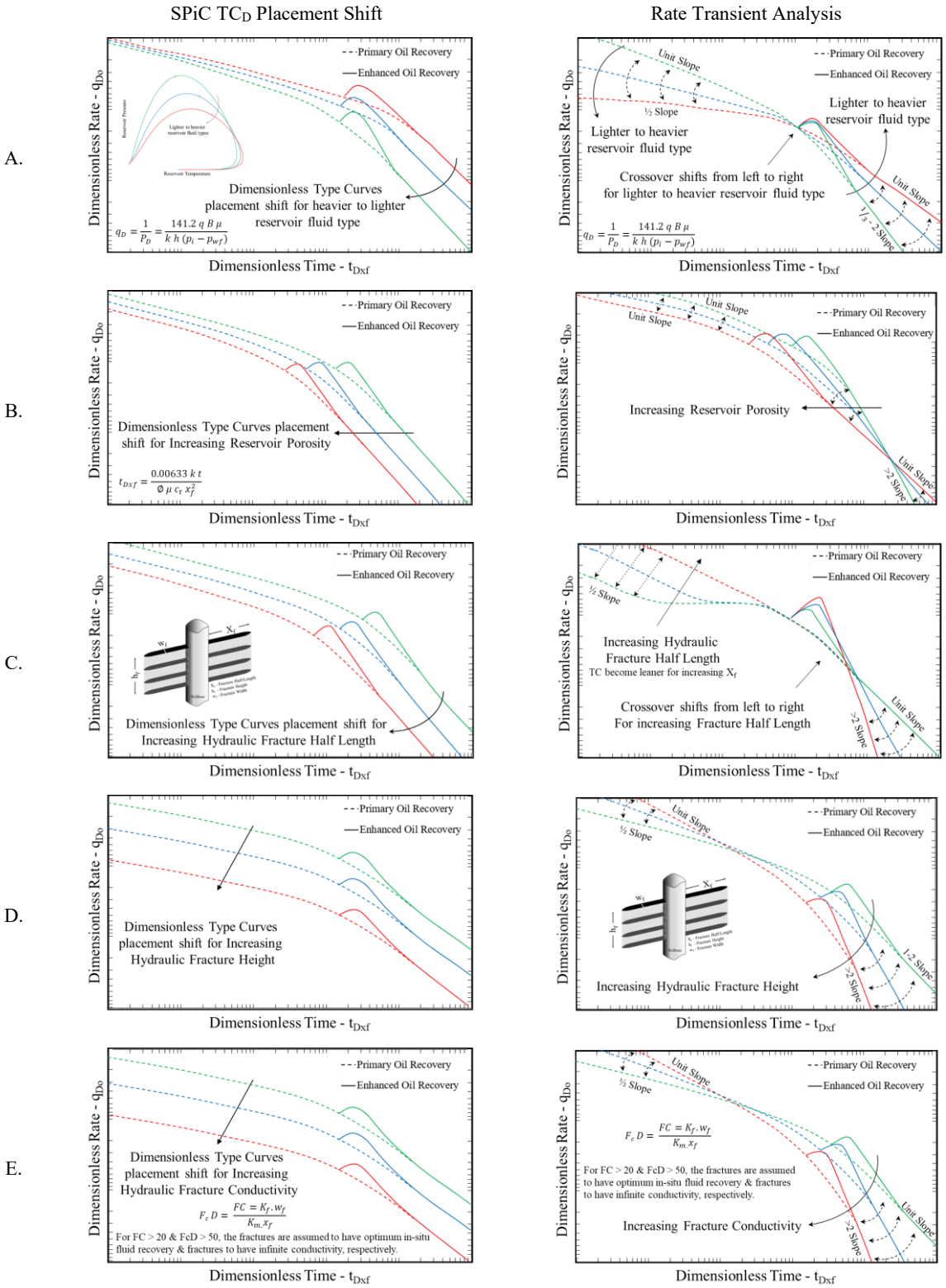

Figure 5.9 UEOR Smart physics-inspired compositional dimensionless type curves for oil production from tight oil reservoi through multi-fractured horizontal wells. Different type curves behaviors and RTA analysis are shown for the response of (A) Reservoir Fluid Types, (B) Reservoir matrix porosity, (C) Fracture half-length, (D) Hydraulic fracture height, (E) Hydraulic fracture conductivity

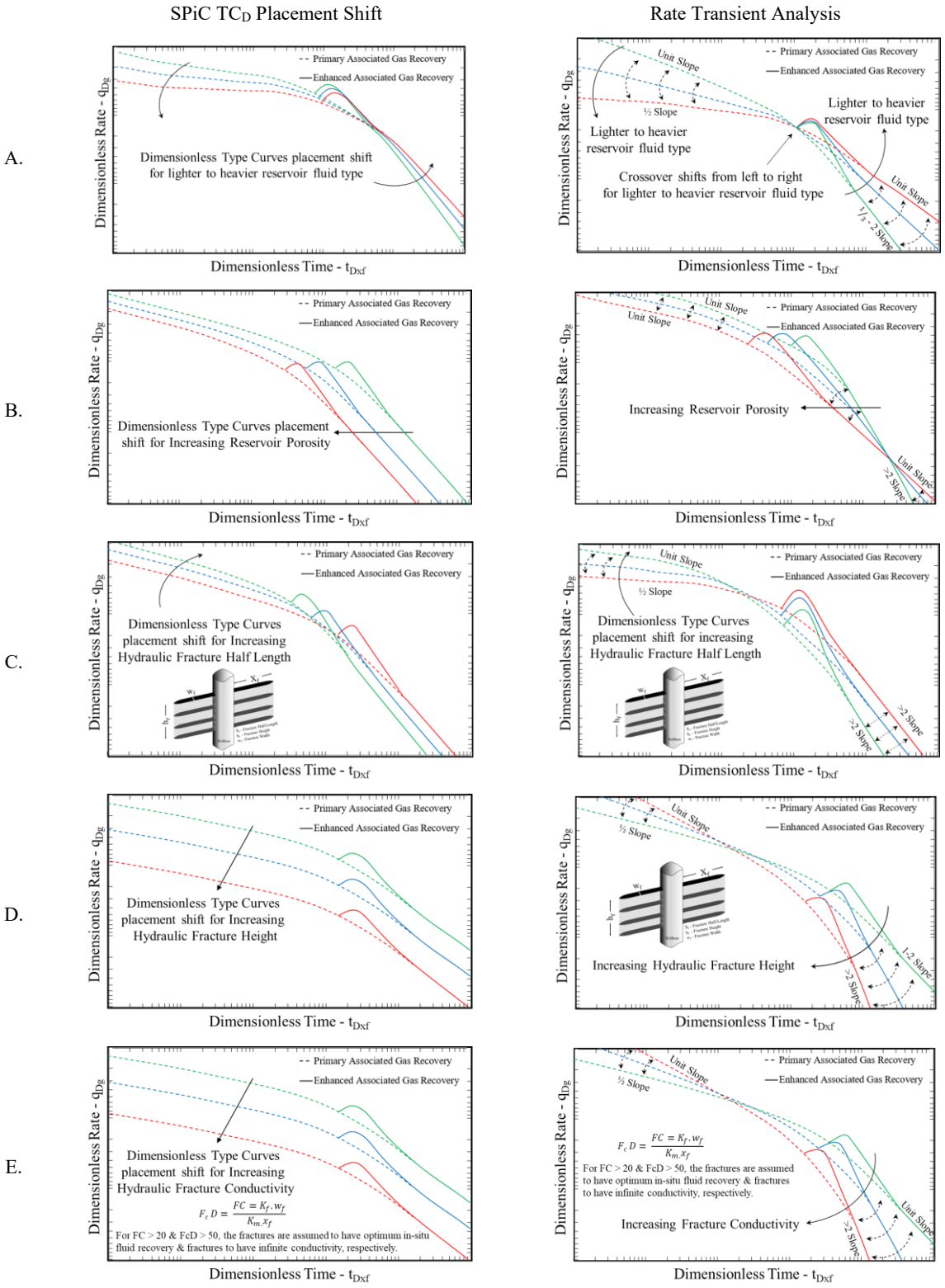

Figure 5.10 UEOR Smart physics-inspired compositional dimensionless type curves for associated hydrocarbon gas production from tight oil reservoir through multi-fractured horizontal wells. Different type curves behaviors and RTA analysis are shown for the response of (A) Reservoir Fluid Types, (B) Reservoir matrix porosity, (C) Fracture half-length, (D) Hydraulic fracture height, (E) Hydraulic fracture conductivity

6

PHYSICS-INSPIRED PROXY MODELS DEVELOPMENT

Proxy model applications are getting routine in the oil industry especially in reservoir engineering applications as an alternative to computationally expensive numerical reservoir simulation. However, well-trained proxy models are a good approach to save computational run time but their accuracy as per the physics-informed governing laws is mandatory for billion-dollar decisions and reservoir developments. In this chapter, a systematic approach and steps are discussed initially to generate random samples, for a numerical simulation-based comprehensive data library, using a physics-inspired design of experiment and the post-training physics-informed performance and quality check through detailed sensitivity analysis.

6.1. Introduction

Numerical modeling and simulation are established techniques that have been used in the oil industry for reservoir development, uncertainty analysis, and optimization of many processes in various areas such as engineering, geology, geophysics, and thermodynamics. Numerical modeling is a mathematical representation of physics-based complex problems within the defined set of limitations. However, for many grid blocks, complex processes such as compositional modeling, and EOR mechanisms with multiple fluid components, the numerical simulation process is computationally expensive. Therefore, the application of computationally efficient Proxy Models (PM) is being performed in recent years as a supportive and reliable alternative for the numerical simulation approach. Successful application of proxy models is only reasonably acceptable if the trained proxy models comply with the physics and the meaningful trends for different physics-based systems. Various terminologies referred to as Proxy models are surrogate models, meta-models, etc. (Bahrami, P., et al., 2022), as they are essentially deployed for similar purposes.

Proxy models can be defined as an input-output relationship (formulas, equations, etc.) that is capable of interpolating within a range of data as an approximation. In the reservoir engineering domain, Proxy models shall be defined as a representative model for a comprehensive numerical simulation that can be utilized and upscaled as a reliable alternative for a full-field reservoir simulation model and reduce execution time (compared to the numerical simulation's approach when obtaining similar solutions).

To fit/train a PM, a decent amount of representative data for all reservoir model parameters is provided. After the Proxy models infer the input-output relationship within the provided range of data, it is ready to be deployed as a reliable alternative to the specific numerical simulation settings/contexts for the prediction of the output. The most important benefit of using proxy models is their execution speed after inferring the input-output relationships. Proxy models in reservoir engineering are used for: sensitivity analysis of uncertain reservoir static/dynamic parameters, history matching and probabilistic forecasting for field development/evaluation, and full field development planning with less time for decision-making.

For most representative ranges of critical parameters in almost all reservoir engineering processes and to ensure interference between them, Proxy models' input-output relationship is commonly inferred through random data sampling using design-of-experiment techniques (such as Latin Hypercube Sampling) to cover the most possible sampling ranges utilizing a reasonable number of sample size.

6.2. Proxy Models Quality

The quality of any Proxy model depends on several factors including the selection of input parameters, selection of algorithms for the proxy models, data quality used for the model training, training techniques and efficiency, and various domain-expertise interpretation requirements.

Due to numerous uncertainties in reservoir engineering, domain expertise play an important role to define an initial skimming on all input parameters (this falls into both the selection of input parameters and the domain-expertise interpretation requirements as mentioned above).

In this study, the input parameters are divided into two main categories: static parameters (i.e., reservoir pressure, porosity, permeability) and dynamic parameters (i.e., bottom hole flowing pressure, time, and numerically encoded case types). Within the "selection of algorithms" aspect, multiple algorithms for proxy models have been applied in reservoir engineering, including polynomial regression, surrogate models, statistical models, and machine learning/ deep learning models. In this study, deep-learning models as ANNs are implied, trained, validated, and deployed using the static and dynamic parameters as aforementioned.

Within the training techniques and efficiency aspect, the following quality controls are applied in this study to make sure the Proxy models comply with the pre-defined and presumable physical conditions in the numerical simulation settings. They are listed below:

i. Train a portion of the prepared dataset (i.e., train set) until an acceptable R^2 and Mean Absolute Error (MAE) are obtained. Different combinations of layers and weights-bias initializations are tested.
ii. Validate and calibrate the Proxy models' prediction performance using the validation set. It is common to execute training and validation (i.e., i and ii) simultaneously.
iii. Monitor and record the optimal proxy models along the training and validation processes.
iv. Test the proxy models' prediction performance using the test set (i.e., simulation cases that do not exist in the training and validation sets, commonly referred to as a blind-test set).
v. Conduct sensitivity analyses for multiple reservoirs and hydraulic fracture parameters to establish meaningful trends following physical laws (physical compliance, referred to the domain-expertise interpretation requirements).

6.3. Deep Neural Network Architecture & Proxy Model Generation

Neural network development is a sophisticated process with multiple steps. A schematic of a typical Deep Neural Network (DNN) architecture and the proxy model generation workflow is previewed in Figure 6.1. In this study, a supervised machine learning technique using DNN architecture. DNNs can recognize and construct complex non-linear patterns via their layers' weights and biases via the feed-forward procedure. Learning and inferring from data inside DNNs are conducted by a backpropagation procedure. The backpropagation procedure in DNN is executed during the training and validation to minimize the pre-set error/loss metrics. One critical component inside the backpropagation procedure is gradient descent which iterates to obtain the optimal values of weights and biases in the layers, from which the DNN produces the minimum values of the loss metric(s). (Ahmad, F., et al., 2010; Wang, J., et al., 2017).

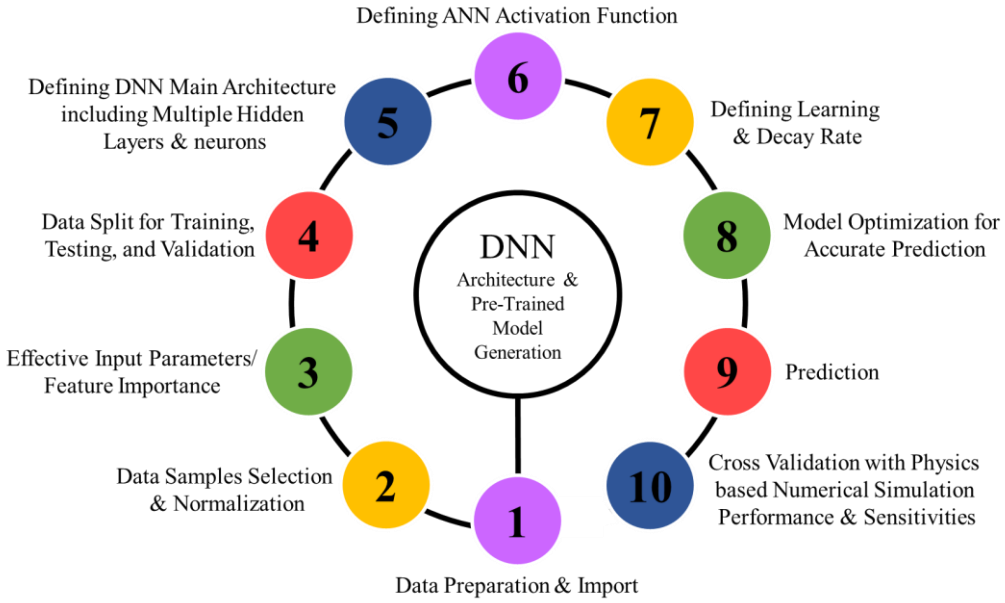

Figure 6.1 Deep neural network architecture and model generation workflow

6.3.1. Data Sensitivity, Characterization, & Preparation

The initial step adopted in this process is the selection of the most impactful reservoir parameters that control the reservoir fluid in-flow performance including reservoir pressure, matrix porosity, and permeability. Secondly, the hydraulic fracture parameters are short-listed that support the reservoir fluid in-flow performance including hydraulic fracture design parameters such as fracture half-length, effective permeability, fracture height, and width, etc. Fracture

conductivity is another important parameter that extensively defines the fluid intake from the reservoir and out-flow towards the wellbore. The dynamic operational parameters including bottom-hole flowing pressure and the injection of an EOR solvent (for the EOR cases) are also important parameters that are used in this study. Table 6.1 summarizes all the parameters and their ranges applied in this study to generate proxy models. Apart from the meaningful parameters representing reservoir characteristics, hydraulic fracture, and the operational design parameters, a few pseudo-encoded parameters are also included that helped the ANN to distinguish the different characteristics of the processes. Essentially, the proxy models are generated for a couple of categories representing natural drive mechanisms and the EOR. Each category is further divided, as listed in Figure 6.2. Generating the oil and gas flow rate well-trained proxy models overall cover the entire flow performance in multiple ways, such as GOR, cumulative oil production, incremental oil recovery, etc.

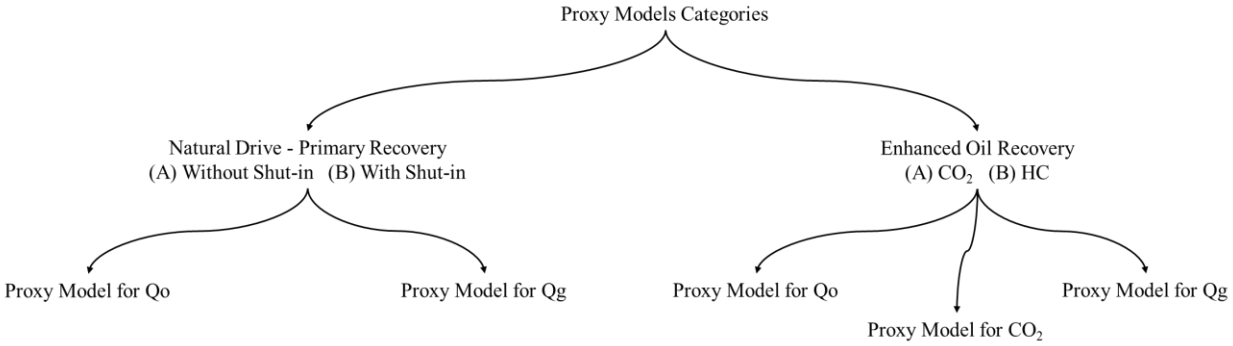

Figure 6.2 DNN-trained proxy model categories

Table 6.1 Parameters and their ranges used for the DNN training and proxy models development

Parameters	**Parameters Used for**		**Range**
	Primary Recovery Models	EOR Models	
Initial Reservoir Pressure	✓	✓	4000 – 12000 Psi
Reservoir Porosity	✓	✓	2 – 15 %
Reservoir Permeability	✓	✓	0.0001 – 0.1 mD
Reservoir Fluid Type	✓	✓	Light to Medium Quality
Fracture Conductivity	✓	✓	0.02 – 50 mD.ft
Fracture Half-Length	✓	✓	25 – 300 ft.
Fracture Height	✓	✓	10 – 120 ft.
Solvent Injection Volume		✓	0.2 – 910 MMScf
Soaking Time		✓	2 – 30 Days
Bottom Hole Flowing Pressure	✓	✓	
Time	✓	✓	
Case Type (Pseudo Parameter)	✓	✓	
EOR Type (Pseudo Parameter)		✓	
Oil Flow Rate	✓	✓	
Gas Flow Rate	✓	✓	
CO_2 Flow Rate		✓	

For each of these parameters, a field-derived practical variation is considered to generate a database that shall cover all possible scenarios for the field applications. For the models training fixed reservoir property value is used as the localized mechanistic simulation model is used for the entire dataset development. Therefore, an end-user would have to come average-out / scale up the actual reservoir property to be used in the proxy model for closed possible prediction. A few most adopted averaging methods are harmonic, geometric, arithmetic, and quadratic averaging methods (Ahmed U., et al., 2016; Jarvie, D.M., et al., 2007). The mathematic representation of these averaging techniques is given below:

$$x_{Harmonic} = \left[\frac{1}{n}\sum_{i=1}^{n}\frac{1}{x_i}\right]^{-1} \quad Eq.6.1$$

$$x_{Geometric} = \left[\sum_{i=1}^{n} x_i\right]^{\frac{1}{n}} \quad Eq.6.2$$

$$x_{Arithmetic} = \frac{1}{n}\sum_{i=1}^{n}\frac{1}{x_i} \quad Eq.6.3$$

$$x_{Quadratic} = \left[\frac{1}{n}\sum_{i=1}^{n} x_i^2\right]^{\frac{1}{2}} \quad Eq.6.4$$

where x_i is the value of the subject parameter at the i^{th} reference location in a reservoir.

It is important that the physical meaning of each of the considered input parameters are unique and important, and the magnitude of one input parameter in the dataset is drastically different from the others. Therefore, data normalization is performed to ensure proper weightage distribution on all input parameters according to their scope in the proxy models during training/validation processes. There are several normalization techniques such as Min-Max normalization, z-score normalization, decimal scaling normalization, etc. In this study, the Min-Max normalization technique is adopted (Al Shalabi, L. and Shaaban, Z., 2006; Mohamad, I.B. and Usman, D., 2013; Saranya, C. and Manikandan, G., 2013). The mathematical expression of the technique is shown below:

$$x_{normalized} = \frac{x - x_{min}}{x_{max} - x_{min}} \quad Eq.6.5$$

$$x_{scaled} = x_{normalized} \times (max - min) + min \quad Eq.6.6$$

$$x_{scaled} = x_{normalized} \times (max - min) + min \qquad Eq.\,6.7$$

Where x is the absolute value of the subject parameter while x_{min} and x_{max} are the minima and the maximum values of the subject parameter used in the dataset for the model preparation, respectively. For scaling, the min and max are normalized to values between these limits. In this study, 0 and 1 are the min and the max limits.

6.3.2. Feature Importance Analysis

Feature Importance Analysis refers to the characterization of all perspective features that control the performance of the output parameter. One step further, this study provides the physical meaning of the important features that control the fluid flow from a reservoir in a defined reservoir and a hydraulic fractured system.

In this work, Feature Importance Analysis is conducted end-to-end within the modeling workflow, i.e., during both pre-processing and post-training steps. During pre-training, Feature Importance Analysis is determined using single variate statistics and R_2 correlation to determine correlations between the output and all individual input parameters. Based on the single variate statistics, all prospective features are scanned, and profound features are extracted (presumably that the impact of the input features on the output is mutually independent). During post-training, feature importance is determined through *SHapley Additive exPlanations* (abbreviated as SHAP). SHAP, a model explain-ability technique, is designed based on the game theoretic approach. It explains machine learning/ deep learning models according to the optimal allocation from local explanations of the input features, given a sufficient sample of data and the corresponding pre-proxy machine learning/deep learning model. Consequently, SHAP is initiated and executed to leverage the use of available proxy modeling techniques and, because of its optimal allocation nature, to interpret the interference between the impact of input features to the output. The benefits of SHAP for post-training Feature Importance Analysis mitigates the presumptions during the pre-processing Feature Importance Analysis and allows domain expertise to reflect the physical meaning of the important features.

Figures 6.3 presents the feature importance ranking for all five models trained during pre-processing, and figures 6.4 to 6.8 show the post-training feature importance interpretation post-processing. The following figures indicate different interpretations in terms of feature importance. Figure 6.3 merely indicates a preview and naive feature ranking between all modeled features and the output since no trained model and no feature interference contribute to the evaluation. In contrast, figures 6.4-6.8 provide a significantly detailed feature ranking, in terms of:

1. One feature's value distribution
2. One feature's degree of impact on the output, given the changes in its value and its interference with the others
3. One feature's uniformity in impact on the output

For example, the feature "Days" has the highest and less uniform impact on the output (since the range of impact on the output from "Days" is highly diverse when this feature's value is low and greatly reduces when this feature's value is higher). The higher the value of the feature "Days" is, the lower impact it has on the output The feature "Fluid type" has the 2nd highest and more uniform impact on the output (since the range of impact on the output from "Fluid type" is similar regardless of the low/high values of this feature). The higher the value of "Fluid type" is, the higher impact it has on the output. Similar explanations can be conducted for the other features in Figures 6.4-6.8 using the understandings 1-3 as aforementioned.

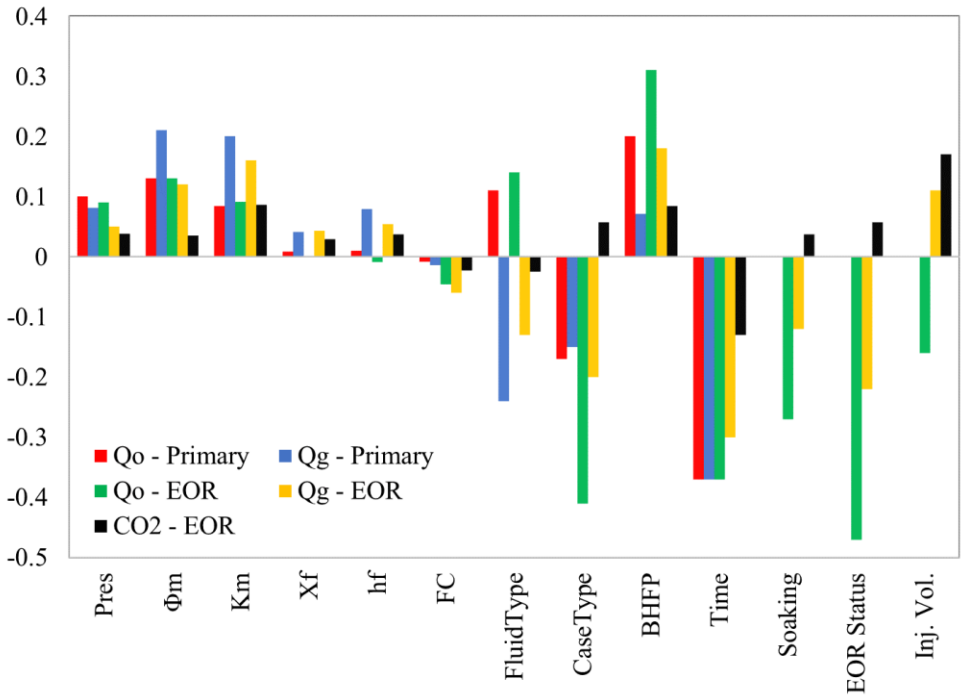

Figure 6.3 Single variate feature importance for all proxy models

Figure 6.4 Post-training feature importance – Oil flow rate for the primary model

Figure 6.5 Post-training feature importance – Gas flow rate for the primary model

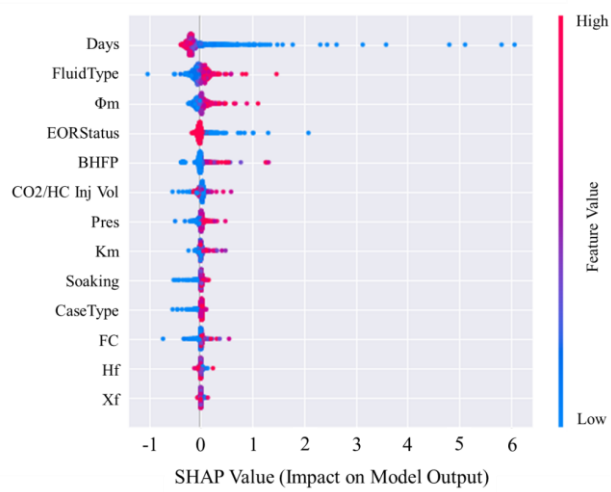

Figure 6.6 Post-training feature importance – Oil flow rate for the GOR model

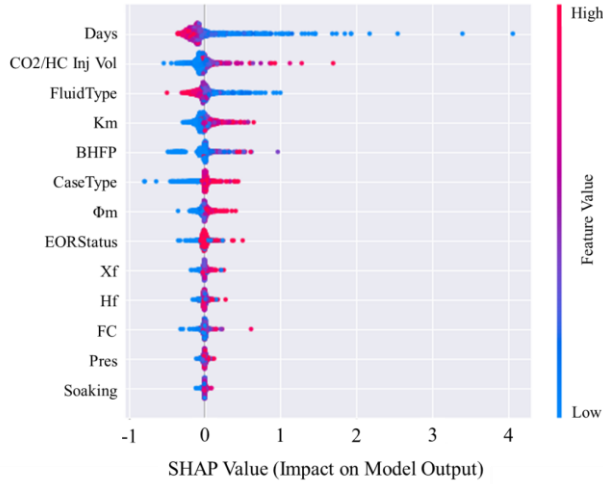

Figure 6.7 Post-training feature importance – Gas flow rate for the EOR model

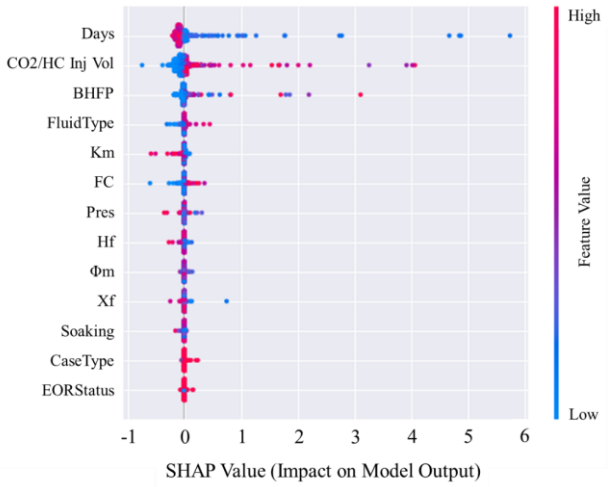

Figure 6.8 Post-training feature importance – CO_2 flow rate for the EOR model

6.3.3. Data Split for Training, Testing, and Validation

The next important step after data preparation and pre-training feature importance determination is to split the prepared data into training, validation, and blind-test sets. In this study, all models are trained using 75% of the prepared data while the remaining 25% of the data is used for validation and blind test. Since approximately a quarter million data points/events are prepared in this study, a slight shift in the split ratio (i.e., 80%/20%, or 70%/30%, or 90%10%) does not heavily impact the performance of the proxy models.

6.3.4. Neural Network Architecture

The next step is to develop an overall ANN architecture by defining the input layer followed by multiple hidden layers, and an output layer. Figure 6.9 is representing a typical ANN architecture that follows the following steps:

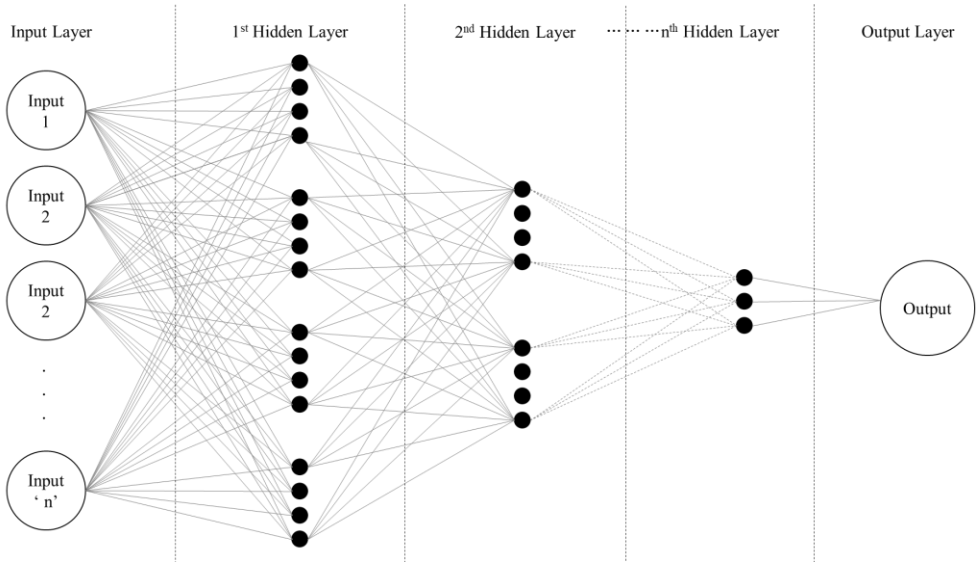

Figure 6.9 Typical neural network architecture

Artificial neural networks can utilize multiple hidden layers; however, the selection of the hidden layers is problem specific. An excessive number of hidden layers may not significantly outperform a reasonable number of hidden layers. In addition, it is equally important to choose the proper number of nodes in the hidden layers. Multiple nodes are beneficial to reduce the error between the predicted and the actual values. Like the number of hidden layers, an excessive number of nodes may not outperform a reasonable number of nodes. Therefore, the number of hidden layers and nodes in an ANN shall be carefully considered. (Chen, H., et al., 2022; Shen, H., et al., 2008; Stathakis, D, 2009). In this study, after multiple realizations through a trial-and-error process, five dense hidden layers are defined

for all models with various neurons for accurate computation of ANN's performance followed by an activation function. The activation functions are responsible for the feed-forward procedure (de Campos, P.V., et al., 2019; Warner, B. and Misra, M., 1996). A variety of activation functions is used in different ANN algorithms such as Sigmoid, Tanh, Soft-max, Rectified Linear Unit (ReLU), and Max-out functions. In this study, the ReLU function is used because of its superiority in the ANN's performance compared to the other activation function variants.

6.3.5. Learning / Decay Rate and Model Optimization

Over- and/or under-fitting are common issues that may happen because of the insufficient or excessive number of training samples, the number of nodes, and the hidden layers defined in an ANN architecture (Chen, H., et al., 2021). Over-fitting refers to the scenario that a machine learning/deep learning model fails to generalize the input-output relationship due to its over-detailing into all samples in the trained set. Under-fitting means a model fails to infer the intrinsic complexity of training and validation sets due to its under-detailing into all samples in the trained set (Smith, L.N., 2008). Therefore, modifying the learning rate (i.e., referred to as the learning rate decay model) is required to train a neural network in this study. Modifying the learning rates is conducted to ensure the optimization to approach the minima and not diverge from the minima. In this study, values between 5×10^{-3} and 5×10^{-4} are taken as the initial learning rate and decay rate, respectively. Eventually, the model optimization step is defined as the last constituent step of the model architecture for an accurate ANN model prediction. Several optimization techniques can be selected based on the ANN architecture and the objective function. In this study, the Adam optimization technique is used to minimize the Mean Absolute Error (MAE). MAE loss metric determines the absolute difference between the actual and the predicted values taken from the dataset. The MAE function is defined in Equation 6.7. Another quantitative method commonly adopted to cross-check the accuracy of the prediction is the coefficient of correlation (R^2), shown in Equation 6.8. Table 6.2 summarizes the MAE and the R^2 for all ANNs in this study. While Figures 6.10 to 6.19 are presenting training & testing loss metrics and the ANNs' performance cross-plots.

$$MAE = \frac{\sum_{i=1}^{n} |Prediction_i - True\ Value_i|}{Total\ No.\ of\ Data\ Points\ (n)} \qquad Eq.\ 6.7$$

$$R^2 = 1 - \frac{\sum_{i-1}^{n} \left(Z_{i\ sample} - Z_{i\ ANN}\right)^2}{\sum_{i-1}^{n} \left(Z_{i\ sample} - \overline{Z_{i\ sample}}\right)^2} \qquad Eq.\ 6.8$$

Table 6.2 Parameters and their ranges used for the DNN training and proxy models development

	MAE Testing	MAE Training	R2_Testing	R2_Training
Qo – Primary Recovery	0.013	0.017	0.985	0.994
Qg – Primary Recovery	0.016	0.021	0.987	0.994
Qo – EOR	0.019	0.027	0.972	0.989
Qg – EOR	0.019	0.046	0.977	0.977
CO_2 – EOR	0.017	0.046	0.955	0.973

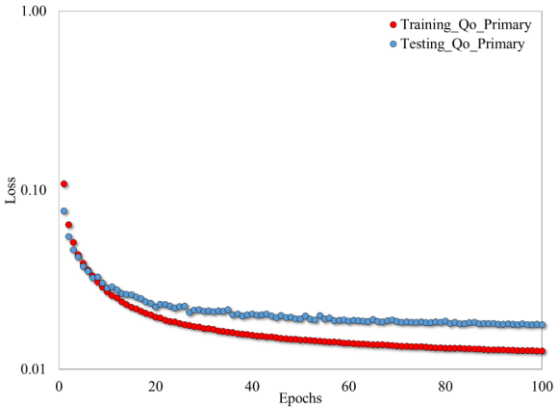

Figure 6.10 training and testing losses for Qo – primary recovery model

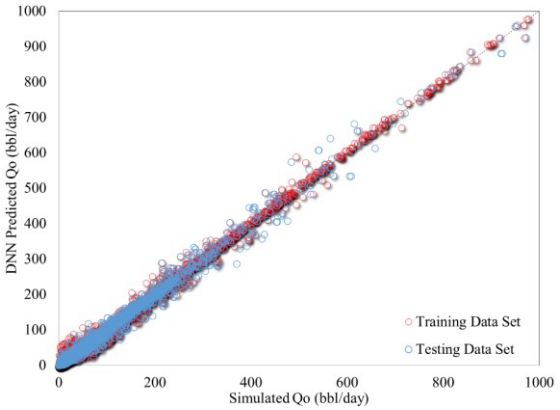

Figure 6.11 DNN post-training diagnostic prediction cross-plots for Qo – Primary recovery proxy model

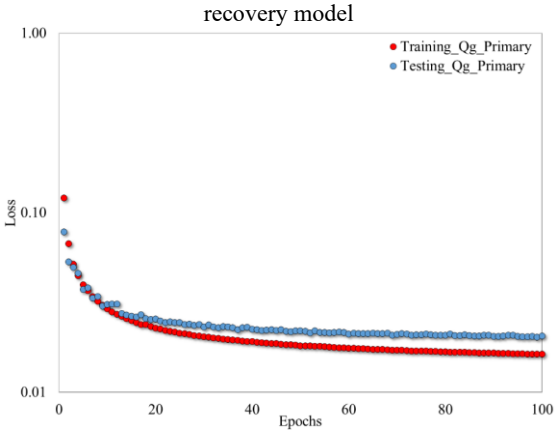

Figure 6.12 Training and testing losses for Qg – Primary recovery model

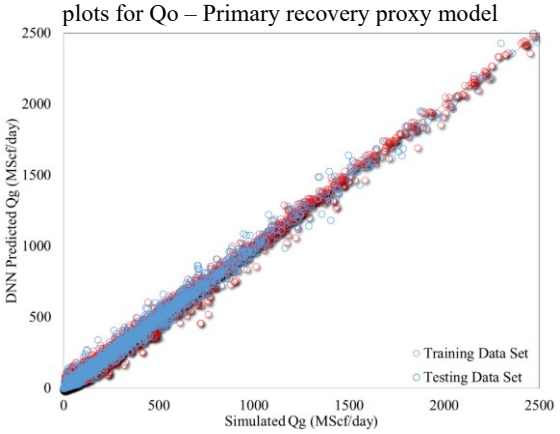

Figure 6.13 DNN post-training diagnostic prediction cross-plots for Qg – Primary recovery proxy model

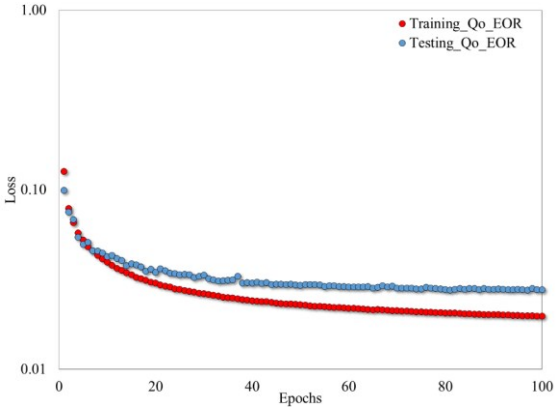

Figure 6.14 Training and testing losses for Qo – EOR model

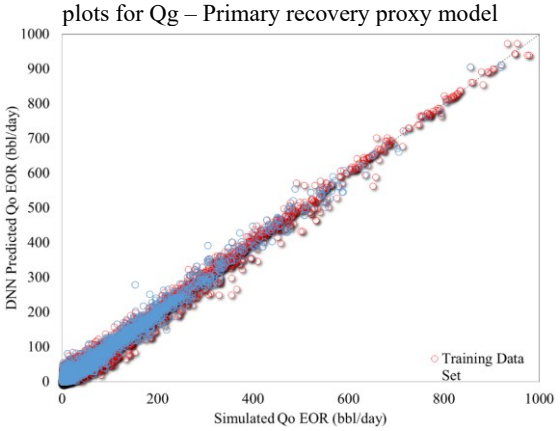

Figure 6.15 DNN post-training diagnostic prediction cross-plots for Qo – EOR proxy model

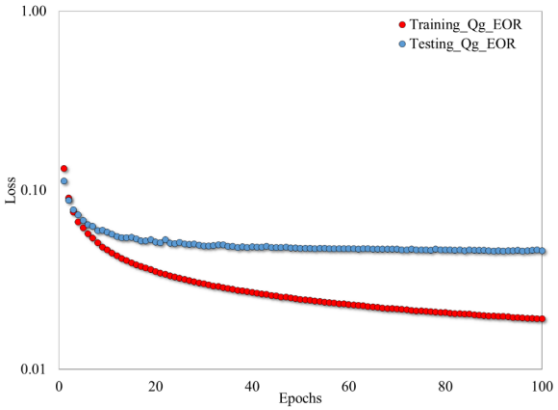

Figure 6.16 Training and testing losses for Qg – EOR model

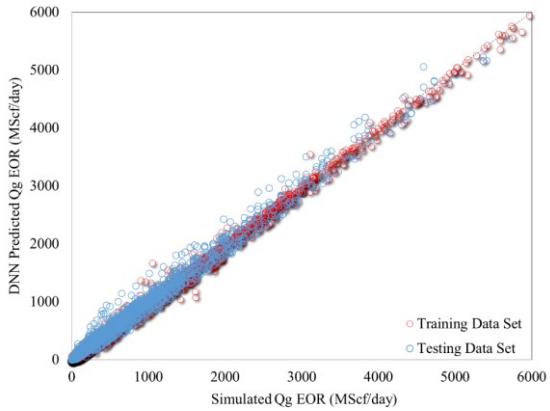

Figure 6.17 DNN post-training diagnostic prediction cross-plots for Qg – EOR proxy model

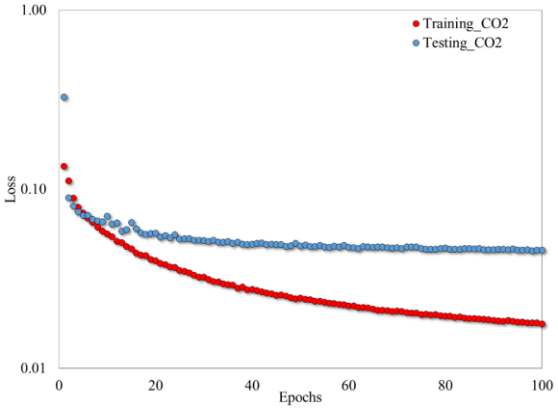

Figure 6.18 Training and testing losses for the CO_2 model

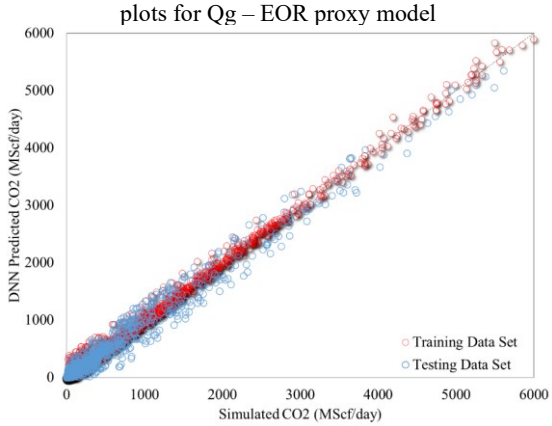

Figure 6.19 DNN post-training diagnostic prediction cross-plots for CO_2 proxy model

6.4. Limitations to Proxy Models Application

There are a few limitations to using DNN-trained physics-informed proxy models as listed below;

1. The DNN-trained proxy models can only be used for unconventional tight oil reservoir recovery performance.
2. The proxy models can be used for similar geological characteristics and hydraulic fracture designs as used in the numerical simulation model that is used to develop the entire training dataset.
3. All proxy models are valid to be used for the given ranges of individual reservoir rock and fluid properties, hydraulic fracture design, and the EOR operating design parameters.
4. The EOR proxy models can only be applied for the CO_2 and lean hydrocarbon gas injection as EOR solvents.

7

PHYSICS-INFORMED PROXY MODELS QUALITY CHECK & CASE STUDIES

Proxy model validation always involves certain subjectivity and is unique to the original specific problem and constraints applied during model training. Since the main emphasis of this study is on physics governing principles, it is crucial to ensure that the trained proxy models are operating and adhering to the physical knowledge for which they were trained. The prediction performance of the proxy models is presented in this chapter using both training and non-training datasets, followed by several actual field case studies to see how the proxy models react to the techno-economic unconventional EOR pilot screening.

7.1. Introduction

This chapter details the most important part of the entire study. ANNs have been commonly referred to as "black boxes" that do not disclose explicitly the understanding of the learned correlation between the input parameters and the corresponding output. In this study, apart from the static input parameters, multiple dynamic parameters are also used that directly affect the performance of the output parameter. If the ANNs are successfully and properly trained, the output prediction shall comply with the physics and the governing laws because the entire data is generated using physics-based numerical simulation. Ideally, the relationship between the reservoir characteristics, hydraulic fracture design parameters, and the bottom hole flowing pressure should depict the response in the reservoir hydrocarbon flow rate.

7.2. Proxy Models Prediction Performance Check Using Training Data

Physics-based prediction performance of the trained proxy models is analyzed in multiple ways. Initially, as discussed earlier, a hydrocarbon reservoir is a dynamic system that is mainly been driven by the reservoir and the bottom hole flowing pressure (i.e., differential pressure). Before proceeding further, it is important to make sure that the incremental system pressure is providing meaningful and logical fluid flow response as per the physics governing laws. Figure 7.1 is presenting the simulated and the ANN-prediction reservoir fluid flow response as the function of pressure. It is important to notice that on a single pressure value, multiple fluid flow responses are obtained that represent the effects of the combination of different reservoir rock properties, in-situ fluid type, hydraulic fracture design parameters, etc. From the proxy model training perspective, the models are evaluated to be good enough to follow the pre-defined physics.

To further investigate the performance of the trained proxy models as per the physics governing laws, it is important to first validate their performance with the training dataset to make sure the prediction is reliable with minimum error to further use the model for blind testing. For the training performance check, multiple sets of events are randomly selected from the training datasets representing different properties including but not limited to reservoir pressure, fluid type, reservoir matrix porosity & permeability, etc. Also, the performance validation has been done using the training dataset having a couple of major hydraulic fracture design parameters including fracture conductivity and the half-length.

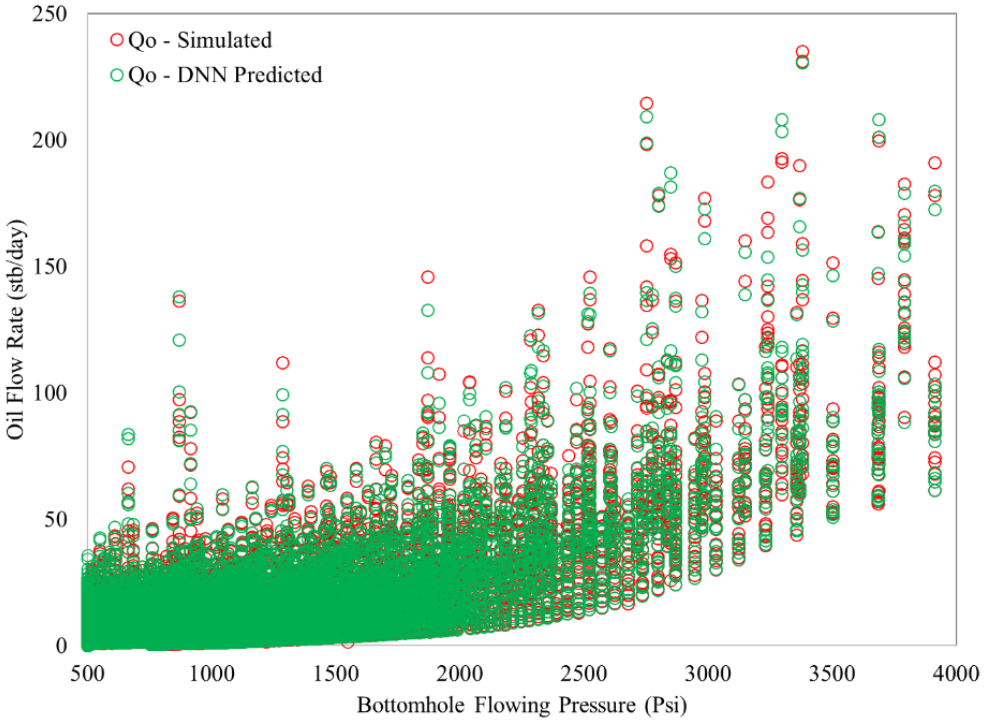

Figure 7.1 Relationship between pressure and reservoir hydrocarbon withdrawal

Figures 7.2 to 7.4 present the proxy models' performance for primary recovery as a function of the reservoir and hydraulic fracture properties. Similarly, for the same properties, the performance plots for the EOR proxy models are presented in Figures 7.5 to 7.7. Using the same testing and the predicted dataset, the dimensionless type curves are also developed for properties as shown in Figures 7.8 to 7.10.

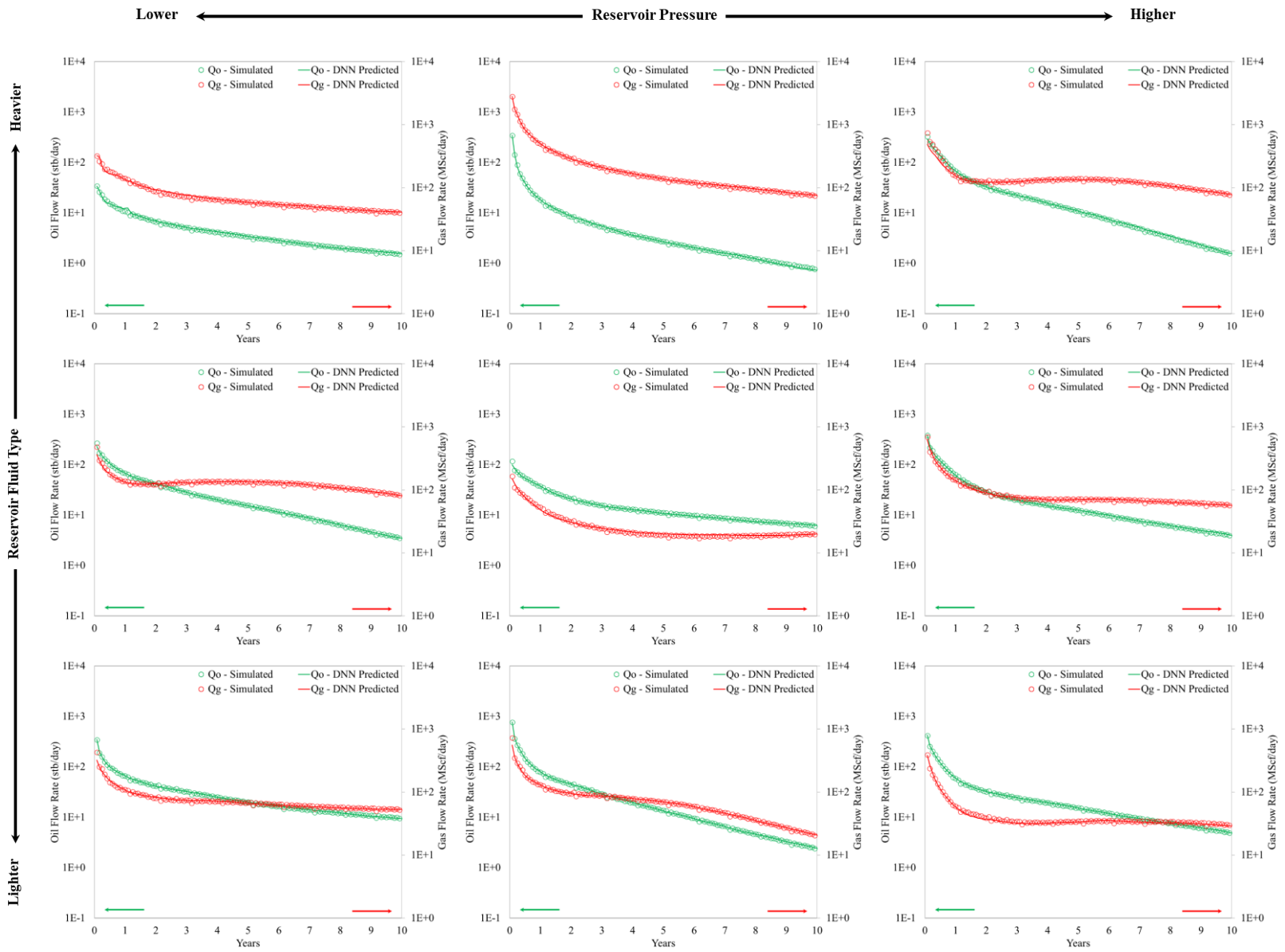

Figure 7.2 Proxy models prediction performance for primary production as the function of Res. pressure & fluid type

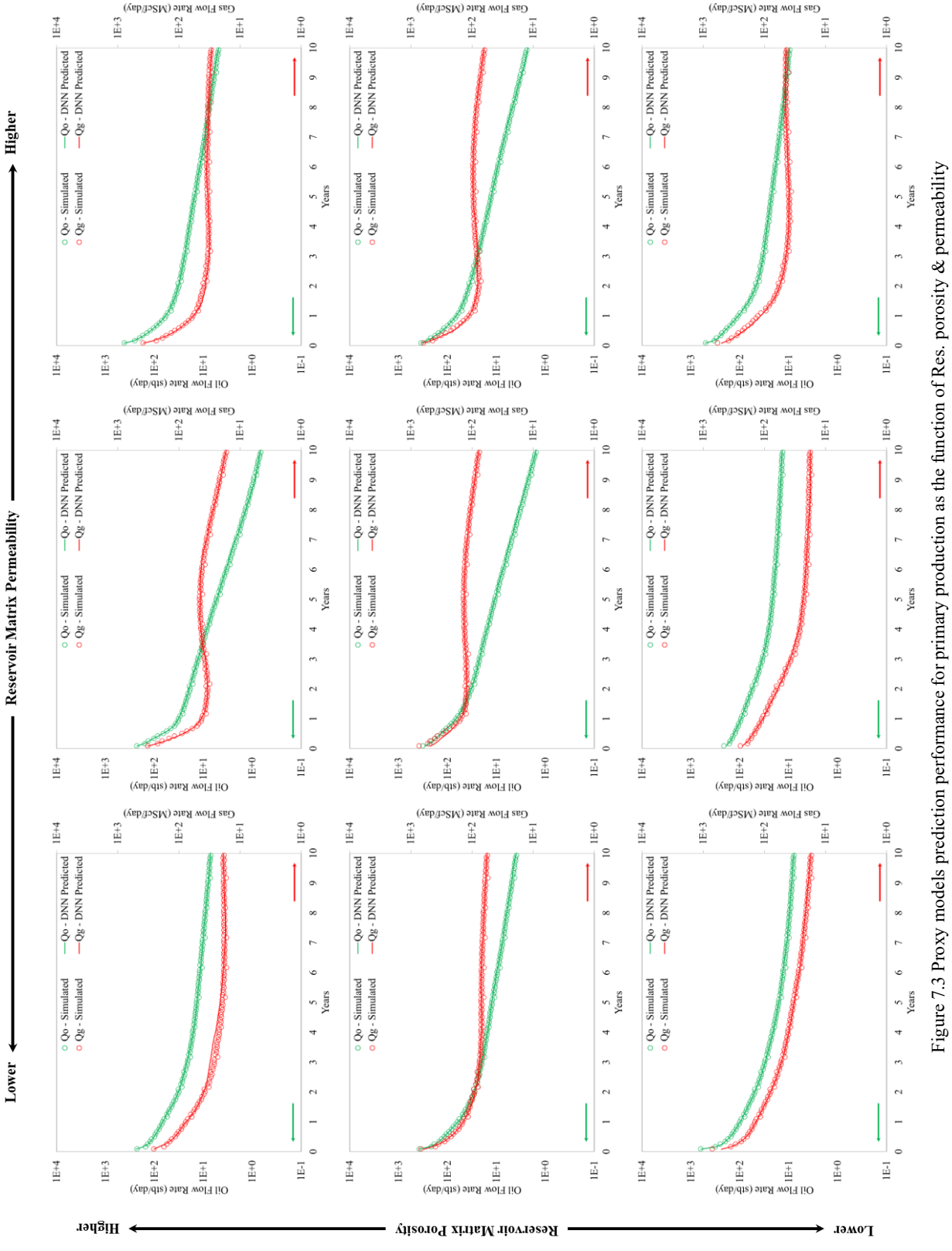

Figure 7.3 Proxy models prediction performance for primary production as the function of Res. porosity & permeability

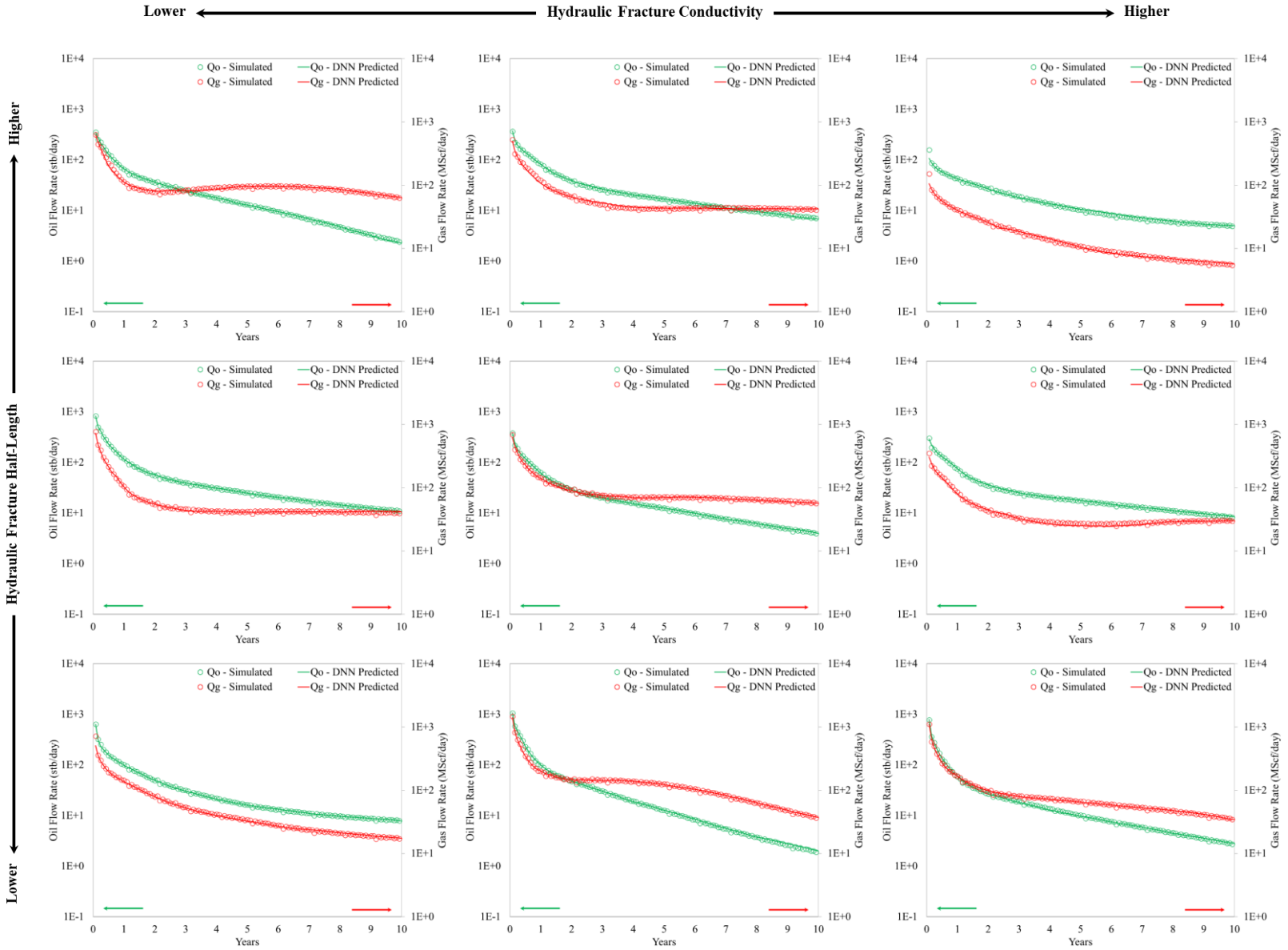

Figure 7.4 Proxy models prediction performance for primary production as the function of hydraulic fracture conductivity and fracture half-length

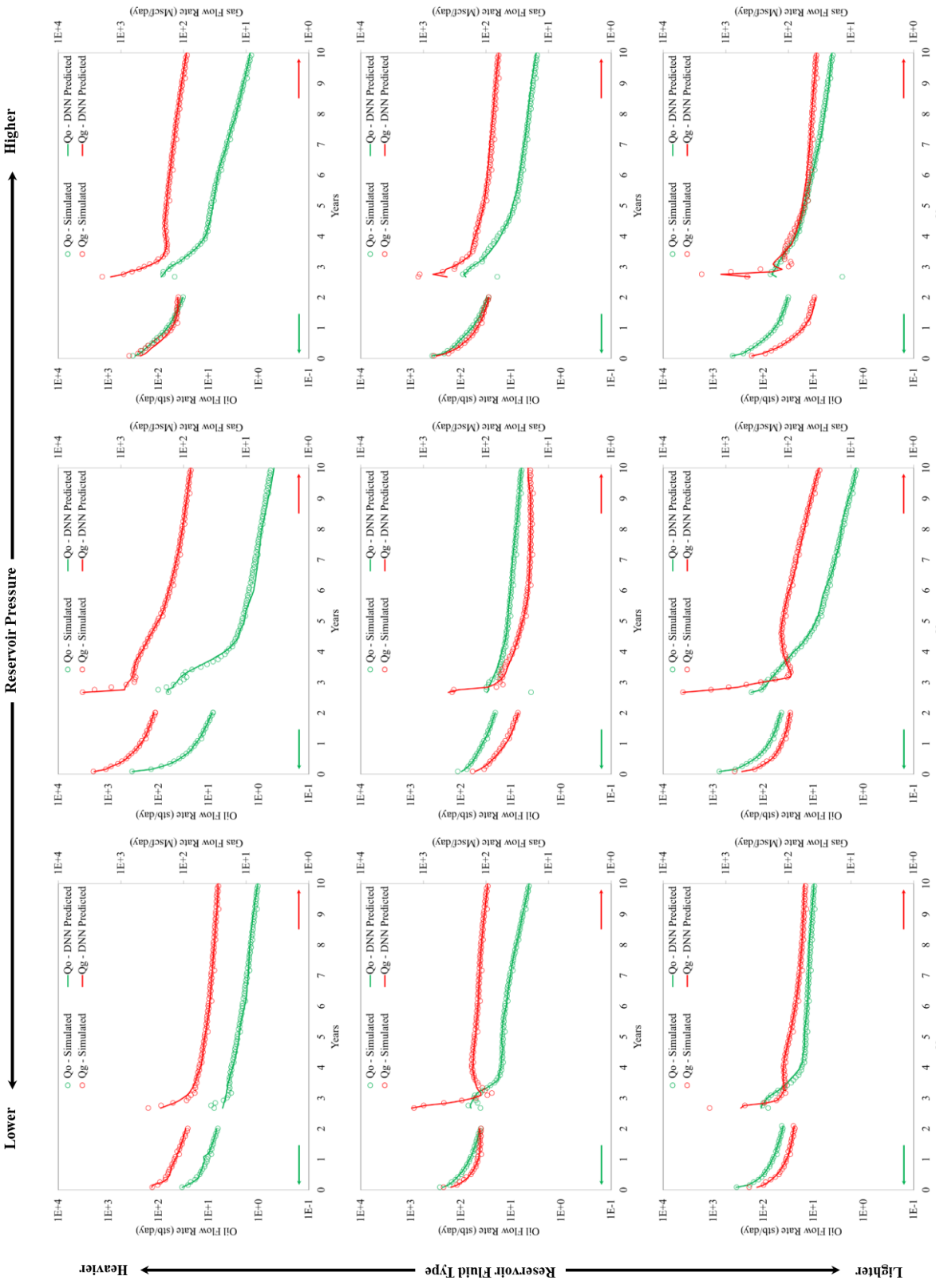

Figure 7.5 Proxy models prediction performance for CO_2 EOR production as the function of Res. pressure & fluid type

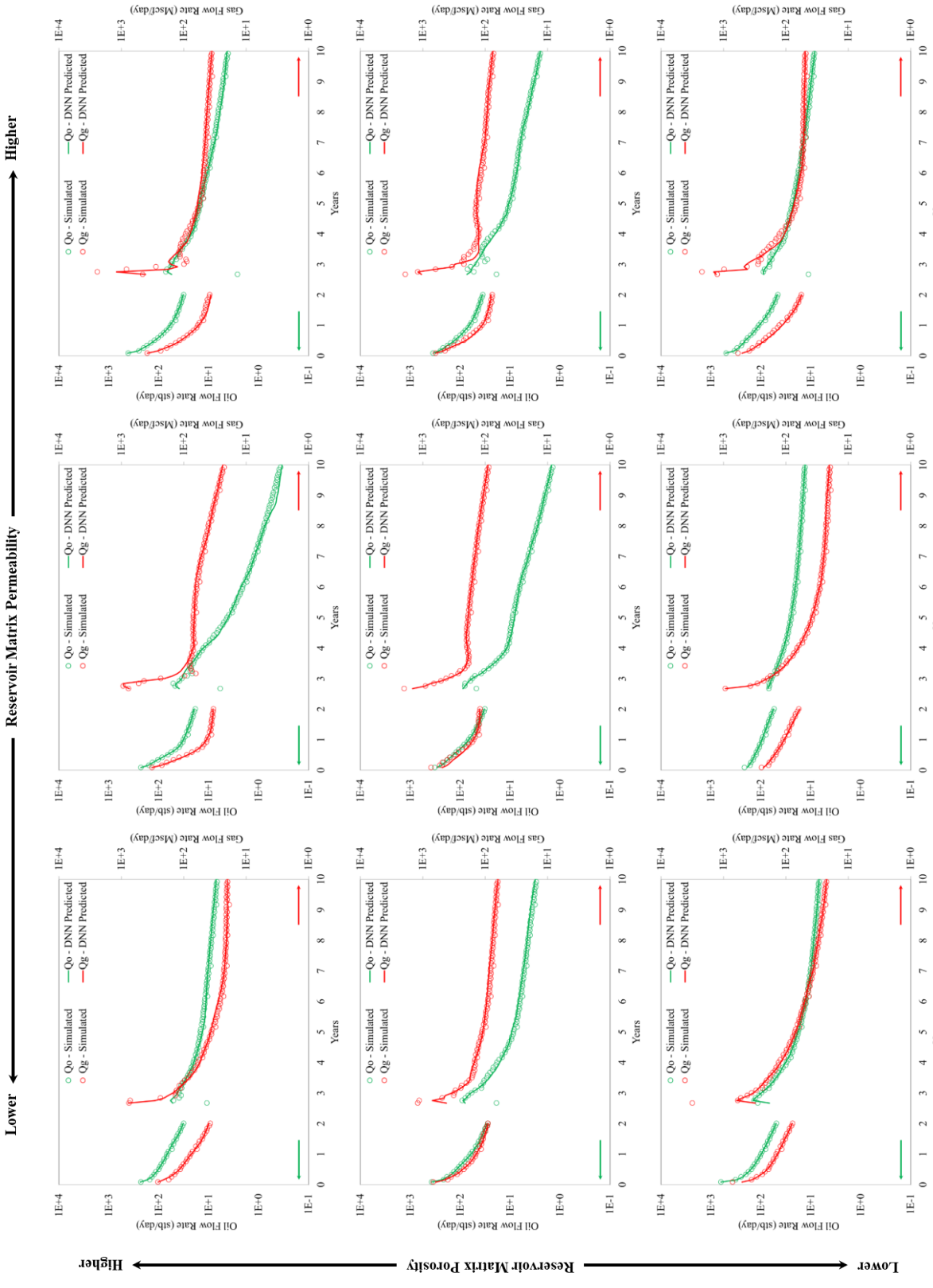

Figure 7.6 Proxy models prediction performance for CO_2EOR production as the function of Res. porosity & permeability

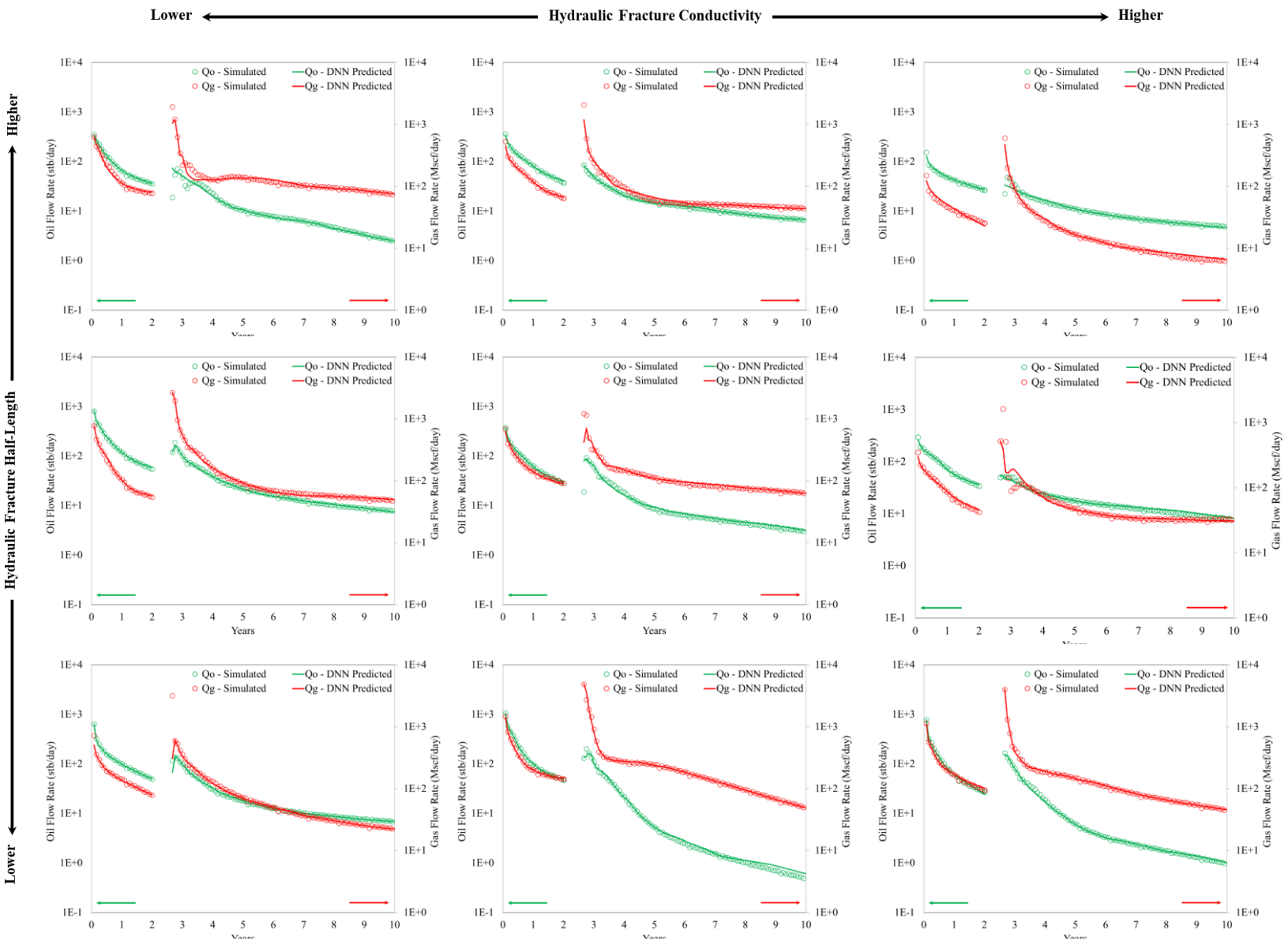

Figure 7.7 Proxy Models prediction performance for CO_2 EOR production as the function of hydraulic fracture conductivity and fracture half-length

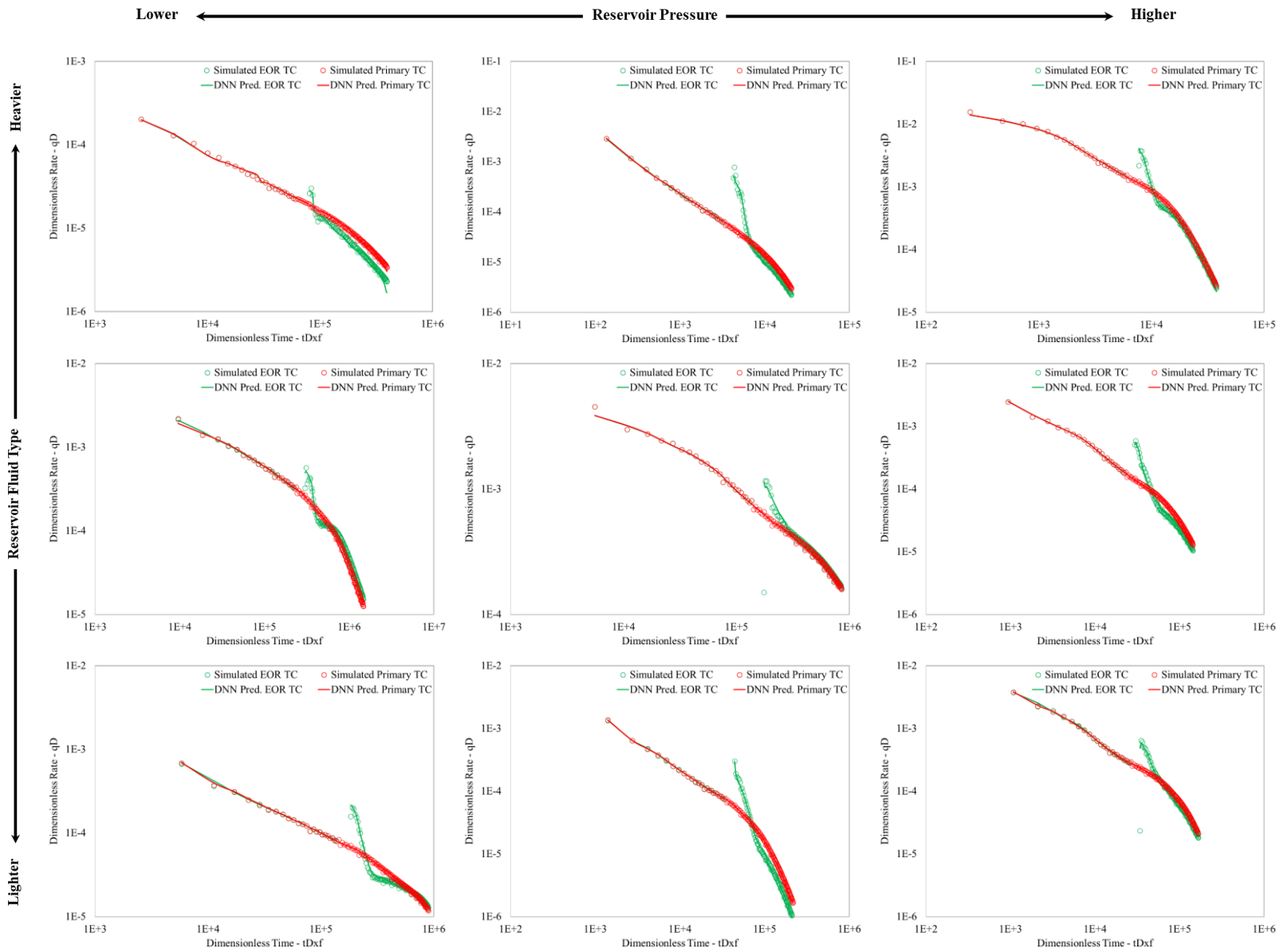

Figure 7.8 Primary & EOR type curves generated for different Res. pressure & fluid types using proxy models

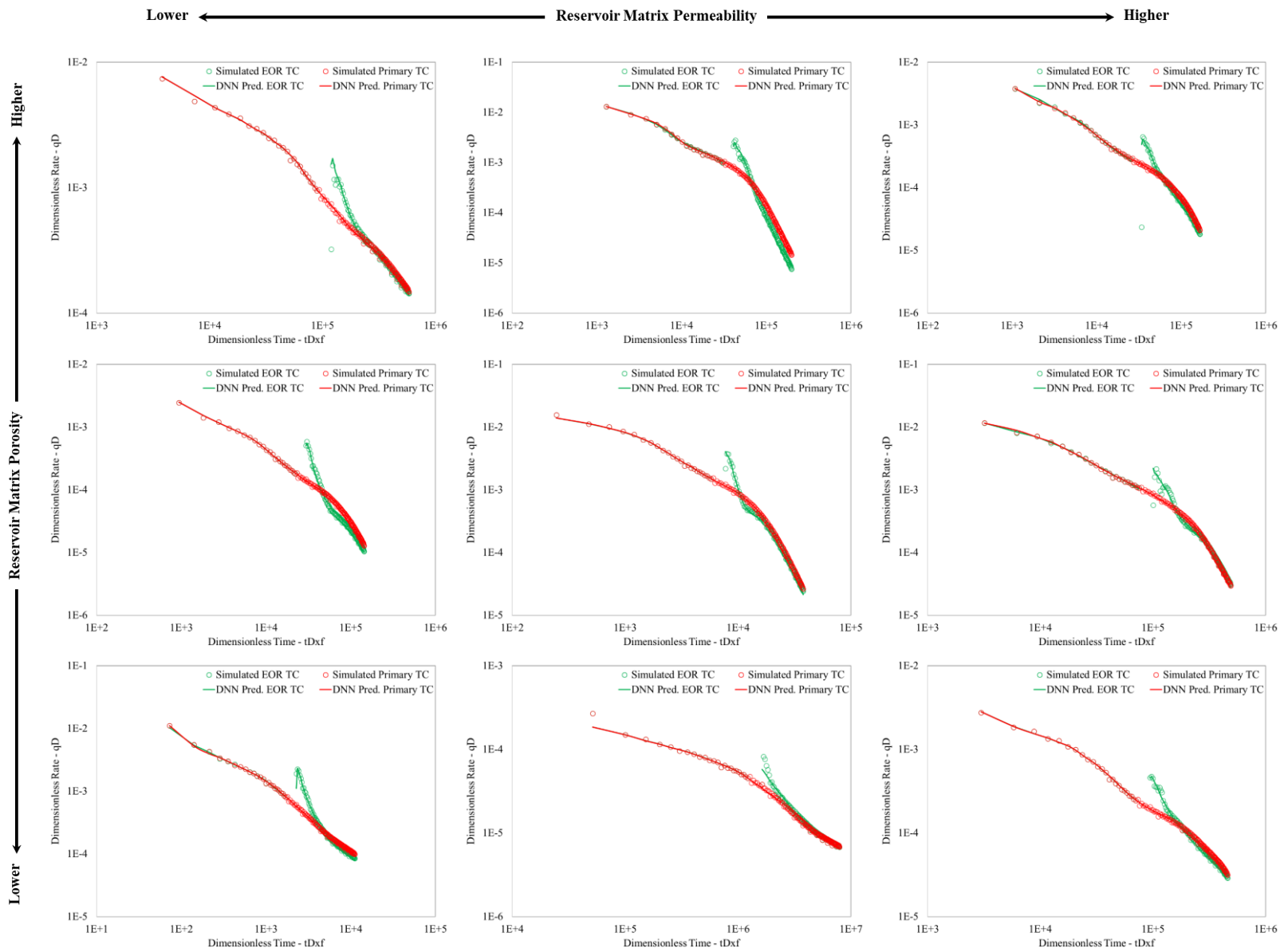

Figure 7.9 Primary & EOR type curves generated for different Res. permeability & porosity using proxy models

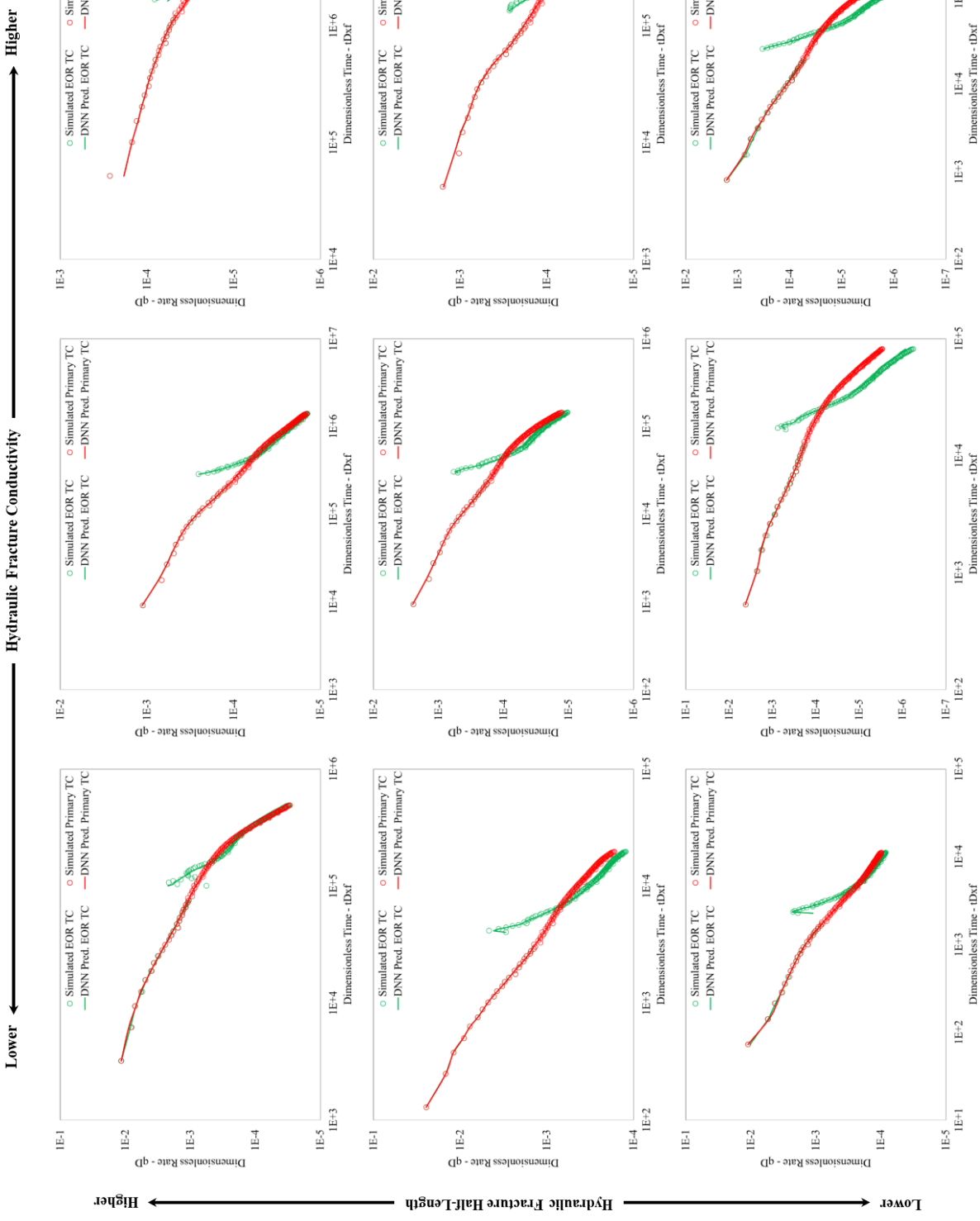

Figure 7.10. Primary & EOR type curves generated for different hydraulic fracture conductivity & fracture half-length using proxy mode

7.3. Physics-Based Proxy Models Blind Prediction Performance

After having satisfactory predictions using the Proxy DNN models for the testing dataset, the next step is to perform blind tests to satisfy the proxy models' physics-based quality check using the dataset that is not used for the DNN models' training or testing purposes. To satisfy the physics, multiple scenarios with different reservoir and hydraulic fracture parameters are considered. Figures 7.11 is presenting a systematic effect of reservoir fluid type on oil flow rate and the corresponding dimensionless type curves. Similarly, Figures 7.12 and 7.13 are presenting the effects of hydraulic fracture half-length and fracture conductivity, respectively.

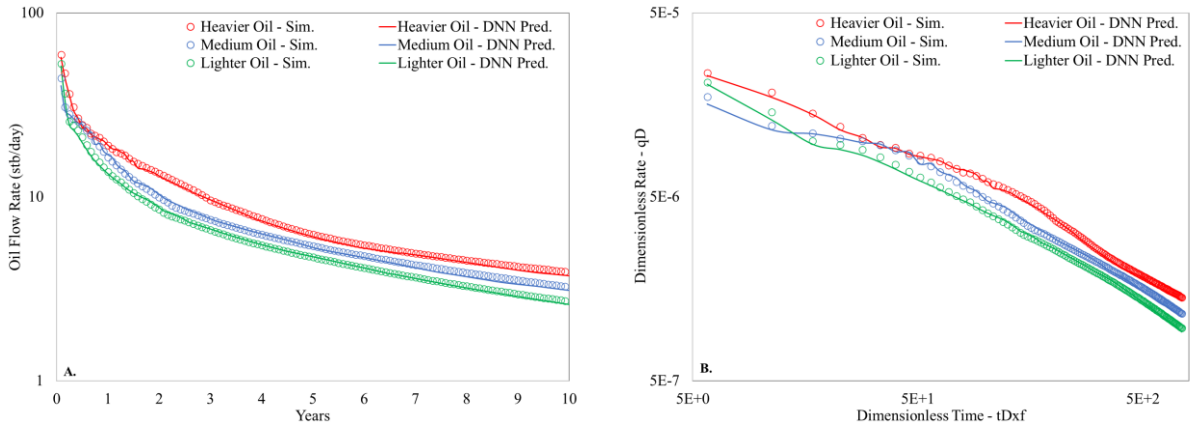

Figure 7.11 Blind physics-based proxy models' performance check for reservoir fluid types
(A) Oil flow rate (B) Dimensionless type curves

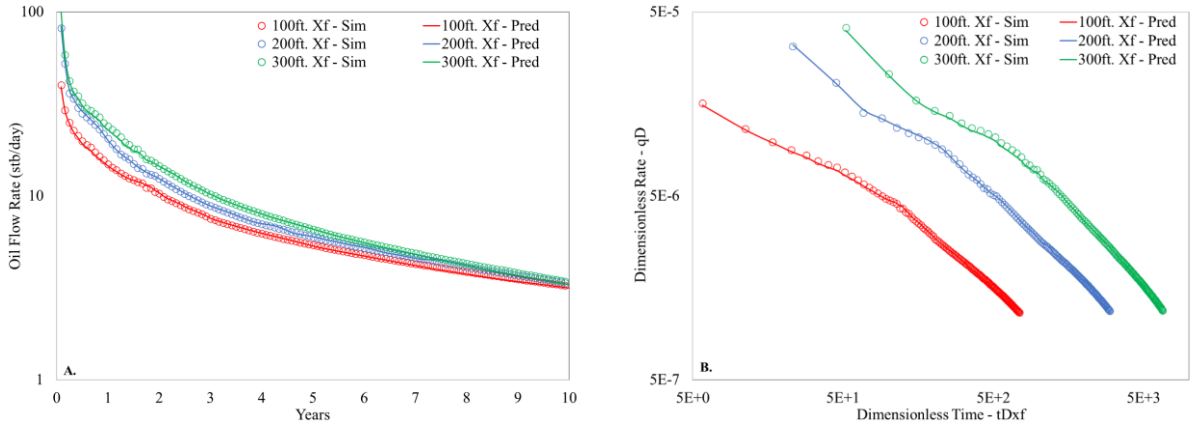

Figure 7.12 Blind physics-based proxy models' performance check for hydraulic fracture half-length
(A) Oil flow rate (B) Dimensionless type curves

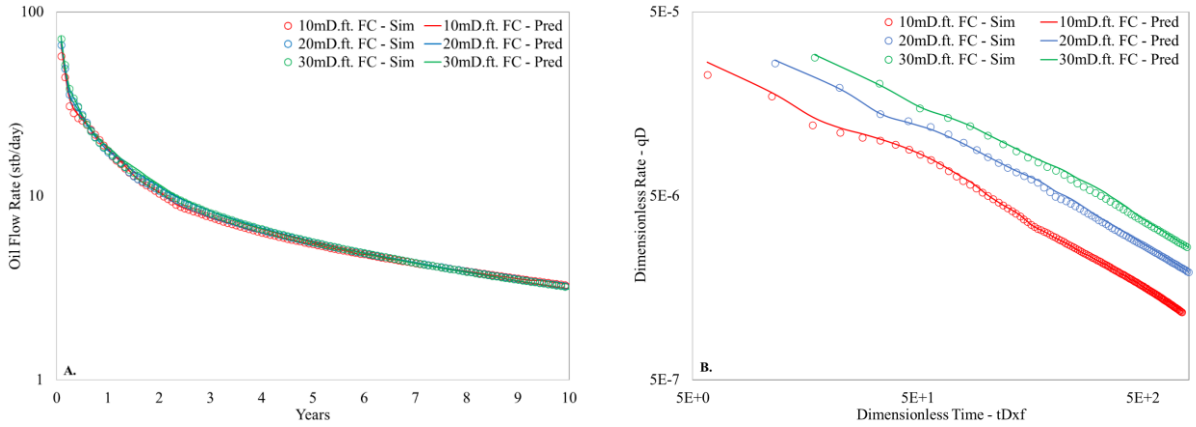

Figure 7.13 Blind physics-based proxy models' performance check for hydraulic fracture conductivity
(A) Oil flow rate (B) Dimensionless type curves

After reviewing all the discussed performances, it is concluded that the proxy models are capable enough to be used for the predictions within the defined training range. As the following step of this study, the verified proxy models are equipped with a smart tool with a Graphical User Interface (GUI) called 'W_3H', for unconventional EOR pilot screening. A detailed discussion about the smart tool, its capabilities, and a few case studies are presented in the following chapter.

7.4. Case Studies

For teaching, research, publication, and development reasons, the SPE Bleeding Edge of RTA Group (BERG) gathered numerous tight oil well performance data from several US-based companies; these datasets are now available on the SPE data repository (https://www.spe.org/en/industry/data-repository). Several tight oil primary recovery datasets from the subject repository are evaluated for the 'W_3H' concept validation. Table 7.1 is a list of the subjective data for each dataset representing the individual well that is used in this investigation.

The 'W_3H' analysis tool is designed to be as simple as possible so that analysis can be performed with limited yet necessary reservoir and hydraulic fracture design information. The necessary reservoir characteristics include in-situ reservoir fluid composition, initial reservoir pressure, porosity, and average matrix permeability. While the primary hydraulic fracture design parameters needed for the analysis include

fracture half-length, height, and fracture conductivity. If any of the required information is not available, the study would begin with the best-guess estimates using indirectly linked information.

Table 7.1 Reservoir and hydraulic fracture information for all wells discussed in case studies

	Well-1	Well-2	Well-3
Field	Osprey	Eagle	Kite
Formation/ Reservoir	Eagle Ford	Eagle Ford	Eagle Ford
Initial Res. Pressure (Psi)	5400	5000	5000
Res. Temperature (^{o}F)	225	235	238
Net Pay Thickness (ft)	78	74	56.5
Matrix Porosity (%)	6.3	6.3	5
Water Saturation (%)	26	27	32
Oil Saturation	74	73	68
Oil API Gravity	37.29	35.46	43.58
Initial GOR (Scf/Stb)	336	558	1035
Saturation Pressure (Psi)	1211	2122	3064
Fracture Stages	28	50	34
Clusters per Fracture	9	9	9

For instance, none of the datasets chosen for this study has reservoir fluid compositions available; nonetheless, a skilled reservoir engineer can use the API gravity as a key indicator to determine which reservoir fluid composition in the tool's offered fluid composition templates is the closest. Similarly, no information regarding the hydraulic fracture design is available except the total number of fracture stages and the cluster count per fracture. In this case at least one of the necessarily needed fracture design properties i.e., fracture height can be guessed using the formation net pay thickness as a starting point. All other necessary parameters that cannot be estimated using the available information will be tuned up while simultaneously being guessed blindly. Keeping this technique in mind, all the information needed to start the performance analysis is divided into three categories: information that is available, information that is best predicted using indirectly linked parameters, and information that is predicted blindly and tuned accordingly while matching the performance plots. For all case studies, the available and the required data for the analysis are categorically distributed as listed in Table 7.2.

Table 7.2 Categorical distribution of the available and the required data for the W_3H analysis

Available Certain Data	Initial Reservoir Pressure
	Matrix Porosity
	Fracture Stages
	Clusters per Fracture
Best Guessed Data	Reservoir Fluid Type (Oil API Gravity)
	Fracture height (Net Pay Thickness)
Blind Guessed Data (Tuning Parameters)	Matrix Permeability
	Fracture Half-Length
	Fracture Conductivity

7.4.1. W_3H Performance Analysis

The entire analysis is carried out primarily in three steps, starting with the collection of static and dynamic data followed by dynamic performance data preparation, then tuning of input parameters to get the closest performance match using dimensionless type curves for the primary recovery, and finally determining of techno-economic unconventional EOR options. The dynamic data preparation is critical; the correct number of fracture stages and clusters per fracture is essentially required such that to normalize the data as per the W_3H tool's data input format. Since there are only one stage and three clusters per fracture in the tool's design as explained in chapter 3 'Reservoir Numerical Model Development', therefore the oil flow rate data must be normalized appropriately.

7.4.2. Primary Recovery Performance Match

Using the available well data after cleaning and normalization based on a single stage and three clusters per fracture, the dimensionless type-curve is matched for the primary recovery performance. Figures 7.14 to 7.16 are showing the dimensionless type curves and the associated well performance data including Oil Flow Rate (Q_o), and Bottom Hole Flowing Pressure (BHFP) for wells 1,2, and 3, respectively. The BHFP in each case is extrapolated to predict the well performance data using the W_3H smart tool.

Traditionally, using a history-matched numerical simulation model to predict well performance would take several hours to a few days. However, the W_3H smart tool was able to make this prediction in only a few minutes, even with blindly guessed parameters' tuning, and the performance match of all selected wells

are found to be in good agreement. Table 7.3 is presenting the complete list of input data including the tuned matching parameters for all three case studies.

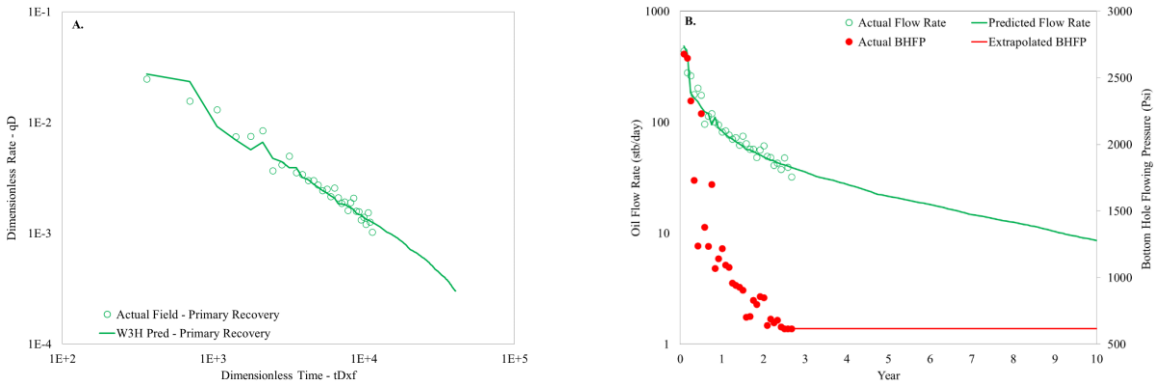

Figure 7.14 Well-1 primary recovery performance matching using the W_3H Smart tool
(A) Dimensionless type curve (B) Oil flow rate & BHFP

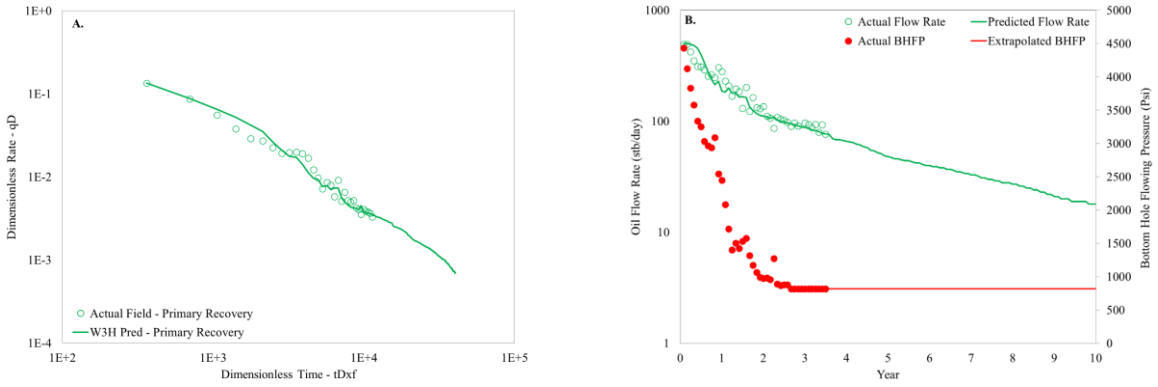

Figure 7.15 Well-2 primary recovery performance matching using the W_3H smart tool
(A) Dimensionless type curve (B) Oil flow rate & BHFP

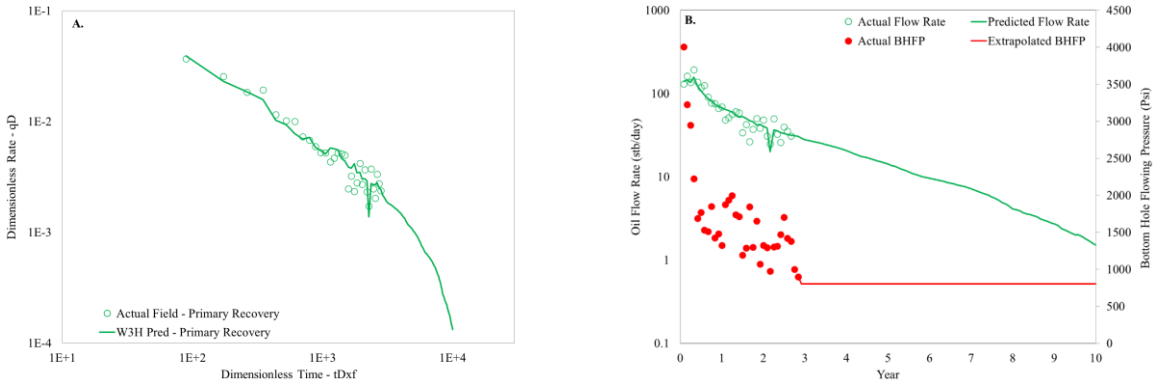

Figure 7.16 Well-3 Primary recovery performance matching using the W_3H smart tool
(A) Dimensionless type curve (B) Oil flow rate & BHFP

Table 7.3 Reservoir and hydraulic fracture information for all wells discussed in case studies

Input Parameter	Well 1	Well 2	Well 3
Initial Res. Pressure (Psi)	5400	5000	5000
Matrix Porosity (%)	6.3	6.3	5.0
Matrix Permeability (mD)	0.015	0.017	0.005
Fluid Type (Ref. Figure 3.11)	4	3	1
Fracture Half-Length (ft)	200	200	180
Fracture Height (ft)	40	40	50
Fracture Conductivity (mD.ft)	5	5	1
Fracture Stages	28	50	34
Clusters per Fracture	9	9	9

7.4.3. Techno-Economic UEOR Analysis

The next stage is to perform techno economic unconventional EOR screening by choosing a suitable EOR solvent and the operational design for the best oil recovery with the least amount of solvent injection and soaking time. The smart tool's design considered the fact that each operator uniquely operates their reservoir. As a result, the tool offers multiple realizations that can be tested with various combinations of EOR Solvent Type (available choices include CO_2 or HC), EOR Solvent Injection Volume (available range 0.2 - 900 MMScf), and Soaking Time (available range 2 – 30 days).

Before analyzing the selected case studies, a modified base case is created for each case study that is nothing more than the main recovery performance with a shut-in time, which is like the EOR solvent injection and soaking period, to create a fair incremental cumulative oil comparison. Before moving on to the EOR screening analysis, the modified base case performance for each well is compared with the true base case, which refers to the flow performance without well shut-in to observe the effect of pressure buildup. Even though there won't be much of a pressure-building impact because of the tight formation, limited pressure support, and isolated pressure transient effect, it would still be worthwhile to evaluate whether any extra barrels of oil may be produced without the use of any EOR applications. The primary recovery dimensionless type curves and the corresponding cumulative oil recovery comparisons are shown in Figures 7.17 to 7.19.

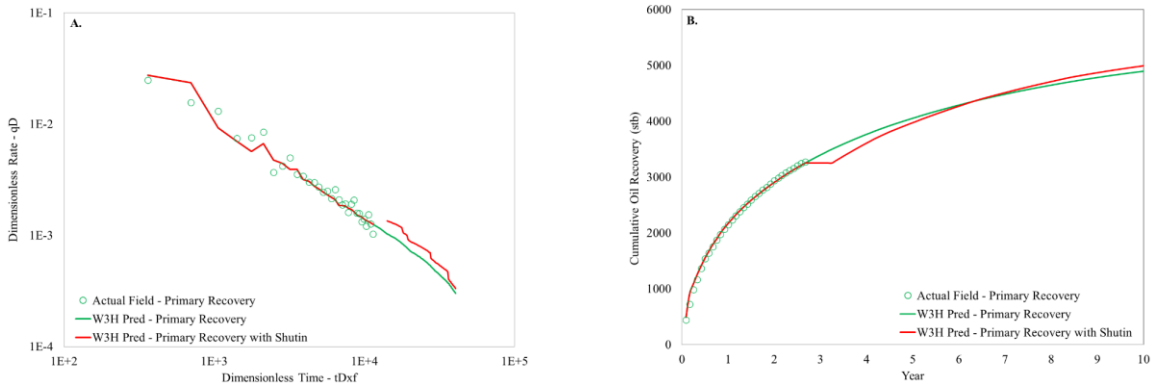

Figure 7.17 Well-1 Primary recovery performance with and without shutting in the producer
(A) Dimensionless type curve (B) Cum. oil

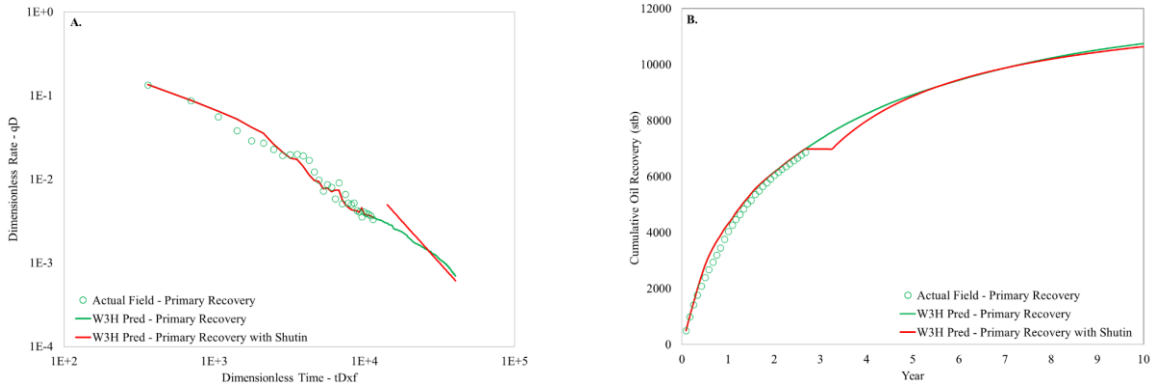

Figure 7.18 Well-2 Primary recovery performance with and without shutting in the producer
(A) Dimensionless type curve (B) Cum. oil

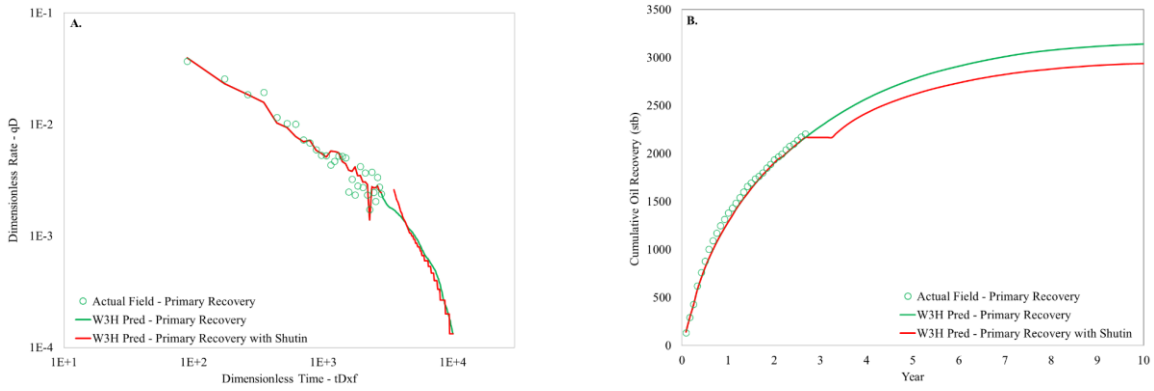

Figure 7.19 Well-3 Primary recovery performance with and without shutting in the producer
(A) Dimensionless type curve (B) Cum. oil

It can be noticed from the above figures, as expected, none of the examples demonstrate any benefit from shutting in the well, infect shutting the well negatively impacted the recovery performance. EOR application is, thus, a sensible choice to increase tight oil recovery. For instance, in this study, EOR

comparison is studied using CO_2 as an EOR solvent. To highlight the capability of the smart tool 'W_3H', multiple EOR operational designs, including the CO_2 injection volume and the soaking period, are considered in this study as listed in Table 7.4.

Table 7.4 EOR scenarios for different CO_2 injection volume and soaking periods

Scenarios	Injection Volume (MMScf)	Soaking Period (Days)
1	250	15
2	500	
3	750	
4	250	30
5	500	
6	750	

The EOR dimensionless type curves and the cumulative oil recovery comparisons are shown in Figures 7.20 to 7.22 for all wells considered in this study. For the performance comparisons, it is very important to consider both, long-term, and short-term benefits. For instance, the EOR application in Well 1 is not providing any extra barrels of oil, infect it is hurting the overall recovery in most of the scenarios with 15 days soaking period on a long-term comparison. However, on a short-term basis, the EOR application significantly boosted the oil recovery. Therefore, it can be concluded that an operator can benefit from the EOR application depending on its objectives based on the production timeline. There is another fact to keep in mind that all the presented performances are generated based on a single Huff-n-Puff cycle purposely to demonstrate the capabilities of the technique introduced in this work and the smart tool developed for the operators.

Despite having identical recovery performance, scenarios 5 and 6 perform better when compared. Well 2's recovery capabilities are virtually identical to those of Well 1. However, well 3; the strongest candidate—shows a large increase in oil recovery across all scenarios. Therefore, depending on the availability of CO_2 volume and the operator's flexibility for how long a well may be left idol in operation to give an adequate soaking period, any method could be chosen. From this study, it can be inferred that more CO_2 injection does not always result in increased oil recovery; there is always a threshold, but

increased CO_2 volume would aim for more in situ oil recovery. Like this, a longer soaking time would help the CO_2 to disperse more oil.

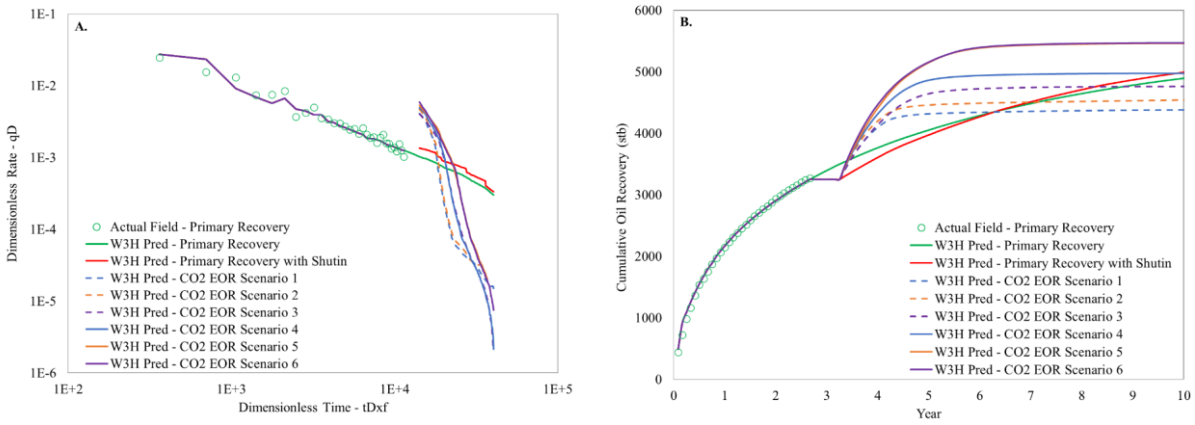

Figure 7.20 Well-1 UEOR SPiC TC_D and the cumulative oil recovery comparisons using the W$_3$H smart tool

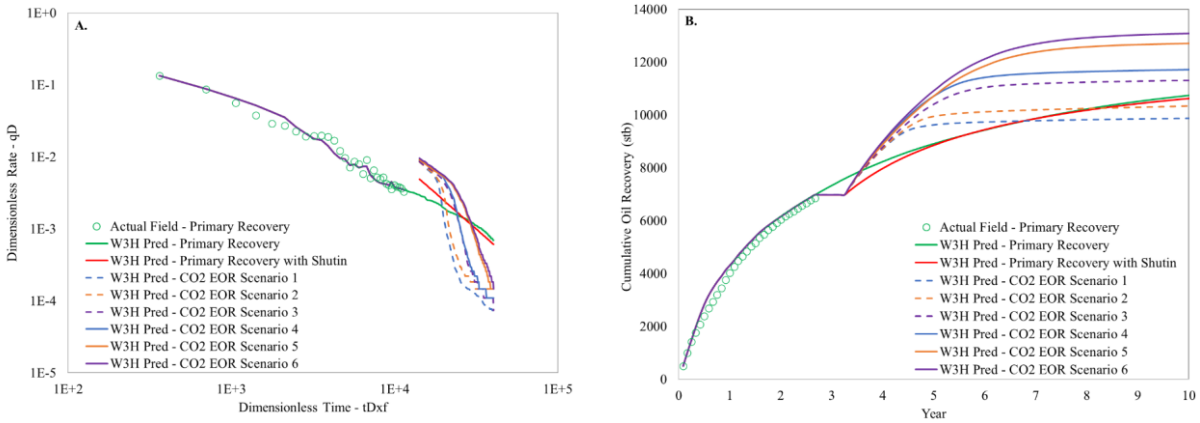

Figure 7.21 Well-2 UEOR SPiC TC_D and the cumulative oil recovery comparisons using the W$_3$H smart tool

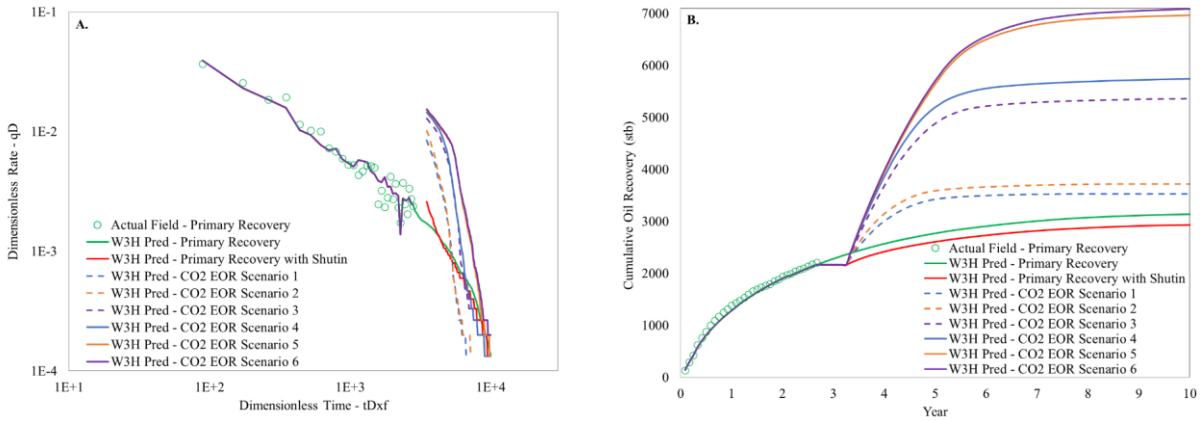

Figure 7.22 Well-3 UEOR SPiC TC_D and the cumulative oil recovery comparisons using the W$_3$H smart tool

7.4.4. Discussion

It is significant to note from the analysis above that the flow performances of the subject wells differ from one another while being produced from the same reservoir (Eagle Ford), despite exploiting different formations. According to the W3H analysis, the reservoir matrix characteristics, such as matrix porosity and permeability, are roughly identical for the formations adjacent to the wells, but the reservoir fluid types are significantly different. Additionally, all wells' hydraulic fracture designs are found to be similar, for example, wells 1 and 2 are having the same fracture half-length, fracture height, and fracture conductivity. While well 3 is found to have a lower fracture conductivity but a little greater half-length and height. All three wells have noticeably different fracture stages, but because the production performance study compares normalized production based on a single-stage fracture, the fracture stage differences are not considered.

The incremental oil recovery responses observed in all three wells are interesting when considering the reservoir and hydraulic fracture design parameters, and most notably, the reservoir fluid type. The fluid type is the key player among other factors. As we know, CO_2 is more active for the EOR in lighter oil in comparison and that is why a comparatively much-improved response is observed in well 3 with the lightest reservoir fluid type, followed by well 2. Tables 7.5 through 7.7 summarize the incremental oil recovery observations, distributed in short- and long-term recovery responses.

It is essential to keep in mind that incremental oil recovery is a time-dependent event, making the comparative sustainability of the incremental recovery a critical issue that must be considered when planning huff-and-puff-based EOR projects. Therefore, in any case, an immediate recovery boost is possible, but the long-term ultimate incremental recovery is not guaranteed. For instance, scenarios 1 through 4 are viable choices for short-term recoveries, but as time passes, the ultimate oil recovery through EOR offers no advantages over the primary recovery. A similar behavior could be observed in well 2, while well 3 is far better in comparison, therefore, a single huff-n-puff cycle with any considered scenario would

work, however, for the other two wells, as soon as the incremental recovery performance flattens, another huff-n-puff cycle should be considered for long term incremental oil recovery benefits.

Table 7.5 Short and long-term EOR incremental oil recovery comparison for Well 1

		Scenario 1	Scenario 2	Scenario 3	Scenario 4	Scenario 5	Scenario 6
Short-Term Recovery (%)	1 Month	2.56	3.06	2.51	3.30	3.62	4.13
	6 Month	6.64	7.87	6.51	8.50	9.23	10.26
	1 Year	9.43	11.11	9.35	12.20	13.23	14.45
Long-Term Recovery (%)	3 Years	10.91	13.66	15.03	18.81	21.98	22.34
	6 Years	-9.76	-6.12	-0.83	3.47	12.08	12.21
	10 Years	-19.35	-14.64	-9.93	-5.24	4.20	4.34

Table 7.6 Short and long-term EOR incremental oil recovery comparison for Well 2

		Scenario 1	Scenario 2	Scenario 3	Scenario 4	Scenario 5	Scenario 6
Short-Term Recovery (%)	1 Month	1.43	1.34	1.38	1.63	1.59	1.74
	6 Month	3.83	3.68	3.77	4.48	4.34	4.79
	1 Year	5.70	5.60	5.81	6.89	6.65	7.35
Long-Term Recovery (%)	3 Years	5.26	8.74	15.24	18.02	19.42	21.01
	6 Years	-4.95	-0.49	8.31	11.53	18.30	20.54
	10 Years	-10.85	-5.30	3.14	6.70	14.04	16.58

Table 7.7 Short and long-term EOR incremental oil recovery comparison for Well 3

		Scenario 1	Scenario 2	Scenario 3	Scenario 4	Scenario 5	Scenario 6
Short-Term Recovery (%)	1 Month	3.84	4.92	6.57	7.51	7.93	8.09
	6 Month	9.73	12.31	16.75	18.77	19.63	19.95
	1 Year	14.02	17.26	24.16	26.78	27.87	28.27
Long-Term Recovery (%)	3 Years	22.83	26.38	47.70	50.79	56.84	57.25
	6 Years	17.82	22.09	45.65	49.21	58.10	58.76
	10 Years	15.95	20.31	44.97	48.62	57.63	58.44

8

W_3H 'Software Package' – USER MANUAL

The Where, When, What, and How of injecting EOR solvent for the best techno-economic incremental oil recovery are typical issues that are addressed by the smart tool 'W_3H', which was created for the unconventional tight oil EOR pilot selection. W_3H is a Physics-based alternative to computationally expensive numerical simulation tools that provide answers in a few hours instead of months to narrow down the list of potential UEOR pilot wells, to be further investigated in detail, based on the wells performance history, regional formation maturity, hydraulic fracture design, and the availability of the EOR agents such as CO_2 and produced hydrocarbon gas. W_3H is simple and easy to use those imports historical well performance data (primary recovery) along with reservoir rock and fluid quality information & hydraulic fracture design parameters and provides multiple EOR options with optimum incremental oil recovery after matching the primary recovery performance with the W_3H dimensionless type curves.

8.1. Introduction

W_3H is a smart plug & play tool developed using Python coding language, capable of analyzing single well-based tight oil production data and providing the suitable EOR options based on the most suited EOR agent selection (i.e., CO_2 or HC), the injection solvent volume, and followed by the soaking period for the optimum incremental oil recovery. Not necessarily, this tool has to be used for the pre-drilled well with prior production history; also, it can be used to design a new well from scratch using the typical reservoir formation and the hydraulic design parameters data. W_3H tool is empowered with Deep Neural Network (DNN) based proxy models and as discussed in the prior chapters the proxy models are developed using a huge compositional numerical simulation-based database. In addition, a Physics-Guided Design of Experiment (PG-DoE) is applied to generate enough random data samples to cover the entire possible sampling space.

8.2. A Quick W_3H Overlook

W_3H is a sophisticated yet simple application with a single interface as shown below in Figure 8.1. Also, all major operational and visualization components of the interface are shown in the same figure which include the W_3H Design Bar, W_3H Toolbox, and multiple data entry and visualization tab windows. The user entry tab window intakes all the necessary reservoir rock and fluid properties, hydraulic fracture design parameters along with the historical (primary recovery) well performance data. Visualization tab windows are used to preview historical performance plots as well as the W_3H performance plots including the SPiC dimensionless type curves in the Type Curve tab window. W_3H designer bar is used to modify reservoir and hydraulic fracture properties to match the primary recovery plots and finally, the EOR operational design properties, including EOR solvent volume and the soaking time, are modified in the W_3H designer bar to perform the Unconventional EOR analysis. Similarly, the W_3H Toolbox is used to visualize the reservoir fluid composition templates and the toolbox contains multiple functional buttons for data handling and plotting.

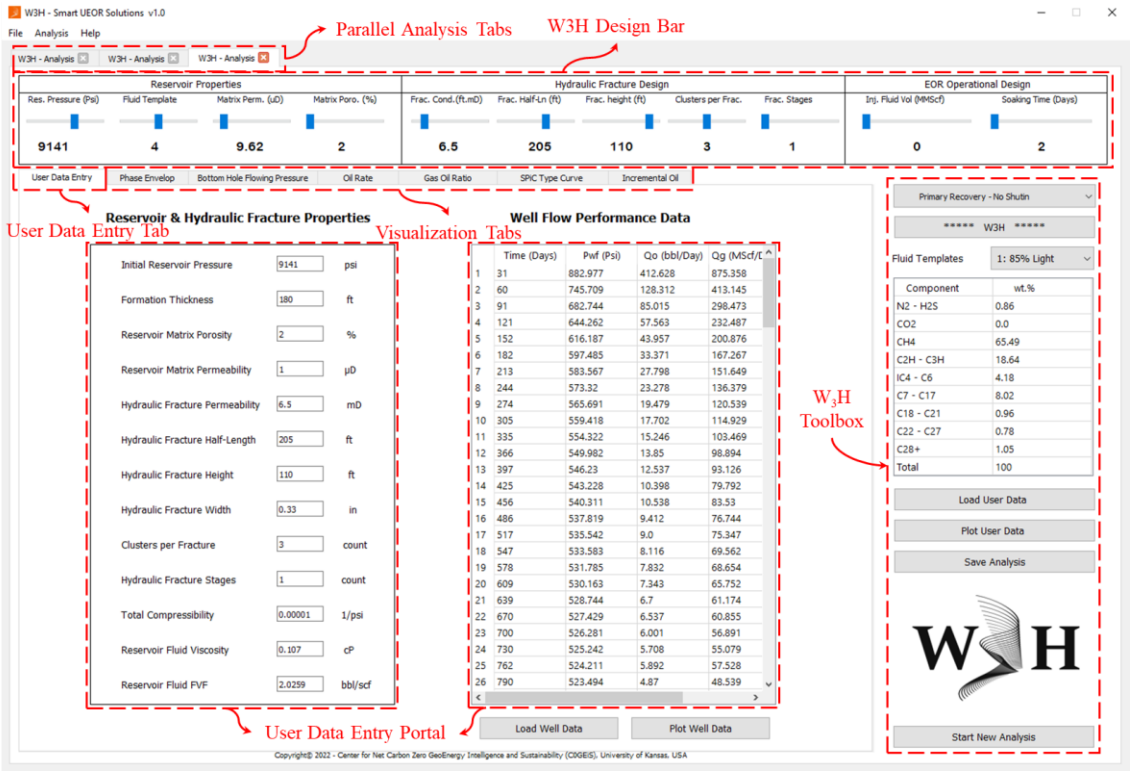

Figure 8.1 W3H – Smart tool interface with operational and visualization components

8.3. W3H Operational Analysis Steps

There are following six major steps to perform W3H analysis as listed in Figure 8.2 while the detailed steps are discussed below as shown in Figure 8.3.

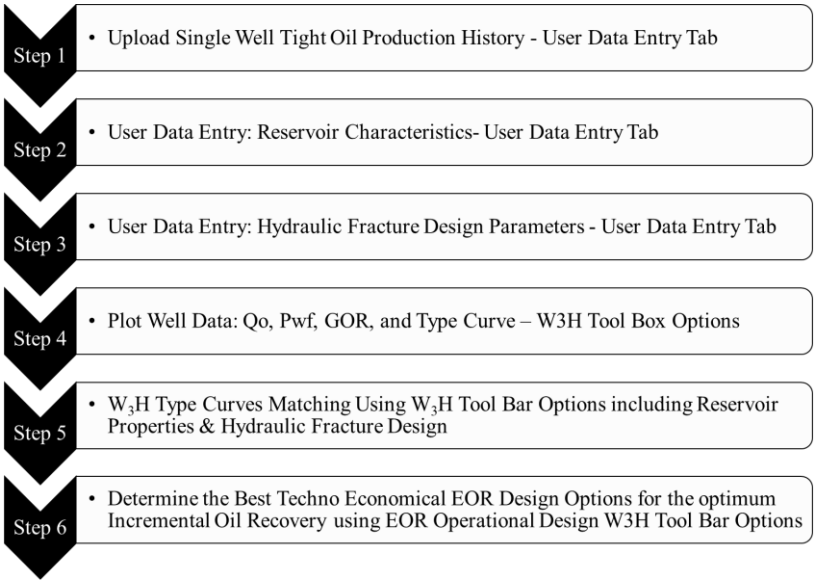

Figure 8.2 W3H – Major operational steps

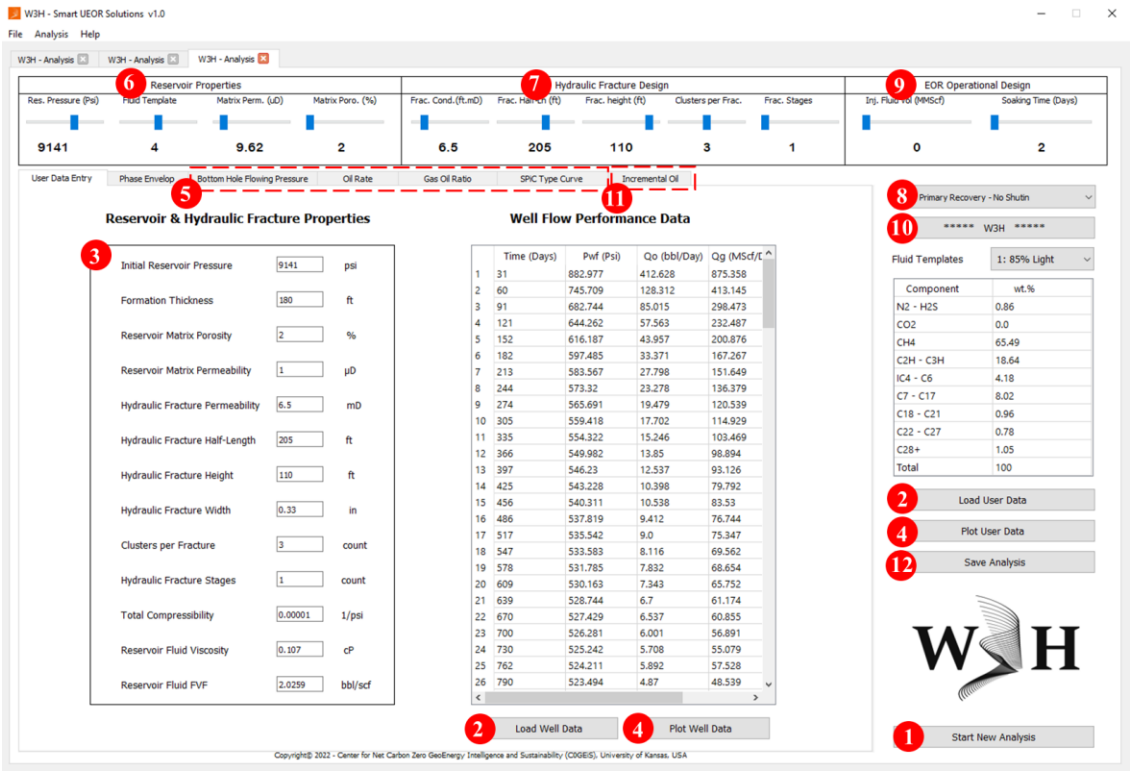

Figure 8.3 Steps for user data entry and visualization steps

Step 1: Press the Start New Analysis button to start a new analysis window. Multiple tabs can be opened in the same window by simply pressing the same button for parallel analysis.

Step 2: Upload the historical well data (primary production) in a specific data format using the '.csv, .xls, .xlm, or .xlsx' file using the Load Well Data button. The data format is required to be in the same sequence as shown in Figure 8.4. In case of having no data for the gas flow rate, leave it black.

	A	B	C	D
1	Days	Pwf (Psi)	Qo (bbl/day)	Qo (MScf/day)
2	31	882.977	412.628	875.358
3	60	745.709	128.312	413.145
4	91	682.744	85.015	298.473
5	121	644.262	57.563	232.487
6	152	616.187	43.957	200.876
7	182	597.485	33.371	167.267
8	213	583.567	27.798	151.649
9	244	573.32	23.278	136.379
10	274	565.691	19.479	120.539

Figure 8.4 User data format for uploading in the application

Step 3: Populate reservoir and hydraulic fracture properties in User Entry Portal on the User Data Entry tab window.

Step 4: Press 'Plot Well Data' to plot well performance data including bottom hole flowing pressure, oil flow rate, gas oil ratio, and the associated dimensionless type curve. It is important to keep in mind that a type curve depends on the reservoir rock and fluid properties as well as hydraulic fracture design charecterstics therefore data quality is important.

Step 5: Next step is to visualize the well flow performance using the bottom hole flowing pressure (Pwf), oil flow rate (Q_o), & gas oil ratio (GOR) tabs and the dimensionless type curve (SPiC TC_D) in their respective visualization tab windows.

Step 6 & 7: After uploading the user data, the next step is to match the given well's flow performance with the W_3H flow performance curves mainly for the flow rate and the SPiC TC_D. GOR could be a useful tool for the performance match but is not mandatorily required. In this step, an appropriate reservoir fluid type selection is critical which directly affects the flow performance and the type curve shape and its slops for different time regions. There are multiple fluid composition templates are provided in the application, such that, the closest possible reservoir fluid type can be selected representing the reservoir in-situ reservoir fluid composition. There are two ways to choose the fluid type including based on the fluid compositions listed in 'W_3H Toolbox', a drop-down window 'Fluid Templates' would provide different fluid type options, or through phase envelop diagrams associated with different fluid compositions that can be visualized in the 'Phase Envelop Tab' window as shown in Figure 8.5. For flow performance matching, the closest reservoir fluid type selection is very important for an accurate prediction and further EOR screening.

Other reservoir properties including reservoir pressure and the matrix porosity are also important. Similarly, the hydraulic fracture design parameters are critical to select. It is recommended to refer Dimensionless Type Curves user guide provided in Chapter 5 (Figure 5.10) for quick SPiC TC_D matching. An excellent example of user entered tight oil well performance data visualization is presented in following fgures. Figure 8.6 is presenting the user entered well's bottom hole flowing pressure.

In Figures 8.7 through 8.9, the cross dot plots are presentation the user well performance data while slid lines in each plot represent the W_3H prediction plots for oil flow rate, gas oil ratio and SPiC dimensionless type curves, respectively, generated through physics based tight oil well performance proxy models.

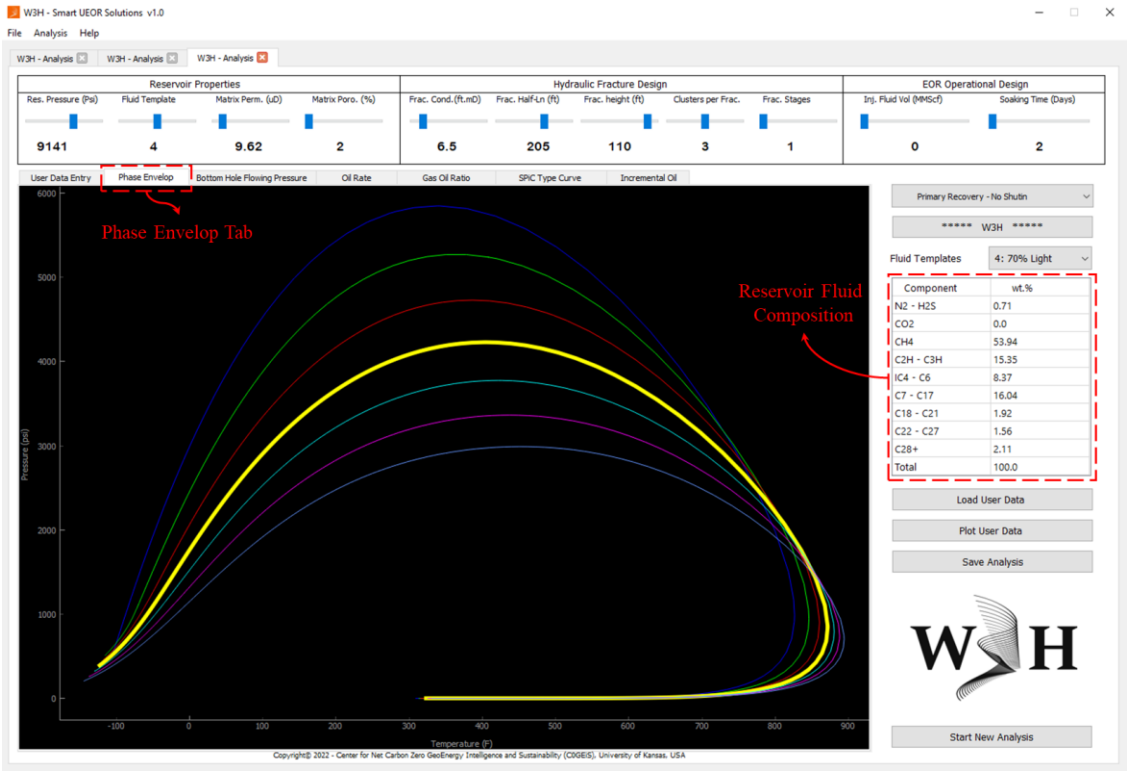

Figure 8.5 Reservoir fluid type selection window through fluid composition or phase envelop

It is very important to have a closest possible performance match, especially for the dimensionless type curve before moving towards the UEOR techno-economic analysis. It is recommended to follow steps listed below for quick and effective performance match.

1. Start with the most certain reservoir and hydraulic fracture design properties in the W_3H design bar. Reservoir fluid type is crucial and a sensitive parameter therefore one has to be careful when selecting the reservoir fluid type.
2. Use all possible available date to guess the missing data, however that can be improved through trial and error process.
3. For the missing data that can not be guessed using the available data at all, use engineering understanding and the experience to start with the possible range of each parameters.

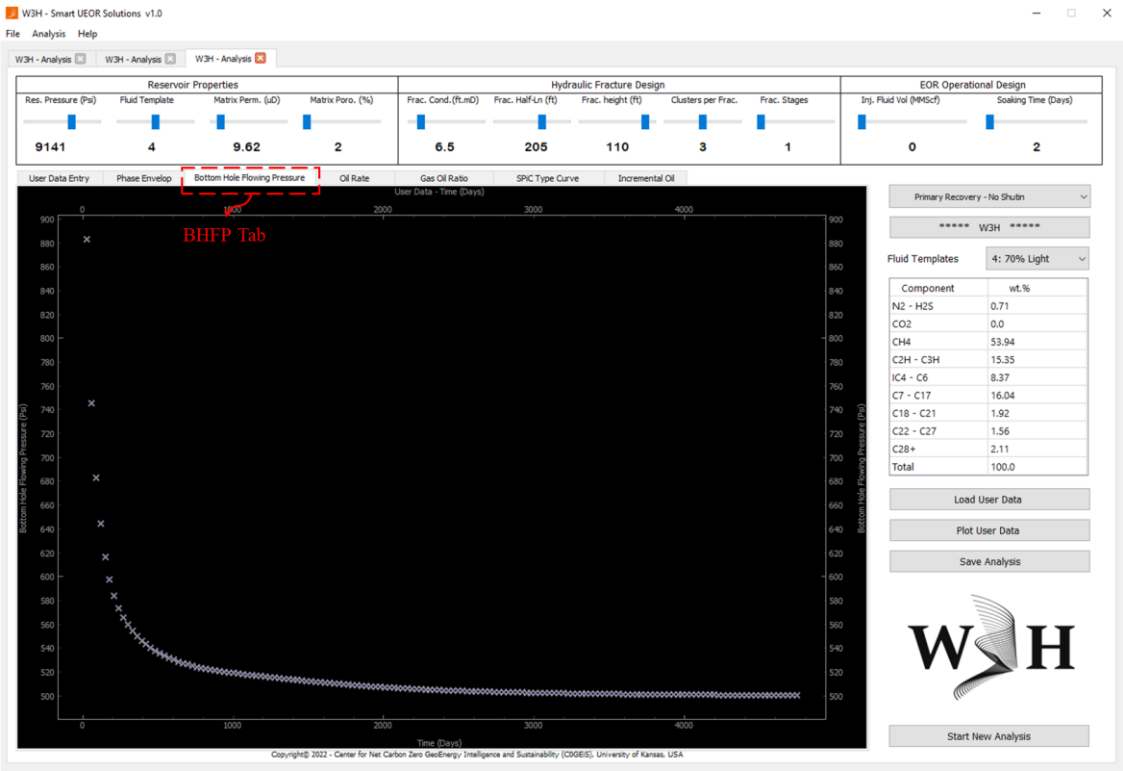

Figure 8.6 User data visualization – Bottom Hole Flowing Pressure

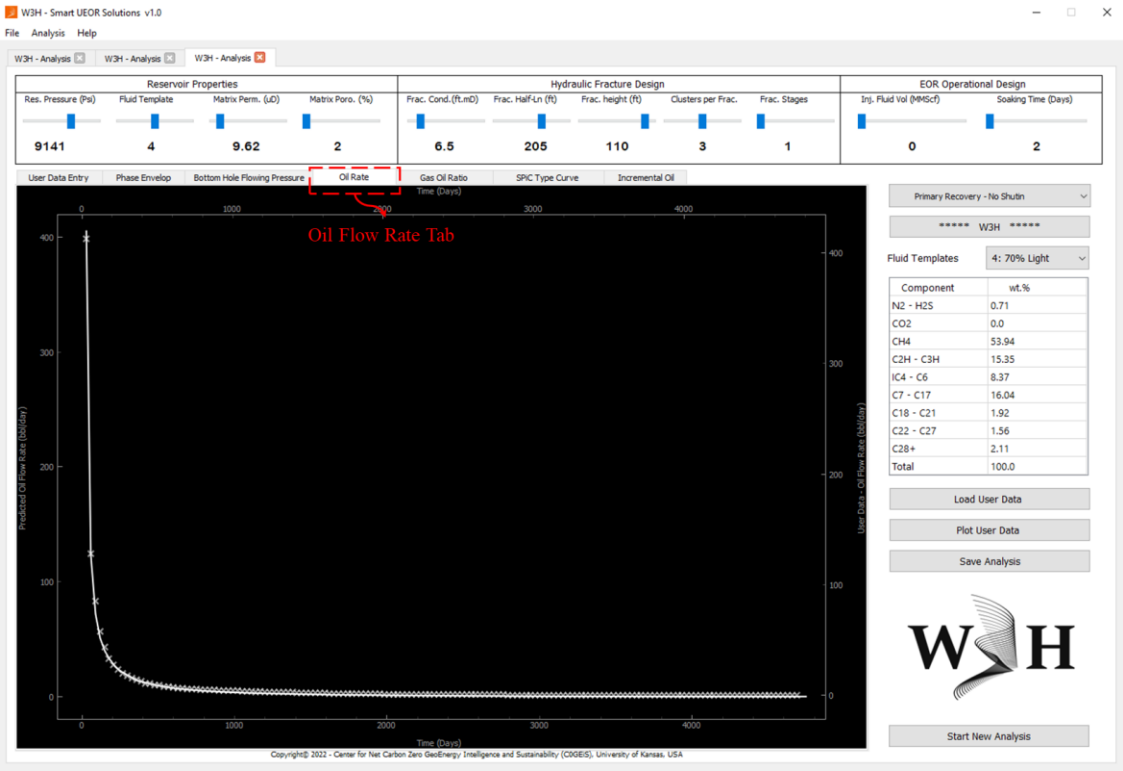

Figure 8.7 User data visualization – Oil flow rate

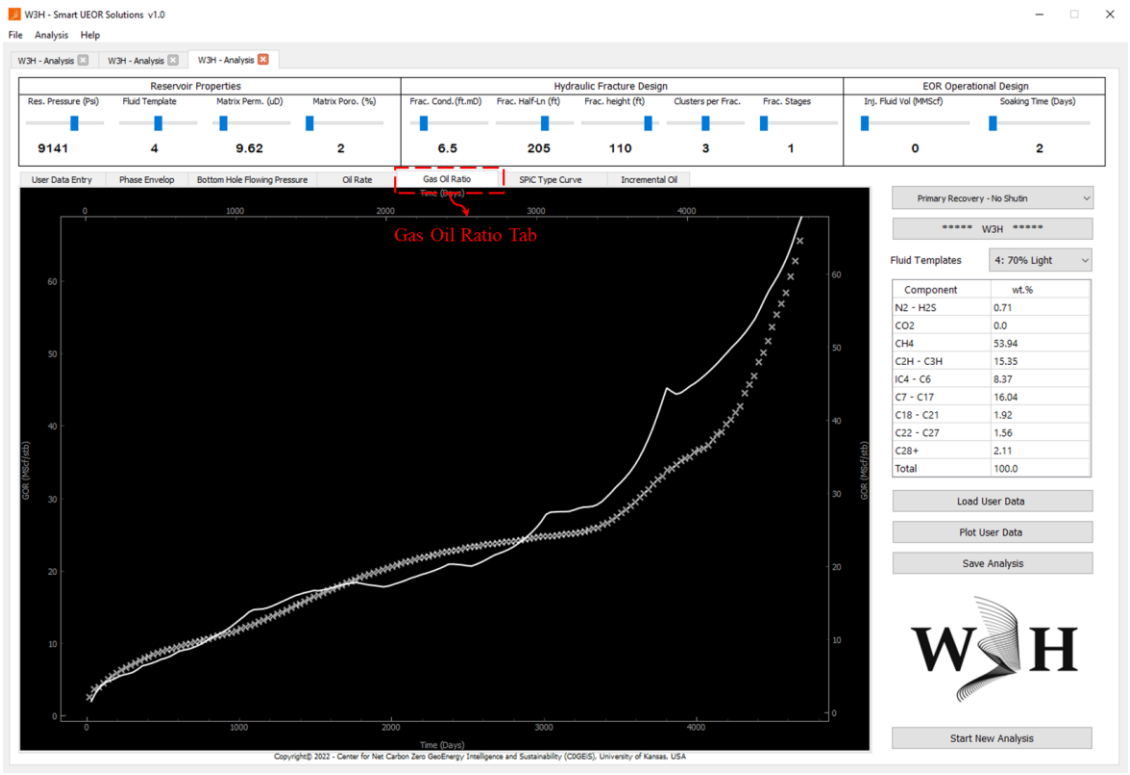

Figure 8.8 User data visualization – Gas Oil Ratio

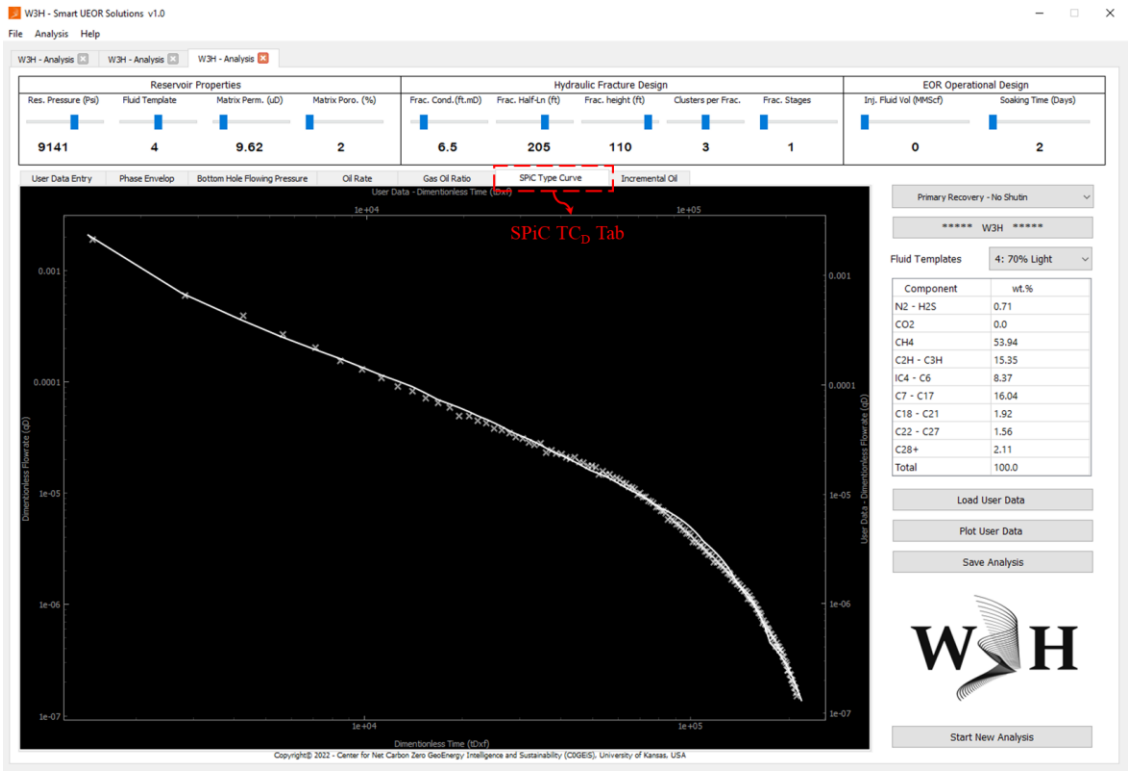

Figure 8.9 User data visualization – Smart Physics-inspired Compositional Dimensionless Type Curve

Step 8: Finally, after having a satisfactory type curve match as shown in Figure 8.9, it's time to move on to UEOR options. The EOR option are listed in the drop-down window as shown in Figure 8.10. There are a couple of options for both primary recovery as well as for EOR. For the primary recovery, there is a 'Primary Recovery – No Shutin' option that makes the well flow without any interruption that is used for the primary well performance matching, while the other option, i.e., 'Primary Recovery with Shut-in', is included as a reference analysis for the EOR options. In this case, the well is kept shut-in for the same duration as the EOR operation is conducted (injection and soaking period) to visualize the effect of pressure build-up (if any). While the EOR, CO_2, and hydrocarbon gas injection options are currently included in the application.

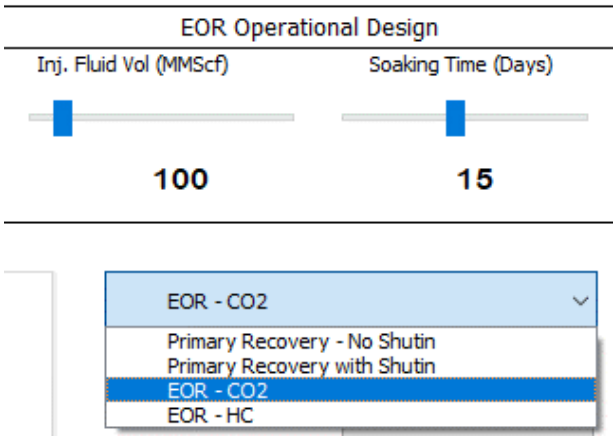

Figure 8.10 Primary recovery and EOR options available to select for the W_3H analysis

Step 9: In this step, the EOR operational design is selected through the EOR solvent injection volume and the soaking period selection.

Step 10 & 11: Operationally, the last step is to hit the 'W_3H' button, located in the W_3H Toolbox, to visualize the UEOR proxy model's results through SPiC dimensionless type curve and the corresponding oil flow rate versus time and the incremental oil recovery. Every time, after changing the EOR operational design or making any changes in any of the listed options, the W_3H button is required to be pressed to update the proxy model's results according to the selected EOR operational design options.

Figure 8.11 is showing the oil flow performance for both primary recovery through scatter plot (as a reference) while the solid line is presenting the W_3H proxy model response for the selected UEOR operational design. For example, in this case, 100 MMScf of CO_2 is injected as a single huff-n-puff cycle followed by 15 days of soaking period. The correspoinding SPiC dimensionless type curve is shown in Figure 8.12 and it is obvious from the figure that the UEOR SPiC TC_D show quite different response in comparison of the primary recovery. The SPiC TC_D use guide is provided in Chapter 5 (Figure 5.10) for individual flow regions analysis.Figure 8.13 is presenting the resultant incremental oil recovery. It is important to keep in mind that the incremental oil recovery is based on single stage huff-n-puff cycle and also most of the incremental oil recovery is assumed to be obtained mainly from the stimulated reservoir volume (SRV).

Step 12: Finally, the entire analysis could be saved through pressing the 'Save Analysis' button.

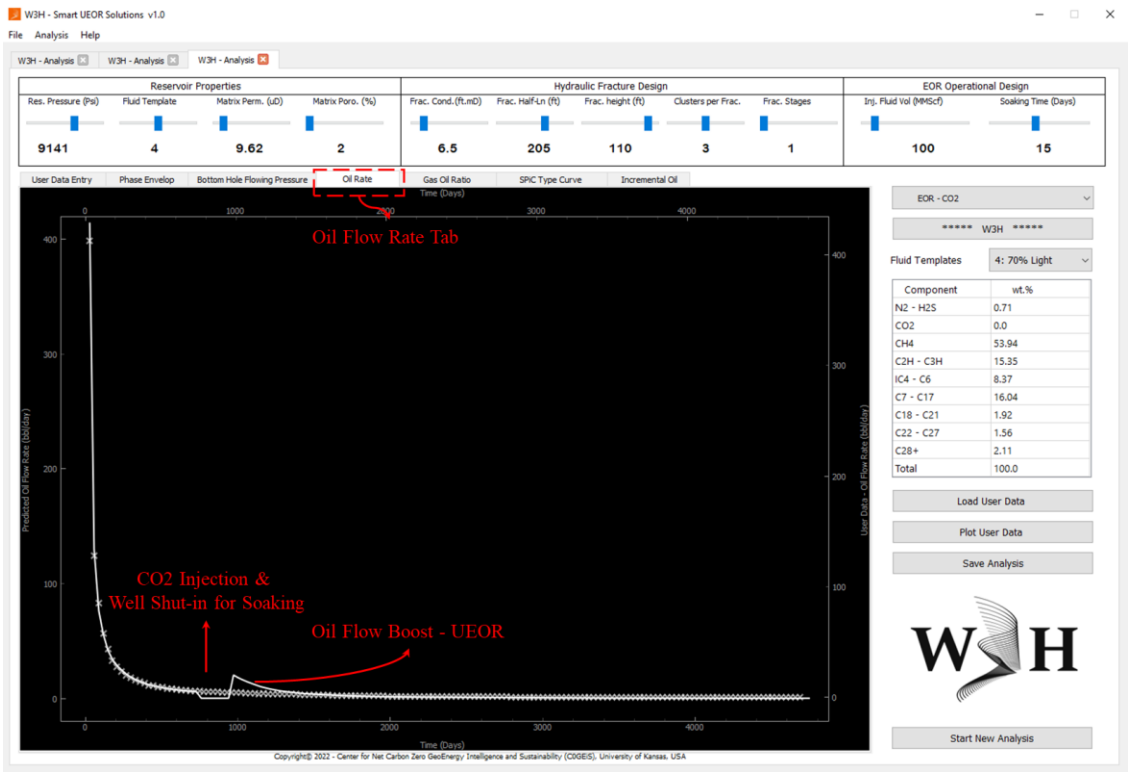

Figure 8.11 Oil flow rate visualization for primary recovery and the UEOR flow performance

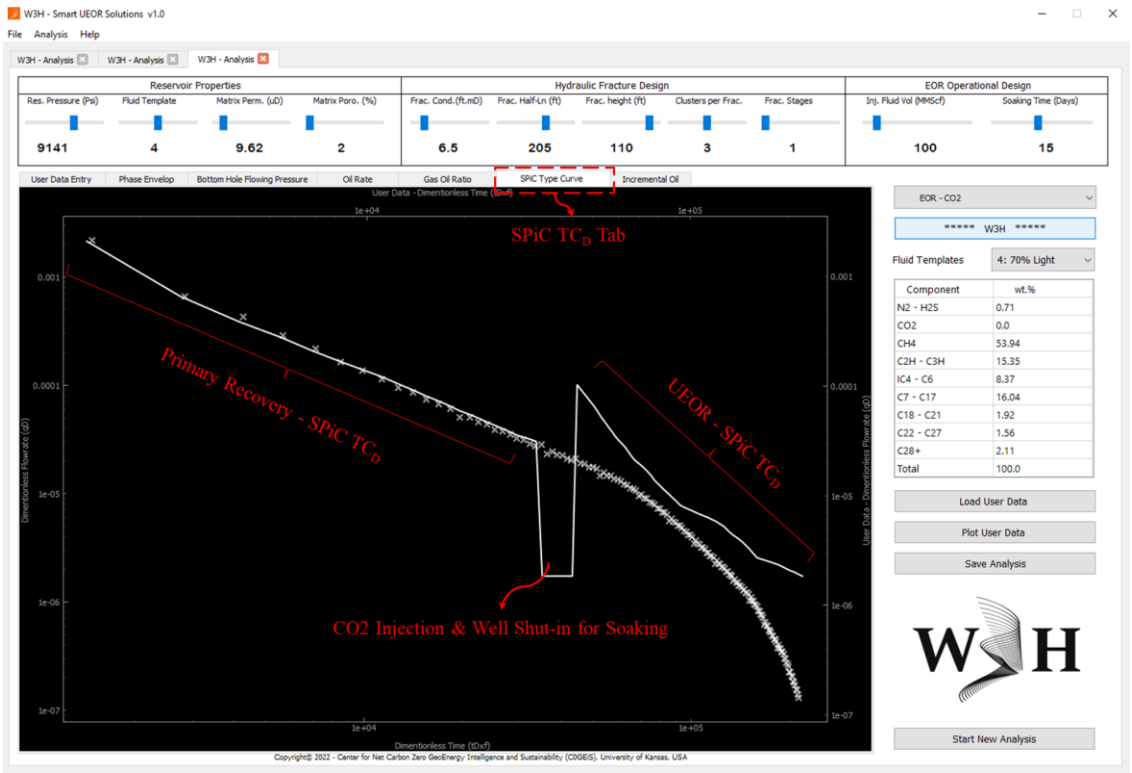

Figure 8.12 Primary and UEOR SPiC Dimensionless Type Curves

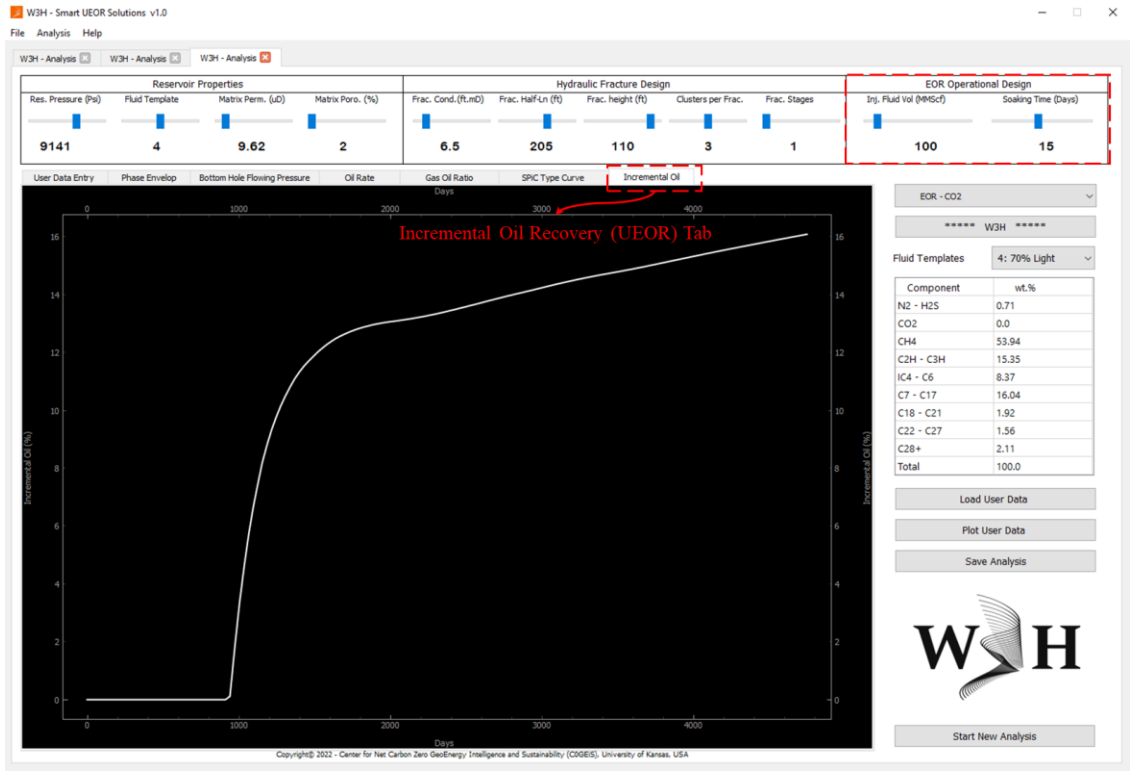

Figure 8.13 Incremental Oil recovery as the result of UEOR application

9

SUMMARY, CONCLUSIONS, & RECOMMENDATIONS

9.1. Summary & Conclusions

Typically, tight oil reservoirs are distinguished by their extremely low inter-pore connectivity and ultra-tight matrix permeability. For such reservoirs to produce profitably, extra measures are traditionally considered, such as long horizontal wells and a significant hydraulic fracture network that can maximize reservoir contact. Even with these specialized and expensive treatments, tight oil wells are observed hardly ever deliver more than 10% of the oil in place.

EOR is therefore believed to be helpful for fast-paced and economical oil recovery when used in the early reservoir development phase. However, to optimize oil recovery through EOR application, it is essential to identify each tight oil reservoir's unique EOR potential and the most effective EOR application design. To do such, a numerical simulation approach is applied that is computationally expensive and time-consuming.

The Smart Physics-Inspired Compositional Dimensionless Type Curves for Unconventional Tight Oil Reservoir EOR are introduced in this dissertation as a substitute to optimize UEOR practice and save millions of dollars and computational run time. These type curves are intended to answer the W_3H issues for operators (i.e., Where to inject, When to inject, What to inject, and How to inject an EOR solvent) while conducting thorough field screening and developing novel EOR pilot projects. In parallel, a user-friendly, plug-and-play application with a Graphical User Interface (GUI) is developed that can suggest optimal UEOR operational design following physics governing laws based on the prior production history, reservoir characteristics, in-situ fluid type, and the pre-existing hydraulic fracture network design. The choice of EOR solvent type, its injection volume, and the soaking time are the primary components of the operational design for EOR.

The smart tool is developed using a Physics-Inspired Design of Experiment (PI-DoE) based on a large number of compositional numerical simulation cases generated through a commercial simulator. PI-DoE covered a wide range of individual reservoir rock and fluid properties, hydraulic fracture design parameters, and the EOR operational design constraints. Deep neural network algorithms are used to train proxy models so that they can reproduce fluid flow performance from a tight oil reservoir in every conceivable

combination of reservoir rock and fluid characteristics as well as the hydraulic fracture and the operational design parameters. The performance of the proxy models is successfully assessed utilizing several physics-based sensitivity analyses, cross-checked using numerical simulation, and a few actual field case studies. As a result of this study, many EOR design possibilities are also examined.

9.2. Recommendations

Due to time restrictions, several limitations and assumptions are considered in this study, therefore, it is highly recommended to extend this study to address the following facts to make this application more robust.

- The database used for proxy model training should be further enhanced with actual field data to such that to consider more robustness of the data and the effect of real field heterogeneity.
- More simulation cases with horizontal well placement at various places should be provided to capture additional boundary dominant flow prospects; currently, in all simulation cases, the well is considered in the middle of the reservoir model.
- To further improve the quality, more examples with varied numbers of clusters and stages as well as non-unique fracture spacing should be taken into consideration. The existing database only has a single-stage hydraulic fracture design with equally spaced three clusters per fracture.
- In future work, multiple huff-n-puff cycles with non-unique cycle durations should be considered to provide additional EOR design options to the end user, the current model is based on a single huff-n-puff cycle.
- Additional cases with wellbore storage and skin factor should be considered to provide an operator more flexibility to match its well performance.
- The training dataset currently uses seven reservoir fluid templates; however, additional fluid compositions might assist to improve the dataset's quality.

10

REFERENCES

Abdullah, M., Emami-Meybodi, H. and Ertekin, T., 2019, June. Development and application of an artificial neural network tool for chemical EOR field implementations. In *SPE Europec featured at 81st EAGE Conference and Exhibition*. OnePetro.

Adel, I.A., Tovar, F.D., Zhang, F. and Schechter, D.S., 2018. The impact of MMP on recovery factor during CO_2–EOR in unconventional liquid reservoirs. SPE Annual Technical Conference and Exhibition. https://doi.org/10.2118/191752-MS

Ahmad, F., Isa, N.A.M., Osman, M.K. and Hussain, Z., 2010, November. Performance comparison of gradient descent and Genetic Algorithm based Artificial Neural Networks training. In *2010 10th International Conference on Intelligent Systems Design and Applications* (pp. 604-609). IEEE.

Ahmed, U. and Meehan, D.N. eds., 2016. Unconventional Oil and Gas Resources: Exploitation and Development. CRC Press.

Akbar, I., Zhou, H., Liu, W., Qureshi, A.S., Memon, A., Muther, T., Ansari, U., UsmanTahir, M., Bakhsh, A., Shaikh, A. and Hamed, H.H., 2021. Nano-suspension combined effect with polymer gels for enhanced oil recovery in low permeability reservoir. Arabian Journal of Geosciences, 14(15), 1-16. https://doi.org/10.1007/s12517-021-07534-0

Al Shalabi, L. and Shaaban, Z., 2006, May. Normalization as a preprocessing engine for data mining and the approach of preference matrix. In *2006 International conference on dependability of computer systems* (pp. 207-214). IEEE.

Alcocer, Y. and Rodrigues, P., 2001, January. Neural networks models for estimation of fluid properties. In SPE Latin American and Caribbean Petroleum Engineering Conference. Society of Petroleum Engineers.

Alder, B.J. and Wainwright, T.E., 1959. Studies in molecular dynamics. I. General method. The Journal of Chemical Physics, 31(2), 459-466. https://doi.org/10.1063/1.1730376

Alder, B.J., and Wainwright, T.E., 1957. Phase transition for a hard sphere system. J. Chem. Phys. 27, 1208–1209. https://doi.org/10.1063/1.1743957

Alfarge, D., Wei, M. and Bai, B., 2017a. IOR Methods in unconventional reservoirs of North America: Comprehensive review. SPE Western Regional Meeting. https://doi. org/10.2118/185640-MS

Alfarge, D., Wei, M. and Bai, B., 2017b. Feasibility of CO_2-EOR in shale-oil reservoirs: Numerical simulation study and pilot tests. Carbon Management Technology Conference. https://doi.org/10.7122/485111-MS

Alfarge, D., Wei, M. and Bai, B., 2017c. Factors affecting CO_2-EOR in shale-oil reservoirs: Numerical simulation study and pilot tests. Energy & Fuels, 31(8), 8462-8480. https://doi.org/10.1021/acs.energyfuels.7b01623

Al-Farisi, O., Belhaj, H., Fahmy, F., Syed, F., Fan, K., Al-Attar, A., Al-Hashmi, E., Memon, S., Al-Hosany, M., Hussain, T. and Obasi, D., 2012. Price projection model for new explorations and the lost control of majors. In GEO 2012 (pp. cp-287). European Association of Geoscientists & Engineers. https://doi.org/10.3997/2214-4609-pdb.287.1133696

Alharthy, N., Teklu, T., Kazemi, H., Graves, R., Hawthorne, S., Braunberger, J. and Kurtoglu, B., 2018a. Enhanced oil recovery in liquid–rich shale reservoirs: Laboratory to field. SPE Reservoir Evaluation & Engineering, 21(01), 137-159. https://doi.org/10.2118/175034-PA

Alvarez, J.O. and Schechter, D.S., 2016. Wettability, oil and rock characterization of the most important unconventional liquid reservoirs in the United States and the impact on oil recovery.

SPE/AAPG/SEG Unconventional Resources Technology Conference. https://doi.org/10.15530/URTEC-2016-2461651

Alvarez, J.O., Neog, A., Jais, A. and Schechter, D.S., 2014. Impact of surfactants for wettability alteration in stimulation fluids and the potential for surfactant EOR in unconventional liquid reservoirs. SPE Unconventional Resources Conference. https://doi.org/10.2118/169001-MS

Alvarez, J.O., Tovar, F.D. and Schechter, D.S., 2017. Improving oil recovery in unconventional liquid reservoirs by soaking-flowback production schedule with surfactant additives. SPE Liquids-Rich Basins Conference-North America. https://doi.org/10.2118/187483-MS

Armstrong, R.T., Wildenschild, D. and Bay, B.K., 2015. The effect of pore morphology on microbial enhanced oil recovery. Journal of Petroleum Science and Engineering, 130, pp.16-25.

Arps, J.J., 1945. Analysis of decline curves. *Transactions of the AIME*, *160*(01), pp.228-247.

Arri, L.E., Yee, D., Morgan, W.D. and Jeansonne, M.W., 1992, May. Modeling coalbed methane production with binary gas sorption. In *SPE rocky mountain regional meeting*. OnePetro.

Aziz, H., Muther, T., Khan, M.J. and Syed, F.I., 2021. A review on nanofluid water alternating gas (N-WAG): application, preparation, mechanism, and challenges. Arabian Journal of Geosciences, 14(14), 1-12. https://doi.org/10.1007/s12517-021-07787-9

Bahrami, P., Sahari Moghaddam, F. and James, L.A., 2022. A Review of Proxy Modeling Highlighting Applications for Reservoir Engineering. *Energies*, *15*(14), p.5247.

Balasubramanian, S., Chen, P., Bose, S., Alzahabi, A. and Thakur, G.C., 2018. Recent advances in enhanced oil recovery technologies for unconventional oil reservoirs. Offshore Technology Conference. https://doi.org/10.4043/28973-MS

Barree, R.D., Barree, V.L. and Craig, D., 2009. Holistic fracture diagnostics: consistent interpretation of prefrac injection tests using multiple analysis methods. SPE Production & Operations, 24(03), 396-406. https://doi.org/10.2118/107877-PA

Barree, R.D., Miskimins, J.L. and Gilbert, J.V., 2015. Diagnostic fracture injection tests: common mistakes, misfires, and misdiagnoses. SPE Production & Operations, 30(02), 84-98. https://doi.org/10.2118/169539-PA

Biresselioglu, M.E., 2016. | Changing trends in the production and consumption of oil and natural gas in the world. MNL 73 Exploration and Production of Petroleum and Natural Gas. American Society for Testing Materials (ASTM). Chapter 22, pp.657-678.

Brons, F. and Miller, W.C., 1961. A simple method for correcting spot pressure readings. Journal of Petroleum Technology, 13(08), pp.803-805.

Butler, B., Roberts, J., Kelsey, M. and van Der Veen, S., 2021. Mature field economic rejuvenation with infill and re-entry multilateral well creation techniques. IADC/SPE Asia Pacific Drilling Technology Conference. https://doi.org/10.2118/200996-MS

Cai, H.Y., Zhang, Y., Liu, Z.Y., Li, J.G., Gong, Q.T., Liao, Q., Zhang, L. and Zhao, S., 2018. Molecular dynamics simulation of binary betaine and anionic surfactant mixtures at decane-water interface. Journal of Molecular Liquids, 266, 82-89. https://doi.org/10.1016/j.molliq.2018.06.047

Caineng, Z., Zhang, G., Zhi, Y., Shizhen, T., Lianhua, H., Rukai, Z., Xuanjun, Y., Qiquan, R., Denghua, L. and Zhiping, W., 2013. Concepts, characteristics, potential and technology of unconventional

hydrocarbons: On unconventional petroleum geology. Petroleum Exploration and Development, 40(4), 413-428. https://doi.org/10.1016/S1876-3804(13)60053-1

Casey, B., Wehner, M., Richards, B. and Moore, C., 2018. Wolfcamp geologic reservoir modeling challenges. Unconventional Resources Technology Conference. https://doi.org/10.15530/urtec-2018-2901856

Chen, C.C. and Raghavan, R., 1997. A multiply-fractured horizontal well in a rectangular drainage region. SPE Journal, 2(04), pp.455-465.

Chen, H., Wang, Y., Zuo, M., Zhang, C., Jia, N., Liu, X. and Yang, S., 2022. A new prediction model of CO2 diffusion coefficient in crude oil under reservoir conditions based on BP neural network. *Energy*, *239*, p.122286.

Chen, H., Zhang, C., Jia, N., Duncan, I., Yang, S. and Yang, Y., 2021. A machine learning model for predicting the minimum miscibility pressure of CO2 and crude oil system based on a support vector machine algorithm approach. *Fuel*, *290*, p.120048.

Chen, P., Al Sowaidi, A.K., Patel, H., Brantferger, K., Bin Buang, K.A., Syed, F.I. and Shehhi, R.A., 2016. Assessment of simultaneous water and gas injection SWAG pilot in a giant offshore carbonate reservoir. Abu Dhabi International Petroleum Exhibition & Conference. https://doi.org/10.2118/183223-MS

Chen, Y. and Xu, G., 2013. Improvement of Ca^{2+}-tolerance by the introduction of EO groups for the anionic surfactants: Molecular dynamics simulation. Colloids and Surfaces A: Physicochemical and Engineering Aspects, 424, 26-32. https://doi.org/10.1016/j.colsurfa.2013.02.026

Cho, Y., Eker, E., Uzun, I., Yin, X. and Kazemi, H., 2016. Rock characterization in unconventional reservoirs: A comparative study of Bakken, Eagle Ford, and Niobrara formations. SPE Low Perm Symposium. https://doi.org/10.2118/180239-MS

Christiansen, R.L. and Haines, H.K., 1987. Rapid measurement of minimum miscibility pressure with the rising-bubble apparatus. SPE Reservoir Engineering, 2(04), 523-527. https://doi.org/10.2118/13114-PA

Chukwu, F.I., 1989. *Pressure derivative analysis of vertically fractured wells in bounded reservoirs* (Doctoral dissertation, University of Oklahoma).

Chun, B.J., Choi, J.I. and Jang, S.S., 2015. Molecular dynamics simulation study of sodium dodecyl sulfate micelle: Water penetration and sodium dodecyl sulfate dissociation. Colloids and Surfaces A: Physicochemical and Engineering Aspects, 474, 36-43. https://doi.org/10.1016/j.colsurfa.2015.03.002

Conte, E., Pierri, G., Federici, A., Mendolicchio, L. and Zbilut, J.P., 2006. A model of biological neuron with terminal chaos and quantum-like features. Chaos, Solitons & Fractals, 30(4), pp.774-780.

Cox, D.O., Kuuskraa, V.A. and Hansen, J.T., 1996, April. Advanced type curve analysis for low permeability gas reservoirs. In *SPE Gas Technology Symposium*. OnePetro.

Culp, J.T., Smith, M.R., Bittner, E. and Bockrath, B., 2008. Hysteresis in the physisorption of CO2 and N2 in a flexible pillared layer nickel cyanide. *Journal of the American Chemical Society*, *130*(37), pp.12427-12434.

Cutler, W.W., 1924. *Estimation of underground oil reserves by oil-well production curves* (No. 228). US Government Printing Office.

Dang, C., Nghiem, L., Fedutenko, E., Gorucu, E., Yang, C. and Mirzabozorg, A., 2018, September. Application of Artificial Intelligence for Mechanistic Modeling and Probabilistic Forecasting of Hybrid Low Salinity Chemical Flooding. In SPE Annual Technical Conference and Exhibition. Society of Petroleum Engineers.

Dawson, M., Nguyen, D., Champion, N. and Li, H., 2015. Designing an optimized surfactant flood in the Bakken. SPE/CSUR Unconventional Resources Conference. https://doi.org/10.2118/175937-MS

de Campos Souza, P.V., Torres, L.C.B., Guimaraes, A.J., Araujo, V.S., Araujo, V.J.S. and Rezende, T.S., 2019. Data density-based clustering for regularized fuzzy neural networks based on nullneurons and robust activation function. *Soft Computing*, *23*(23), pp.12475-12489.

de Lara, L.S., Michelon, M.F. and Miranda, C.R., 2012. Molecular dynamics studies of fluid/oil interfaces for improved oil recovery processes. The Journal of Physical Chemistry B, 116(50), 14667-14676. https://doi.org/10.1021/jp310172j

Demuth, H., Beale, M. and Hagan, M., 2007. Neural Network Toolbox User's GuideMatlab. The Mathworks, Accelerating the pace of engineering and science.

Denney, D., 2001. Neural network for time-lapse seismic reservoir monitoring. Journal of petroleum technology, 53(08), pp.44-47.

Denney, D., 2003. Characterizing partially sealing faults-An artificial neural network approach. Journal of petroleum technology, 55(02), pp.68-69.

DiStefano, V.H., McFarlane, J., Stack, A.G., Perfect, E., Mildner, D.F., Bleuel, M., Chipera, S.J., Littrell, K.C., Cheshire, M.C., Manz, K.E. and Anovitz, L.M., 2019. Solvent-pore interactions in the Eagle Ford shale formation. Fuel, 238, 298-311. https://doi.org/10.1016/j.fuel.2018.10.010

Dong, C. and Hoffman, B.T., 2013. Modeling gas injection into shale oil reservoirs in the Sanish field, North Dakota. Unconventional Resources Technology Conference. https://doi.org/10.1190/urtec2013-185

Doublet, L.E. and Blasingame, T.A., 1995. Decline curve analysis using type curves: Water influx/waterflood cases. paper SPE, 30774, pp.22-25.

Du, F. and Nojabaei, B., 2019. A review of gas injection in shale reservoirs: enhanced oil/gas recovery approaches and greenhouse gas control. Energies, 12(12), p.2355. https://doi.org/10.3390/en12122355

Energy Information Administration (EIA), 2013. Shale Oil and Shale Gas Resources Are Globally Abundant. Available online: https://www.eia.gov/todayinenergy/detail.php?id=11611.

Energy Information Administration (EIA), 2017. World Shale Resource Assessments. Available online: https://www.eia.gov/outlooks/aeo/assumptions/pdf/oilgas.pdf.

Energy Information Administration (EIA), 2019. Annual Energy Outlook 2019 with projections to 2050, U.S. Department of Energy, https://www.eia.gov/outlooks/aeo.

Energy Information Administration (EIA), 2021a. U.S. Tight Oil Production Projection 2020 - 2050. Available online: https://www.eia.gov/todayinenergy/detail.php?id=46656

Energy Information Administration (EIA), 2021b. Weekly U.S. Field Production of Crude Oil. Available online: https://www.eia.gov/dnav/pet/hist/LeafHandler.ashx?n=PET&s=WCRFPUS2&f=W.

Energy Information Administration (EIA), 2022. Low permeabitlity oil and gas plays, Maps. Online Available: https://www.eia.gov/special/shaleplays/ [accessed 03.20.2022].

Fetkovich, M.J., 1973, September. Decline curve analysis using type curves. In *Fall Meeting of the Society of Petroleum Engineers of AIME*. OnePetro.

Fetkovich, M.J., Vienot, M.E., Bradley, M.D. and Kiesow, U.G., 1987. Decline-curve analysis using type curves—case histories. SPE Formation Evaluation, 2(04), pp.637-656.

Fragoso, A., Selvan, K. and Aguilera, R., 2018. An investigation on the feasibility of combined refracturing of horizontal wells and huff and puff gas injection for improving oil recovery from shale petroleum reservoirs. SPE Improved Oil Recovery Conference. https://doi.org/10.2118/190284-MS

Gherabati, S.A., Smye, K.M., McDaid, G. and Hamlin, S., 2020. New Engineering and geologic parameters to predict infill well performance in the Wolfcamp of the Delaware Basin. Unconventional Resources Technology Conference. https://doi.org/10.15530/urtec-2020-3077

Gittings, R.K. and Roach, T., 2020. Who benefits from a resource boom? Evidence from the Marcellus and Utica shale plays. Energy Economics, 87, 104489. https://doi.org/10.1016/j.eneco.2019.104489

Goodman, A., Sanguinito, S., Tkach, M., Natesakhawat, S., Kutchko, B., Fazio, J. and Cvetic, P., 2019. Investigating the role of water on CO_2-Utica Shale interactions for carbon storage and shale gas extraction activities–Evidence for pore scale alterations. Fuel, 242,744-755. https://doi.org/10.1016/j.fuel.2019.01.091

Gringarten, A.C. and Ramey, H.J., 1974. Unsteady-state pressure distributions created by a well with a single horizontal fracture, partial penetration, or restricted entry. Society of petroleum engineers journal, 14(04), pp.413-426.

Gringarten, A.C., Ramey, H.J. and Raghavan, R., 1975. Applied pressure analysis for fractured wells. *Journal of Petroleum Technology*, *27*(07), pp.887-892.

Habibi, A., Yassin, M.R., Dehghanpour, H. and Bryan, D., 2017a. CO_2-oil interactions in tight rocks: an experimental study. SPE Unconventional Resources Conference. https://doi.org/10.2118/185047-MS

Habibi, A., Yassin, M.R., Dehghanpour, H. and Bryan, D., 2017b. Experimental investigation of CO_2-oil interactions in tight rocks: A Montney case study. Fuel, 203, 853-867. https://doi.org/10.1016/j.fuel.2017.04.077

Hall, F.E., Chunhe, Z., Gasem, K.A.M., Robinson, R.L. and Dan, Y., 1994, November. Adsorption of pure methane, nitrogen, and carbon dioxide and their binary mixtures on wet Fruitland coal. In *SPE Eastern Regional Meeting*. OnePetro.

Hamam, H. and Ertekin, T., 2018, August. A Generalized Varying Oil Compositions and Relative Permeability Screening Tool for Continuous Carbon Dioxide Injection in Naturally Fractured Reservoirs. In SPE Kingdom of Saudi Arabia Annual Technical Symposium and Exhibition. Society of Petroleum Engineers.

Hawthorne, S.B., Gorecki, C.D., Sorensen, J.A., Steadman, E.N., Harju, J.A. and Melzer, S., 2013. Hydrocarbon mobilization mechanisms from upper, middle, and lower Bakken reservoir rocks exposed to CO_2. SPE Unconventional Resources Conference. https://doi.org/10.2118/167200-MS

Hawthorne, S.B., Sorensen, J.A., Miller, D.J., Gorecki, C.D., Harju, J.A. and Pospisil, G., 2019. Laboratory studies of rich gas interactions with Bakken crude oil to support enhanced oil recovery. Unconventional Resources Technology Conference. https://doi.org/10.15530/urtec-2019-961

Heart Energy, 2020. Why US shale production declines are higher than you might think. Available online: https://www.hartenergy.com/exclusives/why-us-shale-production-declines-are-higher-you-might-think-188251

Heller, R. and Zoback, M., 2014. Adsorption of methane and carbon dioxide on gas shale and pure mineral samples. *Journal of unconventional oil and gas resources*, *8*, pp.14-24.

Hoffman, B.T., 2012. Comparison of various gases for enhanced recovery from shale oil reservoirs. SPE Improved Oil Recovery Symposium. https://doi.org/10.2118/154329-MS

Hoffman, B.T., 2018a. Bakken IOR model for a pilot injection project. SPE Improved Oil Recovery Conference. https://doi.org/10.2118/190221-MS

Hoffman, B.T., 2018b. Huff-n-puff gas injection pilot projects in the Eagle Ford. SPE Canada Unconventional Resources Conference. https://doi. org/10.2118/189816-MS

Holm, L.W. and Josendal, V.A., 1980. Discussion of determination and prediction of CO_2/minimum miscibility pressures. J. Pet. Technol.; 32(5). https://www.osti.gov/biblio/5587425

Hoteit, H. and Firoozabadi, A., 2006. Numerical modeling of diffusion in fractured media for gas injection and recycling schemes. SPE Annual Technical Conference and Exhibition. https://doi.org/10.2118/103292-PA

Hu, Jinghong, Chong Zhang, Zhenhua Rui, Yanlong Yu, and Zhangxin Chen. "Fractured horizontal well productivity prediction in tight oil reservoirs." *Journal of Petroleum Science and Engineering* 151 (2017): 159-168.

Huang, Y.F., Huang, G.H., Dong, M.Z. and Feng, G.M., 2003. Development of an artificial neural network model for predicting minimum miscibility pressure in CO2 flooding. Journal of Petroleum science and Engineering, 37(1-2), pp.83-95.

Jalili, S. and Akhavan, M., 2009. A coarse-grained molecular dynamics simulation of a sodium dodecyl sulfate micelle in aqueous solution. Colloids and Surfaces A: Physicochemical and Engineering Aspects, 352(1-3), 99-102. https://doi.org/10.1016/j.colsurfa.2009.10.007

Jarvie, D.M., Hill, R.J., Ruble, T.E. and Pollastro, R.M., 2007. Unconventional shale-gas systems: The Mississippian Barnett Shale of north-central Texas as one model for thermogenic shale-gas assessment. *AAPG bulletin*, *91*(4), pp.475-499.

Jessen, K., Tang, G.Q. and Kovscek, A.R., 2008. Laboratory and simulation investigation of enhanced coalbed methane recovery by gas injection. *Transport in Porous Media*, *73*(2), pp.141-159.

Jiang, R., Xu, J., Sun, Z., Guo, C. and Zhao, Y., 2014. Rate transient analysis for multistage fractured horizontal well in tight oil reservoirs considering stimulated reservoir volume. Mathematical Problems in Engineering, 2014.

Jin, L., Hawthorne, S., Sorensen, J., Kurz, B., Pekot, L., Smith, S., Bosshart, N., Azenkeng, A., Gorecki, C. and Harju, J., 2016. A systematic investigation of gas-based improved oil recovery technologies for the Bakken tight oil formation. SPE/AAPG/SEG Unconventional Resources Technology Conference. https://doi.org/10.15530/URTEC-2016-2433692

Jin, X.J., Pavia, M., Samuel, M., Shah, S., Zhang, R. and Thompson, J., 2019. Field pilots of unconventional shale EOR in the Permian basin. Unconventional Resources Technology Conference. https://doi.org/10.15530/urtec-2019-506

Karadkar, P.B., AlTammar, M.J., Alabdrabalnabi, M.I. and Bataweel, M.A., 2019. Use of carbonated slickwater for fracturing unconventional formations. SPE Gas & Oil Technology Showcase and Conference. https://doi.org/10.2118/198583-MS

Karimi, S., Kazemi, H. and Simpson, G.A., 2019. Capillary pressure and wettability indications of middle Bakken core plugs for improved oil recovery. SPE Reservoir Evaluation & Engineering, 22(01), 310-325. https://doi.org/10.2118/185095-PA

Kerr, E., Venepalli, K.K., Patel, K., Ambrose, R. and Erdle, J., 2020. Use of reservoir simulation to forecast field EOR response-An Eagle Ford gas injection huff-n-puff application. SPE Hydraulic Fracturing Technology Conference and Exhibition. https://doi.org/10.2118/199722-MS

Khamidy, N.I., Tariq, Z. and Syihab, Z., 2019, March. Development of ANN-based predictive model for miscible CO2 flooding in sandstone reservoir. In *SPE middle east oil and gas show and conference*. OnePetro.

Khan, M.Y., Tiwari, A., Ikeda, S., Syed, F.I., Al Sowaidi, A.K. and Martin, J., 2016. Co-development plan optimization of complex multiple reservoirs for giant offshore Middle East Oil Field. Abu Dhabi International Petroleum Exhibition & Conference. https://doi.org/10.2118/183221-MS

Kurtoglu, B. and Salman, A., 2015. How to utilize hydraulic fracture interference to improve unconventional development. Abu Dhabi International Petroleum Exhibition and Conference. https://doi.org/10.2118/177953-MS

Kurtoglu, B., Kazemi, H., Rosen, R., Mickelson, W. and Kosanke, T., 2014. A rock and fluid study of middle Bakken formation: key to enhanced oil recovery. SPE/CSUR Unconventional Resources Conference. https://doi.org/10.2118/171668-MS

Kurtoglu, B., Sorensen, J.A., Braunberger, J., Smith, S. and Kazemi, H., 2013b. Geologic characterization of a Bakken reservoir for potential CO_2 EOR. SPE/AAPG/SEG Unconventional Resources Technology Conference. https://doi.org/10.1190/urtec2013-186

Li, C., Ostadhassan, M., Gentzis, T., Kong, L., Carvajal-Ortiz, H. and Bubach, B., 2018. Nanomechanical characterization of organic matter in the Bakken formation by microscopy-based method. Marine and Petroleum Geology, 96, 128-138. https://doi.org/10.1016/j.marpetgeo.2018.05.019

Li, C., Pu, H. and Zhao, J.X., 2019a. Molecular simulation study on the volume swelling and the viscosity reduction of n-alkane/co2 systems. Industrial & Engineering Chemistry Research, 58(20), pp.8871-8877. https://doi.org/10.1021/acs.iecr.9b01268

Li, C., Pu, H., Zhang, S. and Zhao, J., 2019b. Effect of nanoparticles and surfactants on oil/water interfacial tension: A coarse-grained molecular dynamics simulation study. SPE/AAPG/SEG Unconventional Resources Technology Conference. https://doi.org/10.15530/urtec-2019-246

Li, C., Pu, H., Zhong, X., Li, Y. and Zhao, J.X., 2020. Interfacial interactions between Bakken crude oil and injected gases at reservoir temperature: A molecular dynamics simulation study. Fuel, 276, 118058. https://doi.org/10.1016/j.fuel.2020.118058

Li, H., Hart, B., Dawson, M. and Radjef, E., 2015. Characterizing the middle Bakken: Laboratory measurement and rock typing of the Middle Bakken formation. Unconventional Resources Technology Conference. https://doi.org/10.15530/urtec-2015-2172485

Li, L., Su, Y., Sheng, J.J., Hao, Y., Wang, W., Lv, Y., Zhao, Q. and Wang, H., 2019. Experimental and numerical study on CO_2 sweep volume during CO_2 huff-n-puff enhanced oil recovery process in shale oil reservoirs. Energy & Fuels, 33(5), 4017-4032. https://doi.org/10.1021/acs.energyfuels.9b00164

Li, S. and Luo, P., 2017. Experimental and simulation determination of minimum miscibility pressure for a Bakken tight oil and different injection gases. Petroleum, 3(1), 79-86. https://doi.org/10.1016/j.petlm.2016.11.011

Li, S., Zhang, S., Ma, X., Zou, Y., Li, N., Chen, M., Cao, T. and Bo, Z., 2019. Hydraulic fractures induced by water-/carbon dioxide-based fluids in tight sandstones. Rock Mechanics and Rock Engineering, 52(9), 3323-3340. https://doi.org/10.1007/s00603-019-01777-w

Liang, Y. and Zhao, P., 2019, September. A machine learning analysis based on big data for eagle ford shale formation. SPE Annual Technical Conference and Exhibition. https://doi.org/10.2118/196158-MS

Lin, M., Chen, S., Ding, W., Chen, Z.J. and Xu, J., 2015. Effect of fracture geometry on well production in hydraulic-fractured tight oil reservoirs. Journal of Canadian Petroleum Technology, 54(03), pp.183-194.

Liu, B., Shi, J., Wang, M., Zhang, J., Sun, B., Shen, Y. and Sun, X., 2016. Reduction in interfacial tension of water–oil interface by supercritical CO_2 in enhanced oil recovery processes studied with molecular dynamics simulation. The Journal of Supercritical Fluids, 111, 171-178. https://doi.org/10.1016/j.supflu.2015.11.001

Long D., 2022. US Shale Oil Output Poised for Higher Growth, 2022. Available online: https://www.argusmedia.com/en/news/2294701-us-shale-oil-output-poised-for-higher-growth

Luo, S., Lutkenhaus, J.L. and Nasrabadi, H., 2018. Effect of nano-scale pore size distribution on fluid phase behavior of gas IOR in shale reservoirs. SPE Improved Oil Recovery Conference. https://doi.org/10.2118/190246-MS

Makimura, D., Kunieda, M., Liang, Y., Matsuoka, T., Takahashi, S. and Okabe, H., 2013. Application of molecular simulations to CO_2-enhanced oil recovery: Phase equilibria and interfacial phenomena. SPE Journal, 18(02), 319-330. https://doi.org/10.2118/163099-PA

McClelland, J.L. and Rumelhart, D.E., 1989. Explorations in parallel distributed processing: A handbook of models, programs, and exercises. MIT press.

McCormack, K.L., Zoback, M.D. and Kuang, W., 2021. A case study of vertical hydraulic fracture growth, stress variations with depth and shear stimulation in the Niobrara Shale and Codell Sand, Denver-Julesburg Basin, Colorado. Interpretation, 9(4), SG59-SG69. https://doi.org/10.1190/INT-2020-0246.1

McCulloch, W.S. and Pitts, W., 1943. A logical calculus of the ideas immanent in nervous activity. The bulletin of mathematical biophysics, 5(4), pp.115-133.

Memon, A., Li, A., Memon, B.S., Muther, T., Han, W., Kashif, M., Tahir, M.U. and Akbar, I., 2021. Gas adsorption and controlling factors of shale: review, application, comparison and challenges. Natural Resources Research, 30(1), 827-848. https://doi.org/10.1007/s11053-020-09738-9

Memon, A., Li, A., Muther, T. and Ren, X., 2020. An experimental study of gas sorption, adsorbed, and sorbed porosity, and their impact on shale gas-in-place calculations. Journal of Porous Media, 23(10), 985-1000. https://doi.org/10.1615/JPorMedia.2020033387

Metropolis, N. and Ulam, S., 1949. The monte carlo method. Journal of the American statistical association, 44(247), 335-341. https://web.williams.edu/Mathematics/sjmiller/public_html/105Sp10/handouts/MetropolisUlam_TheMonteCarloMethod.pdf

Mohaghegh, S., 2000. Virtual-intelligence applications in petroleum engineering: Part 1—Artificial neural networks. Journal of Petroleum Technology, 52(09), pp.64-73.

Mohamad, I.B. and Usman, D., 2013. Standardization and its effects on K-means clustering algorithm. *Research Journal of Applied Sciences, Engineering and Technology*, *6*(17), pp.3299-3303.

Mohebbinia, S. and Wong, T., 2017. Molecular diffusion calculations in simulationn of gasfloods in fractured reservoirs. SPE Reservoir Simulation Conference. https://doi.org/10.2118/182594-MS

Moosavi, S.R., Wood, D.A., Ahmadi, M.A. and Choubineh, A., 2019. ANN-based prediction of laboratory-scale performance of CO2-foam flooding for improving oil recovery. *Natural Resources Research*, *28*(4), pp.1619-1637.

Morsy, S. and Sheng, J.J., 2014. Effect of water salinity on shale reservoir productivity. Advances in Petroleum Exploration and Development, 8(1), 9-14. https://doi.org/10.3968/5604

Morsy, S., Sheng, J.J. and Soliman, M.Y., 2013. Waterflooding in the Eagle Ford shale formation: Experimental and simulation study. SPE Unconventional Resources Conference and Exhibition. https://doi.org/10.2118/167056-MS

Muther, T., Khan, M.J., Chachar, M.H. and Aziz, H., 2020b. A study on designing appropriate hydraulic fracturing treatment with proper material selection and optimized fracture half-length in tight multilayered formation sequence. SN Applied Sciences, 2(5), 1-12. https://doi.org/10.1007/s42452-020-2729-9

Muther, T., Nizamani, A.A. and Ismail, A.R., 2020a. Analysis on the effect of different fracture geometries on the productivity of tight gas reservoirs. Malays. J. Fundam. Appl. Sci, 16, 201-211.

Muther, T., Qureshi, H.A., Syed, F.I., Aziz, H., Siyal, A., Dahaghi, A.K. and Negahban, S., 2021a. Unconventional hydrocarbon resources: geological statistics, petrophysical characterization, and field development strategies. Journal of Petroleum Exploration and Production Technology, pp.1-26. https://doi.org/10.1007/s13202-021-01404-x

Muther, T., Syed, F.I., Dahaghi, A.K. and Negahban, S., 2022a. Contribution of gas adsorption–desorption in Marcellus shale for different fractured well configurations. Journal of Petroleum Exploration and Production Technology, pp.1-16. https://doi.org/10.1007/s13202-022-01456-7

Muther, T., Syed, F.I., Dahaghi, A.K. and Negahban, S., 2022b. Socio-inspired multi-cohort intelligence and teaching-learning-based optimization for hydraulic fracturing parameters design in tight formations. Journal of Energy Resources Technology, 144(7). https://doi.org/10.1115/1.4052182

Muther, T., Syed, F.I., Dahaghi, A.K. and Neghabhan, S., 2021b. Subsurface physics inspired neural network to predict shale oil recovery under the influence of rock and fracture properties. 2021 International Conference on INnovations in Intelligent SysTems and Applications (INISTA). https://doi.org/10.1109/INISTA52262.2021.9548580

Muther, T., Syed, F.I., Lancaster, A.T., Salsabila, F.D., Dahaghi, A.K. and Negahban, S., 2022c. Geothermal 4.0: AI-enabled geothermal reservoir development-current status, potentials, limitations, and ways forward. Geothermics, 100, p.102348. https://doi.org/10.1016/j.geothermics.2022.102348

Najeh, A., PISHVAEI, M. and Taghikhani, V., 2010. Neural network meta-modeling of steam assisted gravity drainage oil recovery processes.

Nguyen, D., Wang, D., Oladapo, A., Zhang, J., Sickorez, J., Butler, R. and Mueller, B., 2014. Evaluation of surfactants for oil recovery potential in shale reservoirs. SPE Improved Oil Recovery Symposium. https://doi.org/10.2118/169085-MS

O'Bryan, P.L. and Bourgoyne, A.T., 1990. Swelling of oil-based drilling fluids resulting from dissolved gas. SPE Drilling Engineering, 5(02), 149-155. https://doi.org/10.2118/16676-PA

Parmar, R., 2018. Training Deep Neural Networks. *Towards Data Science, Sept*. Retrieved from https://towardsdatascience.com/

Peng, F., Wang, R., Guo, Z. and Feng, G., 2018. Molecular dynamics simulation to estimate minimum miscibility pressure for oil with pure and impure CO_2. Journal of Physics Communications, 2(11), p.115028. https://doi.org/10.1088/2399-6528/aaf090

Pereira, L.M., Chapoy, A., Burgass, R. and Tohidi, B., 2016. Measurement and modelling of high pressure density and interfacial tension of (gas+ *n*-alkane) binary mixtures. The Journal of Chemical Thermodynamics, 97, 55-69. https://doi.org/10.1016/j.jct.2015.12.036

Perrin, J., 2019. Horizontally drilled wells dominate US tight formation production. US Energy Information Administration URL: https://www. eia. gov/todayinenergy/detail. php.

Pu, H. and Li, Y., 2016, April. Novel capillarity quantification method in IOR process in Bakken shale oil reservoirs. SPE Improved Oil Recovery Conference. https://doi.org/10.2118/179533-MS

Qu, G., Xue, C., Zhang, M., Liang, S., Han, Y. and Ding, W., 2016. Molecular dynamics simulation of sulfobetaine-type zwitterionic surfactants at the decane/water interface: structure, interfacial properties. Journal of Dispersion Science and Technology, 37(12), 1710-1717. https://doi.org/10.1080/01932691.2015.1135400

Rao, D.N., 1997. A new vanishing interfacial technique for miscibility determination. Fluid Phase Equilibria, 139, 311-324. https://doi.org/10.1016/S0378-3812(97)00180-5

Rassenfoss, S., 2014. Carbon dioxide may offer an unconventional EOR option. Journal of Petroleum Technology, 66(02), 52-56. https://doi.org/10.2118/0214-0052-JPT

Rassenfoss, S., 2017. Shale EOR works, but will it make a difference?. Journal of Petroleum Technology, 69(10), 34-40. https://doi.org/10.2118/1017-0034-JPT

Ribeiro, L.H., Li, H. and Bryant, J.E., 2017. Use of a CO_2-hybrid fracturing design to enhance production from unpropped-fracture networks. SPE Production & Operations, 32(01), 28-40. https://doi.org/10.2118/173380-PA

Ruiz-Morales, Y. and Romero-Martínez, A., 2018. Coarse-grain molecular dynamics simulations to investigate the bulk viscosity and critical micelle concentration of the ionic surfactant sodium dodecyl sulfate (SDS) in aqueous solution. The Journal of Physical Chemistry B, 122(14), 3931-3943. https://doi.org/10.1021/acs.jpcb.7b10770

Saeedi, A., Camarda, K.V. and Liang, J.T., 2007. Using neural networks for candidate selection and well performance prediction in water-shutoff treatments using polymer gels-a field-case study. SPE Production & Operations, 22(04), pp.417-424.

Sammalkorpi, M., Karttunen, M. and Haataja, M., 2007. Structural properties of ionic detergent aggregates: a large-scale molecular dynamics study of sodium dodecyl sulfate. The Journal of Physical Chemistry B, 111(40), 11722-11733. https://doi.org/10.1021/jp072587a

Sanaei, A., Abouie, A., Tagavifar, M. and Sepehrnoori, K., 2018. Comprehensive study of gas cycling in the Bakken shale. Unconventional Resources Technology Conference. https://doi.org/10.15530/urtec-2018-2902940

Sanchez-Rivera, D., Mohanty, K. and Balhoff, M., 2015. Reservoir simulation and optimization of huff-and-puff operations in the Bakken Shale. Fuel, 147, 82-94. https://doi.org/10.1016/j.fuel.2014.12.062

Saranya, C. and Manikandan, G., 2013. A study on normalization techniques for privacy preserving data mining. *International Journal of Engineering and Technology (IJET)*, *5*(3), pp.2701-2704.

Shen, H., Wang, Z., Gao, C., QIN, J., YAO, F. and XU, W., 2008. Determining the number of BP neural network hidden layer units. *Journal of tianjin University of Technology*, *24*(5), p.13.

Sheng, J.J. and Chen, K., 2014. Evaluation of the EOR potential of gas and water injection in shale oil reservoirs. Journal of Unconventional Oil and Gas Resources, 5, 1-9. https://doi.org/10.1016/j.juogr.2013.12.001

Sheng, J.J., 2015. Enhanced oil recovery in shale reservoirs by gas injection. Journal of Natural Gas Science and Engineering, 22, 252-259. https://doi.org/10.1016/j.jngse.2014.12.002

Shuler, P., Tang, H., Lu, Z. and Tang, Y., 2011. Chemical process for improved oil recovery from Bakken shale. Canadian Unconventional Resources Conference.. https://doi.org/10.2118/147531-MS

Sigmund, P.M., 1976. Prediction of molecular diffusion at reservoir conditions. Part 1-Measurement and prediction of binary dense gas diffusion coefficients. Journal of Canadian Petroleum Technology, 15(02). https://doi.org/10.2118/76-02-05

Smith, L.N., 2018. A disciplined approach to neural network hyper-parameters: Part 1--learning rate, batch size, momentum, and weight decay. *arXiv preprint arXiv:1803.09820*.

Smye, K.M., Ikonnikova, S., Yang, Q., McDaid, G. and Goodman, E., 2020. Geologic Variability and well productivity in US oil plays: The efficiency of completion intensity and new designs in various geologic contexts. Unconventional Resources Technology Conference. https://doi.org/10.15530/urtec-2020-3317

Song, C. and Yang, D., 2017. Experimental and numerical evaluation of CO_2 huff-n-puff processes in Bakken formation. Fuel, 190, 145-162. https://doi.org/10.1016/j.fuel.2016.11.041

SPE Data Repository. Online Available at: https://www.spe.org/en/industry/data-repository/

Sprunger, C., Muther, T., Syed, F.I., Dahaghi, A.K. and Neghabhan, S., 2021. State of the art progress in hydraulic fracture modeling using AI/ML techniques. Modeling Earth Systems and Environment, 8, 1-13. https://doi.org/10.1007/s40808-021-01111-w

Stalkup, F.I., 1987. Displacement behavior of the condensing/vaporizing gas drive process. SPE Annual Technical Conference and Exhibition. https://doi.org/10.2118/16715-MS

Stathakis, D., 2009. How many hidden layers and nodes?. *International Journal of Remote Sensing*, *30*(8), pp.2133-2147.

Stubbs, D.F., 1988. Neurocomputers. MD Computing: Computers in Medical Practice, 5(3), pp.14-24.

Sun, Q. and Ertekin, T., 2020. Screening and optimization of polymer flooding projects using artificial-neural-network (ANN) based proxies. *Journal of Petroleum Science and Engineering*, *185*, p.106617.

Syed, F.I., 2012. Analysis of Formation Flow Impairment in carbonate Reservoir due to Asphaltene Precipitation and Deposition during Gas Flooding. Doctoral Dissertation. The Petroleum Institute (United Arab Emirates)). Online Available at: https://www.proquest.com/docview/1329512830?pq-origsite=gscholar&fromopenview=true

Syed, F.I., Al Saadi, S., Khedr, O., Khan, M.Y., Yusuf, R. and Thakur, K.K., 2016. Successful application of a mechanistic coupled wellbore-reservoir dynamic simulation model to history match and plan cleanup operation of long horizontal wells. Abu Dhabi International Petroleum Exhibition & Conference. https://doi.org/10.2118/183190-MS

Syed, F.I., Alnaqbi, S., Muther, T., Dahaghi, A.K. and Negahban, S., **2021d**. Smart shale gas production performance analysis using machine learning applications. Petroleum Research. 7(1), 21-31. https://doi.org/10.1016/j.ptlrs.2021.06.003

Syed, F.I., AlShamsi, A., Dahaghi, A.K. and Neghabhan, S., 2020a. Application of ML & AI to model petrophysical and geo-mechanical properties of shale reservoirs–A systematic literature review. Petroleum. https://doi.org/10.1016/j.petlm.2020.12.001

Syed, F.I., Alshamsi, M., Dahaghi, A.K. and Neghabhan, S., 2020c. Artificial lift system optimization using machine learning applications. Petroleum. https://doi.org/10.1016/j.petlm.2020.08.003

Syed, F.I., Boukhatem, M. and Al Kiyoumi, A.A., 2019. Lean HC gas injection pilots analysis and IPR back calculation to examine the impact of asphaltene deposition on flow performance. Petroleum Research, 4(1), 84-95. https://doi.org/10.1016/j.ptlrs.2018.11.006

Syed, F.I., Dahaghi, A.K. and Muther, T., 2022. Laboratory to field scale assessment for EOR applicability in tight oil reservoirs. Petroleum Science.

Syed, F.I., Ghedan, S.G., Hage, A.R., Tariq, S.M. and Shebl, H., 2012. Formation flow impairment in carbonate reservoirs due to asphaltene precipitation and deposition during hydrocarbon gas flooding. Abu Dhabi International Petroleum Conference and Exhibition. https://doi.org/10.2118/160253-MS

Syed, F.I., Muther, T., Dahaghi, A.K. and Negahban, S., **2021a**. AI/ML assisted shale gas production performance evaluation. Journal of Petroleum Exploration and Production Technology, 11(9), 3509-3519. https://doi.org/10.1007/s13202-021-01253-8

Syed, F.I., Muther, T., Dahaghi, A.K. and Negahban, S., **2021b**. Low-rank tensors applications for dimensionality reduction of complex hydrocarbon reservoirs. Energy, p.122680. https://doi.org/10.1016/j.energy.2021.122680

Syed, F.I., Muther, T., Dahaghi, A.K. and Neghabhan, S., 2022a. CO_2 EOR performance evaluation in an unconventional reservoir through mechanistic constrained proxy modeling. Fuel, 310, p.122390. https://doi.org/10.1016/j.fuel.2021.122390

Syed, F.I., Muther, T., Van, V.P., Dahaghi, A.K. and Negahban, S., 2022b. Numerical trend analysis for factors affecting EOR performance and CO_2 storage in tight oil reservoirs. Fuel, 316, p.123370. https://doi.org/10.1016/j.fuel.2022.123370

Syed, F.I., Negahban, S. and Dahaghi, A.K., **2021c**. Infill drilling and well placement assessment for a multi-layered heterogeneous reservoir. Journal of Petroleum Exploration and Production, 11(2), 901-910. https://doi.org/10.1007/s13202-020-01067-0

Syed, F.I., Neghabhan, S., Zolfaghari, A. and Dahaghi, A.K., 2020b. Numerical validation of asphaltene precipitation and deposition during CO_2 miscible flooding. Petroleum Research, 5(3), 235-243. https://doi.org/10.1016/j.ptlrs.2020.04.002

Syed, F.I., Tunio, A.H. and Ghirano, N.A., 2011. Compositional analysis and screening for enhanced oil recovery processes in different reservoir and operating conditions. International Journal of Applied, 1(4), 143-160.

Tang, X., Koenig, P.H. and Larson, R.G., 2014. Molecular dynamics simulations of sodium dodecyl sulfate micelles in water. The effect of the force field. The Journal of Physical Chemistry B, 118(14), 3864-3880. https://doi.org/10.1021/jp410689m

Teklu, T.W., Alharthy, N., Kazemi, H., Yin, X., Graves, R.M. and AlSumaiti, A.M., 2014. Phase behavior and minimum miscibility pressure in nanopores. SPE Reservoir Evaluation & Engineering, 17(03), 396-403. https://doi.org/10.2118/168865-PA

Thomas, W.R., Helms, L.W., Driggers, T.K., Trice, D.W. and Thomas, G.L., 2016. EOG Resources (EOG) Earnings Call. May, 6, p.2016.

Todd, B.J., Reichhardt, D.K. and Heath, L.A., 2017. An evaluation of EOR potential in the Elm Coulee Bakken Formation, Richland County, Montana. SPE Unconventional Resources Conference. https://doi.org/10.2118/185028-MS

Todd, H.B. and Evans, J.G., 2016. Improved oil recovery IOR pilot projects in the Bakken formation. SPE Low Perm Symposium. https://doi.org/10.2118/180270-MS

Tovar, F.D., Barrufet, M.A. and Schechter, D.S., 2018. Gas injection for EOR in organic rich shales. part II: Mechanisms of recovery. SPE/AAPG/SEG Unconventional Resources Technology Conference. https://doi.org/10.15530/URTEC-2018-2903026

Tsau J., 2011. Near miscible carbon dioxide application in Arbuckle reservoirs to improve oil recovery. TORP IOR Conference. Available online at: https://torp.drupal. ku.edu/sites/torp.drupal.ku.edu/files/docs/rpsea2/RPSEA_TORP2011_near_ miscible1.pdf

Valluri, M.K., Alvarez, J.O. and Schechter, D.S., 2016. Study of the rock/fluid interactions of sodium and calcium brines with ultra-tight rock surfaces and their impact on improving oil recovery by spontaneous imbibition. SPE Low Perm Symposium. https://doi.org/10.2118/180274-MS

Vu, T.V. and Papavassiliou, D.V., 2019. Synergistic effects of surfactants and heterogeneous nanoparticles at oil-water interface: Insights from computations. Journal of Colloid and Interface Science, 553, 50-58. https://doi.org/10.1016/j.jcis.2019.05.102

Wan, T., Yu, Y. and Sheng, J.J., 2015. Experimental and numerical study of the EOR potential in liquid-rich shales by cyclic gas injection. Journal of Unconventional Oil and Gas Resources, 12, 56-67. https://doi.org/10.1016/j.juogr.2015.08.004

Wang, D., Butler, R., Liu, H. and Ahmed, S., 2011. Flow-rate behavior and imbibition in shale. SPE Reservoir Evaluation & Engineering, 14(04), 505-512. https://doi.org/10.2118/138521-PA

Wang, D., Butler, R., Zhang, J. and Seright, R., 2012. Wettability survey in Bakken shale using surfactant formulation imbibition. SPE Improved Oil Recovery Symposium. https://doi.org/10.2118/153853-MS

Wang, D., Zhang, J., Butler, R. and Olatunji, K., 2016. Scaling laboratory-data surfactant-imbibition rates to the field in fractured-shale formations. SPE Reservoir Evaluation & Engineering, 19(03), 440-449. https://doi.org/10.2118/178489-PA

Wang, D., Zhang, J., Butler, R., Koskella, D., Rabun, R. and Clark, A., 2014. Flow rate behavior and imbibition comparison between Bakken and Niobrara Formations. SPE/AAPG/SEG

Unconventional Resources Technology Conference. https://doi.org/10.15530/URTEC-2014-1920887

Wang, J., Wen, Y., Gou, Y., Ye, Z. and Chen, H., 2017. Fractional-order gradient descent learning of BP neural networks with Caputo derivative. *Neural networks*, *89*, pp.19-30.

Wang, X., Hou, J., Li, S., Dou, L., Song, S., Kang, Q. and Wang, D., 2020. Insight into the nanoscale pore structure of organic-rich shales in the Bakken Formation, USA. Journal of Petroleum Science and Engineering, 191, p.107182. https://doi.org/10.1016/j.petrol.2020.107182

Wang, X., Luo, P., Er, V. and Huang, S., 2010. Assessment of CO_2 flooding potential for Bakken formation, Saskatchewan. Canadian Unconventional Resources and International Petroleum Conference. https://doi.org/10.2118/137728-MS

Wang, Y. and Orr Jr, F.M., 1997. Analytical calculation of minimum miscibility pressure. Fluid Phase Equilibria, 139(1-2), 101-124. https://doi.org/10.1016/S0378-3812(97)00179-9

Warner, B. and Misra, M., 1996. Understanding neural networks as statistical tools. *The american statistician*, *50*(4), pp.284-293.

Whitson, C.H. and Sognesand, S., 1990. Application of the van Everdingen-Meyer method for analyzing variable-rate well tests. *SPE Formation Evaluation*, *5*(01), pp.67-75.

Wilke, C.R. and Chang, P., 1955. Correlation of diffusion coefficients in dilute solutions. AIChE Journal, 1(2), 264-270.

Williams, L.L., Rubin, J.B. and Edwards, H.W., 2004. Calculation of Hansen solubility parameter values for a range of pressure and temperature conditions, including the supercritical fluid region. Industrial & Engineering Chemistry Research, 43(16), 4967-4972. https://doi.org/10.1021/ie0497543

Xie, J., Yang, C., Gupta, N., King, M.J. and Datta-Gupta, A., 2015. Integration of shale-gas-production data and microseismic for fracture and reservoir properties with the fast marching method. SPE Journal, 20(02), 347-359. https://doi.org/10.2118/161357-PA

Yan, H., Yuan, S.L., Xu, G.Y. and Liu, C.B., 2010. Effect of Ca^{2+} and Mg^{2+} ions on surfactant solutions investigated by molecular dynamics simulation. Langmuir, 26(13), 10448-10459. https://doi.org/10.1021/la100310w

Yang, D., Song, C., Zhang, J., Zhang, G., Ji, Y. and Gao, J., 2015. Performance evaluation of injectivity for water-alternating-CO_2 processes in tight oil formations. Fuel, 139, 292-300. https://doi.org/10.1016/j.fuel.2014.08.033

Yang, H.S. and Kim, N.S., 1996, January. Determination of rock properties by accelerated neural network. In 2nd North American Rock Mechanics Symposium. American Rock Mechanics Association.

Yin, H., Zhou, J., Xian, X., Jiang, Y., Lu, Z., Tan, J. and Liu, G., 2017. Experimental study of the effects of sub-and super-critical CO_2 saturation on the mechanical characteristics of organic-rich shales. Energy, 132, 84-95. https://doi.org/10.1016/j.energy.2017.05.064

Yu, W., Lashgari, H. and Sepehrnoori, K., 2014. Simulation study of CO_2 huff-n-puff process in Bakken tight oil reservoirs. SPE Western North American and Rocky Mountain Joint Meeting. https://doi.org/10.2118/169575-MS

Yu, Y. and Sheng, J.J., 2016. Experimental investigation of light oil recovery from fractured shale reservoirs by cyclic water injection. SPE Western Regional Meeting. https://doi.org/10.2118/180378-MS

Yue, H., Vieth-Hillebrand, A., Han, Y., Horsfield, B., Schleicher, A.M. and Poetz, S., 2021. Unravelling the impact of lithofacies on the composition of NSO compounds in residual and expelled fluids of the Barnett, Niobrara and Posidonia formations. Organic Geochemistry, 155, p.104225. https://doi.org/10.1016/j.orggeochem.2021.104225

Zabihi, R., Schaffie, M., Nezamabadi-Pour, H. and Ranjbar, M., 2011. Artificial neural network for permeability damage prediction due to sulfate scaling. Journal of Petroleum Science and Engineering, 78(3-4), pp.575-581.

Zhang, F., Adel, I.A., Park, K.H., Saputra, I.W. and Schechter, D.S., 2018. Enhanced oil recovery in unconventional liquid reservoir using a combination of CO_2 huff-n-puff and surfactant-assisted spontaneous imbibition. In SPE Annual Technical Conference and Exhibition. https://doi.org/10.2118/191502-MS

Zhang, J., Pan, Z., Liu, K. and Burke, N., 2013a. Molecular simulation of CO_2 solubility and its effect on octane swelling. Energy & Fuels, 27(5), 2741-2747. https://doi.org/10.1021/ef400283n

Zhang, J., Wang, D. and Butler, R., 2013b. Optimal salinity study to support surfactant imbibition into the Bakken shale. SPE Unconventional Resources Conference Canada. https://doi.org/10.2118/167142-MS

Zhang, K., 2016. Experimental and numerical investigation of oil recovery from Bakken formation by miscible CO_2 injection. SPE ATCE. https://doi.org/10.2118/184486-STU

Zhang, X., Lu, Y., Tang, J., Zhou, Z. and Liao, Y., 2017. Experimental study on fracture initiation and propagation in shale using supercritical carbon dioxide fracturing. Fuel, 190, 370-378. https://doi.org/10.1016/j.fuel.2016.10.120

Zhao, L., Tao, L. and Lin, S., 2015. Molecular dynamics characterizations of the supercritical CO_2–mediated hexane–brine interface. Industrial & Engineering Chemistry Research, 54(9), 2489-2496. https://doi.org/10.1021/ie505048c

Zhao, P., Dong, R. and Liang, Y., 2020. Regional to local machine-learning analysis for unconventional formation reserve estimation: Eagle Ford case study. SPE ATCE. https://doi.org/10.2118/201351-MS

Zhu, J., Chen, J., Wang, X., Fan, L. and Nie, X., 2021. Experimental investigation on the characteristic mobilization and remaining oil distribution under CO_2 huff-n-puff of Chang 7 continental shale oil. Energies, 14(10), p.2782. https://doi.org/10.3390/en14102782

Zick, A.A. 1986. A Combined Condensing/Vaporizing Mechanism in the Displacement of Oil and Enriched Gases. Presented at ATCE, Louisiana, 5–8 October. SPE15493-MS. http://dx.doi.org/10.2118/15493-MS. https://doi.org/10.2118/175131-MS

Zou, J., Han, Y. and So, S.S., 2008. Overview of artificial neural networks. *Artificial Neural Networks*, pp.14-22. https://link.springer.com/protocol/10.1007/978-1-60327-101-1_2

Zou, J., Liao, X., Li, X., Zhu, Z., Chu, H., Yuan, Z., Luo, W. and Shen, X., 2018, October. An experimental study on carbonated water injection of core samples from tight oil reservoirs from Ordos Basin. In SPE Russian Petroleum Technology Conference. OnePetro. https://doi.org/10.2118/191474-18RPTC-MS